JOURNAL OF CAVE AND KARST STUDIES

December 2011
Volume 73, Number 3
ISSN 1090-6924
A Publication of the National Speleological Society

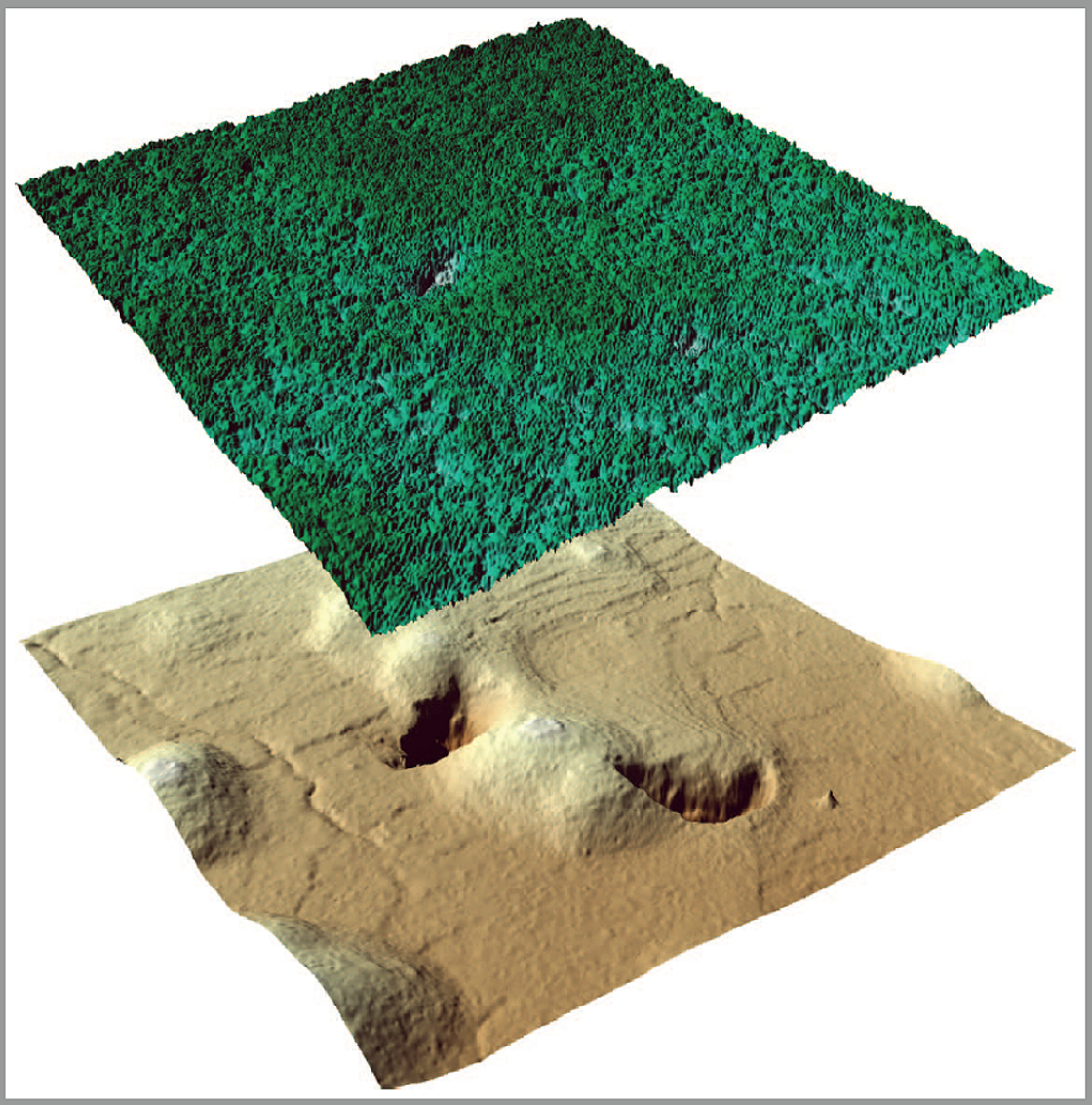

IN THIS ISSUE:

USING LIDAR TO LOCATE CAVE OPENINGS, GEOGRAPHY AND GEOLOGY OF WHITE-NOSE SYNDROME, QUATERNARY CAVE FAUNAS OF CANADA, AND MORE.

Published By
The National Speleological Society

The *Journal of Cave and Karst Studies* (ISSN 1090-6924, CPM Number #40065056) is a multi-disciplinary, refereed journal published three times a year by the National Speleological Society, 2813 Cave Avenue, Huntsville, Alabama 35810-4431 USA; Phone (256) 852-1300; Fax (256) 851-9241, email: nss@caves.org; World Wide Web: http://www.caves.org/pub/journal/.
Check the *Journal* website for subscripion rates. Back issues and cumulative indices are available from the NSS office.

POSTMASTER: send address changes to the *Journal of Cave and Karst Studies*, 2813 Cave Avenue, Huntsville, Alabama 35810-4431 USA.

The *Journal of Cave and Karst Studies* is covered by the following ISI Thomson Services Science Citation Index Expanded, ISI Alerting Services, and Current Contents/Physical, Chemical, and Earth Sciences.

Front cover: Cover figure depicts ability of LiDAR to remove forest canopy to reveal karst land surface. Figure courtesy of J. Weishampel.

C.S. Swezey and C.P. Garrity – Geographical and geological data from caves and mines infected with white-nose syndrome (WNS) before September 2009 in the eastern United States. *Journal of Cave and Karst Studies,* v. 73, no. 3, p. 125–157. DOI: 10.4311/jcks2010es0162

GEOGRAPHICAL AND GEOLOGICAL DATA FROM CAVES AND MINES INFECTED WITH WHITE-NOSE SYNDROME (WNS) BEFORE SEPTEMBER 2009 IN THE EASTERN UNITED STATES

Christopher S. Swezey and Christopher P. Garrity
U.S. Geological Survey, 12201 Sunrise Valley Drive, MS 926A, Reston, VA 20192 U.S.A., cswezey@usgs.gov; cgarrity@usgs.gov

Abstract: Since 2006, a white fungus named *Geomyces destructans* has been observed on the muzzles, noses, ears, and (or) wings of bats in the eastern United States, and bat colonies that are infected with this fungus have experienced dramatic incidences of mortality. Although it is not exactly certain how and why these bats are dying, this condition has been named white-nose syndrome (WNS). WNS appears to have spread from an initial infection site at a cave that is connected to a commercial cave in New York, and by the end of August 2009 was identified in at least 74 other sites in the eastern United States. Although detailed geographical and geological data are limited, a review of the available data shows that sites infected with WNS before September 2009 include both natural caves and mines. These infected sites extend from New Hampshire to Virginia, and known site elevations range from 84 to 2693 feet above sea level. In terms of geological setting, the infected sites include sedimentary, metamorphic, and igneous rocks of ages ranging from Precambrian to Jurassic. However, by the end of August 2009, no infected sites had been identified in strata of Mississippian, Cretaceous, or Triassic age. Meteorological data are sparse, but most of the recorded air temperatures in the known WNS-infected caves and mines range from 0 to 13.9 °C, and humidity measurements range from 68 to 100 percent. Although it is not certain which environmental parameters are important for WNS, it is hoped that the geographical and geological information presented in this paper will inform and clarify some of the debate about WNS, lead to greater understanding of the environmental parameters associated with WNS, and highlight the paucity of scientific data from caves in the eastern United States.

Introduction

In 2006 and 2007, unusually great numbers of emaciated and dead bats were discovered in several caves in Schoharie County (New York), yet studies of these bats revealed no obvious disease-causing parasites, no viral pathogens, and no unusual bacteriological problems (Blehert et al., 2009). However, a percentage of these bats was characterized by a notable decrease in body fat. In addition, many of these bats exhibited erratic behavior such as a shift in roosting locations closer to cave entrances, out-of-season emergence from hibernation, and flying outside during the daytime. Furthermore, the bats were characterized by the presence of a visually striking white fungus growing on their muzzles, noses, ears, and (or) wings. This condition was named white-nose syndrome (WNS) and all of the sites where this condition has appeared have experienced dramatic incidences of bat mortality. Blehert et al. (2009), for example, have calculated bat population declines in excess of 75 percent at WNS-infected sites. Although exact numbers are difficult to determine, it is estimated that more than 1 million bats may have died from WNS as of December 2009 (Sleeman, 2009). These population declines are likely to have far-reaching ecological consequences because bats play critical roles in insect population control, plant pollination, and seed dissemination (Ransome, 1990; Pierson, 1998; Dumont, 2003; Jones and Rydell, 2003; von Helversen and Winter, 2003).

The white fungus associated with WNS is a newly identified fungus named *Geomyces destructans* (Gargas et al., 2009). *Geomyces* is a genus of terrestrial saprophytes that has been identified in soils in many places throughout the world, usually in colder regions such as northern Europe, Russia, Canada, and the South Orkney Islands of the Antarctic region (e.g., Traaen, 1914; Carmichael, 1962; Sigler and Carmichael, 1976; Van Oorschot, 1980; Marshall, 1998; Rice and Currah, 2006; Kochkina et al., 2007). However, *Geomyces* is a very diverse genus, and it has also been reported from Costa Rica (Sigler and Carmichael, 1976).

The species *Geomyces destructans* has spores with a distinctive and unusual hook shape (Gargas et al., 2009). Until recently, *G. destructans* had been identified only at the WNS-infected sites in the eastern North America (Blehert et al., 2009). However, in March 2009 *G. destructans* was identified on a bat near Périgueux, France (Puechmaille et al., 2010), and subsequently the fungus has been identified at other sites in Europe (Wibbelt et al.,

2010). In contrast with the sites in North America, the occurrences of *G. destructans* in Europe do not appear to be associated with dramatic incidences of bat mortality.

In North America, *Geomyces destructans* is seen on sick bats but not on healthy bats. The fungus invades living skin tissue of bats, but does not typically cause inflammation or an immune response (Meteyer et al., 2009; Reichard and Kunz, 2009). Other than attacking skin tissue, it is not yet known if the fungus affects bats in other ways. In fact, it is not yet known whether *G. destructans* is the primary cause of the unusual bat mortality in North America or whether the fungus is simply a secondary infection. However, at the time of this writing, all isolates of *G. destructans* in North America have been genetically identical within the marker genes examined. This observation suggests that the fungus in North America probably disseminated from a point source.

Since it first appeared in New York, *Geomyces destructans* has spread rapidly among bats in the eastern North America. Bats infected with the fungus were first photodocumented on 16 February 2006 in a cave that is connected to Howe Caverns, which are commercial caverns in Schoharie County, New York (Blehert et al., 2009). During early 2007, bats infected with *G. destructans* were discovered in other caves in New York. During January to March 2008, *G. destructans* was identified on hibernating bats at several other locations in New York, as well as locations in Vermont, Massachusetts, and Connecticut. During November 2008, *G. destructans* appeared on bats in Pennsylvania (Mifflin County). During December 2008 to February 2009, the fungus appeared on bats in New Hampshire, New Jersey, and new sites in New York, Vermont, Connecticut, and Pennsylvania. The fungus also appeared in West Virginia (Pendleton County) during January 2009 and in Virginia (Bath County) during February 2009. During March and April 2009, the fungus appeared on bats in southwestern Virginia (Giles County) and at new sites in New York, Connecticut, and Pennsylvania. During May and August 2009, the fungus appeared on bats at new sites in Virginia. After August 2009, very few records of new WNS occurrences are available, other than statements that document the appearance of WNS in previously uninfected counties and states.

According to Blehert et al. (2009) and Turner and Reeder (2009), bat species infected with the fungus include the big brown bat (*Eptesicus fuscus*), the eastern small-footed bat (*Myotis leibii*), the little brown bat (*Myotis lucifugus*), the northern long-eared bat (*Myotis septentrionalis*), the Indiana bat (*Myotis sodalis*), and the tricolored bat (*Perimyotis subflavus*). It is not known if the fungus affects other animals besides bats.

Although studies of *Geomyces destructans* are still in their infancy, there is great interest in how the fungus has spread in the past, and concern about where and how the fungus might spread in the future. Preliminary studies suggest that the fungus may be transmitted from bat to bat, and that the fungus may also be transmitted as an unwanted hitchhiker upon humans, clothing, and caving gear (Sleeman, 2009; Turner and Reeder, 2009). Studies by Blehert et al. (2009) have shown that *G. destructans* prefers cold temperatures for growth, that optimal temperatures for fungus growth are between 5 °C and 10 °C, and that the fungus does not grow at temperatures greater than approximately 20 °C. Anecdotal field evidence suggests that the fungus may prefer relatively high humidity, although no laboratory studies on this topic have been published yet.

At present, it is not certain which environmental parameters are important for predicting the spread of *Geomyces destructans* and WNS. This uncertainty is due, in part, to the lack of a publicly available list of WNS-infected sites and the paucity of detailed scientific data from caves and mines in the United States. In order to improve understanding of the environmental parameters associated with WNS, this paper presents a chronology of where and when WNS appeared in the United States prior to September 2009 (Table 1). This paper then presents (in stratigraphic order from oldest to youngest) a series of short paragraphs that summarize geological and meteorological data from each of the infected sites. These paragraphs are followed by a discussion of observations regarding the distribution of WNS with respect to various geographical, geological, and meteorological parameters. At this early stage of investigation, it is difficult to know which data may or may not be important with regards to WNS. Nevertheless, it is hoped that the information presented in this paper will inform and clarify the debate about WNS, and lead to greater understanding of the environmental parameters associated with WNS.

GEOLOGIC SETTINGS OF CAVES AND MINES INFECTED WITH WNS

By the end of August 2009, 75 sites were known to be infected with WNS, and 42 of these sites were located within the Appalachian Basin (Table 1, Figs. 1 and 2). This basin extends from New York and Ontario in the north to Alabama in the south, and the basin contains strata that range in age from Precambrian to Permian. As shown in Figure 3, the Precambrian rocks (older than ~542 Ma) consist of various igneous, metamorphic, and clastic sedimentary lithologies. The Lower Cambrian strata (~542 to 513 Ma) are predominantly sandstone and mudstone. The Middle Cambrian through Middle Ordovician strata (~513 to 461 Ma) are predominantly carbonate. The Upper Ordovician through lower Silurian strata (~461 to 428 Ma) are predominantly sandstone and mudstone. The upper Silurian through Lower Devonian strata (~428 to 398 Ma) are predominantly carbonate. The Middle Devonian to Upper Devonian strata (~398 to 359 Ma) are predominantly sandstone and mudstone. The Mississippian strata (~359 to 318 Ma) are predominantly carbonate, and the Pennsylvanian and Permian strata (~318 to 251 ma) are predominantly sandstone, mudstone,

and coal. Several regional unconformities are present in the Appalachian Basin (Fig. 3). Of particular note for this paper are the Ordovician Owl Creek Unconformity (''Knox Unconformity''), which caps carbonate strata of the Cambrian-Ordovician Knox Group, and the Devonian Wallbridge Unconformity, which caps carbonate strata of the Silurian-Devonian Helderberg Group. Both of these unconformities are overlain in most places by clean, quartz sandstone (Ordovician St. Peter Sandstone, Devonian Oriskany Sandstone).

Thirty-three of the 75 sites that were known to be infected with WNS before September 2009 are located to the north and east of the Appalachian Basin (Fig. 1). This region to the north and east of the Appalachian Basin consists of igneous rocks and various metamorphic rocks that may be correlated with age-equivalent sandstone, mudstone, limestone, and dolomite in the Appalachian Basin. In addition, this region beyond the Appalachian Basin contains numerous small rift basins that formed during the opening of the Atlantic Ocean (e.g., Benson, 1992; Weems and Olsen, 1997). In the United States, these rift basins contain mostly sandstone and mudstone of Triassic and Jurassic age (~226 to 190 Ma).

Geographical and geological data from each of the infected sites are described below in stratigraphic order from oldest to youngest. The descriptions include information on hydrology and meteorology, where such information is available. The descriptions also include any available information on cave sediment/soil, because *Geomyces* are terrestrial saprophytes that are known to reside in soils. Finally, each description provides information on when and who reported the WNS infection at that site.

Precambrian-Cambrian Igneous and Metamorphic Rocks

Nine of the sites infected with WNS before September 2009 are located in Precambrian and (or) Cambrian igneous and metamorphic rocks (Fig. 3). These sites are present in New York, New Jersey, and Vermont. Seven of these sites are mines, and two of these sites are caves. Three of the sites are located in granite or gneiss (W Mountain Cave, Hibernia Mine, Mount Hope Mine), three of the sites are located in meta-volcanic rocks (Barton Hill Mine, Fisher Hill Mine, Fahnestock State Park Mine), and three of the sites are located in meta-sedimentary rocks (Main Graphite Mine, Williams Cave, Bridgewater Mines).

W Mountain Cave, Franklin County, NY (Site 71 on Fig. 1):

Note: Initial reports erroneously placed this cave in Clinton County (Carroll, 1972b, 1974), but subsequent reports indicate that the cave is located in Franklin County (Cole, 1974; Carroll, 1997, 2009; Porter, 2009c).

Cave Map: Map dated 1973 in Carroll (2009).

Stratigraphy: Precambrian granitic gneiss (Cole, 1974; Carroll, 1997, 2009; Porter, 2009c).

Cave Meteorology: Carroll (2009) reported temperatures of 5.0 to 5.6 °C) 100 feet inside the cave, and temperatures of 2.8 to 3.3 °C 300 feet inside the cave.

WNS Infection Report: Anonymous (2009a) and Porter (2009c). In addition, a WNS infection in Clinton County (NY) was confirmed by the U.S. Geological Survey (USGS) National Wildlife Health Center (NWHC) Quarterly Mortality Reports, 2009, Quarter 1. These USGS reports are available online at http://www.nwhc.usgs.gov/publications/quarterly_reports/.

Hibernia Mine, Morris County, NJ (Site 52 on Fig. 1):

Mine Map: Undated map in Sims (1953).

Stratigraphy: Precambrian granite (Bayley, 1910; Sims, 1953; McManus and Esher, 1971).

Mined Commodity: Iron, mined from approximately 1722 to 1916.

Mine Meteorology: McManus and Escher (1971) reported an air temperature gradient ranging from 0 to 6 °C along a horizontal mine shaft 350 to 650 meters from the entrance. McManus (1974) reported relative humidity of 99 to 100 percent and average air temperature ranging from 1.39 to 4.38 °C.

WNS Infection Report: USGS NWHC (Quarterly Mortality Reports, 2008, Quarter 4).

Mount Hope Mine, Morris County, NJ (Site 53 on Fig. 1):

Mine Map: Undated map in Sims (1953).

Stratigraphy: Precambrian oligoclase-quartz-biotite gneiss enclosed within granite (Bayley, 1910; Sims, 1953; James and Dennen, 1962; Ross, 1982).

Mined Commodity: Iron, mined from approximately 1710 to at least 1959.

WNS Infection Report: USGS NWHC (Quarterly Mortality Reports, 2008, Quarter 4).

Barton Hill Mine, Essex County, NY (Site 43 on Fig. 1):

Mine Map: None published.

Stratigraphy: Magnetite ore in Precambrian meta-volcanic rocks (Kemp, 1898; Newland, 1921; Britzke et al., 2006).

Mined Commodity: Iron, mined during the mid-1800s.

WNS Infection Report: Anonymous (2008), Porter (2008a), and Bat Conservation and Management, Inc. (http://www.batmanagement.com/wns/WNSphotoalbum1/index.html). In addition, a WNS infection in Essex County (NY) was confirmed by the USGS NWHC (Quarterly Mortality Reports, 2009, Quarter 1).

Fisher Hill Mine, Essex County, NY (Site 44 on Fig. 1):

Mine Map: None published.

Stratigraphy: Magnetite ore in Precambrian meta-volcanic rock (Kemp, 1898; Newland, 1921).

Mined Commodity: Iron, mined periodically from 1845 to 1971

WNS Infection Report: Porter (2008a). In addition, a WNS infection in Essex County (NY) was confirmed by

Table 1. List of sites infected with WNS before September 2009 in the eastern United States.

Site Number on Figures 1 and 2	Cave or Mine Name	Location		Stratigraphic Age	Stratigraphic Name	Elevation		WNS First Identified	
		State	County			m	ft	Month	Year
1	Howe Caverns	N.Y.	Schoharie	Silurian-Devonian	Helderberg Group	319	1047	February	2006
2	Barytes Cave	N.Y.	Schoharie	Silurian-Devonian	Helderberg Group	244	799	March	2006
3	Schoharie Caverns	N.Y.	Schoharie	Silurian-Devonian	Helderberg Group	304	997	January	2007
4	Gage Caverns	N.Y.	Schoharie	Silurian-Devonian	Helderberg Group	387	1271	March	2007
5	Hailes Cave	N.Y.	Albany	Silurian-Devonian	Helderberg Group	356	1167	March	2007
6	Knox Cave	N.Y.	Albany	Silurian-Devonian	Helderberg Group	401	1315	April	2007
7	Merlin's Cave	N.Y.	Columbia	Ordovician	Stockbridge Group	223	731	December	2007
8	Mass Hole	Mass.	Berkshire	Ordovician	Stockbridge Group	33	108	January	2008
9	Williams Preserve Mine	N.Y.	Ulster	Silurian-Devonian	Helderberg Group	65	214	January	2008
10	Williams Hotel Mine	N.Y.	Ulster	Silurian-Devonian	Helderberg Group	77	253	January	2008
11	mine	Vt.	Windham	…	…	…	…	January	2008
12	Morris Cave	Vt.	Rutland	Ordovician	Stockbridge Group	250	820	January	2008
13	Elizabeth Mine	Vt.	Orange	Devonian	Gile Mountain Formation	356	1167	January	2008
14	…	Vt.	Washington	…	…	…	…	January	2008
15	Glen Park Caves	N.Y.	Jefferson	Ordovician	Trenton Limestone	134	439	January	2008
16	Clarksville Cave	N.Y.	Albany	Devonian	Onondaga Limestone	232	761	February	2008
17	Mitchell's Cave	N.Y.	Montgomery	Cambrian	Little Falls Dolomite	215	705	February	2008
18	Williams Lake Mine	N.Y.	Ulster	Silurian-Devonian	Helderberg Group	81	266	February	2008
19	Bat's Den Cave	Mass.	Berkshire	Cambrian-Ordovician	Stockbridge Group	329	1081	February	2008
20	Old Mine	Mass.	Hampden	Ordovician	Chester Amphibolite	206	675	February	2008
21	Bakers Quarry Cave	Mass.	Berkshire	Cambrian-Ordovician	Stockbridge Group	460	1510	February	2008
22	Red Bat Cave	Mass.	Berkshire	Ordovician	Stockbridge Group	457	1500	February	2008
23	mine	Mass.	Franklin	…	…	…	…	February	2008
24	Aeolus Bat Cave	Vt.	Bennington	Ordovician	Stockbridge Group	763	2503	February	2008
25	Benson's Cave	N.Y.	Schoharie	Silurian-Devonian	Helderberg Group	330	1082	March	2008
26	Hell's Wells	N.Y.	Schoharie	Silurian-Devonian	Helderberg Group	298	977	March	2008

Table 1. Continued.

Site Number on Figures 1 and 2	Cave or Mine Name	Location		Stratigraphic Age	Stratigraphic Name	Elevation		WNS First Identified	
		State	County			m	ft	Month	Year
27	Lasell's Hell Hole	N.Y.	Schoharie	Silurian-Devonian	Helderberg Group	367	1203	March	2008
28	Ain't No Catchment Cave	N.Y.	Schoharie	Silurian-Devonian	Helderberg Group	277	910	March	2008
29	South Bethlehem Cave	N.Y.	Albany	Silurian-Devonian	Helderberg Group	66	216	March	2008
30	Martin Mine	N.Y.	Ulster	Silurian-Devonian	Helderberg Group	74	244	March	2008
31	unnamed cave	Conn.	Litchfield	Cambrian-Ordovician	Stockbridge Group	101	331	March	2008
32	…	Conn.	Hartford	…	…	…	…	March	2008
33	Williams Cave	Vt.	Bennington	Precambrian-Cambrian	Nassau Formation	564	1850	March	2008
34	Skinnner Hollow Cave	Vt.	Bennington	Ordovician	Stockbridge Group	585	1920	March	2008
35	Main Graphite Mine	N.Y.	Warren	Precambrian	Metasedimentary rock	486	1596	March	2008
36	Greeley Mine	Vt.	Windsor	Ordovician	Serpentinite	272	892	March	2008
37	McFails Cave	N.Y.	Schoharie	Silurian-Devonian	Helderberg Group	375	1231	April	2008
38	Nature's Way Cave	N.Y.	Albany	Silurian-Devonian	Helderberg Group	261	856	April	2008
39	Shindle Mine	Pa.	Mifflin	Silurian	Tuscarora Sandstone	389	1277	November	2008
40	Hasbrouck Mine	N.Y.	Ulster	Silurian-Devonian	Helderberg Group	26	84	December	2008
41	Indian Oven Cave	N.Y.	Columbia	Cambrian-Ordovician	Stockbridge Group	300	984	December	2008
42	Surprise Cave	N.Y.	Sullivan	Silurian-Devonian	Helderberg Group	221	726	December	2008
43	Barton Hill Mine	N.Y.	Essex	Precambrian	Metavolcanic rock	455	1493	December	2008
44	Fisher Hill Mine	N.Y.	Essex	Precambrian	Metavolcanic rock	499	1638	December	2008
45	cave	N.Y.	Onondaga	…	…	…	…	January	2009
46	…	N.Y.	Hamilton	…	…	…	…	January	2009
47	cave	N.Y.	Washington	…	…	…	…	January	2009
48	Bridgewater Mines	Vt.	Windsor	Cambrian	Pinney Hollow Formation	361	1184	January	2009
49	mine	N.H.	Merrimack	…	…	…	…	January	2009
50	mine	N.H.	Grafton	…	…	…	…	January	2009
51	Fahnestock State Park Mine	N.Y.	Putnam	Precambrian	Amphibolite	305	1000	January	2009

Table 1. Continued.

Site Number on Figures 1 and 2	Cave or Mine Name	Location		Stratigraphic Age	Stratigraphic Name	Elevation		WNS First Identified	
		State	County			m	ft	Month	Year
52	Hibernia Mine	N.J.	Morris	Precambrian	Granite	262	861	January	2009
53	Mount Hope Mine	N.J.	Morris	Precambrian	Granite	244	800	January	2009
54	Pahaquarry Copper Mine	N.J.	Warren	Silurian	Bloomsburg Red Beds	168	552	January	2009
55	Dunmore Mine	Pa.	Lackawanna	Pennsylvanian	Llewellyn Formation	316	1036	January	2009
56	Shickshinny mine	Pa.	Luzerne	Pennsylvanian	Llewellyn Formation	260	853	January	2009
57	Hamilton Cave	W.Va.	Pendleton	Silurian-Devonian	Helderberg Group	640	2100	January	2009
58	Trout Cave	W.Va.	Pendleton	Silurian-Devonian	Helderberg Group	622	2040	January	2009
59	Cave Mountain Cave	W.Va.	Pendleton	Silurian-Devonian	Helderberg Group	683	2240	February	2009
60	Breathing Cave	Va.	Bath	Silurian-Devonian	Helderberg Group	716	2350	February	2009
61	Alexander Caverns	Pa.	Mifflin	Ordovician	Trenton Limestone	194	636	February	2009
62	Roxbury Mine	Conn.	Litchfield	Ordovician	Mine Hill Granite Gneiss	215	705	February	2009
63	Brandon Mine	Vt.	Rutland	Cambrian	Winooski Dolomite	125	410	February	2009
64	Single X Cave	N.Y.	Schoharie	Silurian-Devonian	Helderberg Group	180	590	March	2009
65	New-Gate Prison Mine	Conn.	Hartford	Jurassic	Portland Formation	293	960	March	2009
66	Carbondale mine #1	Pa.	Lackawanna	Pennsylvanian	Llewellyn Formation	137	450	March	2009
67	Carbondale mine #2	Pa.	Lackawanna	Pennsylvanian	Llewellyn Formation	342	1123	March	2009
68	Seawra Cave	Pa.	Mifflin	Silurian-Devonian	Helderberg Group	342	1123	March	2009
69	Aitkin Cave	Pa.	Mifflin	Ordovician	Trenton Limestone	220	723	March	2009
70	Clover Hollow Cave	Va.	Giles	Ordovician	Witten Limestone	220	723	March	2009
71	W Mountain Cave	N.Y.	Franklin	Precambrian	Granitic Gneiss	744	2440	April	2009
72	Saltpeter Cave	W.Va.	Pendleton	Silurian-Devonian	Helderberg Group	821	2693	May	2009
73	Newberry-Bane Cave	Va.	Bland	Ordovician	Witten Limestone	527	1729	May	2009
74	Hancock Cave	Va.	Smyth	Ordovician	Witten Limestone	780	2560	May	2009
75	Endless Caverns	Va.	Rockingham	Ordovician	New Market & Lincolnshire Ls.	358	1175	August	2009

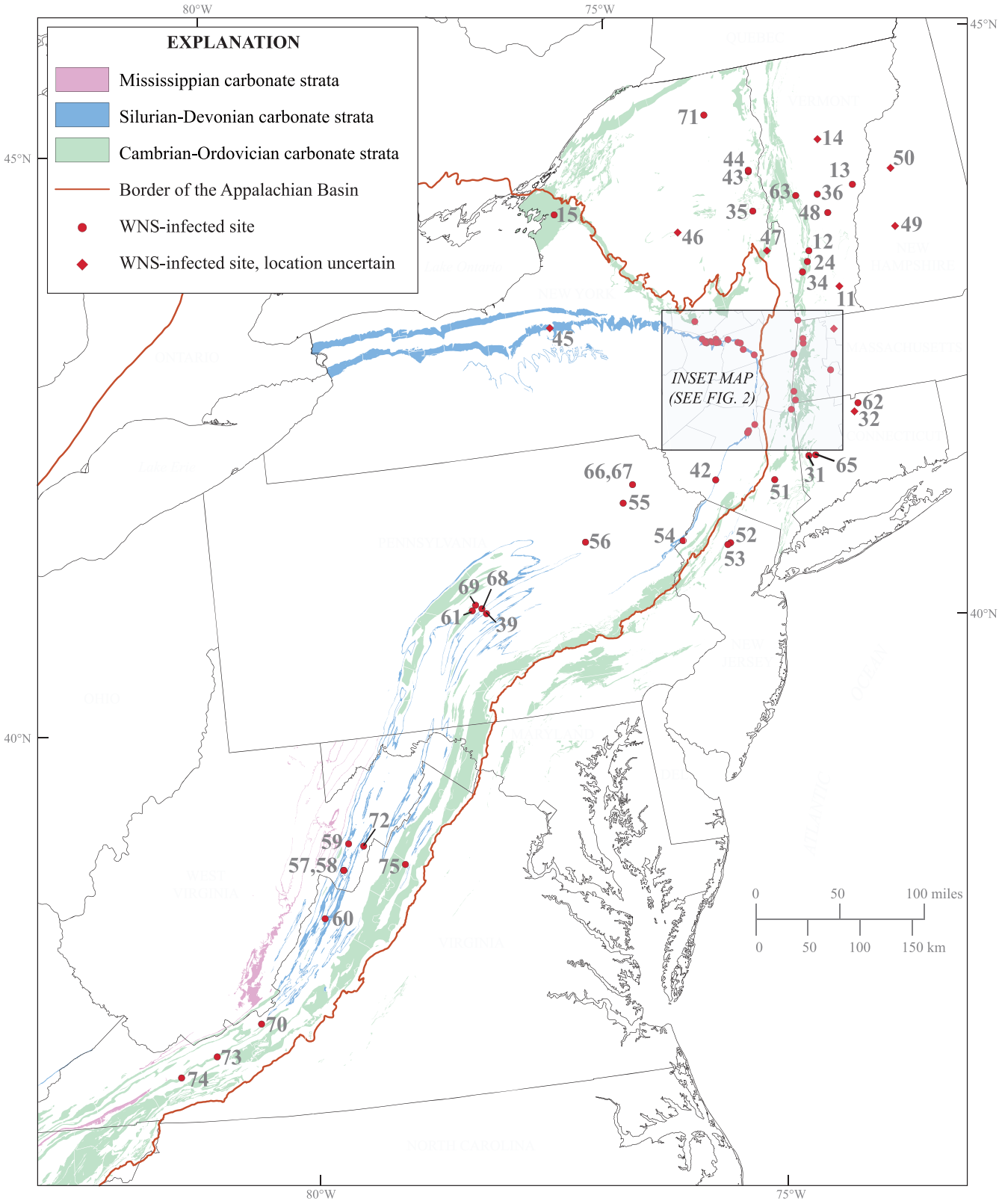

Figure 1. Map showing the locations of sites infected with white-nose syndrome (WNS) before September 2009 in the eastern United States. Sites are numbered in the approximate order in which WNS infection was detected, and the key to location numbers is given in the first column of Table 1. Outline of the Appalachian Basin is from Swezey (2009). Geological data were derived from the U.S. Geological Survey (USGS) Mineral Resources On-Line Spatial Data, which are available online at http://tin.er.usgs.gov/geology/state/ [accessed September 15, 2010].

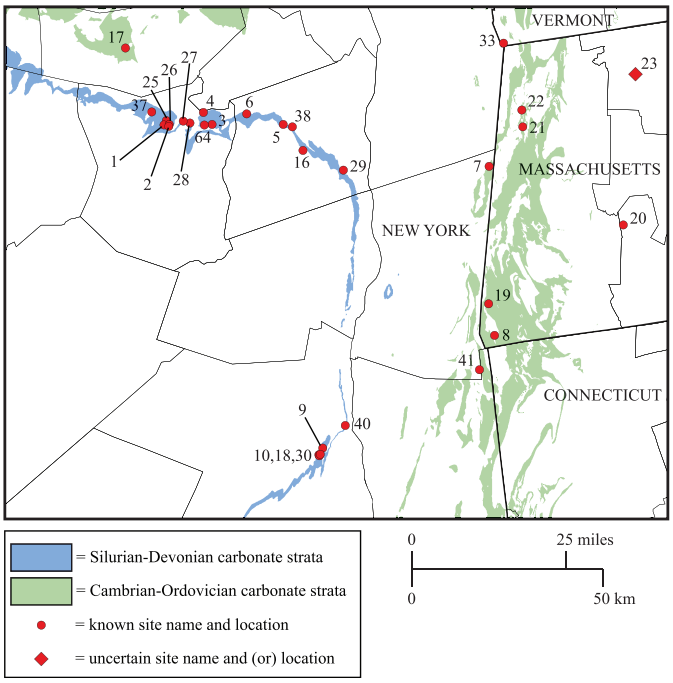

Figure 2. Detailed map showing the locations of sites infected with WNS before September 2009 in part of the northeastern United States (map location is shown on Fig. 1). Sites are numbered in the approximate order in which WNS infection was detected, and the key to location numbers is given in the first column of Table 1. Geological data were derived from the USGS Mineral Resources On-Line Spatial Data, which are available online at http://tin.er.usgs.gov/geology/state/ [accessed September 15, 2010].

the USGS NWHC (Quarterly Mortality Reports, 2009, Quarter 1).

Abandoned mine, Fahnestock State Park, Putnam County, NY (Site 51 on Fig. 1):

Mine Map: None published.

Stratigraphy: Precambrian amphibolite.

Mined Commodity: Iron, mined during the 1800s.

WNS Infection Report: Fred Koontz (http://teatown-blog.wordpress.com/2009/04/22/bats-threatened/). In addition, a WNS infection in Putnam County (NY) was confirmed by the USGS NWHC (Quarterly Mortality Reports, 2009, Quarter 1).

Main Graphite Mine, Warren County, NY (Site 35 on Fig. 1):

Mine Map: None published.

Stratigraphy: Precambrian graphite-rich schist (Kemp and Newland, 1897; Craytor, 1969).

Mined Commodity: Graphite, mined from 1887 to 1921.

Hydrology: Lower levels of the mine are filled with water, and patches of ice are present throughout the year.

Mine Meteorology: Patches of ice are present throughout the year.

WNS Infection Report: Porter (2008a) and Blehert et al. (2009).

Williams Cave, Bennington County, VT (Site 33 on Fig. 2):

Cave Map: Map dated 1999 in Keough (2000).

Stratigraphy: Schist of the Precambrian to Cambrian Nassau Formation (Porter, 1968; Keough, 2000; Ratcliffe et al., 2010, in prep.). According to Ratcliffe (1974), the Nassau Formation is stratigraphically equivalent to the Cambrian Everett Formation (depicted in Fig. 5).

WNS Infection Report: Porter (2008a).

Bridgewater Mines, Windsor County, VT (Site 48 on Fig. 1):

Mine Map: None published.

Stratigraphy: Schist of the Cambrian Pinney Hollow Formation (Hitchcock et al., 1861; Perry, 1929; Ratcliffe, 1994).

Mined Commodity: Gold, mined from 1851 to 1855.

WNS Infection Report: Anonymous (2009a,b). In addition, a WNS infection in Windsor County (VT) was confirmed by the USGS NWHC (Quarterly Mortality Reports, 2009, Quarter 1).

CAMBRIAN-ORDOVICIAN CARBONATE STRATA BELOW THE KNOX UNCONFORMITY

Twelve of the sites infected with WNS before September 2009 are located in Cambrian-Ordovician carbonate strata below the Knox Unconformity (Figs. 3 and 4). These sites are present in New York, Vermont, Massachusetts, and Connecticut. One of these sites is a mine, and 11 of these sites are caves. All of these sites are located in limestone, dolomite, or marble of the Middle Cambrian-Middle Ordovician Stockbridge Group (Fig. 4) or equivalent strata (Bat's Den Cave, Mass Hole, Bakers Quarry, Red Bat, Indian Oven Cave, Merlin's Cave, Mitchell's Cave, Brandon Mine, Morris Cave, Aeolus Bat Cave, Skinner Hollow Cave, and an unnamed cave in Litchfield County). Although these Middle Cambrian-Middle Ordovician carbonate rocks occupy a stratigraphic position immediately below the Knox Unconformity, the WNS-infected caves are located in an area where schist has been thrust over the carbonate rocks (Fig. 5), and the carbonate rocks have experienced some metamorphism. Estimates for the age of the schist range from Precambrian to Ordovician.

Bat's Den Cave, Berkshire County, MA (Site 19 on Fig. 2):

Cave Map: Map dated 1991 in Plante (1991).

Stratigraphy: Cambrian-Ordovician Stockbridge Formation (Hauer, 1969; Plante, 1991, 1992), as shown in Figure 5.

Cave Meteorology: Veilleux (2007) reported air temperatures ranging from 4.5 to 8.3 °C.

WNS Infection Report: Porter (2008a) and supporting online material for Blehert et al. (2009).

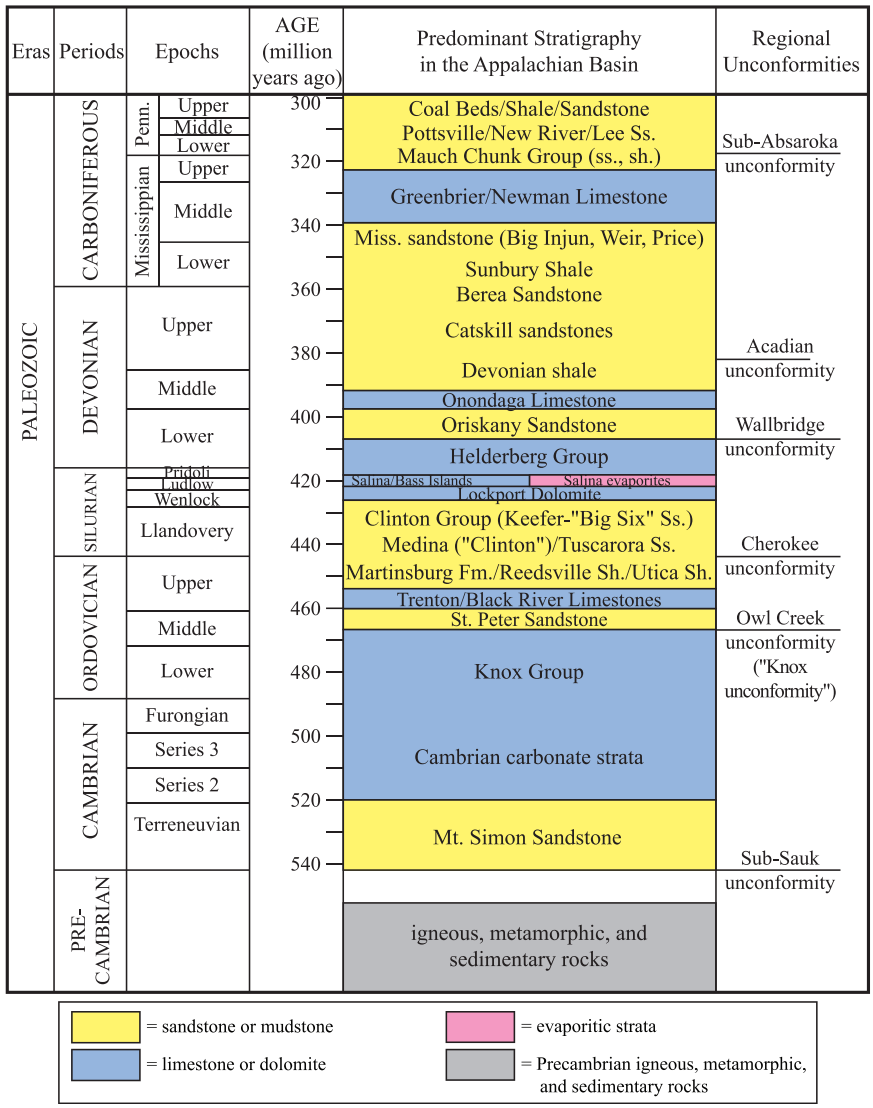

Figure 3. Schematic stratigraphy of the Appalachian Basin in the eastern United States, and some common stratigraphic names used in the basin (modified from Swezey, 2002). Time scale is from Gradstein et al. (2004). Penn. = Pennsylvanian; Sh. = Shale; Ss. = Sandstone; Miss. = Mississippian.

Mass Hole, Berkshire County, MA (Site 8 on Fig. 2):

Cave Map: Map dated 2008 in Goodman (2009).

Stratigraphy: Cambrian-Ordovician Stockbridge Formation (Berkshire Diggers and the Rockeaters, 2008; Goodman, 2009; Hackley, 2009).

Hydrology: The cave contains a stream and waterfalls.

Cave Sediments: Breakdown blocks in all of the major passages, and one room contains a lot of mud.

WNS Infection Report: Berkshire Diggers and the Rockeaters (2008) and Anonymous (2009a).

Bakers Quarry Cave, Berkshire County, MA (Site 21 on Fig. 2):

Cave Map: Map dated 1990 in Plante (1992).

Stratigraphy: Ordovician Shelburne Marble (Fig. 4) of the Cambrian-Ordovician Stockbridge Group (Barr, 1958; Anonymous, 1960; Hauer, 1969; Plante, 1992).

Hydrology: A stream flows in the cave entrance and along the most of the main passage.

WNS Infection Report: Porter (2008a).

Red Bat Cave, Berkshire County, MA (Site 22 on Fig. 2):

Cave Map: Undated map in Hauer (1969).

Stratigraphy: Cambrian-Ordovician Stockbridge Group (Davis and Palmer, 1959; Hauer, 1969).

WNS Infection Report: Porter (2008a).

Indian Oven Cave, Columbia County, NY (Site 41 on Fig. 2):

Cave Map: Undated map in van Beynen and Febbroriello (2006).

Stratigraphy: Cambrian-Ordovician Stockbridge Formation (Fisher, 1954; Seigel, 1957; van Beynen and Febbroriello, 2006). At this site, the Stockbridge Formation is

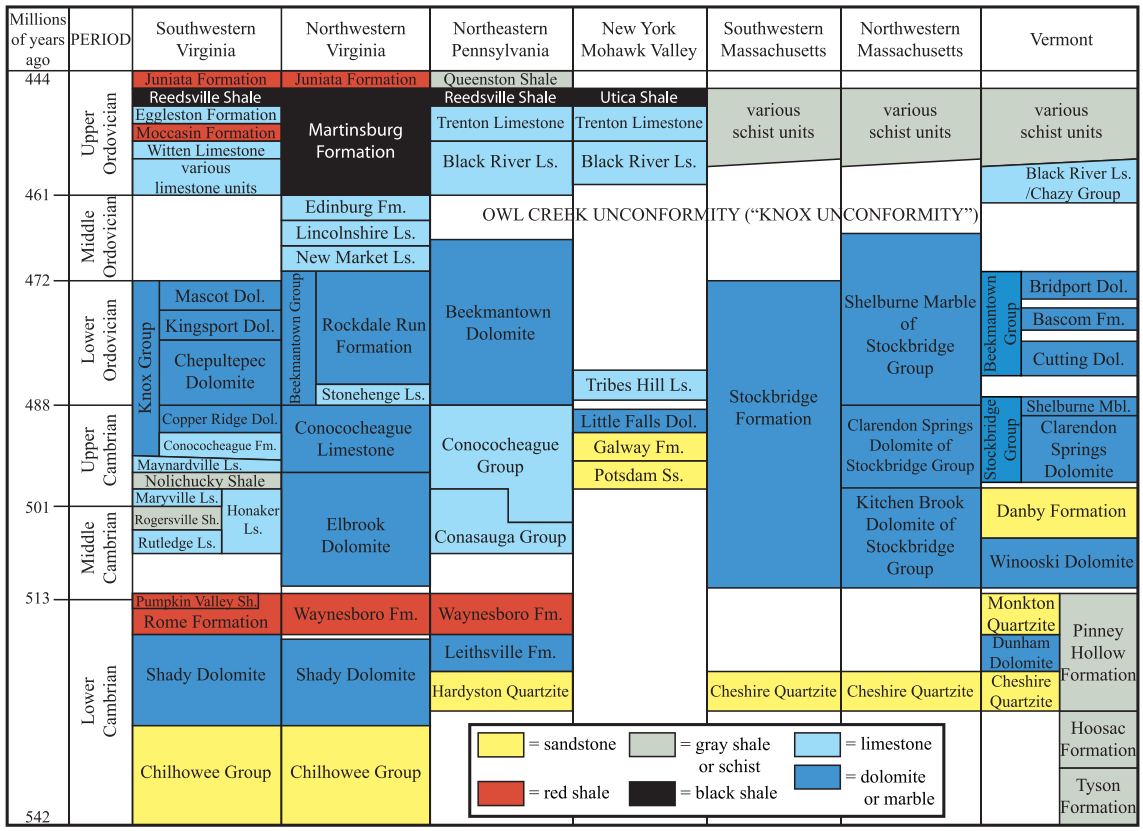

Figure 4. Cambrian through Ordovician strata in selected regions of the eastern United States (modified from Rader and Biggs, 1976, p. 6–25; Le Van and Rader, 1983; Read, 1989; Ratcliffe, 1994; Swezey, 2002; Landing, 2007; Ryder et al., 2008, 2009). Time scale is from Gradstein et al. (2004). Dol. = Dolomite; Fm. = Formation; Ls. = Limestone; Mbl. = Marble; Sh. = Shale; Ss. = Sandstone.

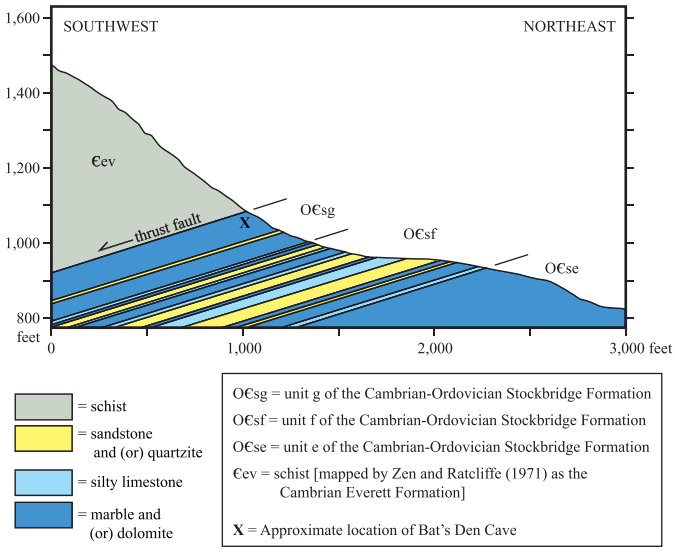

Figure 5. Geologic cross-section in the vicinity of Bat's Den Cave, Berkshire County, Massachusetts (modified from Plante, 1991; additional data from Zen and Hartshorn, 1966; Zen and Ratcliffe, 1971; Stanley and Ratcliffe, 1985). The vertical scale is in feet relative to sea level.

overlain by the Berkshire Schist, which is thought by Weaver (1957) to be stratigraphically equivalent to the black shale above the Upper Ordovician Trenton Limestone (Fig. 4).

Hydrology: A stream flows along the length of the cave.

Cave Meteorology: Air is reported to have relative humidity >95 percent (van Beynen and Febbroriello, 2006).

WNS Infection Report: Porter (2008a).

Merlin's Cave (XTC Cave), Columbia County, NY (Site 7 on Fig. 2):

Cave Map: Map dated 2008 in Porter (2009a).

Stratigraphy: Cambrian-Ordovician Stockbridge Formation (Botto, 2007; Dunham, 2007, 2009; Porter, 2009a).

Hydrology: The cave contains streams and waterfalls.

Cave Sediments: Mud is present throughout much of the cave (Dunham, 2010).

Cave Meteorology: Botto (2007) reported air temperature of 8.9 °C in one room.

WNS Infection Report: Porter (2008a).

Mitchell's Cave, Montgomery County, NY (Site 17 on Fig. 2):

Cave Map: Map dated 1954 in Curl and Peters (1954) and Evans et al. (1979).

Stratigraphy: Upper Cambrian Little Falls Dolomite (Curl and Peters, 1954; Jurgens, 1960; Anonymous, 1965; Porter, 1972), which is equivalent stratigraphically to the middle part of the Stockbridge Group (Fig. 4).

Hydrology: Water is present in some parts of the cave.

WNS Infection Report: Porter (2008a) and Armstrong (2009).

Brandon Mine, Rutland County, VT (Site 63 on Fig. 1):

Mine Map: None published.

Stratigraphy: Middle Cambrian Winooski Dolomite (Clark, 1990), which is equivalent stratigraphically to the lower part of the Stockbridge Group (Fig. 4).

Mined Commodity: Iron, mined during the 1870s, the 1950s, and possible other times.

Mine Meteorology: A data logger recorded nearly constant air temperature of 6.5 °C for four months (Kennedy, 2002).

WNS Infection Report: Dave McDevitt (http://www.nature.org/wherewework/northamerica/states/vermont/science/art27325.html#Feb_11). In addition, a WNS infection in Rutland County (VT) was confirmed by the USGS NWHC (Quarterly Mortality Reports, 2009, Quarter 1).

Morris Cave, Rutland County, VT (Site 12 on Fig. 1):

Cave Map: Map dated 1978 in Schweyen (1987) and Quick (1994).

Stratigraphy: Cambrian-Ordovician carbonate strata below the Knox Unconformity (Thayer, 1967; Schweyen, 1987; Higham, 1992, 1996; Quick, 1994; Porter, 2009b). The cave is located either in the Upper Cambrian-Lower Ordovician Shelburne Marble of the Stockbridge Group near the contact between the Stockbridge Group and schist that has been thrust over the Stockbridge Group (Thayer, 1967; Schweyen, 1987; Higham, 1992), or in the Upper Cambrian Clarendon Springs Dolomite (Fig. 4), which lies directly below the Shelburne Marble in Vermont (Quick, 1994).

Hydrology: Streams and waterfalls are present within parts of the cave.

Cave Meteorology: Thayer (1967) reported an air temperature of 6.1 °C.

WNS Infection Report: Porter (2008a,b). In addition, a WNS infection in Rutland County (VT) was confirmed by the USGS NWHC (Quarterly Mortality Reports, 2009, Quarter 1).

Aeolus Bat Cave (Dorset Bat Cave), Bennington County, VT (Site 24 on Fig. 1):

Cave Map: Map dated 1980 in Quick (1994).

Stratigraphy: Cambrian-Ordovician Shelburne Marble of the Stockbridge Group (Scott, 1959; Carroll, 1969; Quick, 1994; Porter, 2009b).

Cave Meteorology: Kennedy (2002) reported the air temperature to be approximately 6.1 °C, although Griffin (1945) mentions one instance when sub-freezing temperatures occurred during the winter.

WNS Infection Report: Porter (2008a,b), the USGS NWHC (Quarterly Mortality Reports, 2008, Quarter 4), and supporting online material for Blehert et al. (2009).

Skinner Hollow Cave, Bennington County, VT (Site 34 on Fig. 1):

Cave Map: Map dated 2000 in Quick (2001).

Stratigraphy: Marble of the Lower Ordovician Bascom Formation of the Beekmantown Group (Fig. 4), a few hundred feet below the contact between the marble and schist that has been thrust over the marble (Perry, 1942; Scott, 1959; Carroll, 1988; Quick, 1994, 2001).

Hydrology: A stream flows through parts of the cave.

Cave Meteorology: The entrance of the cave gets little direct sunlight, and snow and ice may persist in the cave well into the summer (Perry, 1942; Quick, 2001). Cave air temperatures as low as 1.7 °C have been measured in August (Quick, 2001).

WNS Infection Report: Porter (2008a) and Anonymous (2009a).

Unnamed cave near New Milford, Litchfield County, CT (Site 31 on Fig. 1):

WNS infection at this site was suggested by Kocer (2009) and reported in supporting online material for Blehert et al. (2009). Additional information has not been reported, but all known caves in Litchfield County are located within the Cambrian-Ordovician Stockbridge Formation (Huntington, 1963).

Ordovician Carbonate Strata Above the Knox Unconformity

Seven of the sites infected with WNS before September 2009 are located in Ordovician carbonate strata above the Knox Unconformity (Figs. 3 and 4). These sites include a group of caves in New York (Glen Park Caves), two caves in Pennsylvania (Aitkin Cave, Alexander Caverns), and four caves in Virginia (Endless Caverns, Clover Hollow Cave, Newberry-Bane Cave, Hancock Cave). The Glen Park Caves, Aitkin Cave, and Alexander Caverns have developed mainly in the Upper Ordovician Trenton Limestone (Fig. 4). Endless Caverns in Virginia are located in Middle Ordovician limestone beneath the Upper Ordovician Martinsburg Formation. The three other caves in Virginia (Clover Hollow Cave, Newberry-Bane Cave, Hancock Cave) are located in Upper Ordovician limestone, immediately below shale of the Upper Ordovician Moccasin Formation (Fig. 4).

Glen Park Caves, Jefferson County, NY (Site 15 on Fig. 1):

Cave Maps: Map dated 1979 of Glen Park Commercial Cave (Nekvasil-Coraor, 1979); Map dated 1972 of Glen Park Labyrinth System (Nekvasil-Coraor, 1979); Undated map of Glen Park Labyrinth System (Engel, 2009); Maps

of other Glen Park caves (Fisher, 1958; Carroll, 1972a; Evans et al., 1979).

Stratigraphy: Upper Ordovician Black River Limestone and the overlying Upper Ordovician Trenton Limestone (Fisher, 1958; Carroll, 1970, 1972a; Nekvasil-Coraor, 1979; Engel, 1987, 2009).

Hydrology: Many of the Glen Park Caves are wet and (or) contain ice.

Cave Sediments: Mud is present in many of the Glen Park Caves.

WNS Infection Report: Porter (2008a,b).

Aitkin Cave, Mifflin County, PA (Site 69 on Fig. 1):

Cave Map: Map dated 1980 in Dayton et al. (1981).

Stratigraphy: Upper Ordovician Trenton Limestone (Stone, 1932, 1953; Dayton et al., 1981).

Hydrology: A canyon-like water course traverses the cave passage 20 feet inside the entrance, and a stream flows along the length of the cave during the winter. The ground water level in this area fluctuates greatly, and at times the entire cave is filled with water.

WNS Infection Report: Bat Conservation and Management, Inc. (http://www.batmanagement.com/wns/WNSphotoalbum1/index.html) and the Pennsylvania Department of Conservation and Natural Resources (http://www.dcnr.state.pa.us/news/resource/res2009/09-0311-resource.aspx#blurb2).

Alexander Caverns, Mifflin County, PA (Site 61 on Fig. 1):

Cave Map: Map dated 1951 in Dayton et al. (1981).

Stratigraphy: Upper Ordovician Trenton Limestone (Stone, 1932; Dayton et al., 1981; Ibberson, 1988).

Hydrology: The caverns are essentially a master trunk drainage system that receives water from many tributary streams that sink in the area. One part of the caverns is dry, whereas another part is wet. The caverns have three entrances, one of which is a spring mouth.

Cave Sediments: Mud and gravel are present at various locations within the caverns.

Cave Meteorology: Air temperature is 11.1 °C throughout the year (Stone, 1932).

WNS Infection Report: Danielle Moxley (http://thesnapper.com/2009/11/12/bye-bye-bats-white-nose-syndrome-waking-bats-from-their-sleep/) and Kiernam Schalk (http://mobile.lewistownsentinel.com/page/wap.home/?id=512320).

Endless Caverns, Rockingham County, VA (Site 75 on Fig. 1):

Cave Map: Map dated 1966 in Holsinger (1975).

Stratigraphy: Middle Ordovician limestone. The commercial part of the caverns is located in the Middle Ordovician New Market Limestone (Douglas, 1964; Holsinger, 1975; Hubbard, 1995; Jones, 1999, 2009). Beyond the commercial part, the main passages have developed along the contact of the New Market Limestone and the overlying Middle Ordovician Lincolnshire Limestone (Fig. 4). In a few areas, the caverns extend above the Lincolnshire Limestone and into the overlying Middle Ordovician Edinburg Formation, which lies immediately below the Upper Ordovician Martinsburg Formation (Fig. 4).

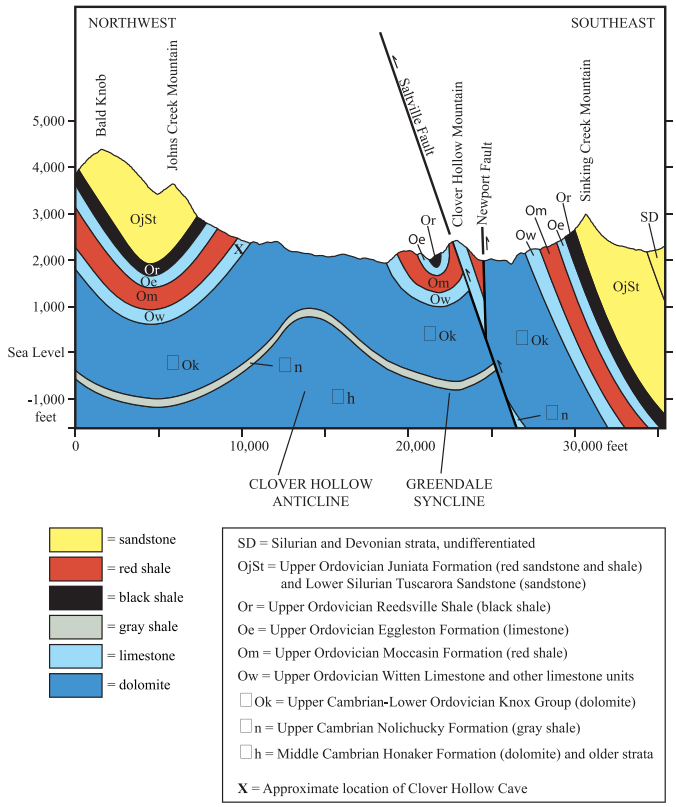

Figure 6. Geologic cross-section in the vicinity of Clover Hollow Cave, Giles County, Virginia (modified from Le Van and Rader, 1983; Schultz et al., 1986; Orndorff, 1995). The Knox Unconformity is present at the top of unit Ok (Upper Cambrian-Lower Ordovician Knox Group). The vertical scale is in feet relative to sea level.

Hydrology: A stream flows north and west through the non-commercial lower level of the caverns. This stream water arises from colluvium on the western slope of Massanutten Mountain, sinks underground and flows through the caverns, and then rises to the surface as a spring in the Edinburg Formation below the Endless Caverns gift shop.

Cave Sediments: Large clasts of Silurian sandstone fill many of the western passages of the caverns (Hubbard and Grady, 1999).

Cave Meteorology: Reeds (1925) states that the air temperature is 13.3 °C.

WNS Infection Report: Dasher (2009b) and the Virginia Department of Conservation and Recreation (DCR) Natural Heritage Program (http://www.dgif.virginia.gov/wildlife/bats/white-nose-syndrome/white-nose-syndrome-recommendations.pdf).

Clover Hollow Cave, Giles County, VA (Site 70 on Fig. 1):

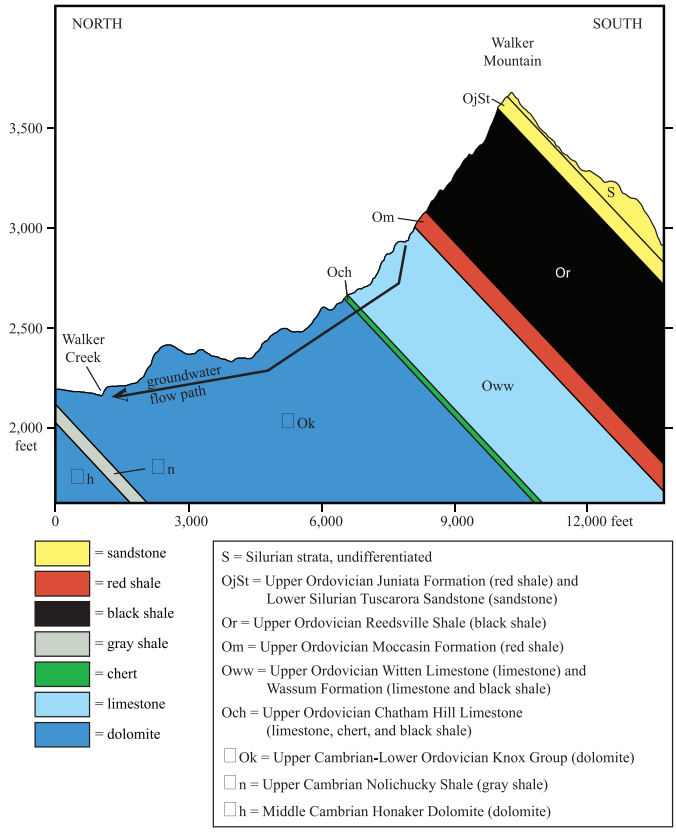

Figure 7. Geological cross-section in the vicinity of Newberry-Bane Cave, Bland County, Virginia (modified from Le Van and Rader, 1983; Wright, 1995). Newberry-Bane Cave is located along the extent of the ground water flow path shown. The Knox Unconformity is present at the top of unit □Ok (Upper Cambrian–Lower Ordovician Knox Group). The vertical scale is in feet relative to sea level.

Cave Map: Map dated 1978 in Zokaites (1995b).

Stratigraphy: Upper Ordovician limestone (Douglas, 1964; Sluzarski, 1972; Saunders, 1974; Holsinger, 1975; Saunders et al., 1981; Orndorff, 1995). The cave entrance is located near the contact between the Upper Ordovician Witten Limestone and the overlying Upper Ordovician Moccasin Formation (Figs. 4 and 6).

Hydrology: Surface water flows down Johns Creek Mountain across relatively impermeable Silurian and Ordovician strata (Fig. 6). Upon encountering the Upper Ordovician Witten Limestone, water flows into the cave near the entrance and flows through the rest of the cave. Dye tracing has shown that this water resurges about 8 km southwest of the cave at Tawney Spring and Smokehole Spring along Sinking Creek.

WNS Infection Report: Dasher (2009b), Youngbaer (2009b), the Virginia Department of Conservation and Recreation (DCR) Natural Heritage Program (http://www.dgif.virginia.gov/wildlife/bats/white-nose-syndrome/white-nose-syndrome-recommendations.pdf), and the Virginia Department of Game and Inland Fisheries (http://www.dgif.virginia.gov/news/release.asp?id=214). In addition, a WNS infection in Giles County (VA) was confirmed by the USGS NWHC (Quarterly Mortality Reports, 2009, Quarter 1).

Newberry-Bane Cave, Bland County, VA (Site 73 on Fig. 1):

Cave Map: Map dated 1995 in Zokaites (1995b).

Stratigraphy: Limestone of the Upper Ordovician Wassum Formation (Figs. 4 and 7) and the overlying Upper Ordovician Witten Limestone (Douglas, 1964; Holsinger, 1975; Wright, 1982, 1995; Zokaites, 1995a; Schwartz et al., 2009).

Hydrology: Surface water flows down the north slope of Walker Mountain across relatively impermeable Silurian and Ordovician strata (Fig. 7). Upon encountering the Upper Ordovician Witten Limestone, water flows into pits and sinkholes and eventually reaches Newberry-Bane Cave. In the cave, chert and black shale of the Upper Ordovician Chatham Hill Limestone (which underlies the Wassum Formation) act as a hydrological barrier that inhibits cave development in older strata. At one location, however, water in the cave penetrates the Chatham Hill Limestone, flows north through the underlying Cambrian-Ordovician Knox Group, and resurges at Burnt House Spring, which flows north into Walker Creek (Fig. 7).

Cave Meteorology: Air temperatures range from 7.0 to 11 °C (Brack et al., 2005).

WNS Infection Report: Dasher (2009a,b), Youngbaer (2010), and the Virginia Department of Conservation and Recreation (DCR) Natural Heritage Program (http://www.dgif.virginia.gov/wildlife/bats/white-nose-syndrome/white-nose-syndrome-recommendations.pdf).

Hancock Cave, Smyth County, VA (Site 74 on Fig. 1):

Cave Map: None published.

Stratigraphy: Upper Ordovician limestone on the northwest flank of Walker Mountain.

WNS Infection Report: Dasher (2009b), the Virginia Department of Conservation and Recreation (DCR) Natural Heritage Program (http://www.dgif.virginia.gov/wildlife/bats/white-nose-syndrome/white-nose-syndrome-recommendations.pdf), and the U.S. Fish and Wildlife Service (http://www.fws.gov/northeast/whitenose/PDF/WNSBulletinJune2009-Final.pdf).

Ordovician-Silurian Non-Carbonate Strata

Five of the sites infected with WNS before September 2009 are located in Ordovician-Silurian non-carbonate rock (Fig. 3). These sites are mines in Connecticut, Massachusetts, Vermont, New Jersey, and Pennsylvania. One site is located in Ordovician granite gneiss (Roxbury Mine), two sites are associated with Ordovician schist (The Old Mine, Greeley Mine), and two sites are located in Silurian sandstone and (or) mudstone (Pahaquarry Copper Mine, Shindle Mine).

Roxbury Mine, Litchfield County, CT (Site 62 on Fig. 1):

Mine Map: Map dated 2005 in Jacobs (2006).

Stratigraphy: Ordovician Mine Hill Granite Gneiss (Gates, 1959; Echols, 1961; Jacobs, 2006).

Mined Commodity: Iron (siderite), mined from 1760 to 1872.

Hydrology: Parts of the lower level of the mine contain standing water.

WNS Infection Report: Suggested by Kocer (2009) and in the Helderberg-Hudson Grotto newsletter ''Mudslinger'' (February 2009, v. 24, no. 2), and subsequently reported in ''The Northeastern Caver'' (June 2009, v. 40, p. 44–45). In addition, a WNS infection near the town of Roxbury in Litchfield County (CT) was confirmed by the USGS NWHC (Quarterly Mortality Reports, 2008, Quarter 4).

The Old Mine (Upper Chester Mine), Hampden County, MA (Site 20 on Fig. 2):

Mine Map: None published.

Stratigraphy: Ordovician Chester Amphibolite, near the contact of the Chester Amphibolite with the Ordovician Savoy Schist (Hartline, 1965; Lincks, 1978). The Savoy Schist is approximately equivalent stratigraphically to the Upper Ordovician siliciclastic strata shown in Figure 3.

Mined Commodity: Emery, mined from approximately 1856 to 1950.

Hydrology: Water flows through some parts of the mine.

WNS Infection Report: Porter (2008a,b), and supporting online material for Blehert et al. (2009). In addition, a WNS infection in Hampden County (MA) was confirmed by the USGS NWHC (Quarterly Mortality Reports, 2009, Quarter 1).

Greeley Mine, Windsor County, VT (Site 36 on Fig. 1):

Mine Map: None published.

Stratigraphy: Ordovician serpentinite (Gillson, 1927; Trombulak et al., 2001).

Mined Commodity: Talc, mined prior to 1930.

WNS Infection Report: Porter (2009d) and the U.S. Fish and Wildlife Service (http://www.fws.gov/northeast/wnspics.html).

Pahaquarry Copper Mine, Delaware Water Gap National Recreation Area, Warren County, NJ (Site 54 on Fig. 1):

Mine Map: None published.

Stratigraphy: Red and gray sandstone of the Upper Silurian Bloomsburg Red Beds (Weed, 1911; Woodward, 1944; Burns Chavez and Clemensen, 1995; Monteverde, 2001). The Bloomsburg Red Beds overlie the Silurian Shawangunk Conglomerate, which in turn overlies the Upper Ordovician Martinsburg Formation (Fig. 4).

Mined Commodity: Copper, mined at various times from approximately 1750 to 1912.

WNS Infection Report: USGS NWHC (Quarterly Mortality Reports, 2008, Quarter 4).

Shindle Mine, Mifflin County, PA (Site 39 on Fig. 1):

Mine Map: None published.

Stratigraphy: Lower Silurian Tuscarora Sandstone (Fig. 3).

Mined Commodity: Iron, although dates of operation are not known.

WNS Infection Report: USGS NWHC (Quarterly Mortality Reports, 2009, Quarter 1).

CARBONATE STRATA OF THE LOWER PART OF THE SILURIAN-DEVONIAN HELDERBERG GROUP

Twenty of the sites infected with WNS before September 2009 are located in carbonate strata of the lower part of the Silurian-Devonian Helderberg Group, specifically within the Coeymans Limestone, Manlius Limestone, and Keyser Limestone (Figs. 3 and 8). Fourteen of these sites are caves in New York (Howe Caverns, McFail's Cave, Benson's Cave, Hell's Wells, Barytes Cave, Ain't No Catchment Cave, Gage Caverns, Schoharie Caverns, Single X Cave, Knox Cave, Hailes Cave, Nature's Way Cave, South Bethlehem Cave, Surprise Cave), and five of these sites are mines in New York (Hasbrouck Mine, Williams Preserve Mine, Williams Hotel Mine, Williams Lake Mine, Martin Mine). One site is a cave in Virginia that has formed in limestone confined between two beds of low-permeability sandstone (Breathing Cave).

Howe Caverns, Schoharie County, NY (Site 1 on Fig. 2):

Note: Howe Caverns is the name of a large cave system, part of which is commercial. In some publications, the name ''Howe Caverns'' is restricted to only the commercial section of the cave system, and the name ''Howe Cave'' is given to the non-commercial sections of the cave system (Davis et al., 1966).

Cave Map: Map dated 1977 in Mylroie (1977).

Stratigraphy: Upper Silurian-Lower Devonian Manlius Limestone and the overlying Lower Devonian Coeymans Limestone (Fig. 9) of the Helderberg Group (Schweiker et al., 1958; Olesen, 1961; Davis et al., 1966; Addis, 1969; Egemeier, 1969; Mylroie, 1972, 1977; Gregg, 1974; Kastning, 1975; Cullen et al., 1979).

Hydrology: Howe Caverns are wet, and a river flows southeast through part of the cave system. Dye tracing indicates that at least some of the water comes from McFail's Cave (Site 37 on Fig. 2), approximately 3 miles northwest of Howe Caverns (Baker, 1976). Water from the caverns resurges on the banks of Cobleskill Creek (Mylroie, 1977).

Cave Sediments: Brown clay, gray laminated clay and sandy gravel containing chert pebbles are present in the caverns (Engel, 2009; Rubin, 2009). At one location (the ''Lake of Venus''), a bed of sandy gravel is overlain by a bed of brown clay, which is overlain by bed of gray laminated clay (Rubin, 2009).

Cave Meteorology: Meteorological measurements taken February 26 to April 30, 1971 from the commercial part of Howe Caverns revealed air temperatures ranging from 9.4

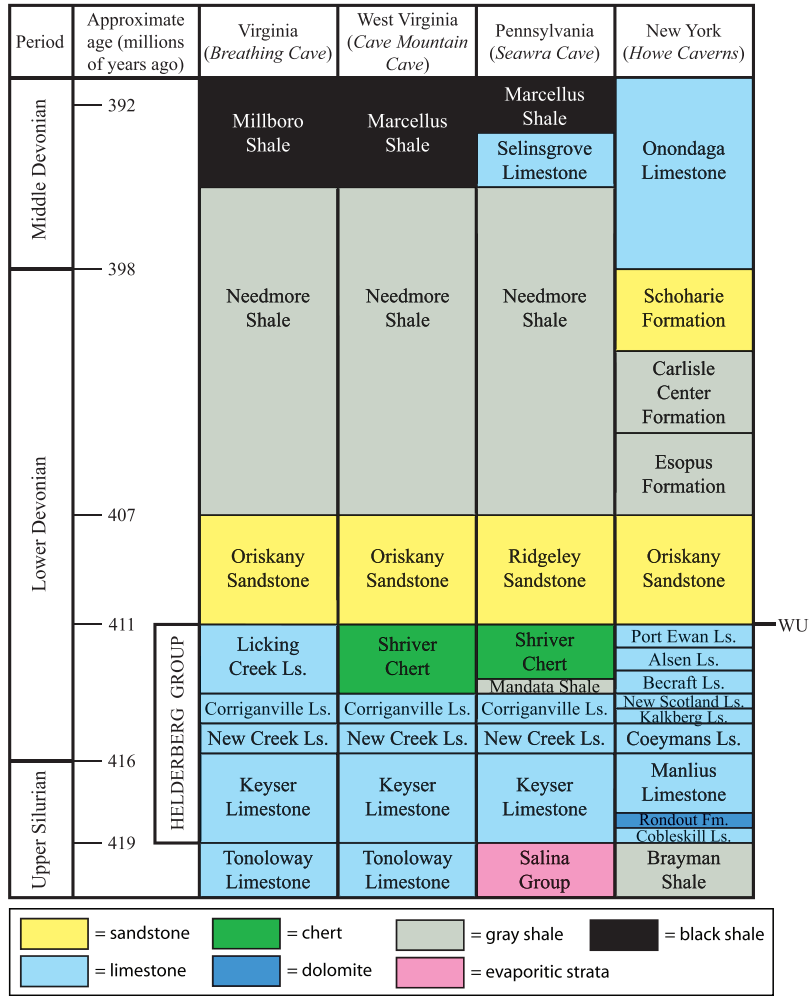

Figure 8. Selected Upper Silurian through Middle Devonian stratigraphic units in the Appalachian Basin (from Head, 1974; Kastning, 1975; Dennison and Hasson, 1979; Dorobek and Read, 1986; Fisher, 1987; Smosna, 1988; Harris et al., 1994; Van Tyne, 1996; Swezey, 2002). Time scale is from Gradstein et al. (2004). Fm. = Formation; Ls. = Limestone. In many places, a regional unconformity is present below the Devonian Oriskany Sandstone and Ridgeley Sandstone (WU: Wallbridge Unconformity). Unconformities are also present in New York on top of the Silurian Brayman Shale and on top of the Devonian Schoharie Formation. Example caves are listed in italics at the tops of columns.

to 10.6 °C and relative humidity ranging from 68 to 72 percent (Mylroie, 1972).

WNS Infection Report: Porter (2008a,b), Armstrong (2009), and Blehert et al. (2009).

McFail's Cave, Schoharie County, NY (Site 37 on Fig. 2):

Cave Map: Map dated 1991 in Haberland (1991).

Stratigraphy: The two active entrances to McFail's Cave are located in the Lower Devonian Kalkberg Limestone (Figs. 8, 9, and 10), but most of the cave has formed in the Upper Silurian-Lower Devonian Manlius Limestone and the overlying Lower Devonian Coeymans Limestone of the Helderberg Group (Olesen, 1961; Egemeier, 1969; Kastning, 1975; Baker, 1976; Mylroie, 1977; Palmer, 2002). In addition, the southernmost portion of the cave has formed partially in the Upper Silurian Rondout Formation.

Hydrology: Water flows through much of the cave and dye tracing has revealed that this water flows to Doc Shaul's Spring (Fig. 10), to Howe Caverns, and to some other springs in the vicinity (Baker, 1970, 1973, 1976).

Cave Sediments: Breakdown blocks, gravel, and mud are present in the cave (Olesen, 1961; Baker, 1973; Kastning, 1975). In addition, Porter (1985) mentioned sediments that are interpreted as glacial varves, and Rubin (1985) described a stream channel incised into a clay bank.

Cave Meteorology: The annual average air temperature is 7.3 °C (van Beynen et al., 2004).

WNS Infection Report: Porter (2008a) and Armstrong (2009).

Benson's Cave, Schoharie County, NY (Site 25 on Fig. 2):

Cave Map: Map dated 1976 in Mylroie (1977).

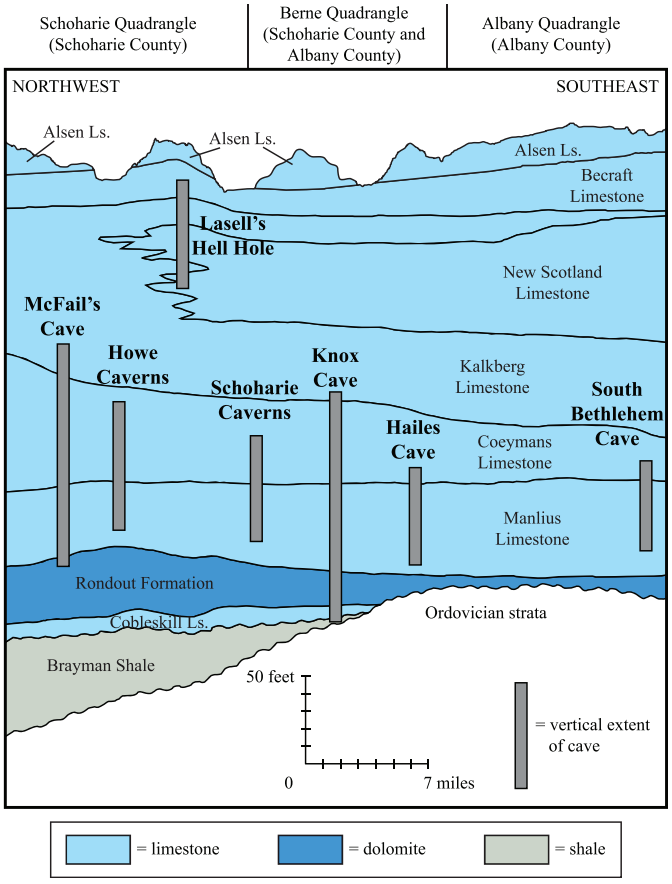

Figure 9. Geologic cross-section through Schoharie, Berne, and Albany 15-minute topographic quadrangles (Schoharie County and Albany County, New York) showing the distribution of selected caves in the Silurian-Devonian Helderberg Group (modified from Kastning, 1975; data on Knox Cave from Palmer, 2000, 2001).

Stratigraphy: Upper Silurian-Lower Devonian Manlius Limestone and the overlying Lower Devonian Coeymans Limestone of the Helderberg Group (Schweiker et al., 1958; Davis et al., 1966; Egemeier, 1969; Kastning, 1975; Dimbirs and Wood, 1977; Mylroie, 1977).

Hydrology: Water enters the cave at several locations, eventually joins a stream from nearby Secret Caverns, and then flows south and east to Barytes Cave.

WNS Infection Report: Porter (2008a).

Hell's Wells, Schoharie County, NY (Site 26 on Fig. 2):

Cave Map: Map dated 1976 in Mylroie (1977).

Stratigraphy: Lower Devonian Coeymans Limestone of the Helderberg Group (Schweiker et al., 1958; Davis et al., 1966; Mylroie, 1977).

Hydrology: The cave is described as "semi-abandoned pit insurgences" (Mylroie, 1977).

WNS Infection Report: Alan Hicks of the New York State Department of Environmental Conservation (http://www.necaveconservancy.org/files/wns_3-30-08.pdf) and Armstrong (2009).

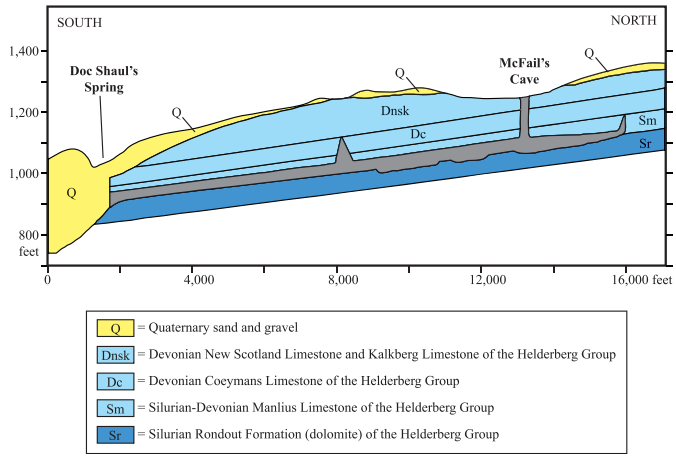

Figure 10. Geologic cross-section through McFail's Cave, Schoharie County, New York (modified from Baker, 1976). The vertical scale is in feet relative to sea level.

Barytes Cave, Schoharie County, NY (Site 2 on Fig. 2):

Cave Map: Map dated 1978 in Middleton (1979).

Stratigraphy: Upper Silurian Rondout Formation and the overlying Upper Silurian-Lower Devonian Manlius Limestone of the Helderberg Group (Schweiker et al., 1958; Davis et al., 1966; Dimbirs and Wood, 1977; Mylroie, 1977; Middleton, 1979).

Hydrology: The cave is connected hydrologically with the nearby Secret-Bensons Cave System (Dimbirs and Wood, 1977; Mylroie, 1977; Siemion et al., 2003; Siemion, 2005). Water in Secret Caverns flows into Bensons Cave, and then flows south and east to Barytes Cave. Dimbirs and Wood (1977) stated that water in Barytes Cave resurges further south at No Admittance Spring, whereas Mylroie (1977) stated that water in Barytes Cave resurges at an occluded bluff spring named Corners Spring.

WNS Infection Report: Alan Hicks of the New York State Department of Environmental Conservation (http://www.necaveconservancy.org/files/wns_3-30-08.pdf).

Ain't No Catchment (ANC) Cave, Schoharie County, NY (Site 28 on Fig. 2):

Cave Map: Map dated 2005 in Armstrong et al. (2005).

Stratigraphy: Upper Silurian Cobleskill Formation and the overlying Upper Silurian Rondout Formation of the Helderberg Group (Hopkins, 1996b; Rubinstein, 1998; Armstrong et al., 2005).

Hydrology: A perennial spring flows from the cave, and at times the entrance is completely flooded.

WNS Infection Report: Porter (2008a) and Armstrong (2009).

Gage Caverns, Schoharie County, NY (Site 4 on Fig. 2):

Cave Map: Map dated 1976 in Mylroie (1977).

Stratigraphy: Upper Silurian-Lower Devonian Manlius Limestone and the overlying Lower Devonian Coeymans

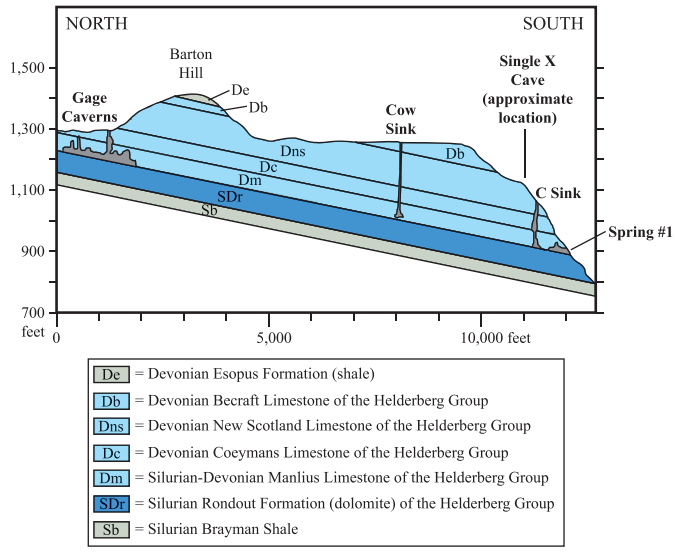

Figure 11. Geologic cross-section through Barton Hill (Schoharie County, New York), showing the location of Gage Caverns and other nearby karst features (modified from Anderson, 1961). The vertical scale is in feet relative to sea level.

Limestone (Fig. 11) of the Helderberg Group (Gurnee, 1957; Schweiker et al., 1958; Anderson, 1961; Baker, 1976; Mylroie, 1977; Engle, 1988).

Hydrology: The caverns are wet, and contain a stream and lakes. Anderson (1961) stated that water in the caverns resurges at Spring #1 (Fig. 11), located approximately 10,800 feet south of the caverns. However, dye tracing has shown that water in Gage Caverns exits at Young's Spring, which is 4,200 feet southwest of the dye injection site (Baker, 1970).

Cave Meteorology: Gurnee (1957) reported air temperature measurements ranging from 8.9 to 12.2 °C from seven locations in the caverns, whereas Moore (1958) stated that the air temperature is approximately 7.8 °C throughout the year.

WNS Infection Report: Folsom (2008), Porter (2008a,b), and Armstrong (2009).

Schoharie Caverns, Schoharie County, NY (Site 3 on Fig. 2):

Cave Map: Map dated 1989 in Schweyen (1989).

Stratigraphy: Upper Silurian-Lower Devonian Manlius Limestone and the overlying Lower Devonian Coeymans Limestone (Fig. 9) of the Helderberg Group (Schweiker et al., 1958; Davis et al., 1966; Kastning, 1975; Dimbirs and Wood, 1977; Mylroie, 1977; Cullen et al., 1979; Schweyen, 1989).

Hydrology: At the back end of the caverns, a perennial stream emerges at the contact between the Manlius Limestone and the overlying Coeymans Limestone (Mylroie, 1977). This stream flows along the entire length of the caverns, and exits at the cavern entrance. Dimbirs and Wood (1977) claimed that water in the caverns overflows into another cave system named the Spider Cave System, whereas Cullen et al. (1979) claimed that water in the caverns overflows into a nearby cave named Tufa Cave.

WNS Infection Report: Folsom (2008), Porter (2008a,b), the USGS NWHC (Quarterly Mortality Reports, 2008, Quarter 4), and supporting online material for Blehert et al. (2009).

Single X Cave, Schoharie County, NY (Site 64 on Fig. 2):

Cave Map: Map dated 1975 in Mylroie (1977).

Stratigraphy: Silurian-Devonian Helderberg Group (Fig. 11). From the cave entrance, a passage trends northwest along strike in the Upper Silurian Cobleskill Limestone and the overlying Upper Silurian Rondout Formation (Middleton, 1977; Mylroie, 1977, 1980). After 715 feet, this entrance passage intersects the main cave passage, which trends north-northeast and is located primarily in the Upper Silurian-Lower Devonian Manlius Limestone and the overlying Lower Devonian Coeymans Limestone. Some high dome pits along this passage may extend up into the Lower Devonian Kalkberg Limestone.

Hydrology: The cave contains a stream, which is incised into mud banks in places. This stream flows south-southwest along the main passage and then flows southeast along the entrance passage and out the cave entrance (a location named Traux Spring).

Cave Sediments: Breakdown blocks, cobbles, and mud (including mud spatter cones) are present within the cave. In some places, cobbles are cemented to the passage walls by flowstone up to 20 feet above the modern stream level.

WNS Infection Report: Armstrong (2009).

Knox Cave, Albany County, NY (Site 6 on Fig. 2):

Cave Map: Map dated 2000 in Palmer (2000).

Stratigraphy: Most of the cave has developed within the Upper Silurian-Lower Devonian Manlius Limestone and the overlying Lower Devonian Coeymans Limestone (Figs. 9 and 12) of the Helderberg Group (Hornung, 1953; Schweiker, 1958; Palmer, 1963, 2000, 2001; Kastning, 1975; Rubin, 1986). At a few locations, passages extend below the Manlius Limestone and into the underlying Upper Silurian Rondout Formation, Cobleskill Formation, and the Brayman Shale (Fig. 12).

Hydrology: A stream flows through much of the cave (Palmer, 1963). Dye traces indicate that the stream in Knox Cave and a stream in nearby Skull Cave both resurge at the same spring south of the two caves (Egemeier, 1969).

Cave Meteorology: Measurements taken at multiple locations in the cave on October 20, 1962 revealed dry bulb air temperatures ranging from 6.0 to 10.0 °C, wet bulb air temperatures ranging from 5.8 to 9.7 °C, and relative humidity ranging from 93 to 100 percent (Kreider, 1963).

WNS Infection Report: Folsom (2008), Porter (2008a,b), and Armstrong (2009).

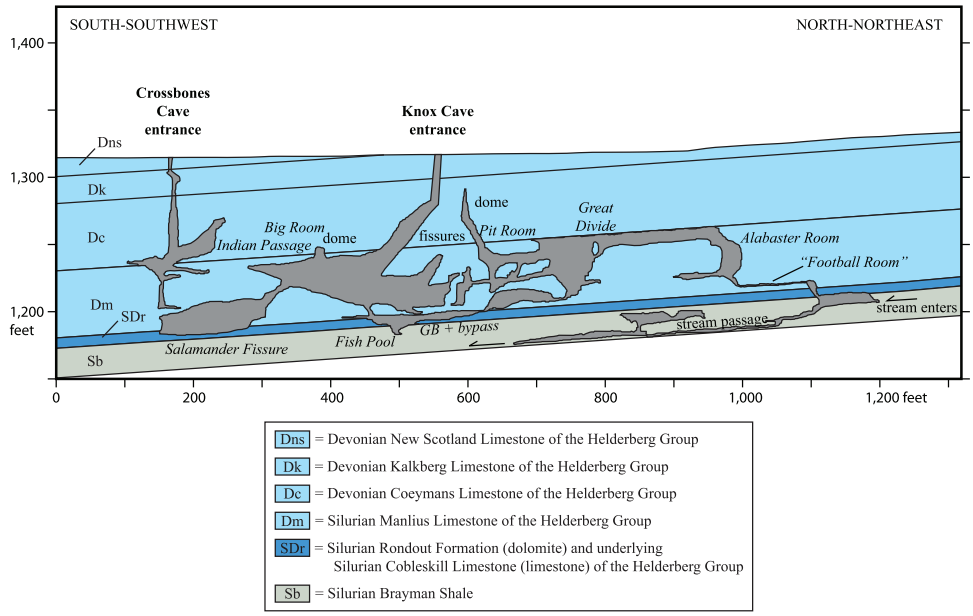

Figure 12. Geologic cross-section through Knox Cave and Crossbones Cave, Albany County, New York (modified from Palmer, 1963, 2000). GB = The Gunbarrel (a straight passage that is 15 m long and 35 cm in diameter). The vertical scale is in feet relative to sea level.

Hailes Cave, Albany County, NY (Site 5 on Fig. 2):

Cave Map: Map dated 1906 in Engle (1979).

Stratigraphy: Upper Silurian-Lower Devonian Manlius Limestone and the overlying Lower Devonian Coeymans Limestone (Fig. 9) of the Helderberg Group (Thurston, 1942; Schweiker, 1958; Kastning, 1975; Baker, 1976; Lundy, 2001).

Hydrology: The cave is relatively wet, and contains pools of water.

WNS Infection Report: Folsom (2008), Porter (2008a,b), the USGS NWHC (Quarterly Mortality Reports, 2008, Quarter 4), and supporting online material for Blehert et al. (2009).

Nature's Way Cave (Zinzow's Cave), Albany County, NY (Site 38 on Fig. 2):

Cave Map: Map dated 2000 in Haberland et al. (2000).

Stratigraphy: Upper Silurian-Lower Devonian Manlius Limestone and the overlying Lower Devonian Coeymans Limestone of the Helderberg Group (Hopkins, 1996a,b; Haberland et al., 2000; Martuscello, 2000).

Hydrology: The cave entrance is a spring, and the cave contains a stream, waterfalls, and sumps.

WNS Infection Report: Porter (2008a) and Armstrong (2009).

South Bethlehem Cave, Albany County, NY (Site 29 on Fig. 2):

Cave Map: Map dated 1968 in Kastning (1975).

Stratigraphy: Silurian-Devonian Helderberg Group (Schweiker, 1958; Kastning, 1968, 1975; Cullen et al., 1979). Most of the cave is within the Upper Silurian-Lower Devonian Manlius Limestone, although some parts extend into the overlying Lower Devonian Coeymans Limestone (Fig. 9).

Hydrology: Kastning (1968) stated that the lower passages of the cave drop down into water and siphons, whereas Cullen et al. (1979) stated that a standing pool of water is present in one area and that the rest of the cave is relatively dry except during times of extreme flood when water flows out of the lower entrance of the cave.

Cave Sediments: Mud is present throughout much of the cave (Kastning, 1968).

Cave Meteorology: The cave is "relatively dry" (Schweiker, 1958).

WNS Infection Report: Porter (2008a).

Surprise Cave (Mystery Cave), Sullivan County, NY (Site 42 on Fig. 1):

Cave Map: Map dated 1982 in Febroriello (1984) and Engel (2009).

Stratigraphy: Upper Silurian Rondout Formation and Lower Devonian Coeymans Limestone of the Helderberg Group (Peck, 1967; Febroriello, 1984; Engel, 2009).

Hydrology: The lower parts of the cave contain at least two active streams.

WNS Infection Report: Porter (2008a).

Hasbrouck Mine at Kingston, Ulster County, NY (Site 40 on Fig. 2):

Mine Map: None published.

Stratigraphy: Upper Silurian Rondout Formation of the Helderberg Group (Chu, 2006; Perlmann, 2006).

Mined Commodity: Limestone.

Hydrology: The lower levels of the mine are flooded.

WNS Infection Report: Porter (2008a). In addition, a WNS infection in Ulster County (NY) was confirmed by the USGS NWHC (Quarterly Mortality Reports, 2009, Quarter 1).

Williams Preserve Mine, near Rosendale, Ulster County, NY (Site 9 on Fig. 2):

Mine Map: None published.

Stratigraphy: Upper Silurian Rondout Formation of the Helderberg Group.

Mined Commodity: Limestone, mined during the 1800s and early 1900s.

WNS Infection Report: Porter (2008a) and the USGS NWHC (Quarterly Mortality Reports, 2008, Quarter 4).

Williams Hotel Mine near Rosendale, Ulster County, NY (Site 10 on Fig. 2):

Mine Map: None published.

Stratigraphy: Upper Silurian Rondout Formation of the Helderberg Group.

Mined Commodity: Limestone, mined during the 1800s and early 1900s.

WNS Infection Report: Porter (2008a,b), the USGS NWHC (Quarterly Mortality Reports, 2008, Quarter 4), and supporting online material for Blehert et al. (2009).

Williams Lake Mine near Rosendale, Ulster County, NY (Site 18 on Fig. 2):

Mine Map: None published.

Stratigraphy: Upper Silurian Rondout Formation of the Helderberg Group.

Mined Commodity: Limestone, mined during the 1800s and early 1900s.

WNS Infection Report: Porter (2008a). In addition, a WNS infection in Ulster County (New York) was confirmed by the USGS NWHC (Quarterly Mortality Reports, 2009, Quarter 1).

Martin Mine near Rosendale, Ulster County, NY (Site 30 on Fig. 2):

Mine Map: None published.

Stratigraphy: Upper Silurian Rondout Formation of the Helderberg Group.

Mined Commodity: Limestone, mined during the 1800s and early 1900s.

WNS Infection Report: Supporting online material for Blehert et al. (2009). In addition, a WNS infection in Ulster County (NY) was confirmed by the USGS NWHC (Quarterly Mortality Reports, 2009, Quarter 1).

Breathing Cave, Burnsville Cove, Bath County, VA (Site 60 on Fig. 1):

Cave Map: Map dated 1975 in Wefer and Nicholson (1982).

Stratigraphy: The cave is located within the Upper Silurian-Lower Devonian Keyser Limestone (Fig. 8) of the Helderberg Group (Deike, 1960; Douglas, 1964; Holsinger, 1975; White and Hess, 1982; Clemmer, 2005). Within the Keyser Limestone, the cave is confined almost entirely to a 77-foot thick unit of shaly limestone between two 12-foot thick beds of sandstone, which have been named informally the upper Breathing sandstone and the lower Breathing sandstone. These sandstone beds are tongues of the Upper Silurian Clifton Forge Sandstone (which interfingers with the Keyser Limestone).

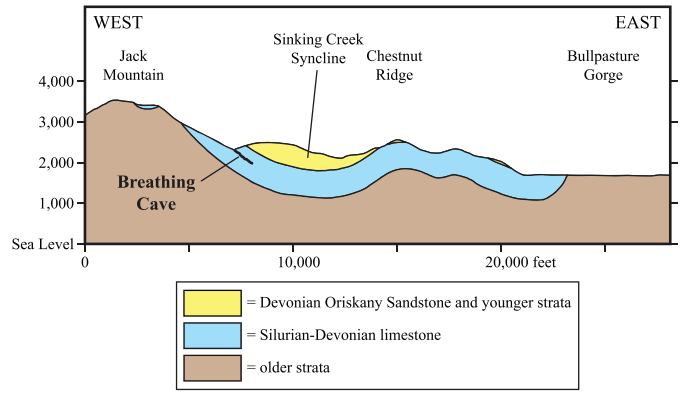

Figure 13. Geologic cross-section through Burnsville Cove (Bath County, Virginia), showing the location of Breathing Cave (modified from Deike, 1960). The vertical scale is in feet relative to sea level.

Hydrology: Surface water flows down Jack Mountain across relatively impermeable strata (Fig. 13). Near the cave, this water sinks into the limestone, and then resurges approximately 3 miles to the northeast at Bullpasture Gorge (Fig. 13).

Cave Sediments: Conglomeratic silt and sand, and cobbles up to 12 inches in diameter, are present in many passages (Deike, 1960). During the American Civil War, sediment in the cave was mined for nitrate to make gunpowder (Faust, 1964; Clemmer, 2005).

Cave Meteorology: Faust (1947) published early descriptions of oscillating air flow (the "Breathing Phenomenon") at Breathing Cave. Cournoyer (1954) published measurements taken during a 1.5 hour interval on January 9, 1954 that revealed air temperatures ranging from −3.3 to 11.1 °C, atmospheric pressure ranging from approximately 1002 to 1003 millibars, and 5 episodes of air flowing into the cave and then out of the cave at speeds attaining approximately 350 feet per minute. Cournoyer (1956) also published a subsequent set of measurements (taken at four locations during a 1.5 hour interval on December 10, 1955) that revealed air temperatures ranging from 0.6 to 10.6 °C. Finally, Moore (1958) stated that air temperature in the cave is approximately 11.1 °C throughout the year.

WNS Infection Report: Dasher (2009b), Lambert (2009), the Virginia Department of Conservation and Recreation (DCR) Natural Heritage Program (http://www.dgif.virginia.gov/wildlife/bats/white-nose-syndrome/

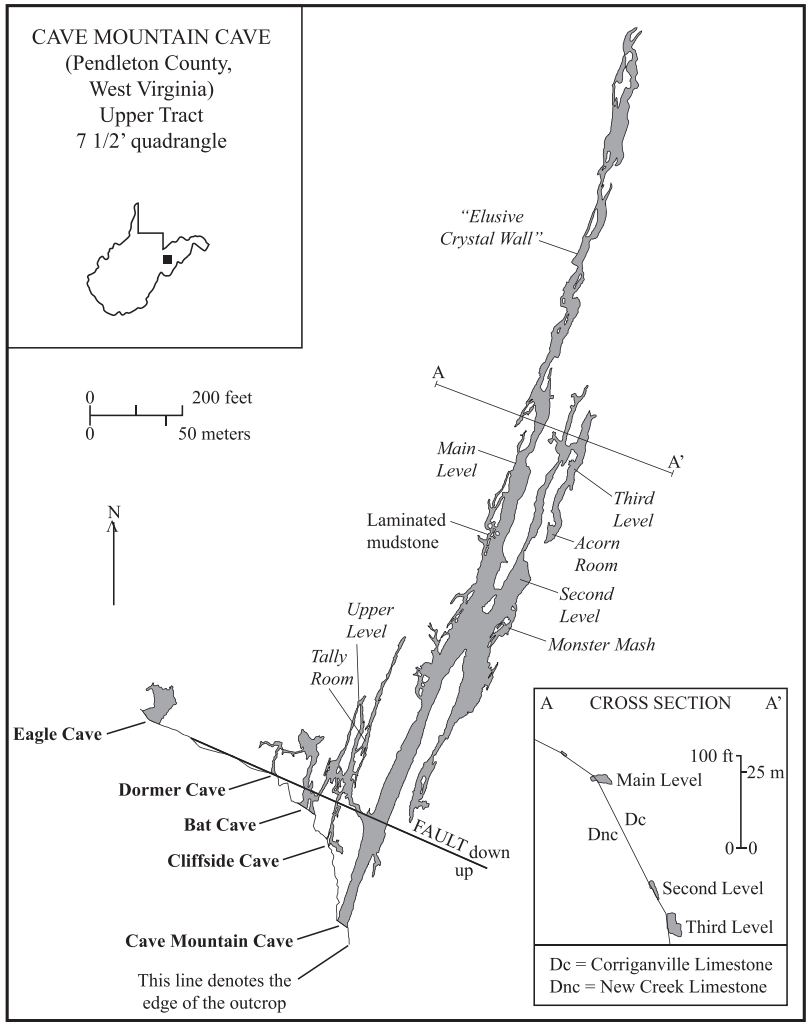

Figure 14. Map of Cave Mountain Cave, Pendleton County, West Virginia (from Swezey and Dulong, 2010). On the south side of the fault, the cave has formed in the Keyser Limestone of the Silurian-Devonian Helderberg Group. On the north side of the fault, the cave has formed in the New Creek Limestone and Corriganville Limestone of the Helderberg Group.

white-nose-syndrome-recommendations.pdf), and the Virginia Department of Game and Inland Fisheries (http://www.dgif.virginia.gov/news/release.asp?id=214). In addition, a WNS infection in Bath County (VA) was also confirmed by the USGS NWHC (Quarterly Mortality Reports, 2008, Quarter 4).

CARBONATE STRATA OF THE MIDDLE PART OF THE SILURIAN-DEVONIAN HELDERBERG GROUP

Five of the sites infected with WNS before September 2009 are located in caves in carbonate strata of the middle part of the Silurian-Devonian Helderberg Group, primarily at the boundary between the New Creek Limestone and the overlying Corriganville Limestone (Figs. 3 and 8). One of these sites is in Pennsylvania (Seawra Cave), and four of these sites are in West Virginia (Cave Mountain Cave, Saltpeter Cave, Hamilton Cave, Trout Cave).

Seawra Cave, Mifflin County, PA (Site 68 on Fig. 1):

Cave Map: Map dated 1960 in Dayton et al. (1981).

Stratigraphy: Silurian-Devonian Helderberg Group (Stone, 1932, 1953; Dayton et al., 1981).

Cave Meteorology: The air temperature is reported to be 13.9 °C, and the cave is described as being relatively dry (Stone, 1932).

WNS Infection Report: Bat Conservation and Management, Inc. (http://www.batmanagement.com/wns/WNSphotoalbum1/index.html) and the Pennsylvania Department of Conservation and Natural Resources (http://www.dcnr.state.pa.us/news/resource/res2009/09-0311-resource.aspx#blurb2).

Cave Mountain Cave, Pendleton County, WV (Site 59 on Fig. 1):

Cave Map: Map dated 2001 in Dasher (2001).

Stratigraphy: Silurian-Devonian Helderberg Group (Davies, 1965; Dyas, 1976a,b; Dasher, 2001; Swezey and Dulong, 2010). A northwest-trending fault is present about 200 feet inside the main entrance of the cave (Fig. 14). On

the south side of this fault (i.e., between the cave entrance and the fault), the cave passages have developed within the Keyser Limestone of the Helderberg Group. On the north side of this fault, the cave passages have developed along the contact between the New Creek Limestone and the overlying Corriganville Limestone of the Helderberg Group.

Hydrology: Most of the cave is relatively dry with no flowing water, although some stalactites drip water near the front part of the cave on the Main Level and the underlying Second Level (Fig. 14).

Cave Sediments: Mud, sand, and gravel are present in most of the cave. Large breakdown blocks are common in places. A laminated mudstone on the Main Level (Fig. 14) is interpreted as a lacustrine deposit (Swezey and Dulong, 2010). In addition, lenses of rust-red clay within unconsolidated sand are present in the rear of the Main Level (Haas, 1960). This clay is a mixture of very fine-grained quartz and metahalloysite, which is a hydrated alumina silicate [$Al_4Si_4(OH)8O_{10}$•$8H_2O$]. During and before the American Civil War, sediment in the cave was mined for nitrate to make gunpowder (Davies, 1965; Anonymous, 1970; Ellen and Garton, 2001). Nitrate samples from the sediment range from about 300 to 2,200 parts per million (Hoke, 2005).

WNS Infection Report: Anonymous (2010), Dasher (2009b), Stihler (2009), and the West Virginia Division of Natural Resources (http://www.fws.gov/northeast/whitenose/WVPressRelease13Feb09.pdf).

Saltpeter Cave, Pendleton County, WV (Site 72 on Fig. 1):

Cave Map: Map dated 1997 in Dasher (2001).

Stratigraphy: Lower Devonian Corriganville Limestone of the Helderberg Group (Davies, 1958, 1965; Dasher, 2001).

Hydrology: The cave is reported to be very dry (Dasher, 2001).

WNS Infection Report: Anonymous (2010) and Dasher (2009b).

Hamilton Cave, Pendleton County, WV (Site 57 on Fig. 1):

Cave Map: Map dated 1988 in Dasher (2001).

Stratigraphy: Silurian-Devonian Helderberg Group (Davies, 1958; Palmer, 1975; Dyas, 1977; Medville, 2000a; Dasher, 2001). The front part of the cave is a maze of passages that have developed at the contact of the New Creek Limestone and the overlying Corriganville Limestone, whereas the back part of the cave consists of northeast-trending passages (without well-developed maze morphologies) that have developed primarily in the New Creek Limestone.

Hydrology: Most of the cave is relatively dry with no flowing water, although in a few rooms some stalactites drip water and damp mud is present on the floor.

Cave Sediments: Mud is present on the cave floor in many places.

Cave Meteorology: Dyroff (1977) published an account of a one-day study (April 10, 1977), which found that air flowed consistently out of the cave during the morning and afternoon, and that the average air temperature inside the cave was 11.7 °C. Hoke (2009a,b) reported that air always flows out of the cave during the winter, and that data loggers just inside the cave entrance recorded air temperatures that ranged from 12.8 °C at the beginning of winter to 10.8 °C at the end of winter.

WNS Infection Report: Anonymous (2010), Dasher (2009b), Hoke (2009a,b), Stihler (2009), and the USGS NWHC (Quarterly Mortality Reports, 2009, Quarter 1).

Trout Cave, Pendleton County, WV (Site 58 on Fig. 1):

Cave Map: Map dated 1993 in Dasher (2001).

Stratigraphy: Silurian-Devonian Helderberg Group, in most places at the contact between the New Creek Limestone and the overlying Corriganville Limestone (Davies, 1958; Haas, 1961; Palmer, 1975; Medville, 2000b; Dasher, 2001). However, Swezey (2003) noted that at least one location (the "Square Room") extends from the Corriganville Limestone into the overlying Lower Devonian Shriver Chert (Fig. 8).

Hydrology: The cave is relatively dry, with no flowing water.

Cave Sediments: Mud, sand, and gravel are present in the cave. Breakdown blocks are common near the entrance. During the American Civil War, sediment in the cave was mined for nitrate to make gunpowder (Faust, 1964; Davies, 1965; Powers, 1981; Ellen and Garton, 2001; Taylor, 2001). Analysis of one sediment sample revealed a nitrate concentration of about 2,100 parts per million (Swezey et al., 2004).

Cave Meteorology: Davies (1958) reported air temperatures of approximately 12 °C, Hoke (2001) reported air temperatures ranging from 6.7 to 8.9 °C, and Swezey et al. (2004) reported air temperatures ranging from 6 to 13 °C and relative humidity ranging from 81 to 92 percent. In addition, Dyroff (1977) published an account of a one-day study (April 10, 1977), which found that during the morning when the outside air temperature was 0 °C, air flowed into the cave along the bottom of the cave passage and air flowed out of the cave along the top of the cave passage. In that study, the mean air temperature was 8.9 °C approximately 500 feet inside the cave, although the air temperature near the ceiling was several degrees warmer than the air temperature near the floor. During the afternoon when the outside air temperature was 12.8 °C, the air currents reversed so that warm air flowed in along the top of the cave passage and cooler air flowed out along the bottom of the cave passage. Despite this reversal in flow directions, the mean air temperature inside the cave remained at 8.9 °C.

WNS Infection Report: Anonymous (2010), Dasher (2009b), and USGS NWHC (Quarterly Mortality Reports, 2009, Quarter 1).

CARBONATE STRATA OF THE UPPER PART OF THE SILURIAN-DEVONIAN HELDERBERG GROUP

Only one site infected with WNS before September 2009 is located in the upper part of the Silurian-Devonian Helderberg Group (Figs. 3 and 8). This site is a cave in New York named Lasell's Hell Hole.

Lasell's Hell Hole, Schoharie County, NY (Site 27 on Fig. 2):

Cave Map: Undated map in Hopkins (1996b).

Stratigraphy: Lower Devonian Kalkberg Limestone, New Scotland Limestone, and Becraft Limestone (Fig. 8) of the Helderberg Group (Schweiker et al., 1958; Davis et al., 1966; Eckler, 1966; Gregg, 1974; Kastning, 1975; Baker, 1976; Hopkins, 1996b). The cave entrance is a 62-foot deep pit in the Becraft Limestone, and the contact between the Becraft Limestone and the underlying Kalkberg Limestone is visible within the first 10 feet of the pit. The Kalkberg Limestone in this area is a relatively thin upper tongue of the main Kalkberg Limestone (Fig. 9).

Hydrology: The New Scotland Limestone at this site is a shaly limestone that inhibits the downward flow of water (Baker, 1976). In other words, the New Scotland Limestone is relatively impermeable and forms a hydrological confining unit beneath the cave-bearing interval. Dye tracing indicates that water in Lasell's Hell Hole exits at Sitzer's Spring, which is said to be 0.5 miles east of the dye injection site (Baker, 1976).

WNS Infection Report: Porter (2008a).

H. CARBONATE STRATA OF THE DEVONIAN ONONDAGA LIMESTONE

Only one site infected with WNS before September 2009 is located in the Devonian Onondaga Limestone (Figs. 3 and 8). This site is Clarksville Cave in New York.

Clarksville Cave (Ward-Gregory Cave), Albany County, NY (Site 16 on Fig. 2):

Cave Map: Map dated 1995 in Engel (1999).

Stratigraphy: Lower part of the Middle Devonian Onondaga Limestone (Gregg, 1974; Kastning, 1975; Cullen et al., 1979; Rubin, 1986, 1991; Engel, 1999, 2009).

Hydrology: A perennial stream flows through much of the cave.

Cave Meteorology: Porter (2004) described several months of air temperature records at two locations in the cave. At one location, air temperature ranged from 7.8 to 8.3 °C from mid-March through late June 2003, and air temperature increased from 8.3 to 10.6 °C from late June through late August 2003. At the other location, air temperature ranged from 4.4 to 9.4 °C from late October 2003 through early July 2004, with the lower temperatures occurring from late January to late February.

WNS Infection Report: Porter (2008a,b), Armstrong (2009), and Youngbaer (2009a).

DEVONIAN SCHIST

Only one site infected with WNS before September 2009 is located in Devonian schist (metamorphosed mudstone; Figs. 3 and 8). This site is Elizabeth Mine in Vermont.

Elizabeth Mine, Orange County, VT (Site 13 on Fig. 1):

Mine Maps: Undated maps in Howard (1969), Annis et al. (1983), and Slack et al. (2001).

Stratigraphy: Lower Devonian Gile Mountain Formation, which consists of schist, quartzite, and amphibolite (Howard, 1959a,b, 1969; Annis et al., 1983; Slack et al., 1993; Kierstead, 2001; Slack et al., 2001; Balistrieri et al., 2007). The Gile Mountain Formation is approximately equivalent stratigraphically to the Lower Devonian siliciclastic strata shown in Figures 3 and 8.

Mined Commodities: Iron from 1793 to 1809, pyrrhotite from 1809 to 1830, and copper from 1830 to 1919 and from 1943 to 1958.

WNS Infection Report: USGS NWHC (Quarterly Mortality Reports, 2008, Quarter 4). A WNS infection in Orange County (VT) was also reported by the USGS NWHC (Quarterly Mortality Reports, 2009, Quarter 1), although it is not clear whether this 2009 report describes the infection at Elizabeth Mine or at a different location.

MISSISSIPPIAN STRATA

No WNS-infected caves or mines were identified in Mississippian strata (Figs. 3 and 15) prior to September 2009. However, in March 2010, Cassell Cave in Pocahontas County of West Virginia became the first WNS infection site identified in Mississippian strata (reported online at http://www.forums.caves.org/viewtopic.php?f=58&p=84299). The lack of WNS infection sites in Mississippian strata prior to March 2010 is notable because the Mississippian carbonate interval is one of the three major cave-forming intervals in the Appalachian region (the other two intervals being the Cambrian-Ordovician carbonate strata and the Silurian-Devonian carbonate strata; Fig. 3). In the Appalachian Basin, most caves in Mississippian strata (including Cassell Cave) have formed in the lower Greenbrier Limestone (Fig. 15). In southwestern Pennsylvania, however, many caves have formed in the Mississippian Loyalhanna Member of the Mauch Chunk Formation (Fig. 15), which is a quartz sandstone that is cemented by calcite (Krezoski et al., 2006).

PENNSYLVANIAN STRATA

Four of the sites infected with WNS before September 2009 are located in Pennsylvanian strata (Fig. 3). These sites are abandoned coal mines in the State of Pennsylvania (two mines at Carbondale, the Dunmore Mine, and the Shickshinny Mine).

Two mines at Carbondale, Lackawanna County, PA (Sites 66 and 67 on Fig. 1):

Mine Map: None published.

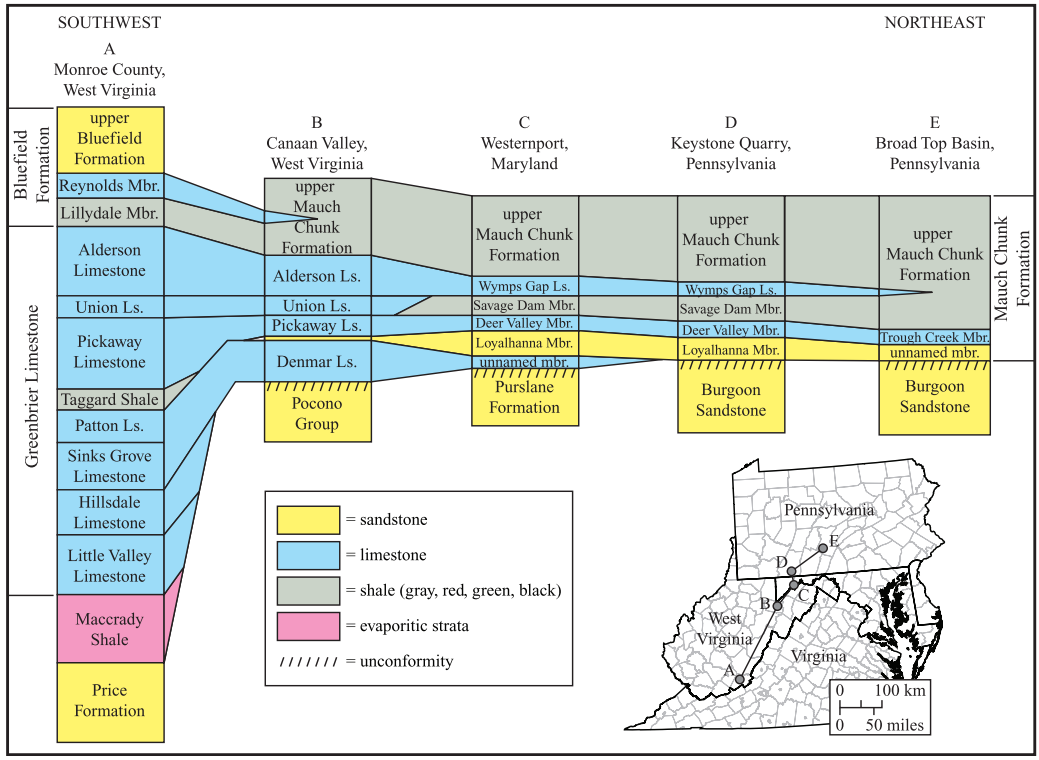

Figure 15. Southwest to northeast cross-sections of the Mississippian Greenbrier Limestone and associated strata from southern West Virginia to central Pennsylvania (modified from Wells, 1950; Cecil et al., 2004). Horizontal and vertical distances are not to scale.

Stratigraphy: A coal bed or coal beds of the Pennsylvanian Llewellyn Formation.

Mined Commodity: Coal (anthracite).

WNS Infection Report: The Pennsylvania Game Commission (http://www.portal.state.pa.us/portal/server.pt/gateway/PTARGS_0_2_112129_9109_615025_43/http%3B/pubcontent.state.pa.us/publishedcontent/publish/marketingsites/game_commission/content/wildlife/wildlife_diseases/white_nose_syndrome/wns_documents/2009_press_releases_019_09.pdf) and the Pennsylvania Department of Conservation and Natural Resources (http://www.dcnr.state.pa.us/news/resource/res2009/09-0311-resource.aspx#blurb2).

The Dunmore Mine, Lackawanna County, PA (Site 55 on Fig. 1):

Mine Map: None published.

Stratigraphy: A coal bed or coal beds of the Pennsylvanian Llewellyn Formation (Baughman and Gadinski, 1997).

Mined Commodity: Coal (anthracite).

WNS Infection Report: USGS NWHC (Quarterly Mortality Reports, 2008, Quarter 4).

The Shickshinny Mine, Luzerne County, PA (Site 56 on Fig. 1):

Mine Map: None published.

Stratigraphy: A coal bed or coal beds of the Pennsylvanian Llewellyn Formation.

Mined Commodity: Coal (anthracite).

WNS Infection Report: The Pennsylvania Department of Conservation and Natural Resources (http://www.dcnr.state.pa.us/news/resource/res2009/09-0311-resource.aspx#blurb2).

Jurassic Strata

Only one of the sites infected with WNS before September 2009 is located in strata of Jurassic age (~200 to 146 Ma, according to Gradstein et al., 2004). This site is a mine in Connecticut named New-Gate Prison Mine.

New-Gate Prison Mine, Hartford County, CT (Site 65 on Fig. 1):

Mine Map: Undated map in Huntington (1963).

Stratigraphy: Redbeds and sandstone of the Jurassic Portland Formation of the Newark Supergroup (Huntington, 1963; Penn and Gray, 1987).

Mined Commodity: Copper, mined prior to 1837.

WNS Infection Report: Suggested by Kocer (2009) and reported by Anonymous (2009a). In addition, a WNS infection in Hartford County (CT) was confirmed by the USGS NWHC (Quarterly Mortality Reports, 2009, Quarter 1).

UNKNOWN LOCATIONS

In addition to the sites described above, nine sites infected with WNS before September 2009 have been identified by state and county location, but the names of these sites and more detailed location information are not available. These nine sites are displayed on a map by Cal Butchkoski of the Pennsylvania Game Commission available online at http://www.portal.state.pa.us/portal/server.pt/gateway/PTARGS_0_2_112129_9109_615025_43/http%3B/pubcontent.state.pa.us/publishedcontent/publish/marketingsites/game_commission/content/wildlife/wildlife_diseases/white_nose_syndrome/images/wnsmap.jpg. Versions of Butchkoski's map have been published in Blehert (2009) and Turner and Reeder (2009). The available information about these sites is listed below as follows:

1) One cave in Onondaga County, NY (Site 45 on Fig. 1).
2) One site in Hamilton County, NY (Site 46 on Fig. 1).
3) One cave in Washington County, NY (Site 47 on Fig. 1): Although an exact site name was not given, a WNS infection in Washington County (NY) was confirmed by the USGS NWHC (Quarterly Mortality Reports, 2009, Quarter 1).
4) One site in Washington County, VT (Site 14 on Fig. 1). Although an exact site name was not given, a WNS infection in Washington County (VT) was confirmed by the USGS NWHC (Quarterly Mortality Reports, 2009, Quarter 1).
5) One mine in Windham County, VT (Site 11 on Fig. 1). Although an exact site name was not given, a WNS infection in Windham County (VT) was confirmed by the USGS NWHC (Quarterly Mortality Reports, 2009, Quarter 1).
6) One mine in Grafton County, NH (Site 50 on Fig. 1). WNS infection at this site was also reported at the following website: http://www.wildlife.state.nh.us/Newsroom/News_2009/News_2009_Q3/bats_WNS_July_09.html. Although an exact site name was not given, a WNS infection in Grafton County (NH) was confirmed by the USGS NWHC (Quarterly Mortality Reports, 2009, Quarter 1).
7) One mine in Merrrimack County, NH (Site 49 on Fig. 1). WNS infection at this site was reported at the following website: http://www.wildlife.state.nh.us/Newsroom/News_2009/News_2009_Q3/bats_WNS_July_09.html.
8) One mine in Franklin County, MA (Site 23 on Fig. 2).
9) One site in Hartford County, CT (Site 32 on Fig. 2). WNS infection at this site was suggested by Kocer (2009). This site is not the New-Gate Prison Mine site (Site 65 on Fig. 1), which is also located in Hartford County (CT). Although an exact site name was not given, a WNS infection in Hartford County (CT) was confirmed by the USGS NWHC (Quarterly Mortality Reports, 2009, Quarter 1).

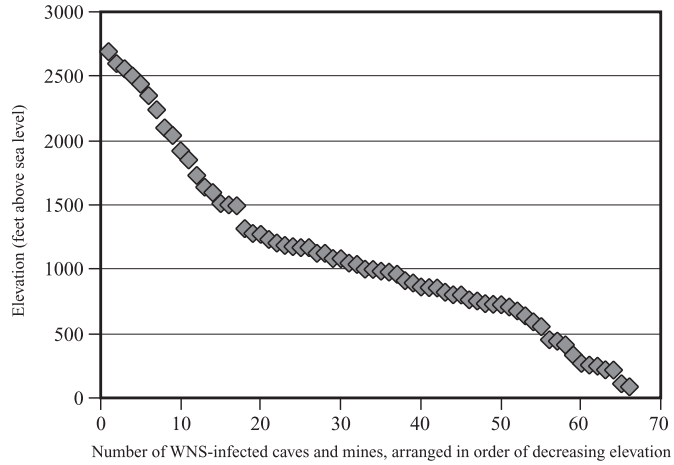

Figure 16. Elevation (feet above sea level) of caves and mines infected with WNS before September 2009, arranged in order of decreasing elevation. Data are given in Table 1.

DISCUSSION

The data presented in this paper reveal that sites infected with WNS before September 2009 are characterized by a wide range of geographical parameters (latitude, longitude, elevation, type of bat hibernaculum). These data also show that the infected sites encompass a wide range of geological parameters (lithology, age of strata) and meteorological parameters (air temperature, humidity).

GEOGRAPHICAL PARAMETERS

The sites infected with WNS before September 2009 are found throughout a wide geographical range in the eastern United States, but most of these sites are located in the State of New York. In order of abundance, the infected sites are listed according to State as follows: New York (n=33), Vermont (n=10), Pennsylvania (n=8), Massachusetts (n=6), Virginia (n=5), West Virginia (n=4), Connecticut (n=4), New Jersey (n=3), and New Hampshire (n=2). The preponderance of infected sites in New York is probably related to the location of the initial infection site. As stated above, the WNS infection is thought to have appeared first in a cave connected to Howe Caverns in New York, and to have spread subsequently to all of the other sites.

The available data show that the known elevations of sites infected with WNS before September 2009 range from 84 to 2693 feet above sea level, although there is no specific elevation around which most of these infected sites are clustered (Fig. 16). These data suggest that elevation alone may not exert a strong control on the spread of WNS. However, all of the sites infected with WNS prior to September 2009 are restricted to the eastern side of the Appalachian Basin geological province and locations immediately north and east of the Appalachian Basin. It is not apparent why WNS has spread primarily north, south, and east from the initial infection site, rather than to

the west. One possible explanation is that the Appalachian Mountains may present some barrier to the spread of WNS, even though elevation alone does not appear to exert a strong control. For example, the presence of the Appalachian Mountains may influence bat migration pathways (re: bat transmission of WNS) as well as human travel patterns (re: human transmission of WNS). The first occurrence of WNS infection west of the Appalachian Mountains occurred in March 2010, at a commercial cave in the Dunbar Cave State Natural Area, Montgomery County, Tennessee (reports available online at http://www.dunbarcave.org/ and at http://www.theleafchronicle.com/article/20100324/NEWS01/100324016/Bat-in-Clarksville-s-Dunbar-Cave-tests-positive-for-deadly-fungusC:/Documents%20and%20Settings/schillers/My%20Documents/Advisement).

All of the sites infected with WNS before September 2009 are bat hibernacula, but the WNS infection is not restricted to one specific type of hibernacula. According to the data in Table 1, 44 of the sites infected with WNS before September 2009 are natural caves, 28 of these infected sites are abandoned mines, and 3 of these sites are of undetermined settings. The preponderance of natural cave settings is probably due to the fact that natural caves make up the preponderance of locations where bats hibernate in large groups.

Geological Parameters

With respect to lithology, most of the sites infected prior to September 2009 are located in sedimentary rocks (n=53), although some of the infected sites are located in metamorphic rocks (n=10), igneous rocks (n=3), and undetermined geological settings (n=9). Of the infected sites that are known to be in sedimentary rocks, 46 are located in carbonate strata, and 7 are located in sandstone or mudstone. The infected sites that are known to be in metamorphic rock are located in both meta-sedimentary and meta-igneous rock, whereas the infected sites that are known to be in igneous rocks are located in granite and serpentinite. In this list, amphibolite and granite gneiss are considered to be metamorphosed igneous rocks. The preponderance of WNS infection sites being located in carbonate strata is probably due to the fact that most bat hibernacula are natural caves in carbonate strata.

With respect to stratigraphic age, the sites infected with WNS before September 2009 are located in rocks that range from Precambrian to Jurassic. However, it is interesting to note that none of these sites (pre-September 2009) are located in rocks of Mississippian, Cretaceous, or Triassic age. Nine of the known infection sites are located in Precambrian-Cambrian igneous or metamorphic rocks, 19 of the sites are located in Cambrian-Ordovician carbonate strata, 5 of the sites are located in Ordovician-Silurian non-carbonate strata (gneiss, schist, sandstone), 27 of the sites are located in Silurian-Devonian carbonate strata, 1 site is located in Devonian schist, 4 sites are located in Pennsylvanian coal-bearing strata, and 1 site is located in Jurassic sandstone. Nine sites are situated in an unknown stratigraphic context.

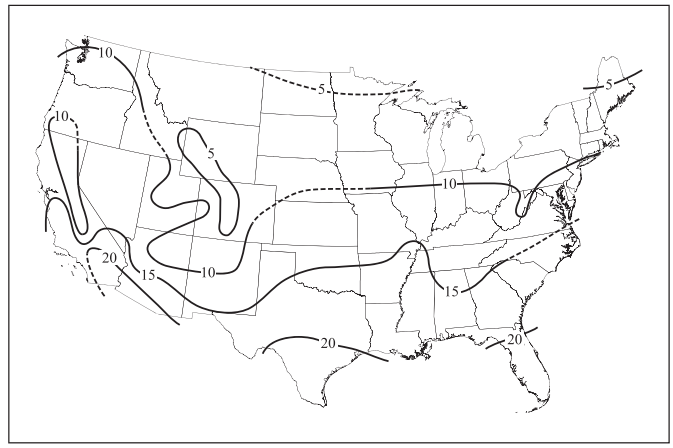

Figure 17. Map of mean cave temperatures (degrees Celsius) in the United States (from Moore and Sullivan, 1978, p. 28). This map is based primarily on theoretical calculations, rather than measured data.

It is not clear why most of the WNS-infected sites are located in Silurian-Devonian carbonate strata. However, the initial infection site is believed to be a cave that is connected to Howe Caverns, which are commercial caverns located in Silurian-Devonian carbonate strata. Thus, the preponderance of infection sites in Silurian-Devonian carbonate strata may have something to do with the location and setting of the initial infection site. Likewise, it is not clear why no infected sites were identified in Mississippian strata prior to March 2010, even though many caves are present in Mississippian limestone. However, Mississippian strata are located to the west of most of the other identified sites (Fig. 1), and thus the lack of infected sites in Mississippian strata (prior to March 2010) may be related to some of the geographical parameters discussed above. [Note: The first appearance of WNS infection in Mississippian strata was reported in March 2010 from Cassell Cave in Pocahontas County, West Virginia (reported online at: http://www.forums.caves.org/viewtopic.php?f=58&p=84299)].

Meteorological Parameters

Information on temperature and humidity conditions in caves and mines might be useful for predicting the spread of WNS because *Geomyces destructans* apparently prefers cold, humid conditions. Unfortunately, not much data have been published on meteorological conditions in caves or mines, and much of the available data are single measurements taken on only one day. Nevertheless, a brief review of some governing principles and assumptions is presented below, followed by a discussion of the meteorology of the WNS-infected sites.

It is generally assumed that the air temperature in a cave is approximately equal to the annual average outside air temperature at a given location (e.g., Davies, 1958). This assumption has been used to produce a map of assumed cave temperatures in the United States (Fig. 17). Fowler (1941),

however, noted that the assumption of cave temperature being approximately equal to the annual average outside air temperature appears to be true only of caves or portions of caves that have a very low rate of air circulation.

For a cave without flowing water and with only one entrance, air circulation is usually limited and the air temperature in deep parts of the cave is controlled by the temperature of the surrounding rock, which is approximately equal to the average annual air temperature at the surface (Wigley and Brown, 1976; Moore and Sullivan, 1978). The air temperature at the surface is controlled by daily and seasonal temperature fluctuations, which in turn are functions of latitude and altitude. The effects of air temperature fluctuations at the surface diminish as heat moves down through the rock. Thus, fluctuations in air temperature are greater at cave entrances and in shallow caves, and these fluctuations diminish at greater distances from the cave entrances and greater depths below the surface. In some instances, where a cave extends directly downward from the entrance, the air temperature in the cave may be cooler than one might predict (Moore and Sullivan, 1978). With these caves, which are called "cold-trap caves," dense cold air flows into the cave during the winter. During the summer, however, air circulation ceases and the cold air is trapped in the cave.

For caves with more than one entrance, air temperature and pressure differences inside and outside the cave may create an air flow pattern that is referred to as a "chimney effect" (Wigley and Brown, 1976; Moore and Sullivan, 1978). In this situation, a temperature difference produces a pressure difference between the cave entrances, and air flows either into or out of the cave in order to equilibrate the temperature and pressure differences between the entrances. This effect is usually more prominent where a cave has two entrances at very different elevations.

Some caves exhibit a phenomenon of oscillating air flow in and out of the cave (referred to as "cave breathing"). This phenomenon was the subject of much speculation and study during the 1940s through 1960s (Faust, 1947; Cournoyer, 1954, 1956; Plummer, 1962; Wigley, 1967). A review by Lewis (1991) suggests that many reports of "cave breathing" are caused by variations in atmospheric pressure at the entrance of a cave, although falling water in a resonant cavity may also cause the phenomenon of "cave breathing."

For caves in which water flows, cave air temperature may be affected by the water (Wigley and Brown, 1976; Moore and Sullivan, 1978). For example, where relatively warm water flows into a cave, this water may transport warmth into the cave further than would be transported by air flow alone. In contrast, where relatively cold water flows into a cave (e.g., caves that receive large quantities of snowmelt in the spring), this water may transport cold air into the cave further than would be transported by air flow alone. In addition, the flow of water can induce the flow of air adjacent to the water, thus generating air currents deeper in the cave than would otherwise occur.

From the sparse data available, the sites infected with WNS before September 2009 appear to have air temperatures ranging from 0 to 13.9 °C. Most of these temperatures are within the range of 5 °C and 10 °C that is reported as being optimal for growth of *Geomyces destructans*. If Blehert et al. (2009) are correct that *G. destructans* does not grow at temperatures greater than 20 °C, then mapping the distribution of a 20 °C temperature threshold would be important for predicting the spread of WNS. Judging from the sparse data that are available, a 20 °C cave temperature threshold is likely to lie south of most of the continental United States (Fig. 17) and north of Puerto Rico (where air temperatures in many caves are approximately 25 to 26 °C; Rodríguez-Durán, 1998).

The available measurements on air temperatures from these caves and mines infected with WNS before September 2009 do not show clear geographic correlations such as one might expect from Figure 17. Although most of the recorded air temperatures in the infected caves and mines range from 4.4 to 13.9 °C, there does not appear to be any particular correlation of cave (or mine) air temperature with latitude (Fig. 18A), longitude (Fig 18B), or elevation (Fig. 19). This lack of apparent correlation could be caused by a variety of reasons. For example, some of the infected caves and mines have single entrances, whereas other infected caves and mines have multiple entrances. Some of the infected caves and mines may be associated with air circulation patterns such that the sites function as "cold-trap caves" or "cold-trap mines." In addition, some of the infected caves and mines have flowing water, whereas others do not. Finally, it is possible that some data may be erroneous because of human effects (e.g., the presence of humans may increase the air temperature in a cave when measurements are taken).

The data on humidity at sites infected with WNS before September 2009 are sparser than the data on air temperature. Published data are available from only four sites, showing a range of humidity measurements from 68 to 100 percent. With regards to *Geomyces destructans*, a humidity threshold below which the fungus does not grow has not been identified, although anecdotal field evidence suggests that the fungus may prefer relatively high humidity.

As with the air temperature data, there does not appear to be any particular correlation of cave or mine humidity with latitude (Fig. 20A), longitude (Fig 20B), or elevation (Fig. 21). However, reliable measurements of cave humidity can be very difficult to obtain (Wefer, 1991; Mitchie, 2006), and certain correlations might become apparent if more data were available.

OTHER ENVIRONMENTAL PARAMETERS

It is possible that several other environmental parameters may influence WNS, in addition to the geographical, geological, and meteorological parameters discussed above. For example, there may be a relation between WNS and the chemistry of cave sediments. Likewise, there may be a relation between WNS and the presence and (or) distribution of other

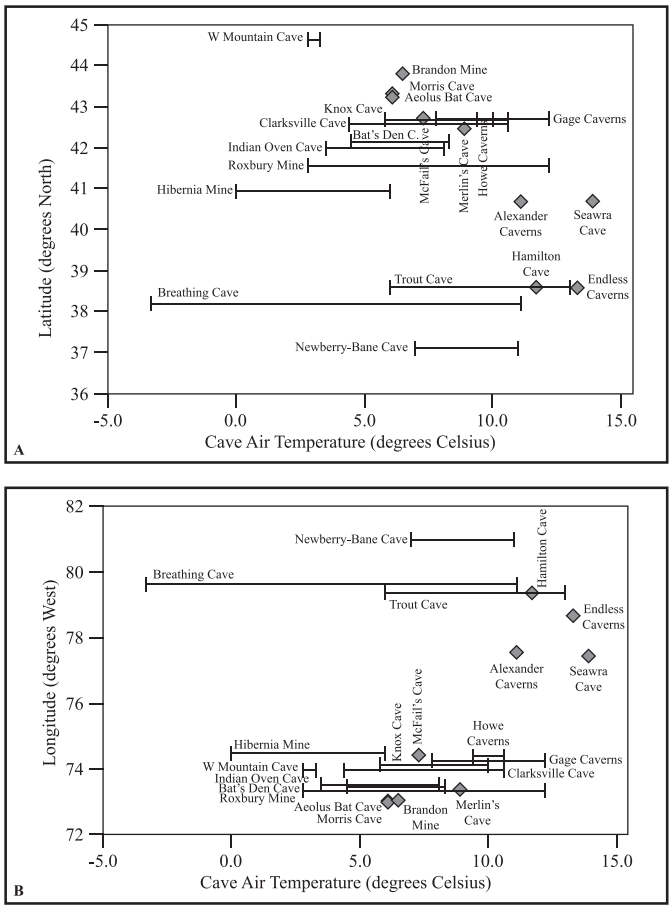

Figure 18. A (upper chart) = Cave air temperature versus latitude. B (lower chart) = Cave air temperature vs. longitude. Latitude and longitude data were calculated for the WNS-infected sites while constructing Figures 1 and 2. However, specific latitude and longitude values are not given in Table 1 for reasons of cave security. Where only one temperature measurement is recorded, this value is represented by a diamond. Where multiple temperature measurements are recorded, the most frequent value is represented by a diamond and the full range of values is represented by the horizontal lines that extend from the diamond.

fauna besides bats. At present, it is not known if WNS affects other animals (e.g., cave rats). Finally, there may be a relation between WNS and specific behaviors of bats.

Conclusions

As of September 2009, 75 known sites in the United States contained bats that were infected with the white-nose syndrome (WNS) fungus named *Geomyces destructans*. WNS appears to have spread from an initial infection site in a cave that is connected to commercial caverns (Howe Caverns) in New York, and by the end of August 2009 WNS had been identified in at least 74 other sites in the eastern United States. These WNS-infected sites extend from New Hampshire to Virginia, but most of the sites are located in the

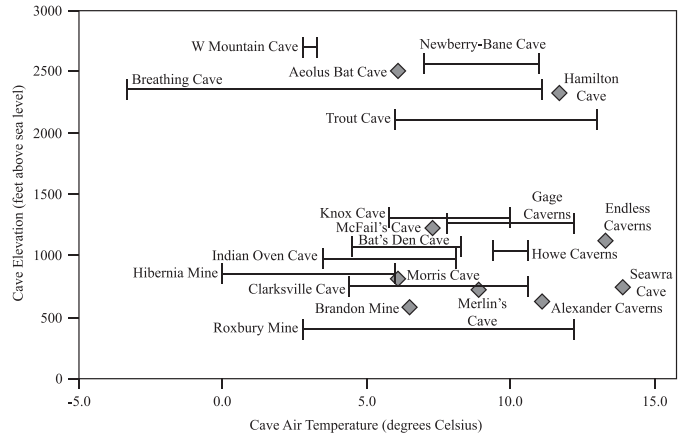

Figure 19. Cave air temperature versus elevation. Elevation data are given in Table 1. Where only one temperature measurement is recorded, this value is represented by a diamond. Where multiple temperature measurements are recorded, the most frequent value is represented by a diamond and the full range of values is represented by the horizontal lines that extend from the diamond.

State of New York (33 of 75). The elevations of these WNS-infected sites (for which data are available) range from 84 to 2693 feet above sea level, but there is no specific elevation at which most of the infected sites are located. The infected sites include both natural caves and mines, although most of the known infected sites for which data are available are natural caves (n=44). In terms of geological setting, the infected sites are located in sedimentary, metamorphic, and igneous rocks, although most of the infected sites for which data are available are located in sedimentary rocks (n=53). Of the infected sites that are known to be in sedimentary rocks, 46 are in located carbonate strata and 7 are located in sandstone or mudstone. Furthermore, these WNS-infected sites are located in rocks that range in age from Precambrian to Jurassic, although as of the end of August 2009 no infected sites were located in strata of Mississippian, Cretaceous, or Triassic age. The majority of the infected sites for which data are available are located in either Silurian-Devonian carbonate strata (n=27) or Cambrian-Ordovician carbonate strata (n=19). Meteorological data are sparse, but most of the recorded air temperatures range from 0 to 13.9 °C in caves and mines infected with WNS before September 2009, and humidity measurements range from 68 to 100%.

Many questions still remain about the nature and origin of WNS, and it is not yet clear which environmental parameters may exert controls on the distribution and behavior of WNS. Based on the information presented in this paper, it appears that the spread of WNS will not be restricted by the elevation of the sites, the lithology in which caves or mines are located, or the age of the strata in which caves or mines are located. Air temperature of 20 °C is reported to be a temperature threshold above which *Geomyces destructans* does not grow, and this temperature threshold is likely to lie south of most of

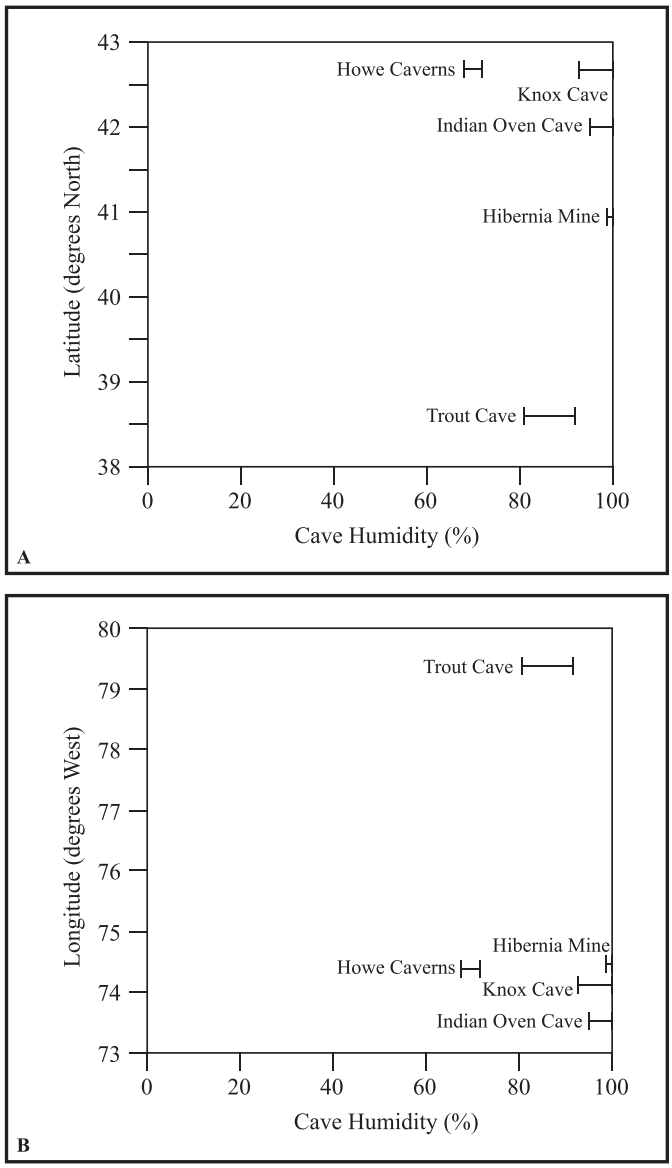

Figure 20. A (upper chart) = Cave humidity vs. latitude. B (lower chart) = Cave humidity vs. longitude. Latitude and longitude data were calculated for the WNS-infected sites while constructing Figures 1 and 2. However, specific latitude and longitude values are not given in Table 1 for reasons of cave security. For each location, the range of measured values is denoted by vertical and horizontal lines.

the continental United States and north of Puerto Rico. It is also possible that the spread of WNS may be restricted by low humidity, although a humidity threshold below which the fungus does not grow has not been identified.

ACKNOWLEDGEMENTS

This manuscript benefited from reviews by USGS microbiologist David Blehert, and USGS geologist David Weary. Subsequently, this manuscript was improved by suggestions from Selene Deike, and journal editors Scott Engel, Malcolm Field, and Gregory Springer. Thanks to Peter Quick for information on caves in Vermont, Nicholas Ratcliffe for information on stratigraphy of Vermont, John Repetski for information on Ordovician stratigraphy, and Kenneth Walsh for information on Hancock Cave in Virginia. Thanks also to Steven Cahan for assistance drafting some of the figures, and to various members of the DC Grotto and the Potomac Speleological Club for critiques and discussions. Publication costs of this manuscript were paid for by David Bornholdt (USGS Eastern Region Coordinator for Biology).

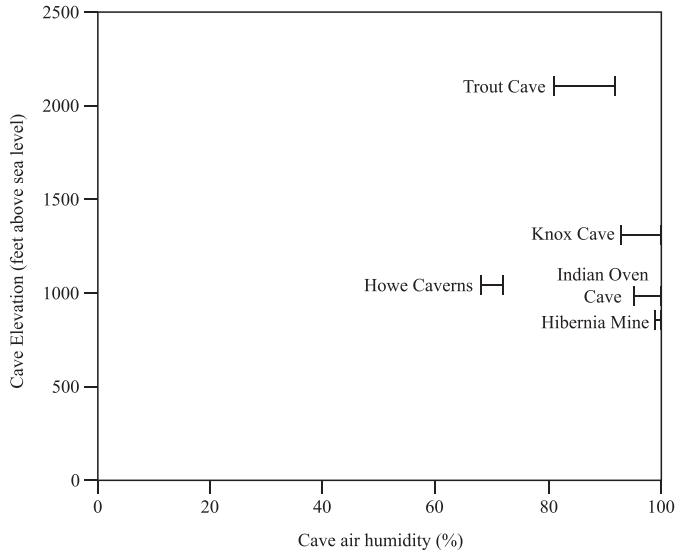

Figure 21. Cave air humidity vs. elevation. Elevation data are given in Table 1. For each location, the range of measured values is denoted by vertical and horizontal lines.

REFERENCES

Addis, B., 1969, The non-commercial sections of Howe Caverns, part III: The Northeastern Caver, v. 1, no. 12, p. 142–145.

Anderson, R., 1961, Geology of Barton Hill: Bulletin of the National Speleological Society, v. 23, pt. 1, p. 11–14.

Annis, M.P., Slack, J.F., and Rolph, A.L., 1983, Stratabound massive sulfide deposits of the Elizabeth Mine, Orange County, Vermont, *in* Sangster, D.F., ed., Field Trip Guidebook to Stratabound Sulfide Deposits, Bathurst Area, N.B., Canada and West-Central New England, U.S.A.: Geological Survey of Canada Miscellaneous Report 36, p. 41–51.

Anonymous, 1960, Baker's Quarry Cave [map]: Journal of the Yale Speleological Society, v. 3, no. 1, p. 12–14.

Anonymous, 1965, Mitchell's Cave: The Massachusetts Caver, v. 4, no. 3, p. 49.

Anonymous, 2008, Bat die-off prompts investigation [New York State Department of Environmental Conservation press release, 30 January 2008]: The Northeastern Caver, v. 39, no. 1, p. 8.

Anonymous, 2009a, Northeast news: The Northeastern Caver, v. 40, no. 2, p. 39–47.

Anonymous, 2009b, White Nose Syndrome news: The Northeastern Caver, v. 40, no. 4, p. 112–113.

Armstrong, J., 2009, New York cave and mine biology notes, 2006–2009: The Northeastern Caver, v. 40, no. 3, p. 97–99.

Armstrong, J., Carley, S., Hopkins, T., Perlman, S., and Siemion, J., 2005, Another breakthrough at ANC Cave: The Northeastern Caver, v. 36, no. 4, p. 125–127.

Baker, V., 1970, Compilation of Albany-Schoharie dye results: The Northeastern Caver, v. 2, no. 3, p. 21.
Baker, V.R., 1973, Geomorphology and hydrology of karst drainage basins and cave channel networks in east central New York: Water Resources Research, v. 9, no. 3, p. 695–706. doi:10.1029/WR009i003p00707.
Baker, V., 1976, Hydrogeology of a cavernous limestone terrane and the hydrochemical mechanisms of its formation, Mohawk River Basin, New York: Empire State Geogram, v. 12, no. 2, p. 2–65.
Balistrieri, L.S., Seal, R.R. II., Piatak, N.M., and Paul, B., 2007, Assessing the concentration, speciation, and toxicity of dissolved metals during mixing of acid-mine drainage and ambient river water downstream of the Elizabeth Copper Mine, Vermont, USA: Applied Geochemistry, v. 22, no. 5, p. 930–952.
Barr, T., 1958, Baker's Quarry Cave (Lanesboro, Massachusetts), *in* Dunn, J.R., and McCrady, A.D., eds., Speleo Digest 1958, p. 1/146–147.
Baughman, S.H., and Gadinski, R., 1997, A new use for an old tool, *in* Inners, J.D., ed., Geology of the Wyoming-Lackawanna Valley and its Mountain Rim, Northeastern Pennsylvania: Guidebook for the 62nd Annual Field Conference of Pennsylvania Geologists, p. 61–63.
Bayley, W.S., 1910, Iron mines and mining in New Jersey: Geological Survey of New Jersey, Final Report Series, v. 7, 512 p.
Benson, R.N., 1992, Map of exposed and buried early Mesozoic rift basins/synrift rocks of the U.S. Middle Atlantic continental margin: Delaware Geological Survey Miscellaneous Map Series Report 5 (1:1,000,000 scale), 1 sheet.
Berkshire Diggers and the Rockeaters, 2008, An alpine cave in the Berkshires: The Northeastern Caver, v. 39, no. 2, p. 46–50.
Blehert, D.S., 2009, Investigating white-nose syndrome in bats: U.S. Geological Survey Fact Sheet 2009-3058, 2 p.
Blehert, D.S., Hicks, A.C., Behr, M., Meteyer, C.U., Berlowski-Zier, B.M., Buckles, E.L., Coleman, J.T.H., Darling, S.R., Gargas, A., Niver, R., Okoniewski, J.C., Rudd, R.J., and Stone, W.B., 2009, Bat white-nose syndrome: An emerging fungal pathogen?: Science, v. 323, no. 5911, p. 227. doi: 10.1126/science.1163874.
Botto, L., 2007, XTC Cave … finally!: The Northeastern Caver, v. 38, no. 2, p. 56–57.
Brack, V. Jr., Reynolds, R.J., Orndorff, W., Zokaites, J., and Zokaites, C., 2005, Bats of Skydusky Hollow, Bland County, Virginia: Virginia Journal of Science, v. 56, no. 2, p. 93–106.
Britzke, E.R., Hicks, A.C., von Oettingen, S.L., and Darling, S.R., 2006, Description of spring roost trees used by female Indiana Bats (*Myotis sodalis*) in the Lake Champlain Valley of Vermont and New York: American Midland Naturalist, v. 155, no. 1, p. 181–187.
Burns Chavez, S.R., and Clemensen, A.B., 1995, Final cultural landscape report: Pahaquarry Copper Mine, Delaware Water Gap National Recreational Area, New Jersey: U.S. National Park Service, Denver Service Center, v. 1 (373 p.) and v. 2 (308 p.).
Carmichael, J.W., 1962, Chrysosporium and some other aleuriosporic hyphomycetes: Canadian Journal of Botany, v. 40, no. 8, p. 1137–1173.
Carroll, R.W. Jr., 1969, Some significant caves in Vermont: The Northeastern Caver, v. 1, no. 3, p. 30–33.
Carroll, R.W. Jr., 1970, Between-season status of Glen Park Caves: The Northeastern Caver, v. 2, no. 1, p. 4–5.
Carroll, R.W. Jr., 1972a, Some recommended caves for the Fall NRO: The Northeastern Caver, v. 3, n. 9, p. 106–115.
Carroll, R.W. Jr., 1972b, Tectono-speleology: The Northeastern Caver, v. 3, no. 12, p. 144, 150.
Carroll, R.W. Jr., 1974, "W" Mountain Cave: The Northeastern Caver, v. 5, no. 6–7, p. 76–77.
Carroll, R.W. Jr., 1988, Caves and karst in the Equinox Range: The Massachusetts Caver, v. 6, no. 1, p. 6–11. Reprinted in Adler, J., and Adler, M., eds., Speleo Digest 1988, p. 231–233.
Carroll, R.W. Jr., 1997, 1997 reassessment of talus caves and snowtubes: The Northeastern Caver, v. 28, no. 3, p. 92–93.
Carroll, R.W. Jr., 2009, W Mountain Cave: The Northeastern Caver, v. 40, no. 1, p. 26–27.
Cecil, C.B., Brezinski, D.K., and Dulong, F., 2004, The Paleozoic record of changes in global climate and sea level: Central Appalachian Basin, *in* Southworth, S., and Burton, W., eds., Geology of the National Capital Region – Field Trip Guidebook: U.S. Geological Survey Circular 1264, p. 77–135.
Chapman, M.E., 1970, Pendleton County's Saltpetre Caves and their role in the Civil War: Karst Kaver, v. 4, no. 4, p. 13–17. Reprinted in Kramer, J., and Mixon, B., eds., Speleo Digest 1970, p. 308–310.
Chu, M., 2006, On the caver cover: The Northeastern Caver, v. 37, no. 2, cover photograph and photograph description.
Clark, S.H.B., 1990, Stratabound zinc-lead-copper deposits in the Cambrian carbonate-siliciclastic shelf sequence at Lion Hill, west-central Vermont: U.S. Geological Survey Bulletin 1887-K, 9 p.
Clemmer, G.S., 2005, Burnsville Cove, Virginia, *in* Culver, D.C., and White, W.B., eds., Encyclopedia of Caves: Amsterdam, Elsevier Academic Press, p. 60–71.
Cole, G., 1974, The mystery of the lost cave: The Northeastern Caver, v. 5, no. 6–7, p. 78–79.
Cook, J.H., 1908, Limestone caverns of eastern New York, *in* Clarke, J.M., ed., Report of the Director 1906: New York State Museum, 60th Annual Report 1906, v. 1, p. 32–51.
Cournoyer, D.N., 1954, The Speleo-Barometer: The American Caver (Bulletin of the National Speleological Society), no. 16, p. 91–93.
Cournoyer, D.N., 1956, Recent work in Breathing Cave: D.C. Speleograph, v. 11, no. 3, p. 1–3.
Craytor, S., 1969, Some Warren County caves: The Northeastern Caver, v. 1, no. 8, p. 97–98.
Cullen, J.J., Mylroie, J.E., and Palmer, A.N., 1979, Karst hydrogeology and geomorphology of eastern New York: A Guidebook to the Geology Field Trip, National Speleological Society Annual Convention, Pittsfield, Massachusetts, August 5–12, 1979, 83 p.
Curl, R., and Peters, D., 1954, Boston Grotto maps Mitchell's Cave: The Northeastern Regional Organization of the National Speleological Society Publication, v. 1, no. 1, p. iii–iv.
Dasher, G.R., ed., 2001, The Caves and Karst of Pendleton County: West Virginia Speleological Survey Bulletin 15, 404 p.
Dasher, G., ed., 2009a, Rockin' Chair: The West Virginia Caver, v. 27, no. 4, p. 7–9.
Dasher, G., 2009b, WNS updates: The West Virginia Caver, v. 27, no. 3, 12 p.
Dasher, G., ed., 2010, Rockin' Chair: The West Virginia Caver, v. 28, no. 3, p. 10–12.
Davies, W.E., 1965, Caverns of West Virginia: West Virginia Geological and Economic Survey v. 19A (330 p.) with Supplement (72 p).
Davis, G., and Palmer, A., 1959, Red Bat Cave: Boston Grotto Newsletter, Nov. 1959, Reprinted in Dunn, J.R., and McCrady, A.D., eds., Speleo Digest 1959, p. 1–8.
Davis, H., Hartline, D., Hauer, P., and Sease, M., eds., 1966, Caves of Schoharie County, NewYork: Boston Grotto for the Northeastern Regional Organization of the National Speleological Society, 124 p.
Dayton, G.O., White, W.B., and White, E.L., eds., 1981, The caves of Mifflin County, PA: Mid-Atlantic Region of the National Speleological Society Bulletin 12, 72 p.
Deike, G.H. III., 1960, Origin and geologic relations of Breathing Cave, Virginia: Bulletin of the National Speleological Society, v. 22, no. 1, p. 30–42.
Dennison, J.M., and Hasson, K.O., 1979, Stratigraphic cross section of Devonian shales along the Allegheny Front from Maryland to Highland County, Virginia: Proceedings of the West Virginia Academy of Science, v. 49, no. 2–4, p. 104–110.
Dimbirs, A., and Wood, L., 1977, Selected dye tests in the Schoharie County karst: The Northeastern Caver, v. 8, no. 3, p. 68–76. Reprinted in Mixon, B., ed., Speleo Digest 1977, p. 225–229.
Dorobek, S.L., and Read, J.F., 1986, Sedimentology and basin evolution of the Siluro-Devonian Helderberg Group, central Appalachians: Journal of Sedimentary Petrology, v. 56, no. 5, p. 601–613.
Douglas, H.H., 1964, Caves of Virginia: Falls Church, Virginia, Virginia Cave Survey, 761 p.
Dumont, E.R., 2003, Bats and fruit: An ecomorphological approach, *in* Kunz, T.H., and Fenton, M.B., eds., Bat Ecology: Chicago, The University of Chicago Press, p. 398–429.
Dunham, J., 2007, XTC: The Northeastern Caver, v. 38, no. 2, p. 50–55.
Dunham, J., 2009, Merlins Cave bat survey: The Northeastern Caver, v. 40, no. 2, p. 48.
Dunham, J., 2010, Descending the Slime Climb: The Northeastern Caver, v. 41, no. 2, p. 50–52.
Dyas, M., 1976a, Cave Mountain project summary: D.C. Speleograph, v. 32, no. 3, p. 3–5. Reprinted in Erh, B., ed., Speleo Digest 1976, p. 109–110.
Dyas, M., 1976b, Further notes on Cave Mountain Cave: D.C. Speleograph, v. 32, no. 6, p. 3–4. Reprinted in Erh, B., ed., Speleo Digest 1976, p. 108–109.
Dyas, M., 1977, Hamilton Cave – new information: D.C. Speleograph, v. 33, no. 1, p. 6–7.

Dyroff, T., 1977, Hamilton Trout connection?: D.C. Speleograph, v. 33, no. 7, p. 11–12.
Echols, P.E. Jr., 1961, Roxbury Mine Trip: Met Grotto News, v. 11, no. 1, 3 p. Reprinted in Black, H.L., and Haarr, A.P., eds., Speleo Digest 1961, p. 1/3.
Eckler, A.R., 1966, Geology of Schoharie County, *in* Davis, H., Hartline, D., Hauer, P., and Sease, M., eds., Caves of Schoharie County, New York: Boston Grotto for the Northeastern Regional Organization of the National Speleological Society, p. 5–10.
Egemeier, S.J., 1969, Origin of caves in eastern New York as related to unconfined groundwater flow: Bulletin of the National Speleological Society, v. 31, no. 4, p. 97–111.
Engel, T.D., 1987, New York's long caves: The Northeastern Caver, v. 18, no. 1, p. 3–9.
Engel, T.D., 1988, Barton Hill Karst Preserve management plan: The Northeastern Caver, v. 19, no. 2, p. 57–65, 48. Reprinted in Adler, J., and Adler, M., eds., Speleo Digest 1988, p. 404–407.
Engel, T.D., 1999, Clarksville Cave: The Northeastern Caver, v. 30, no. 2, p. 61–63.
Engel, T.D., 2009, New York State, *in* Palmer, A.N., and Palmer, M.V., eds., Caves and Karst of the USA: Huntsville, Alabama, National Speleological Society, p. 27–32.
Evans, J., Quick, P., and Sloane, B., eds., 1979, An introduction to caves of the Northeast: National Speleological Society Guidebook 20, 76 p.
Faust, B., 1947, An unusual phenomenon: Bulletin of the National Speleological Society, no. 9, p. 52–54.
Faust, B., 1964, Saltpeter caves and Virginia history, *in* Douglas, H.H., Caves of Virginia: Falls Church, Virginia, Virginia Cave Survey, p. 31–55.
Febroriello, P., 1984, Mystery Cave: The Northeastern Caver, v. 15, no. 3, p. 45–47, 55–56. Reprinted in Speece, J., ed., Speleo Digest 1984, p. 259–262.
Fisher, D.W., 1987, Lower Devonian limestones, Helderberg Escarpment, New York, *in* Roy, D.C., ed., Geological Society of America Centennial Field Guide v. 5 – Northeastern Section: Boulder, Colorado, Geological Society of America, p. 119–122.
Fisher, J., 1954, Cave index of Met, North Jersey and E.D.S. Grotto areas: Met Grotto News, v. 4, no. 1, p. 3–6.
Fisher, J., ed., 1958, Caves of Watertown, New York State: Northeastern Regional Organization of the National Speleological Society Special Publication 5, 52 p.
Folsom, B., 2008, Northeastern Cave Conservancy closes caves: The Northeastern Caver, v. 39, no. 1, p. 7.
Fowler, J.A., 1941, Long eared bats: Bulletin of the National Speleological Society, no. 2, p. 35–37.
Gargas, A., Trest, M.T., Christensen, M., Volk, T.J., and Blehert, D.S., 2009, *Geomyces destructans* sp. nov. associated with bat white-nose syndrome: Mycotaxon, v. 108, p. 147–154.
Garton, M.E., and Garton, R., 2001, Pendleton County's saltpeter caves and their role in the Civil War, *in* Dasher, G.R., ed., The Caves and Karst of Pendleton County: West Virginia Speleological Survey Bulletin 15, p. 70–73.
Gates, R.M., 1959, Bedrock geology of the Roxbury Quadrangle, Connecticut: U.S. Geological Survey Geologic Quadrangle Map GQ-121 (1:24 000 scale), 1 sheet.
Gillson, J.L., 1927, Origin of the Vermont talc deposits, with a discussion on the formation of talc in general: Economic Geology, v. 22, no. 3, p. 246–287.
Goodman, C., 2009, Mass Hole: The Northeastern Caver, v. 40, no. 1, p. 23.
Gradstein, F.M., Ogg, J.G., and Smith, A.G., 2004, A Geologic Time Scale 2004: Cambridge, UK, Cambridge University Press, 589 p.
Griffin, D.R., 1945, Travels of banded cave bats: Journal of Mammalogy, v. 26, no. 1, p. 15–23.
Gregg, W.J., 1974, Structural control of cavern development in Howe Caverns, Schoharie County, New York: Bulletin of the National Speleological Society, v. 36, no. 4, p. 1–6.
Gurnee, J., 1957, Gage Caverns (Schoharie County, New York): Northeastern Regional Organization of the National Speleological Society Bulletin No. 4. Reprinted in Dunn, J.R., and McCrady, A.D., eds., Speleo Digest 1958, p. 1/92–101.
Haas, J.L., 1960, Metahalloysite in Cave Mountain Cave: Nittany Grotto Newsletter, v. 8, no. 4, p. 63. Reprinted in Black, H., Haarr, A.P., and McGrew, W.C., eds., Speleo Digest 1960, p. 2/37–38.
Haas, J., 1961, Trout and Hamilton Cave (Pendleton County, West Virginia): The Cleve-O-Grotto News, v. 8, no. 1, p. 5–6. Reprinted in Black, H.L., and Haarr, A.P., eds., Speleo Digest 1961, p. 1/78–79.
Haberland, P., 1991, Recent discoveries and current exploration in the Northwest Passage Extension of McFail's: NSS News, v. 49, no. 3, p. 82–86.
Haberland, P., Hopkins, T., Fortuin, K., and Whittemore, M., 2000, New discoveries in Natures Way: The Northeastern Caver, v. 31, no. 3, p. 79–87. Reprinted in Fee, S., ed., Speleo Digest 2000, p. 194–197.
Hackley, C., 2009, Rebound theory for the formation of Mass Hole and many other New England caves: The Northeastern Caver, v. 40, no. 4, p. 134–136.
Harris, A.G., Stamm, N.R., Weary, D.J., Repetski, J.E., Stamm, R.G., and Parker, R.A., 1994, Conodont color alteration index (CAI) map and conodont-based age determinations for the Winchester 30′ × 60′ quadrangle and adjacent area, Virginia, West Virginia, and Maryland: U.S. Geological Survey Miscellaneous Field Studies Map MF-2239 (1:100,000 scale), 1 sheet with 40-page pamphlet.
Hartline, D., 1965, Speleologizing in the Chester Emery Mine: The Massachusetts Caver, v. 4, no. 3, p. 51–53.
Hauer, P.M., 1969, Caves of Massachusetts: Altoona, Pennylvania, A Speece Production, 62 p.
Head, J.W., 1974, Correlation and paleogeography of upper part of Helderberg Group (Lower Devonian) of Central Appalachians: American Association of Petroleum Geologists Bulletin, v. 58, no. 2, p. 247–259.
Higham, S., 1992, The caves of Dorset Mountain: The Northeastern Caver, v. 23, no. 2, p. 39–49. Reprinted in Adler, J., and Alder, M., eds., Speleo Digest 1992, p. 267–275.
Higham, S., 1996, New England explorations, 1994–1996: The Northeastern Caver, v. 27, no. 3, p. 88–90. Reprinted in Lau, S.C., ed., Speleo Digest 1996, p. 168–169.
Hitchcock, E., Hitchcock, E. Jr., Hager, A.D., and Hitchcock, C.H., 1861, Report on the Geology of Vermont: Descriptive, Theoretical, Economical, and Scenographical: Proctorsville, Vermont, A.D. Hager, v. 1 (p. 1–558) and v. 2 (p. 559–988).
Hoke, B., 2001, 2001 Trout Rock caves bat counts: The West Virginia Caver, v. 19, no. 2, p. 11.
Hoke, B., 2005, Cave Mountain Cave soil sampling trip November 19, 2005: D.C. Speleograph, v. 61, no. 5–6, p. 5–7.
Hoke, B., 2009a, White nose syndrome has come to West Virginia: D.C. Speleograph, v. 65, no. 1, p. 5.
Hoke, B., 2009b, White-nose syndrome appears to have come to West Virginia: The West Virginia Caver, v. 27, no. 2, p. 12.
Holsinger, J.R., 1975, Descriptions of Virginia Caves: Virginia Division of Mineral Resources Bulletin 85, 450 p.
Hopkins, T., 1996a, Nature's Way: The Northeastern Caver, v. 27, no. 3, p. 85.
Hopkins, T., 1996b, Terrace Mountain again: The Northeastern Caver, v. 27, no. 1, p. 12–15. Reprinted in Lau, S.C., ed., Speleo Digest 1996, p. 192–194.
Hornung, K., 1953, Knox Cave trip: Met Grotto News, v. 3, no. 1, p. 3–4.
Howard, P.F., 1959a, Structure and rock alteration at the Elizabeth Mine, Vermont; Part I, Structure at the Elizabeth Mine: Economic Geology, v. 54, no. 7, p. 1214–1249. doi: 10.2113/gsecongeo.54.7.1214.
Howard, P.F., 1959b, Structure and rock alteration at the Elizabeth Mine, Vermont; Part II, Rock alteration at the Elizabeth Mine: Economic Geology, v. 54, no. 8, p. 1414–1443. doi: 10.2113/gsecongeo.54.8.1414.
Howard, P.F., 1969, The geology of the Elizabeth Mine, Vermont: Vermont Geological Survey, Economic Geology Publication 5, 73 p.
Hubbard, D.A. Jr., 1995, Commercial caves of the Old Dominion, *in* Zokaites, C., ed., Underground in the Appalachians: A Guidebook for the 1995 Convention of the National Speleological Society: Huntsville, Alabama, National Speleological Society, p. 106–111.
Hubbard, D.A. Jr., and Grady, F., 1999, Mammoth tooth found in Endless Caverns: Virginia Minerals, v. 45, no. 1, p. 1–3.
Huntington, D.A., ed., 1963, The caves of Connecticut [2nd edition]: New Haven, Connecticut, Yale Speleological Society, 26 p.
Ibberson, D., 1988, Speleo-canoeing in Alexander Caverns: York Grotto Newsletter, v. 22, no. 4, p. 65–66. Reprinted in Adler, J., and Adler, M., eds., Speleo Digest 1988, p. 181.
Jacobs, B., 2006, Roxbury Mine survey: The Northeastern Caver, v. 37, no. 2, p. 60–67.
James, A.H., and Dennen, W.H., 1962, Trace ferrides in the magnetite ores of the Mount Hope Mine and the New Jersey Highlands: Economic Geology, v. 57, no. 3, p. 439–449. doi: 10.2113/gsecongeo.57.3.439.
Jones, G., and Rydell, J., 2003, Attack and defense: Interactions between echolocating bats and their insect prey, *in* Kunz, T.H., and Fenton, M.B., eds., Bat Ecology: Chicago, University of Chicago Press, p. 301–345.

Jones, W.K., 1999, Field trip to Endless Caverns, New Market, Virginia, *in* Palmer, A.N., Palmer, M.V., and Sasowsky, I.D., eds., Karst Modeling: Karst Waters Institute Special Publication 5, p. 262–264.

Jones, W.K., 2009, Field trip to Endless Caverns, New Market, Virginia, *in* Engel, A.S., and Engel, S.A., eds., Select Field Guides to Cave and Karst Lands of the United States: Karst Waters Institute Special Publication 15, p. 3–6.

Jurgens, B., 1960, Mitchell's Cave: Met Grotto News, v. 10, no. 6, p. 52. Reprinted in Black, H., Haarr, A.P., and McGrew, W.C., eds., Speleo Digest 1960, p. 1/13.

Kastning, E.H., 1968, South Bethlehem Cave (Albany Co., New York): The New York Caver, v. 1, no. 6, p. 96–97, 99. Reprinted in Davis, J.O., Smith, A.R., Sherborne, W.B., and Power, L., eds., Speleo Digest 1968, p. 1/89, 92.

Kastning, E.H., 1975, Cavern development in the Helderberg Plateau, east-central New York: M.S. thesis, Storrs, Connecticut, The University of Connecticut, 194 p. Reprinted in 1975 as New York Cave Survey Bulletin 1, 194p.

Kemp, J.F., 1898, The geology of the magnetites near Port Henry, N.Y., and especially those of Mineville: Transactions of the American Institute of Mining Engineers, v. 27, p. 146–203.

Kemp, J.F., and Newland, D.H., 1899, Preliminary report on the geology of Washington, Warren and parts of Essex and Hamilton Counties: New York State Museum 51st Annual Report 1897, v. 2, p. 499–553.

Kennedy, J., 2002, BCI visits northeastern bat hibernacula: The Northeastern Caver, v. 33, no. 4, p. 121–124.

Keough, J., 2000, Williams Cave remapped: The Northeastern Caver, v. 31, no. 1, 19 p. Reprinted in Fee, S., ed., Speleo Digest 2000, p. 258.

Kierstead, M.A., 2001, History and historical resources of the Vermont Copper Belt, *in* Hammarstrom, J.M., and Seal, R.R. II., eds., Part II. Environmental Geochemistry and Mining History of Massive Sulfide Deposits in the Vermont Copper Belt: Society of Economic Geologists Guidebook Series, v. 35, p. 165–191.

Kocer, C., 2009, White-nose syndrome devastates CT's hibernating bats: Connecticut Wildlife, v. 29, no. 2, p. 7.

Kochkina, G.A., Ivanushkina, N.E., Akimov, V.N., Gilichinskii, D.A., and Ozerskaya, S.M., 2007, Halo- and psychrotolerant *Geomyces* fungi from Arctic cryopegs and marine deposits: Microbiology, v. 76, no. 1, p. 31–38. doi: 10.1134/S0026261707010055.

Kreider, M.B., 1963, Meteorology, *in* Palmer, A., ed., Knox Cave, Albany County, N.Y.: Northeastern Regional Organization of the National Speleological Society Special Publication 9, p. 20.

Krezoski, G.M., Havholm, K.G., and Swezey, C.S., 2006, Petrographic analysis of the Mississippian (Chesterian) Loyalhanna Member of the Mauch Chunk Formation, Keystone Quarry, southwestern Pennsylvania [abs].: Geological Society of America, Abstracts with Programs, v. 38, no. 4, p. 6.

Lambert, R., 2009, Breathing Cave closed due to WNS: D.C. Speleograph, v. 65, no. 1, p. 6.

Landing, E., 2007, Ediacaran-Ordovician of East Laurentia—Geologic setting and controls on deposition along the New York Promontory region, *in* Landing, E., ed., S.W. Ford Memorial Volume: Ediacaran-Ordovician of East Laurentia: New York State Museum Bulletin 510, p. 5–24.

Le Van, D.C., and Rader, E.K., 1983, Relationship of stratigraphy to occurrences of oil and gas in western Virginia: Virginia Division of Mineral Resources Publication 43, 1 sheet.

Lewis, W.C., 1991, Atmospheric pressure changes and cave airflow: A review: Bulletin of the National Speleological Society, v. 53, no. 1, p. 1–12.

Lincks, G.F., 1978, The Chester emery mines: The Mineralogical Record, v. 9, no. 4, p. 235–242.

Lundy, J., 2001, Dyeing to know about Hailes Cave: The Northeastern Caver, v. 32, no. 2, p. 58–60. Reprinted in Adler, J., Adler, M., and Parvin, S., eds., Speleo Digest 2001, p. 168–169.

Marshall, W.A., 1998, Aerial transport of keratinaceous substrate and distribution of the fungus *Geomyces pannorum* in Antarctic soils: Microbial Ecology, v. 36, no. 2, p. 212–219. doi: 10.1007/s002489900108.

Martuscello, M., 2000, Natures Way, Sump Two and beyond: The Northeastern Caver, v. 31, no. 4, p. 122–127. Reprinted in Fee, S., ed., Speleo Digest 2000, p. 198–200.

McManus, J.J., 1974, Activity and thermal preference of the Little Brown Bat, *Myotis lucifugus*, during hibernation: Journal of Mammalogy, v. 55, no. 4, p. 844–846.

McManus, J.J., and Esher, R.J., 1971, Notes on the biology of the Little Brown Bat, *Myotis lucifugus*, hibernating in New Jersey: Bulletin of the New Jersey Academy of Science, v. 16, nos. 1–2, p. 19–24.

Medville, D., 2000a, Hamilton Cave, *in* Dasher, G.R., ed., The Caves of East-Central West Virginia: The Guidebook of the National Speleological Society's 2000 Convention: West Virginia Speleological Survey Bulletin 14, p. 92.

Medville, D., 2000b, Trout Cave (Trout Rock Cave), *in* Dasher, G.R., ed., The Caves of East-Central West Virginia: The Guidebook of the National Speleological Society's 2000 Convention: West Virginia Speleological Survey Bulletin 14, p. 130–131, 133.

Meteyer, C.U., Buckles, E.L., Blehert, D.S., Hicks, A.C., Green, D.E., Shearn-Bochsler, V., Thomas, N.J., Gargas, A., and Behr, M.J., 2009, Histopathologic criteria to confirm white-nose syndrome in bats: Journal of Veterinary Diagnostic Investigations, v. 21, no. 4, p. 411–414.

Middleton, J., 1977, Access policy for Single-X Cave: The Northeastern Caver, v. 8, no. 2, 35 p.

Middleton, J., 1979, New discoveries in Barytes Cave, Schoharie County, N.Y.: The Northeastern Caver, v. 10, no. 3, p. 53–54.

Mitchie, N., 2006, Humidity and caves: NSS News, v. 64, no. 8, p. 17, 19.

Monteverde, D.H., 2001, Pahaquarry Copper Mine, *in* Inners, J.D., and Fleeger, G.M., eds., 2001: A Delaware River Odyssey: Guidebook for the 66th Annual Field Conference of Pennsylvania Geologists, p. 150–155.

Moore, G.W., 1958, Time of stalactite growth: Journal of the Yale Speleological Society, v. 1, no. 2, 12 p. Reprinted in Dunn, J.R., and McCrady, A.D., eds., Speleo Digest 1958, p. 2/46–48.

Moore, G.W., and Sullivan, G.N., 1978, Speleology, The Study of Caves [revised 2nd edition]: Teaneck, New Jersey, Zephyrus Press, 150 p.

Mylroie, J., 1972, Growth, colonization, and distribution of mosses in Howe Caverns, N.Y.: The Northeastern Caver, v. 3, no. 4, p. 46–47. Reprinted in Moody, J., ed., Speleo Digest 1972, p. 186–187.

Mylroie, J.E., 1977, Speleogenesis and karst geomorphology of the Helderberg Plateau, Schoharie County, New York: Ph.D. dissertation, Troy, New York, Rensselaer Polytechnic Institute, 336 p. Reprinted in 1977 as New York Cave Survey Bulletin 2, 336 p.

Mylroie, J., 1980, Cave location and exploration in Schoharie County, New York: National Speleological Society Bulletin, v. 42, no. 1, p. 15–20.

Nekvasil-Coraor, H., 1979, Caves as environmental indicators: The Dripstone, v. 10, no. 1, p. 2–14. Reprinted in Garton, E.R., Gaton, M.E., Deem, K., and Deem, D., eds., Speleo Digest 1979, p. 221–224.

Newland, D.H., 1921, The mineral resources of the State of New York: New York State Museum Bulletin, no. 223–224, 152 p.

Olesen, N.R., 1961, Howe Cave Project: NSS News, v. 19, no. 1, p. 4–5.

Orndorff, W., 1995, Bedrock geologic setting of karst near the Central and Southern Appalachian transition: Geology Field Trip, *in* Zokaites, C., ed., Underground in the Appalachians: A Guidebook for the 1995 Convention of the National Speleological Society: Huntsville, Alabama, National Speleological Society, p. 126–154.

Palmer, A., 1963, The geology of Knox Cave, *in* Palmer, A., ed., Knox Cave, Albany County, N.Y.: Northeastern Regional Organization of the National Speleological Society Special Publication 9, p. 9–17.

Palmer, A.N., 1975, The origin of maze caves: Bulletin of the National Speleological Society, v. 37, no. 3, p. 57–76.

Palmer, A., 2000, Knox Cave update: The Northeastern Caver, v. 31, no. 4, p. 116–120. Reprinted in Fee, S., ed., Speleo Digest 2000, p. 201–206.

Palmer, A., 2001, The geology and hydrology of Knox Cave: The Northeastern Caver, v. 32, no. 2, p. 51–53. Reprinted in Adler, J., Adler, M., and Parvin, S., eds., Speleo Digest 2001, p. 359–360.

Palmer, A.N., 2002, Karst in Paleozoic rocks: How does it differ from Florida?, *in* Martin, J.B., Wicks, C.M., and Sasowsky, I.D., eds., Hydrogeology and Biology of Post-Paleozoic Carbonate Aquifers: Karst Waters Institute Special Publication 7, p. 185–191.

Peck, S., 1967, Biological notes on caves in the northeastern U.S.: V: The Massachusetts Caver, v. 6, no. 4, 63 p. Reprinted in McCutchen, G.D., ed., Speleo Digest 1967, p. 2/67–68.

Penn, W.E., and Gray, N.H., 1987, Geology and hydrology of the sedimentary bedrock of Old New-Gate Prison and Copper Mine, East Granby, CT [abs.]: Geological Society of America, Abstracts with Programs, v. 19, no. 1, p. 51.

Perlman, S., 2006, A visit to Hasbrouck Mine: Met Grotto News, v. 56, no. 2, p. 6.

Perry, C., 1942, Skinner's Hollow Cave: Bulletin of the National Speleological Society, no. 3, p. 20–21.

Perry, E.L., 1929, The geology of Bridgewater and Plymouth Townships, Vermont: Report of the State Geologist on the Mineral Industries and Geology of Vermont 1927–1928 [16th of this series], p. 1–64.

Pierson, E.D., 1998, Tall trees, deep holes, and scarred landscapes – Conservation biology of North American bats, *in* Kunz, T.H., and

Racey, P.A., eds., Bat Biology and Conservation: Washington, D.C., Smithsonian Institution Press, p. 309–325.
Plante, A.R., 1991, Berkshire caves and karsts – The Jug End Karst: The Northeastern Caver, v. 22, no. 3, p. 82–91. Reprinted in O'Malley, E., and Fee, S., eds., Speleo Digest 1991, p. 524–531.
Plante, A., 1992, Berkshire caves and karst – The Disappearing Brook Karst: The Northeastern Caver, v. 23, no. 2, p. 54–70. Reprinted in Adler, J., and Adler, M., eds., Speleo Digest 1992, p. 131–146.
Plummer, B., 1962, A note on cave breathing: The Baltimore Grotto News, v. 5, no. 12, p. 282–287. Reprinted in Haarr, A.P., and Plummer, W.T., eds. Speleo Digest 1962, p. 2/101–107.
Porter, C., 1968, Williams Cave: The New York Caver, v. 1, no. 2, p. 22–24, 30. Reprinted in Davis, J.O., Smith, A.R., Sherborne, W.B., and Power, L., eds., Speleo Digest 1968, p. 1/158–161.
Porter, C., 1972, "Mitchells Cave": The Northeastern Caver, v. 3, no. 12, p. 145, 150.
Porter, C., 1985, The Northeastern Caver interview: Chuck Porter: The Northeastern Caver, v. 16, no. 1, p. 23–25.
Porter, C., 2004, Clarksville Cave temperature study: The Northeastern Caver, v. 35, no. 4, p. 118–119.
Porter, C., 2008a, White Nose Syndrome developments: The Northeastern Caver, v. 39, no. 2, p. 43–45.
Porter, C., 2008b, White Nose synopsis: The Northeastern Caver, v. 39, no. 1, p. 9–10.
Porter, C., 2009a, Merlins Cave acquisition nears: The Northeastern Caver, v. 40, no. 2, p. 47–48.
Porter, C., 2009b, New England, *in* Palmer, A.N., and Palmer, M.V., eds., Caves and Karst of the USA: Huntsville, Alabama, National Speleological Society, p. 24–27.
Porter, C., 2009c, The history of W Mountain/Norton Range Cave: The Northeastern Caver, v. 40, no. 2, p. 53–56.
Porter, C., 2009d, White Nose spread, bat numbers dwindle: The Northeastern Caver, v. 40, no. 1, p. 5–12.
Powers, J., 1981, Confederate niter production: Bulletin of the National Speleological Society, v. 43, no. 4, p. 94–97.
Puechmaille, S.J., Verdeyroux, P., Fuller, H., Ar Gouilh, M., Bekaert, M., and Teeling, E.C., 2010, White-nose syndrome fungus (*Geomyces destructans*) in bat, France: Emerging Infectious Diseases, v. 16, no. 2, p. 290–293. doi: 10.3201/eid1602.091391.
Quick, P.G., 1994, Vermont Caves – A Geologic and Historical Guide: Ypsilanti, Michigan, Paleoflow Press, 74 p.
Quick, P., 2001, Skinner Hollow Cave: Vermont Cavers Association Newsletter, v. 10, no. 5, Reprinted in Adler, J., Adler, M., and Parvin, S., eds., Speleo Digest 2001, p. 221–222.
Rader, E.K., and Biggs, T.H., 1976, Geology of the Strasburg and Toms Brook Quadrangles, Virginia: Virginia Division of Mineral Resources Report of Investigations 45, 104 p.
Ransome, R., 1990, The Natural History of Hibernating Bats: London, UK, Christopher Helm, 235 p.
Ratcliffe, N.M., 1974, Bedrock geologic map of the State Line Quadrangle, Columbia County, New York, and Berkshire County, Massachusetts: U.S. Geological Survey Geologic Quadrangle Map GQ-1142 (1:24,000 scale), 1 sheet.
Ratcliffe, N.M., 1994, Changes in stratigraphic nomenclature in the eastern cover sequence in the Green Mountain Massif from Ludlow to West Bridgewater, Vermont, *in* Stratigraphic notes, 1992; Four short papers propose changes in stratigraphic nomenclature in Vermont, Virginia, Maryland, and the District of Columbia: U.S. Geological Survey Bulletin 2060, p. 1–10.
Ratcliffe, N.M., Stanley, R.S., Gale, M.H., and Thompson, P.J., 2010 (in prep.), Bedrock geologic map of Vermont: U.S. Geological Survey Scientific Investigations Map (1:100,000 scale).
Read, J.F., 1989, Correlation chart of latest Precambrian, Cambrian and Ordovician formations, passive margin sequence, U.S. Appalachians, *in* Hatcher, R.D. Jr., Thomas, W.A., and Viele, G.W., eds., The Appalachian-Ouachita Orogen in the United States: Boulder, Colorado, Geological Society of America, The Geology of North America series, v. F-2, Plate 3A.
Reeds, C.A., 1925, The Endless Caverns of the Shenandoah Valley: New York, The Evans-Brown Company, 48 p.
Reichard, J.D., and Kunz, T.H., 2009, White-nose syndrome inflicts lasting injuries to the wings of little brown myotis (*Myotis lucifugus*): Acta Chiropterologica, v. 11, no. 2, p. 457–464. doi: 10.3161/150811009X485684.
Rice, A.V., and Currah, R.S., 2006, Two new species of *Pseudogymnoascus* with *Geomyces* anamorphs and their phylogenetic relationship with *Gymnostellatospora*: Mycologia, v. 98, no. 2, p. 307–318. doi: 10.3852/mycologia.98.2.307.
Rodríguez-Durán, A., 1998, Nonrandom aggregations and distribution of cave-dwelling bats in Puerto Rico: Journal of Mammalogy, v. 79, no. 1, p. 141–146.
Ross, C., 1982, Mount Hope Mine: New Jersey Outdoors, v. 9, no. 1, p. 17–18, 24.
Rubin, P.A., 1985, Journey to the center of Schoharie County, or karst hydrology predicts integrated McFail's–Howe–Secret Caverns system, Cobleskill Quad., New York: The Northeastern Caver, v. 16, no. 3, p. 59–84. Reprinted in Kambesis, P., ed. Speleo Digest 1985, p. 80–91.
Rubin, P.A., 1986, New York State's mega cave systems: Hydrology and speleogenesis: The Northeastern Caver, v. 17, no. 2–3, p. 29–81.
Rubin, P.A., 1991, Modification of preglacial caves by glacial meltwater invasion in east-central New York, *in* Kastning, E.H., and Kastning, K.M., eds., Appalachian Karst: Huntsville, Alabama, National Speleological Society, p. 91–99.
Rubin, P.A., 2009, Geological evolution of the Cobleskill Plateau, New York State, USA, *in* Proceedings, 15th International Congress of Speleology, v. 2, part 2, p. 972–978.
Rubinstein, J., 1998, Strontium mines and Ain't No Catchment Cave: A history of a mine exploration of a cave: The Northeastern Caver, v. 29, no. 1, p. 10–12. Reprinted in Reyome, J., and Reyome, S., eds., Speleo Digest 1998, p. 344–345.
Ryder, R.T., Swezey, C.S., Crangle, R.D. Jr., and Trippi, M.T., 2008, Geologic cross section *E-E′* through the central Appalachian Basin from the Findlay Arch, Wood County, Ohio, to the Valley and Ridge Province, Pendleton County, West Virginia: U.S. Geological Survey Scientific Investigations Series Map SIM-2985 (2 sheets with 48-page pamphlet).
Ryder, R.T., Crangle, R.D. Jr., Trippi, M.H., Swezey, C.S., Lentz, E.E., Rowan, E.L., and Hope, R.S., 2009, Geologic cross section *D-D′* through the central Appalachian basin from the Findlay arch, Sandusky County, Ohio, to the Valley and Ridge province, Hardy County, West Virginia: U.S. Geological Survey Scientific Investigations Series Map SIM-3067 (2 sheets with 52-page pamphlet).
Saunders, J., 1974, The Sinking Creek project: The Tech Troglodyte, v. 12, no. 3, p. 15–19. Reprinted in Mixon, B., ed., Speleo Digest 1974, p. 209–211.
Saunders, J.W., Ortiz, R.K., and Koerschner, W.F. III., 1981, Major groundwater flow directions in the Sinking Creek and Meadow Creek drainage basins of Giles and Craig Counties, Virginia, USA, *in* Proceedings of the 8th International Congress of Speleology, v. 1, p. 398–400.
Schultz, A.P., Stanley, C.B., Gathright, T.M. II., Rader, E.K., Bartholomew, M.J., Lewis, S.E., and Evans, N.H., 1986, Geologic map of Giles County, Virginia: Virginia Division of Mineral Resources Publication 69 (1:50 000 scale), 1 sheet.
Schwartz, B.F., Orndorff, W.D., Futrell, M.S., and Lucas, P.C., 2009, Virginia, *in* Palmer, A.N., and Palmer, M.V., Caves and Karst of the USA: Huntsville, Alabama, National Speleological Society, p. 39–51.
Schweiker, R., ed., 1959, Boston Grotto cave file, *in* Dunn, J.R., and McCardy, A.D., eds., Speleo Digest 1958, p. 1/145–163.
Schweiker, R., Anderson, R.R., and Van Note, P., 1958, Field Guide to New York Caves, Schoharie County: Northeastern Regional Organization of the National Speleological Society Special Publication 6, 83 p.
Schweyen, J., 1987, Northeast cave diving notes: The Northeastern Caver, v. 18, no. 3, p. 79–82, 76.
Schweyen, J., 1989, A brief review of diving exploration in Schoharie Caverns: The Northeastern Caver, v. 20, no. 2, p. 36–39. Reprinted in Fee, S. ed., Speleo Digest 1989, p. 150–151.
Scott, J., 1959, Caves in Vermont: Hancock, Vermont, Killooleet Independent Speleological Society, p. 45.
Seigel, R., 1957, The east passage of Indian Oven Cave (New York): Met Grotto News, v. 7, no. 3, p. 3. Reprinted in Dunn, J.R., and White, W.B., eds., Speleo Digest 1957, p. 1/81.
Siemion, J., 2005, Barytes-Wolferts Cave map: The Northeastern Caver, v. 36, no. 4, p. 128–130.
Siemion, J., Armstrong, J., Folsom, B., Hopkins, T., and Porter, C., 2003, Breakthroughs in Barytes and Wolferts Cave: The Northeastern Caver, v. 34, no. 3, p. 82–92. Reprinted in Johnson, K. and Johnson, M.H., eds., Speleo Digest 2003, p. 215–219.
Sigler, L., and Carmichael, J.W., 1976, Taxonomy of *Malbranchea* and some other hyphomycetes with arthroconidia: Mycotaxon, v. 4, no. 2, p. 349–488.

Sims, P.K., 1953, Geology of the Dover magnetite district, Morris County, New Jersey: U.S. Geological Survey Bulletin 982-G, p. 245–305.

Slack, J.F., Offield, T.W., Woodruff, L.G., and Shanks, W.C. III., 2001, Geology and geochemistry of Besshi-type massive sulfide deposits of the Vermont Copper Belt, *in* Hammarstrom, J.M., and Seal, R.R. II., eds., Part II. Environmental Geochemistry and Mining History of Massive Sulfide Deposits in the Vermont Copper Belt: Society of Economic Geologists Guidebook Series, v. 35, p. 193–211.

Slack, J.F., Offield, T.W., Shanks, W.C. III, and Woodruff, L.G., 1993, Besshi-type massive sulfide deposits of the Vermont Copper Belt, *in* Slack, J.F., and Offield, T.W., eds., Selected Mineral Deposits of Vermont and the Adirondack Mountains, New York. II. Besshi-Type Massive Sulfide Deposits of the Vermont Copper Belt: Society of Economic Geologists Guidebook Series, v. 17, p. 32–72.

Sleeman, J., 2009, Wildlife Health Bulletin 2009-03, http://www.fws.gov/northeast/whitenose/PDF/WHB2009-03WNSFinal.pdf [accessed September 15, 2010].

Sluzarski, M.L., 1972, Hydrogeologic determination of the origin of stream flow in Smoke Hole Cave, Giles County, Virginia: The Region Record [Virginia Region of the National Speleological Society], v. 2, no. 4, p. 102–105. Reprinted in Moody, J., ed., Speleo Digest 1972, p. 166–168.

Smosna, R., 1988, Paleogeographic reconstruction of the Lower Devonian Helderberg Group in the Appalachian Basin, *in* McMillan, N.J., Embry, A.F., and Glass, D.J., eds., Devonian of the World: Canadian Society of Petroleum Geology Memoir 14, v. 1, p. 265–275.

Stanley, R.S., and Ratcliffe, N.M., 1985, Tectonic synthesis of the Taconian orogeny in western New England: Geological Society of America Bulletin, v. 96, no. 10, p. 1227–1250. doi:10.1130/0016-7606(1985)96<1227:TSOTTO>2.0.CO;2.

Stihler, C., 2009, Laboratory results confirm white-nose syndrome in West Virginia: The West Virginia Caver, v. 27, no. 2, p. 18–19.

Stihler, C., 2010, White-nose syndrome update April 2010: The West Virginia Caver, v. 28, no. 3, p. 15–16.

Stone, R.W., 1932, Pennsylvania Caves, 2nd edition: Pennsylvania Geological Survey Bulletin G3, 143 p.

Stone, R.W., 1953, Descriptions of Pennsylvania's undeveloped caves: The American Caver (Bulletin of the National Speleological Society), no. 15, p. 51–137.

Swezey, C.S., 2002, Regional stratigraphy and petroleum systems of the Appalachian Basin, North America: U.S. Geological Survey Geologic Investigations Series Map I-2768, 1 sheet.

Swezey, C., 2003, Trout Cave (Pendleton County, WV): D.C. Speleograph, v. 59, no. 10–11, p. 7.

Swezey, C.S., 2009, Regional stratigraphy and petroleum systems of the Illinois Basin, U.S.A.: U.S. Geological Survey Scientific Investigations Series Map SIM-3068, 1 sheet.

Swezey, C.S., and Dulong, F.T., 2010, Some notes on the geology of Cave Mountain Cave, Pendleton County, West Virginia: The West Virginia Caver, v. 28, no. 2, p. 5–10.

Swezey, C.S., Hadden, R.L., and Piatak, N.M., 2004, Nitrate concentrations of soils in "saltpeter caves" in West Virginia (USA): NSS News, v. 62, no. 12, p. 342–345.

Taylor, J.C., 2001, The early history of Pendleton County caves 1760 to 1860, *in* Dasher, G.R., ed., The Caves and Karst of Pendleton County: West Virginia Speleological Survey Bulletin 15, p. 42–59.

Thayer, C.W., 1967, Mud stalagmites and the conulite: Bulletin of the National Speleological Society, v. 29, no. 3, p. 91–95.

Thurston, A.W., 1942, Some New York caves: Rocks and Minerals, v. 17, no. 12, p. 410–411.

Traaen, A.E., 1914, Untersuchungen über bodenpilze aus Norwegen: Nyt Magazin for Naturvidenskaberne, v. 52, p. 20–121.

Trombulak, S.C., Higuera, P.E., and DesMeules, M., 2001, Population trends of wintering bats in Vermont: Northeastern Naturalist, v. 8, no. 1, p. 51–62.

Turner, G.G., and Reeder, D.M., 2009, Update of white nose syndrome in bats, September 2009: Bat Research News, v. 50, no. 3, p. 47–53.

van Beynen, P., and Febbroriello, P., 2006, Seasonal isotopic variability of precipitation and cave drip water at Indian Oven Cave, New York: Hydrological Processes, v. 20, no. 8, p. 1793–1803. doi: 10.1002/hyp.5957.

van Beynen, P.E., Schwarcz, H.P., and Ford, D.C., 2004, Holocene climatic variability recorded in a speleothem from McFail's Cave, New York: Journal of Cave and Karst Studies, v. 66, no. 1, p. 20–27.

Van Oorschot, C.A.N., 1980, A revision of *Chrysosporium* and allied genera: Studies in Mycology, no. 20, 89 p.

Van Tyne, A.M., 1996, Play Dol: Middle Devonian Onondaga Limestone reef play, *in* Roen, J.B., and Walker, B.J., eds., The Atlas of Major Appalachian Gas Plays: West Virginia Geological and Economic Survey Publication V-25, p. 100–102.

Veilleux, J.P., 2007, A noteworthy hibernation record of *Myotis leibii* (Eastern Small Footed Bat) in Massachusetts: Northeastern Naturalist, v. 14, no. 3, p. 501–502.

von Helversen, O., and Winter, Y., 2003, Glossophagine bats and their flowers: Costs and benefits for plants and pollinators, *in* Kunz, T.H., and Fenton, M.B., eds., Bat Ecology: Chicago, University of Chicago Press, p. 346–397.

Weaver, J.D., 1957, Stratigraphy and structure of the Copake Quadrangle, New York: Geological Society of America Bulletin, v. 68, no. 6, p. 725–762. doi:10.1130/0016-7606(1957)68[725:SASOTC]2.0.CO;2.

Weed, W.H., 1911, Copper deposits of the Appalachian states: U.S. Geological Survey Bulletin 455, 166 p.

Weems, R.E., and Olsen, P.E., 1997, Synthesis and revision of groups within the Newark Supergroup, eastern North America: Geological Society of America Bulletin, v. 109, no. 2, p. 195–209. doi:10.1130/0016-7606(1997)109<0195:SAROGW>2.3.CO;2.

Wefer, F.L., 1991, Meteorology of the Butler Cave–Sinking Creek Cave System, *in* Kastning, E.H., and Kastning, K.M., eds., Appalachian Karst: Huntsville, Alabama, National Speleological Society, p. 65–73.

Wefer, F.L., and Nicholson, I.K., 1982, Exploration and mapping of the Sinking Creek System: Bulletin of the National Speleological Society, v. 44, no. 3, p. 48–63.

Wells, D., 1950, Lower Middle Mississippian of southeastern West Virginia: American Association of Petroleum Geologists Bulletin, v. 34, no. 5, p. 882–922.

White, W.B., and Hess, J.W., 1982, Geomorphology of Burnsville Cove and the geology of the Butler Cave–Sinking Creek System: Bulletin of the National Speleological Society, v. 44, no. 3, p. 67–77.

Wibbelt, G., Kurth, A., Hellmann, D., Weishaar, M., Barlow, A., Veith, M., Prüger, J., Görföl, T., Grosche, L., Bontadina, F., Zöphel, U., Seidl, H.-P., Cryan, P., and Blehert, D.S., 2010, White-nose syndrome fungus (*Geomyces destructans*) in bats, Europe: Emerging Infectious Diseases, v. 16, no. 8, p. 1237–1242. doi: 10.3201/eid1608.100002.

Wigley, T.M.L., 1967, Non-steady flow through a porous medium and cave breathing: Journal of Geophysical Research, v. 72, no. 12, p. 3199–3205. doi: 10.1029/JZ072i012p03199.

Wigley, T.M.L., and Brown, M.C., 1976, The physics of caves, *in* Ford, T.D., and Cullingford, C.H.D., eds., The Science of Speleology: New York, Academic Press, p. 329–358.

Woodward, H.P., 1944, Copper mines and mining in New Jersey: New Jersey Department of Conservation and Development, Division of Geology and Topography Bulletin 57, 156 p.

Wright, W., 1982, Geohydrology of the Skydusky Hollow Cave System, Bland County, Virginia: The Tech Troglodyte, v. 21, no. 2, p. 59–65.

Wright, W., 1995, Hydrology of the Skydusky Hollow Cave System, *in* Zokaites, C., ed., Underground in the Appalachians: A Guidebook for the 1995 Convention of the National Speleological Society: Huntsville, Alabama, National Speleological Society, p. 26–29.

Youngbaer, P., 2009a, White Nose Syndrome—A conservation challenge for cavers and conservancies: NSS News, v. 67, no. 3, p. 5–7.

Youngbaer, P., 2009b, WNS appears in Clover Hollow Cave: D.C. Speleograph, v. 65, no. 2, p. 8.

Youngbaer, P., 2010, White nose syndrome: A second year look at the conservation challenges: NSS News, v. 68, no. 3, p. 24–25.

Zen, E., and Hartshorn, J.H., 1966, Geologic map of the Bashbish Falls Quadrangle, Massachusetts, Connecticut, and New York: U.S. Geological Survey Geologic Quadrangle Map GQ-507 (1:24,000 scale), 1 sheet with 5-page pamphlet.

Zen, E., and Ratcliffe, N.M., 1971, Bedrock geologic map of the Egremont Quadrangle and adjacent areas, Berkshire County, Massachusetts, and Columbia County, New York: U.S. Geological Survey Miscellaneous Geologic Investigations Map I-628 (1:24,000 scale), 1 sheet with 4-page pamphlet.

Zokaites, C., 1995a, Skydusky Hollow Cave System, *in* Zokaites, C., ed., Underground in the Appalachians: A Guidebook for the 1995 Convention of the National Speleological Society: Huntsville, Alabama, National Speleological Society, p. 23–25.

Zokaites, C., ed., 1995b, Underground in the Appalachians: A Guidebook for the 1995 Convention of the National Speleological Society: Huntsville, Alabama, National Speleological Society, 217 p.

K. Spałek and J. Proćków – Karst springs as habitats for rare and protected plant species: a new inland locality of a halophyte plant *Batrachium baudotii* (Ranunculaceae) in a karst spring in Central Europe. *Journal of Cave and Karst Studies,* v. 73, no. 3, p. 158–161. DOI: 10.4311/jcks2010lsc0165

KARST SPRINGS AS HABITATS FOR RARE AND PROTECTED PLANT SPECIES: A NEW INLAND LOCALITY OF A HALOPHYTE PLANT *BATRACHIUM BAUDOTII* (RANUNCULACEAE) IN A KARST SPRING IN CENTRAL EUROPE

Krzysztof Spałek[1] and Jarosław Proćków[2]

Abstract: A new inland locality of *Batrachium baudotii* was discovered in a karst spring in Central Europe; the species had not been reported from such habitats previously. The locality is situated more than 400 km away from the Baltic coast and about 120 km northwest of the only previously known Polish inland locality; both sites are outside its continuous range and are two of the four easternmost in Central Europe. In the eastern part of its range, *Batrachium baudotii* is very rare and is protected or red-listed in these areas. The main goal of this paper is to draw attention to the karst springs' flora, with some interesting and rare species that can be found there. Within the examined patches, no other saline taxa were recorded. The data show that the species prefers habitats in the zone of discharge of karst waters from Jurassic, Cretaceous, and Triassic water-bearing strata. The locality should be especially protected and constantly monitored.

Introduction

Springs are among the most valuable components of the European landscape. Because of their generally small size and marginal economic importance, they are very little studied (Kucharski, 2007). Springs develop a specific vegetation because the subterranean water reaching the surface usually has a relatively constant temperature throughout the year of about 9 °C (Lindacher, 1995; Zarzycki et al., 2002). In Poland, springs harbor many interesting and rare plant species and communities (Kucharski, 2007; Spałek and Horska-Schwarz, 2009; Spałek et al., 2011).

The brackish water-crowfoot (*Batrachium baudotii*) is found in nearly all of Europe, except northern Scandinavia north of 65° N, and in northwestern Africa. It usually occurs along the coast, in salt water, at depths of 0.5 to 1.5 m on sandy and muddy bottoms (Hocquette, 1927; Braun-Blanquet, 1952; Klement, 1953; den Hartog, 1963; Cook, 1966; Westhoff and Held, 1969; Géhu and Mériaux, 1983; Birse, 1984; Wegener, 1991; Passarge, 1992, 1996; Pott, 1995; Schubert et al., 1995; Rodwell, 1998). It is also frequent in estuaries and on islands. In Poland, it is known from a few localities along the Baltic coast (Zając and Zając, 2001). Within the whole of its range, it is very rare in inland fresh waters, found only where the water is stagnant or slow-flowing, usually over a calcareous substratum. A few inland localities are known from France, Austria, Germany, the Czech Republic, Slovakia, and Hungary (Husák et al., 1982; Jasiewicz, 1985; Hultén and Fries, 1986; Husák and Procházka, 1999; Samková, 1999; Holub and Procházka, 2000; Kaplan, 2005, 2008; K. Šumberová and A. Mesterázy, pers. comm.) and, till now, only one isolated locality from Poland, the Będkowska Valley, near Kraków (Jasiewicz, 1985; Zając and Zając, 2001).

It should be pointed out that in the eastern part of its range *Batrachium baudotii* is particularly rare, known only from scattered localities. For this reason, in some countries, including Poland, it is legally protected and is included in the Red List of Plants of Poland with the E category (= CR), i.e. declining—critically endangered (Zarzycki and Szeląg, 2006). It is also very rare and critically endangered in the Czech Republic (Holub and Procházka, 2000), while in Slovakia it is classified as an endangered species (EN) (Feráková et al., 2001). In Hungary, it is a rare species and is included in the NT category, i.e., near threatened (Király, 2007).

In the literature, there are no detailed data on the physical-chemical properties of waters and substrata in the habitats of the species, especially in its inland localities. The knowledge of such parameters is essential for effective protection of its localities (Spałek et al., 2011). At sites in the Czech Republic, the species finds its optimum in lowland flooded sand pits at succession stages in which the water already contains enough nutrients, but is still not too eutrophic and muddy (Samková, 1999; Kaplan, 2005, 2008). The localities are situated within the warmest regions of the Czech Republic, and they are formed by basic bedrocks (K. Šumberová, pers. comm.). In Hungary,

[1] Laboratory of Geobotany & Plant Conservation, Department of Biosystematics, University of Opole, ul. Oleska 22, PL-45-052 Opole, Poland kspalek@uni.opole.pl
[2] Department of Biodiversity & Plant Cover Protection, Institute of Plant Biology, Wrocław University, ul. Kanonia 6/8, PL-50-328 Wrocław, Poland jprockow@biol.uni.wroc.pl

some localities are situated in gravel pits (A. Mesterázy, pers. comm.).

Based on literature data in Great Britain, both saline (*Zannichellia palustris* subsp. *palustris*) and freshwater (*Ceratophyllum submersum*, *Potamogeton pectinatus*, *Ruppia maritima*, *Callitriche stagnalis*, *C. obtusangula*, *C. platycarpa*, *Riccia fluitans*, *Lemna trisulca*, *L. minor*, *L. gibba*, and *Ceratophyllum demersum*) taxa co-occur in patches with *Batrachium baudotii* (Rodwell, 1998). The situation is similar in Germany: *Ruppia cirrhosa*, *Zannichellia palustris* subsp. *pedicellata*, *Potamogeton pectinatus*, and *P. pusillus* (Klement, 1953; Wegener, 1991; Passarge, 1992, 1996; Pott, 1995; Schubert et al., 1995). The main goal of this paper is to draw attention to the karst springs' flora, with some interesting and rare species which can be found there, even including saline taxa (e.g. *Batrachium baudotii*) that had not been reported from such habitats to date.

Methods

The fieldwork was conducted during the growth seasons in 2008–2009. The species names of vascular plants follow Mirek et al. (2002). The physical and chemical properties of the habitat were assessed in the field, when the pH of the water was measured in the spring at depths of 0 to 20 cm and 20 to 70 cm, on March 17, 2008 and June 23, 2009. Measurements of conductivity, water temperature, and O_2 content were taken at the depth of 0 to 20 cm at the spring and at the zone of its flow into the river with a CX 401 Elmetron multipurpose measuring device. Samples of water at the depth of 0 to 70 cm and samples of the bottom sediments were collected from the spring. Laboratory tests included analysis of the water, with measurements of CO_2 content (mg dm^{-3}), general alkalinity (titration), SO_4^{2-} (mg dm^{-3}) (turbidimetric method), NO_3^-, Cl^-, NH_4^+, PO_4^{3-} (mg dm^{-3}) (colorimetric method with a Slandi LF 2004 spectrophotometer). Bottom sediments were also analyzed, with pH measurements of the water extract (potentiometric method used in soil sciences) and $CaCO_3$ content (mg dm^{-3}) (calicimeter-pressure method).

Results and Discussion

During our geobotanical research in Poland, a new inland locality of *Batrachium baudotii* was discovered in a karst spring in the village of Rożniątów near the town of Strzelce Opolskie in Silesia, southwestern Poland (Fig. 1); the species has not been reported from such habitats previously. The site is situated more than 400 km away from the Baltic coast and about 120 km northwest of the only previously-known Polish inland locality, in the Będkowska Valley near Kraków (Fig. 1). So both Polish inland sites of *B. baudotii* are outside its continuous range and are two of the four easternmost in Central Europe. (The more eastern localities are in Slovakia: Chrámec, Ipel'skorimavska brázda, and Bol', Potisí [Husák and Procházka, 1999]).

Figure 1. Inland localities of *Batrachium baudotii* (Ranunculaceae) in Poland (black circle – a new locality in a karst spring in the village Rożniątów, near the town of Strzelce Opolskie, Silesia; black triangle – the previously known Polish inland site in the Będkowska Valley, near Kraków).

The plant covered 0.2 ha in 2008 and 0.3 ha in 2009 (Figs. 2–3). The accompanying taxa were *Callitriche hamulata*, *Veronica beccabunga* f. *submersa*, *Berula erecta* f. *submersa*, *Potamogeton pectinatus*, *Callitriche verna*, and *Lemna minor*. So no saline taxa were found within *Batrachium baudotii* phytocoenoses (Spałek et al., 2011).

The spring in Rożniątów is located in the village center (Assmann, 1929; Staśko, 1984, 1992; Horska-Schwarz and Spałek, 2008). The subterranean waters emerge at an elevation of 231–232 m (Staśko, 1992; Spałek et al., 2011). Waters in the spring zone are characterized by neutral and slightly alkaline pH: the mean pH is within 7.0–7.4. The water temperature is in the range 8.8–11.5 °C. The analyses showed that the water is dominated by the ions HCO_3^-, Ca^{2+} and Mg^{2+}; also confirmed is the presence of SO_4^{2-}, NO_3^-, PO_4^{3-} and Cl^- ions. Based on the total content of dissolved mineral components, the water was classified as moderately mineralized (Spałek et al., 2011). At present, the spring contains fine sediment of slightly alkaline pH (7.5). The sediment at the confluence with the river has a slightly lower pH (6.98). It should be added, however, that during 1986–1988 the bottom was artificially cleaned (Staśko, 1984, 1992). The analysis of the deposits in 2009 showed that they were rich in Ca, Mg, Al, K, and Na. The heavy metals Zn, Mn, Cu, and Cd occurred there in smaller quantities. At the river, the sediments also contain Pb, which was not detected in the spring zone. Detailed results

Figures 2 – 3. *Batrachium baudotii* (*Ranunculus baudotii*) in the karst spring in Rożniątów village.

of laboratory analysis of the water and bottom deposits for the locality are contained in Spałek et al. (2011).

The similar character of subterranean waters in these sites (HCO_3-Ca and natural content of SO_4, associated with the occurrence of intercalation of anhydrite and gypsum in the substratum), shows that the species prefers habitats in the zone of discharge of karst waters from Jurassic, Cretaceous, and Triassic water-bearing levels (Kryza and Staśko, 2000; Macioszczyk and Dobrzyński, 2002; Kryza and Kryza, 2003, 2006; Spałek et al., 2011). However, the absence of localities of this species in other springs of similar chemical composition shows that its occurrence is also affected by an array of other characteristics of the source: bottom morphology, properties of bottom sediments, substratum pH, water temperature, salinity, spring discharge, and the level of human disturbance. It should be pointed out that at present, with such great pressure from the surroundings, the new locality of *Batrachium baudotii* within the spring area in Rożniątów is exposed to considerable stress, and so it should be especially protected and constantly monitored.

ACKNOWLEDGEMENTS

We wish to thank Dr. Richard Hrivnak (Slovak Academy of Sciences, Bratislava), Prof. Stanisław Staśko (Institute of Geological Sciences, Wrocław University), and Dr. Sylwia Horska-Schwarz (Institute of Geography & Regional Development, Wrocław University) for their cooperation, Dr. Attila Mesterázy (Hungary) for making his unpublished data available to us, and Dr. Kateřina Šumberová (Institute of Botany of the Academy of Science of the Czech Republic, Brno) for the floristical and ecological data from Moravia and Bohemia. Special thanks go to Mr. Jason Schock (Department of Applied Linguistics, Institute of English Studies, Wrocław University), who kindly improved our American English.

REFERENCES

Assmann, P., 1929, Über die Enstehung der Quelle des Rosniontauer Wasser un der sogenanten Quelle von Suchau: Naturkundl, Kolonowska, Basteine aus Osterschlesien.

Birse, E.L., 1984, Phytocoenonia of Scotland: Additions and Revisions, Aberdeen, Macaulay Institute for Soil Research.

Braun-Blanquet, J., 1952, Les Groupements Végétaux de la France Méditerranéenne, Vaison-la-Romaine, Macabet frères.

Cook, C.D.K., 1966, A monographic study of *Ranunculus* subgenus *Batrachium* (DC) A. Gray.: Mitteilung Bototanik Staatssammlung München, v. 6, p. 47–237.

Den Hartog, C., 1963, Enige waterplantengemeenschappen in Zeeland: Gorteria, v. 1, p. 155–164.

Feráková, V., Maglocký, Š., and Marhold, K., 2001, Červený zoznam papraďorastov a semenných rastlín Slovenska (December 2001): Ochrana Prírody, v. 20 (suppl.), p. 44–77. Banská Bystrica.

Géhu, J.-M., and Mériaux, J.-L., 1983, Distribution et synécologie des renoncule du sous-genre *Batrachium* dans le nord de la France: Colloques Phytosociologiques, v. 18, p. 122–166.

Hocquette, M., 1927, Étude sur la végétation et la flore du littoral de la mer du Nord de Nieuport à Sangatte: Archives de Botanique, v. 1, no. 4, p. 1–179.

Holub, J., and Procházka, F., 2000, Red List of vascular plants of the Czech Republic – 2000: Preslia, v. 72, no. 2–4, p. 187–230.

Horska-Schwarz, S., and Spałek, K., 2008, Charakterystyka wybranych źródeł Śląska Opolskiego [A characteristic of selected springs in Opole Silesia], *in* Chmielewski, T.J., ed., Struktura i funkcjonowanie systemów krajobrazowych: meta-analizy, modele, teorie i ich zastosowania [Structure and Function of Landscape Systems: Meta-analyses, Models, Theories and Their Applications], Lublin, Wydawnictwo Print 6, Problemy Ekologii Krajobrazu [Problems of Landscape Ecology], no. 21, p. 311–318.

Hultén, E., and Fries, M., 1986, Atlas of North European Vascular Plants: North of the Tropic of Cancer, Königstein, Koeltz Scientific Books.

Husák, Š., and Procházka, F., 1999, *Batrachium baudotii* (Godron) F.W. Schultz, *in* Čeřovský, J., Feráková, V., Holub, J., Maglocký, Š., and Procházka, F., eds., Červená kniha ohrožených a vzácnych druhov rastlín a živočíchov SR a ČR 5: Vyššie rastliny, Bratislava, Príroda, 53 p.

Husák, Š., Slavík, B., and Futák, J., 1982, *Batrachium* (DC) S.F. Gray, *in* Futák, J., and Bertová, L., eds., Flóra Slovenska III, Bratislava, Veda, p. 197–214.

Jasiewicz, A., ed., 1985, Flora Polski 4: Rośliny naczyniowe. Dwuliścienne, Wolnopłatkowe – Dwuokwiatowe [Flora of Poland 4: Vascular Plants, Dicotyledones], 2nd edition, Warszawa-Kraków, PWN-PAN, Instytut Botaniki.

Kaplan, Z., 2005, *Batrachium baudotii* (Godr.) F. W. Schultz, *in* Hadinec, J., Lustyk, P., and Procházka, F., eds., Additamenta ad floram Reipublicae Bohemicae. IV. [Additions to the flora of the Czech Republic. IV], Praha, Zprávy České Botanické Společnosti, v. 40, p. 77–149.

Kaplan, Z., 2008, *Batrachium baudotii* (Godr.) F. W. Schultz *in* Hadinec, J., and Lustyk, P., eds., Additamenta ad floram Reipublicae Bohemicae. VII. [Additions to the flora of the Czech Republic. VII], Praha, Zprávy České Botanické Společnosti, v. 43, p. 251–336.

Király, G., ed., 2007, Vörös Lista: A magyarországi edényes flóra veszélyeztetett fajai. [Red list of the vascular flora of Hungary], Sopron, Saját kiadás, 73 p.

Klement, O., 1953, Die Vegetation der Nordseeinsel Wangerooge: Veröffentlichungen aus dem Instituts Meeresforschung, Bremerhaven, v. 2, p. 279–379.

Kryza, H., and Kryza, J., 2003, Ocena wpływu ognisk zanieczyszczeń na jakość wód podziemnych w rejonie Strzelec Opolskich [Assessment of the impact of contamination on quality of underground waters within Strzelce Opolskie area]: Współczesne Problemy Hydrogeologii, v. 11, p. 431–439.

Kryza, H., and Kryza, J., 2006, The analytic and model estimation of the direct groundwater inflow to Baltic Sea on the territory of Poland: Geologos, v. 10, p. 153–165.

Kryza, J., and Staśko, S., 2000, Groundwater Flow Rate and Contaminant Migration in Fissure-Karstic Aquifer of Opole Triassic System Southwest Poland: Environmental Geology, v. 39, no. 3–4, p. 384–389. doi: 10.1007/s002540050018.

Kucharski, L., 2007, Flora źródlisk – skład i gatunki wskaźnikowe [Flora of springs – a composition and diagnostic species], *in* Jokiel, P., Moniewski, P., and Ziułkiewicz, M., eds., Źródła Polski. Wybrane problemy krenologiczne [Springs of Poland. Crenological Selected Problems], Łódź, Wydział Nauk Geograficznych Uniwersytetu Łódzkiego, p. 62–68.

Lindacher, R., 1995, Phanart. Datebank der Gefässpflanzen Mitteleuropas. Erklärung der Kennzahlen, Aufbau und Inhalt, Zurich, Veröffentlichungen des Geobotanischen Institutes der ETH, Stiftung Rübel, no. 125, 436 p.

Macioszczyk, A., and Dobrzyński, D., 2002, Hydrogeologia strefy aktywnej wymiany wód podziemnych [Hydrogeology of the area of active exchange of underground waters], Warsaw, Wydawnictwo Naukowe PWN, 448 p.

Mirek, Z., Piękoś-Mirkowa, H., Zając, A., and Zając, M., eds., 2002, Flowering Plants and Pteridophytes of Poland – a Checklist: Biodiversity of Poland, v. 1, p. 1–442. Kraków, W. Szafer Insitute of Botany, Polish Academy of Sciences, Biodiversity of Poland no. 1, 442 p.

Passarge, H., 1992, Mitteleuropäische Potamogetonetea I: Phytocoenologia, v. 20, p. 489–527.

Passarge, H., 1996, Pflanzengesellschaften Nordostdeutschlands. I. Hydro- und Therophytosa, Berlin, J. Cramer, 298 p.

Pott, R., 1995, Die Pflanzengesellschaften Deutschlands, 2 Aufl., Stuttgart, Verl. E. Ulmer, 622 p.

Rodwell, J.S., ed., 1998, British Plant Communities. Vol. 4. Aquatic Communities, Swamps and Tall-Herb Fens, Cambridge University Press, 296 p.

Samková, V., 1999, Příspěvek k rozšíření některých vzácných a ohrožených druhů rostlin ve východních Čechách [Distribution data on some rare and endangered plant species in the eastern part of the Czech Republic]: Acta musei Reginaehradecensis ser. A, v. 27, p. 19–74.

Schubert, R., Hilbig, W., and Klotz, S., 1995, Bestimmungsbuch der Pflanzengesellschaften Mittel- und Nordostdeutschlands, Heidelberg, Spektrum Akademischer Verlag, 403 p.

Spałek, K., and Horska-Schwarz, S., 2009, *Veronico beccabungae-Callitrichetum stagnalis* (Oberd. 1957) Müller 1962, a plant association new to Poland – quality of habitat: Acta Societatis Botanicorum Poloniae, v. 78, no. 4, p. 345–349.

Spałek, K., Proćków, J., Staśko, S., and Horska-Schwarz, S., 2011, Preliminary study of the unusual properties in the habitat of *Ranuculetum baudotii* in central Europe: Central European Journal of Biology, v.6 no.4, p. 632–638.

Staśko, S., 1984, Charakterystyka hydrogeologiczna wybranych źródeł Śląska Opolskiego [Hydrogeological characteristic of selected springs of Opole Silesia]: Materiały i Studia Opolskie, v. 26, no. 52–53, p. 277–298.

Staśko, S., 1992, Wody podziemne w węglanowych utworach triasu opolskiego [Underground waters in carbonate formation of Opole Triassic], Prace geologiczno-mineralogiczne, no. 32, 71 p.

Wegener, K.-A., 1991, Pflanzengesellschaften an der Südküste des Greifswalder Boddens: Gleditschia, v. 19, p. 259–288.

Westhoff, V., and den Held, A.J., 1969, Plantengemeenschappen in Nederland, Zutphen, Thieme.

Zając, A., and Zając, M., eds., 2001, Atlas rozmieszczenia roślin naczyniowych w Polsce. Distribution Atlas of Vascular Plants in Poland, Kraków, Laboratory of Computer Chorology, Institute of Botany, Jagiellonian University, 715 p.

Zarzycki, K., and Szeląg, Z., 2006, Red list of the vascular plants in Poland. Czerwona lista roślin naczyniowych w Polsce, *in* Mirek, Z., Zarzycki, K., Wojewoda, W., and Szeląg, Z., eds., Red list of plants and fungi in Poland. Czerwona lista roślin i grzybów Polski, Kraków, W. Szafer Institute of Botany, Polish Academy of Sciences, p. 9–20.

Zarzycki, K., Trzcińska-Tacik, H., Różański, W., Szeląg, Z., Wołek, J., and Korzeniak, U., 2002, Ecological indicator values of vascular plants of Poland, W. Szafer Insitute of Botany, Polish Academy of Sciences, Biodiversity of Poland no. 2, 183 p.

C.R. Harington – Quaternary cave faunas of Canada: a review of the vertebrate remains. *Journal of Cave and Karst Studies,* v. 73, no. 3, p. 162–180. DOI: 10.4311/jcks2009pa128

QUATERNARY CAVE FAUNAS OF CANADA: A REVIEW OF THE VERTEBRATE REMAINS

C.R. Harington
Canadian Museum of Nature (Paleobiology), Ottawa K1P 6P4 Canada, dharington@mus-nature.ca

Abstract: Highlights of ice-age vertebrate faunas from Canadian caves are presented in geographic order (east to west). They include four each from Quebec and Ontario; three from Alberta; one from Yukon; and ten from British Columbia. Localities, vertebrate species represented, radiocarbon ages, and paleoenvironmental evidence are mentioned where available, as well as pertinent references. Of these caves, perhaps Bluefish Caves, Yukon, are most significant, because they contain evidence for the earliest people in North America. Tables provide lists of species and radiocarbon ages from each site.

Introduction

Although some cave faunas from the United States and Mexico are dealt with in the book *Ice Age Cave Faunas of North America* (Schubert et al., 2003), no Canadian cave faunas are mentioned. To help broaden that perspective, highlights of twenty-two Quaternary vertebrate faunas from Canadian caves (Fig. 1) are summarized here, progressing geographically from east to west. This paper developed from a review of the 2003 book (Harington, 2006).

It is important to study vertebrate faunal remains from Canadian caves for several reasons. Specimens often preserve well in a stratified sedimentary context, allowing a better understanding of the environments occupied by various animals represented. If such strata are sufficiently deep and discrete (bioturbation and cryoturbation can cause problems), they help us understand how climate, environment, and fauna have changed through time, such as across the Pleistocene/Holocene boundary finely recorded at Bluefish and Charlie Lake caves. Furthermore, Canada has been subject to particularly heavy, multiple glaciations in the Quaternary that have greatly disturbed fossil sites on open terrain, with fragmenting of fossil bones. So it is valuable to have pockets such as caves, fissures, and rock shelters in upland areas from coast to coast that can preserve long faunal and environmental records. It is especially valuable to have microfaunal remains, including fragile bones of ecologically-sensistive fish, amphibians, reptiles, and rodents, often well-preserved in quiet cave surroundings that are available for study.

Apart from presenting highlights of the cave faunas and their importance to Canadian Quaternary studies, generally, the purpose of this paper is to list the taxa in each vertebrate fauna and provide radiocarbon ages for them (Tables 1 and 2), as well as illustrating some of the caves.

Localities

Quebec

Caves near Saint-Elzéar and La Rédemption in the Gaspésie region, as well as Mine and Laflèche caves in Gatineau, have yielded fascinating glimpses of Québec's Quaternary faunas (for summaries see Beaupré and Caron, 1986; and Harington, 2003a; Fig. 1a).

Saint-Elzéar Cave (48°14′20″N, 65°21′30″W), situated on a plateau north of Baie des Chaleurs, has produced remains of three species of amphibians, one species of reptile, four species of birds, and thirty-four species of mammals. About 80% of nearly 4,700 fossils are fragments of small mammals. Several species no longer live in the region, and a period of colder climate seems to be indicated by the presence of some of them, such as the arctic shrew *Sorex arcticus*, the arctic hare *Lepus arcticus*, the western heather vole *Phenacomys intermedius*, the Ungava collared lemming *Dicrostonyx hudsonius*, and the least weasel *Mustela nivalis*. Due to soil chemistry, the bones seem unsuitable for radiocarbon dating (LaSalle, 1984; LaSalle and Guilday, 1980). However, a few of the cold-adapted species might be sampled for AMS radiocarbon dating, because they are likely to be relatively old.

Preliminary collections of faunal remains from sediments in caves near La Rédemption (Trou Otis and Spéos de la Fée; 48°27′N, 67°50′W) yielded seven mammal species: Keen's bat *Myotis keenii*, the Ungava lemming, the North American porcupine *Erethizon dorsatum*, the red fox *Vulpes vulpes*, the brown bear *Ursus arctos*, the caribou *Rangifer tarandus*, and the moose *Alces alces*). The lemming and brown bear are of great interest because of their rarity in the faunal record of eastern North America. I postulated that they occupied Gaspésie when patches of tundra-like habitat existed there, perhaps in early postglacial time (Harington, 1980). A radiocarbon date on the bear specimen did not yield conclusive information.

Located some 20 km northeast of Ottawa, Mine Cave (45°28′18″N, 75°51′01″W; Fig. 2) is a natural trap that has accumulated many bones and teeth that are useful for paleoecological reconstruction. It lies on the Eardley Escarpment within the limits of Gatineau Park. The upper 100 cm of the infill, containing relatively recent fauna dating back to about 5,000 B.P. (radiocarbon years before present, taken as 1950), is characterized by the American black bear *Ursus americanus*, the white-

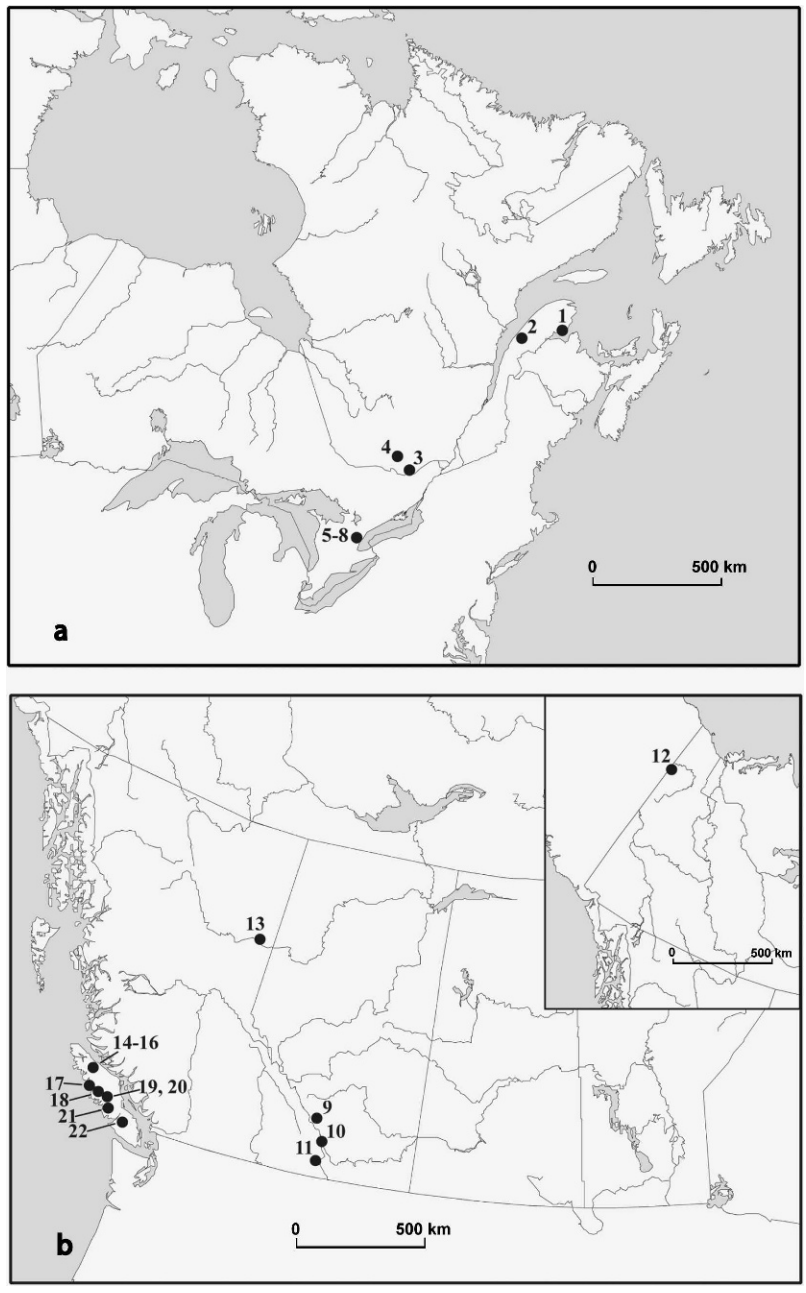

Figure 1. Maps showing sites of most important Quaternary vertebrate faunas in Canadian caves. (a) Eastern Canada. Quebec: 1 Saint-Elzéar Cave, 2 La Rédemption caves (Trou Otis, Spéos-de-la-Fée), 3 Mine Cave, 4 Laflèche Cave. Ontario: 5 Elba Cave, 6 Kelso Cave, 7 Mt. Nemo Cave, 8 Dickson Cave. (b) Western Canada. Alberta: 9 Rats Nest Cave, 10 January Cave, 11 Eagle Cave. Yukon (inset): 12 Bluefish Caves. British Columbia: 13 Charlie Lake Cave, 14 Resonance Cave, 15 Pellucidar I Cave, 16 Pellucidar II Cave, 17 Port Eliza Cave, 18 Windy Link Pot Cave, 19 Mariner Mountain Cave, 20 Golden Hinde Cave, 21 Clayoquot Plateau Cave, 22 Limestone Mountain Cave.

tailed deer *Odocoileus virginianus*, the raccoon *Procyon lotor*, the deer mouse *Peromyscus* sp., and the big brown bat *Eptesicus fuscus* (Carrier, 1989). The bottom 70 cm of infill dates between 8,230 ± 80 and 5,020 ± 70 B.P., and it contains remains of amphibians, reptiles (snakes), and twenty-three species of mammals, but no black bear or deer. Two species, the woodland vole *Microtus pinetorum* and the Ungava lemming, no longer occupy the area. The former is found mainly in the eastern United States, whereas the latter occurs in northern Québec and Labrador, suggesting Holocene range shifts to the south and north, respectively. Most small mammals from the lower infill consist of boreal species (Lauriol et al., 2003).

Laflèche Cave (45°39′00″N, 75°46′48″W) is about 27 km north of Gatineau (formerly Hull). Upper and lower levels are joined by an 18 m vertical shaft. Sandy matrix up to 80 cm deep near the lower (man-made) entrance has yielded four birds and twenty-one species of mammals (Harington, 2003). Several arctic-adapted species are represented in this fauna, such as the snowy owl *Nyctea scandiaca*, the arctic hare, the arctic fox *Alopex lagopus*, and the Ungava lemming, suggesting the presence of tundra-like conditions following the retreat of Laurentide ice from the region in late glacial time. Indeed, an arctic fox mandible yielded a date of 10,800 ± 90 B.P.; an unidentified bone yielded a comparable date of 9,310 ± 80 B.P. It is worth noting that such species retreated northward with the melting Laurentide Ice Sheet, and at present, they survive in northernmost Quebec and Labrador. Perhaps the archaeological and historical evidence for brown bears (*Ursus arctos*) in Labrador and northern Quebec fits this hypothesis, too (Pigott, 1999).

ONTARIO

Four caves worth mentioning in Ontario (Fig. 1a) are Elba, Kelso, Mt. Nemo, and Dickson. Faunal remains for each were summarized by Churcher and Karrow (2008, Table 1). They are situated on the Niagara Escarpment. Elba Cave (44°01′N, 80°10′W) is a fissure deposit in Mono Cliffs Provincial Park in south-central Ontario. The entrance is vertical. Howard Savage (1994) and crew collected 625 bones of twenty mammalian species from various ledges. Eighteen of the twenty taxa are typical of the present-day fauna of the region. Only two, the pika *Ochotona* sp. and the American marten *Martes americana* (locally exterminated in the early 1900s), are not part of the current local community. In such crevice or fissure faunas, the crevices open and close because of karstic solution, rock movement, or infilling by calcium carbonate dripstone (Karrow, 2005), allowing animal remains to be deposited there at more than one time. Thus a single large (extinct giant?) pika femur from a ledge 25 m below the surface in Elba Cave was AMS dated at 8,670 ± 220 B.P., and an American marten skull from that cave yielded a date of 510 ± 60 B.P.

Remains of vertebrates were found in a travertine-cemented dolomite breccia from a demolished cave (Kelso Cave; 43°30′N, 70°55′W) in the Niagara Escarpment west of Milton, Ontario. They represent the American toad *Bufo americanus*, the spruce grouse *Canachites canadensis* or the ruffed grouse *Bonasa umbellus*, the snowshoe hare *Lepus americanus*, the eastern cottontail *Sylvilagus floridanus*, the giant pika, the woodland deer mouse *Peromyscus maniculatus*, the muskrat *Ondatra zibethicus*, the little brown bat *Myotis lucifugus*, and the striped skunk *Mephitis mephitis*. Pollen remains from the matrix with the extinct giant pika *Ochotona whartoni* bone suggest an age of about 10,000 years. Therefore, Mead and Grady (1996) suggest that the giant pika lived, possibly relictually, in southern Ontario into the Early Holocene.

Mt. Nemo Cave was the first of these crevice caves reported (Bateman, 1961). Its fauna consists of two species of bats, the North American beaver *Castor canadensis*, and the white-tailed deer. Because of the cave's elevation, the last two species may have been introduced by a predator that denned in it (Churcher and Karrow, 2008).

The fauna of Dickson Cave, situated in the Niagara Escarpment north of Mt. Nemo, consists of the painted turtle *Chrysemys picta*, the northern short-tailed shrew *Blarina brevicauda*, the smoky shrew *Sorex fumeus*, the big brown bat, the long-eared bat, the southern red-backed vole *Myodes* (*Clethrionomys*) *gapperi*, the meadow vole *Microtus pennsylvanicus*, the red squirrel *Tamiasciurus hudsonicus*, the woodland deer mouse, the muskrat, and the wapiti *Cervus elaphus*. The fauna is considered to be older than AD 1750 based on the presence of wapiti (Churcher and Fenton, 1968; Churcher and Karrow, 2008).

ALBERTA

In Alberta (Fig. 1b), the faunal remains from January and Eagle caves are best known. January Cave (50°11′N, 114°31′W), at an elevation of 2,040 m, is located on Plateau Mountain in the Front Range of the Rocky Mountains, and is about 100 km southeast of Calgary (Fig. 3). The six most common vertebrate remains represented in the cave are the pika, the hoary marmot *Marmota caligata*, the Columbian ground squirrel *Spermophilus columbianus*, the bushy-tailed wood rat *Neotoma cinerea*, the long-tailed vole *Microtus longicaudus*, the deer mouse, and the arctic grayling *Thymallus arcticus*. A shrew *Sorex* sp., a hare *Lepus* sp., the northern pocket gopher *Thomomys talpoides*, several small carnivores, and the bighorn sheep *Ovis canadensis* are also represented. Roughly 90% of all identified fossils are rodents; probably most were derived from raptor pellets and carnivore droppings. Four exotic species (brown lemming *Lemmus sibiricus*, collared lemming *Dicrostonyx torquatus*, Niobrara prairie dog *Cynomys* cf. *C. niobrarius*, and black-footed ferret *Mustela nigripes*) were identified. The lemmings, presently occupying northern Canada, and the ferret and prairie dog, characteristic of a more southern range in the United States plains, were found together, and radiocarbon dates on bone of mixed species extend from about 33,000 to 23,000 B.P., so probably the fauna represents a cool, dry mid-Wisconsin interstadial (Burns, 1991, 2002).

Eagle Cave (49°38′N, 114°38′W) is situated about 10 km west of Coleman, Alberta, at an elevation of 1,377 m in Crowsnest Pass. Like January Cave, the sediments were deposited during the mid-Wisconsin (more than 33,000 to 23,000 B.P.). The northern pocket gopher *Thomomys talpoides* and the water vole *Microtus richardsoni* are perhaps the most interesting species in the fauna. The water vole fossil is the oldest known of the species, and its presence in southwestern Alberta suggests equable climatic conditions during the mid-Wisconsin. The pocket gopher is

Table 1. Quaternary cave faunas of Canada: vertebrate taxa from selected localities.

	Localities[a]																					
Cave Faunas	1	2	3	4	5	6	7	8	9	10	11	12	13	14	15	16	17	18	19	20	21	22
Fishes	…	…	…	…	…	…	…	…	x	…	x	x	x	…	…	…	x	…	x	…	…	…
Arctic grayling (*Thymallus arcticus*)	…	…	…	…	…	…	…	…	x	…	…	x	…	…	…	…	…	…	…	…	…	…
Longnose sucker (*Catostomus catostomus*)	…	…	…	…	…	…	…	…	…	…	…	x	cf	…	…	…	…	…	…	…	…	…
Inconnu (*Stenodus leucichthys*)	…	…	…	…	…	…	…	…	…	…	…	cf	…	…	…	…	…	…	…	…	…	…
Northern pike (*Esox lucius*)	…	…	…	…	…	…	…	…	…	…	…	x	…	…	…	…	…	…	…	…	…	…
Salmon (*Onchorhynchus* sp.)	…	…	…	…	…	…	…	…	…	…	…	…	…	…	…	…	x	…	…	…	…	…
Cuthroat trout (*Onchorhynchus clarkii*)	…	…	…	…	…	…	…	…	…	…	…	…	…	…	…	…	cf	…	…	…	…	…
Greenling (Hexagrammidae)	…	…	…	…	…	…	…	…	…	…	…	…	…	…	…	…	x	…	…	…	…	…
Alaska pollock (*Theragra chalcogramma*)	…	…	…	…	…	…	…	…	…	…	…	…	…	…	…	…	x	…	…	…	…	…
Flatfish (Pleuronectiformes)	…	…	…	…	…	…	…	…	…	…	…	…	…	…	…	…	x	…	…	…	…	…
Irish lord (*Hemilepidotus* sp.)	…	…	…	…	…	…	…	…	…	…	…	…	…	…	…	…	x	…	…	…	…	…
Sculpin (Cottidae)	…	…	…	…	…	…	…	…	…	…	…	…	…	…	…	…	cf	…	…	…	…	…
Pacific tomcod (*Microgadus proximus*)	…	…	…	…	…	…	…	…	…	…	…	…	…	…	…	…	x	…	…	…	…	…
Three-spined stickleback (*Gasterostens aculeatus*)	…	…	…	…	…	…	…	…	…	…	…	…	…	…	…	…	cf	…	…	…	…	…
Amphibians	x	…	x	…	x	x	…	…	…	…	x	x	x	…	…	x	x	…	…	…	…	…
Blue-spotted salamander (*Ambystoma laterale*)	x	…	…	…	…	…	…	…	…	…	…	…	…	…	…	…	…	…	…	…	…	…
American toad (*Bufo americanus*)	x	…	x	…	x	x	…	…	…	…	…	…	…	…	…	…	…	…	…	…	…	…
Western toad (*Bufo boreas*)	…	…	…	…	…	…	…	…	…	…	…	…	…	…	…	…	x	…	…	…	…	…
Toad (*Bufo* sp.)	…	…	…	…	…	…	…	…	…	…	…	…	…	…	…	x	…	…	…	…	…	…
Woodfrog (*Rana palustris*)	x	…	…	…	…	…	…	…	…	…	…	…	…	…	…	…	…	…	…	…	…	…
Bullfrog (*Rana catesbiana*)	…	…	…	…	…	…	…	…	…	…	…	…	…	…	…	…	…	…	…	…	…	…
Frog (*Rana* sp.)	…	…	…	…	…	…	…	…	…	…	…	…	…	…	…	…	…	…	…	…	…	…
Frogs (Anura)	…	…	…	…	…	…	…	…	…	…	…	x	…	…	…	…	…	…	…	…	…	…
Reptiles	…	…	x	…	…	…	…	x	…	…	x	…	x	…	…	x	…	…	…	…	…	…
Snakes (Serpentes)	…	…	x	…	…	…	…	…	…	…	x	…	x	…	…	x	…	…	…	…	…	…
Painted turtle (*Chrysemys picta*)	…	…	…	…	…	…	…	x	…	…	…	…	…	…	…	…	…	…	…	…	…	…
Birds	x	…		x	x	x	…	…	…	x	x	x	x	…	…	x	x	…	x	…	…	…
Red-throated loon (*Gavia stellata*)	…	…	…	…	…	…	…	…	…	…	…	…	…	…	…	…	cf	…	…	…	…	…
Western grebe (*Aechmophorus occidentalis*)	…	…	…	…	…	…	…	…	…	x	…	…	x	…	…	…	…	…	…	…	…	…
Red-necked grebe (*Podiceps grisegena*)	…	…	…	…	…	…	…	…	…	x	…	…	x	…	…	…	…	…	…	…	…	…
Horned grebe (*Podiceps auritus*)	…	…	…	…	…	…	…	…	…	x	…	…	…	…	…	…	…	…	…	…	…	…
Eared grebe (*Podiceps negricollis*)	…	…	…	…	…	…	…	…	…	x	…	…	x	…	…	…	…	…	…	…	…	…
Grebe (Podicepedidae)	…	…	…	…	…	…	…	…	…	x	…	…	…	…	…	…	…	…	…	…	…	…
Double-crested cormorant (*Phalacrocorax auritus*)	…	…	…	…	…	…	…	…	…	…	…	…	x	…	…	…	…	…	…	…	…	…
Cormorant (*Phalacrocorax* sp.)	…	…	…	…	…	…	…	…	…	…	…	…	…	…	…	…	cf	…	…	…	…	…
Swan (Cygnini)	…	…	…	…	…	…	…	…	…	…	…	…	x	…	…	…	…	…	…	…	…	…
Canada goose (*Branta canadensis*)	…	…	…	x	…	…	…	…	…	x	…	…	…	…	…	…	…	…	…	…	…	…
Snow goose (*Chen caerulescens*)	…	…	…	…	…	…	…	…	…	…	…	x	…	…	…	…	…	…	…	…	…	…
Geese (Anserini)	…	…	…	…	…	…	…	…	…	…	…	…	x	…	…	…	…	…	…	…	…	…
Mallard (*Anas platyrhynchos*)	…	…	…	…	…	…	…	…	…	x	…	…	x	…	…	…	…	…	…	…	…	…

Table 1. Continued.

Cave Faunas	Localities[a]																					
	1	2	3	4	5	6	7	8	9	10	11	12	13	14	15	16	17	18	19	20	21	22
American widgeon (*Anas americana*)	…	…	…	…	…	…	…	…	…	…	…	x	…	…	…	…	…	…	…	…	…	…
Green-winged teal (*Anas creca*)	…	…	…	…	…	…	…	…	…	…	…	…	x	…	…	…	…	…	…	…	…	…
Small duck (*Anas* sp.)	…	…	…	…	…	…	…	…	…	…	…	…	…	…	…	…	cf	…	…	…	…	…
Surface-feeding ducks (Anatini)	…	…	…	…	…	…	…	…	…	…	…	…	x	…	…	…	…	…	…	…	…	…
Diving ducks (Aythyini)	…	…	…	…	…	…	…	…	…	…	…	…	x	…	…	…	…	…	…	…	…	…
Common goldeneye (*Bucephala clangula*)	…	…	…	…	…	…	…	…	…	x	…	…	…	…	…	…	…	…	…	…	…	…
Goldeneye (*Bucephala* sp.)	…	…	…	…	…	…	…	…	…	…	…	…	x	…	…	…	…	…	…	…	…	…
Harlequin duck (*Histrionicus histrionicus*)	…	…	…	…	…	…	…	…	…	x	…	x	…	…	…	…	…	…	…	…	…	…
White-winged scoter (*Melanitta fusca*)	…	…	…	…	…	…	…	…	…	x	…	…	x	…	…	…	…	…	…	…	…	…
Ruddy duck (*Oxyura jamaicensis*)	…	…	…	…	…	…	…	…	…	…	…	…	x	…	…	…	…	…	…	…	…	…
Hooded merganser (*Lophodytes cucullatus*)	…	…	…	…	…	…	…	…	…	x	…	…	x	…	…	…	…	…	…	…	…	…
Large merganser (*Mergus* sp.)	…	…	…	…	…	…	…	…	…	…	…	…	x	…	…	…	…	…	…	…	…	…
Swans, geese, ducks (Anatidae)	…	…	…	…	…	…	…	…	…	x	…	…	…	…	…	…	…	…	…	…	…	…
Cooper's hawk (*Accipter cooperi*)	…	…	…	…	…	…	…	…	…	x	…	…	…	…	…	…	…	…	…	…	…	…
Red-tailed hawk (*Buteo jamaicensis*)	…	…	…	…	…	…	…	…	…	cf	…	x	…	…	…	…	…	…	…	…	…	…
Hawk (*Buteo* sp.)	…	…	…	…	…	…	…	…	…	…	…	…	…	…	…	x	…	…	…	…	…	…
Hawks and falcons (Falconiformes)	…	…	…	…	…	…	…	…	…	…	…	…	x	…	…	…	…	…	…	…	…	…
Ruffed grouse (*Bonasa umbellus*)	…	…	…	…	x	…	…	…	…	x	…	…	…	…	…	…	…	…	…	…	…	…
Spruce grouse or Ruffed Grouse (*Canachites canadensis* or *Bonasa umbellus*)	…	…	…	…	…	x	…	…	…	…	…	…	…	…	…	…	…	…	…	…	…	…
Sharp-tailed grouse (*Pediocetes phasianellus*)	…	…	…	…	…	…	…	…	…	x	…	…	…	…	…	…	…	…	…	…	…	…
Ptarmigan or grouse (Tetraonidae)	…	…	…	…	…	…	…	…	…	x	…	x	x	…	…	…	…	…	…	…	…	…
Blue grouse (*Dendragrapus obscurus*)	…	…	…	…	…	…	…	…	…	x	…	…	…	…	…	x	…	…	…	…	…	…
Spruce grouse (*Canachites canadensis*)	…	…	…	…	…	…	…	…	…	x	…	…	…	…	…	…	…	…	…	…	…	…
Partridge or pheasant or grouse (Phasianiidae)	…	…	…	x	…	…	…	…	…	…	…	…	…	…	…	…	…	…	…	…	…	…
Virginia rail or Sora (Rallidae)	…	…	…	…	…	…	…	…	…	…	…	…	x	…	…	…	…	…	…	…	…	…
Ameircan coot (*Fulica americana*)	…	…	…	…	…	…	…	…	…	…	…	…	x	…	…	…	…	…	…	…	…	…
Small wader (Charadriiformes)	…	…	…	…	…	…	…	…	…	…	…	…	x	…	…	…	…	…	…	…	…	…
American golden plover (*Pluvialis dominica/fulva*)	…	…	…	…	…	…	…	…	…	…	…	x	…	…	…	…	…	…	…	…	…	…
Black-bellied plover (*Pluvialis squatarola*)	…	…	…	…	…	…	…	…	…	…	…	x	…	…	…	…	…	…	…	…	…	…
Willet (*Catoptrophorus semipalmatus*)	…	…	…	…	…	…	…	…	…	cf	…	…	…	…	…	…	…	…	…	…	…	…
Eskimo curlew (*Numenius borealis*)	…	…	…	…	…	…	…	…	…	…	…	cf	…	…	…	…	…	…	…	…	…	…
Solitary sandpiper (*Tringa solitaria*)	…	…	…	…	…	…	…	…	…	…	…	cf	…	…	…	…	…	…	…	…	…	…
Small Sandpiper (*Calidris* sp.)	…	…	…	…	…	…	…	…	…	…	…	x	…	…	…	…	…	…	…	…	…	…
Small gull (*Larus* sp.)	…	…	…	…	…	…	…	…	…	…	…	…	x	…	…	…	…	…	…	…	…	…
Small alcid (Alcidae)	…	…	…	…	…	…	…	…	…	…	…	…	…	…	…	…	x	…	…	…	…	…
Passenger pigeon (*Ectopistes migratorius*)[b]	…	…	…	…	…	…	…	…	…	x	…	…	x	…	…	…	…	…	…	…	…	…
Short-eared owl (*Asio flammeus*)	…	…	…	…	…	…	…	…	…	…	…	…	x	…	…	…	…	…	…	…	…	…
Hawk owl (*Surnia ulula*)	…	…	…	-	…	…	…	…	…	-	…	x	x	…	…	…	…	…	…	…	…	…

Table 1. Continued.

Cave Faunas	Localities[a]																					
	1	2	3	4	5	6	7	8	9	10	11	12	13	14	15	16	17	18	19	20	21	22
Snowy owl (*Nyctea scandiaca*)	…	…	…	x	…	…	…	…	…	-	…	x	-	…	…	…	…	…	…	…	…	…
Owls (Strigiformes)	…	…	…	…	…	…	…	…	…	x	…	…	x	…	…	…	…	…	…	…	…	…
Belted kingfisher (*Ceryle alcyon*)	…	…	…	…	…	…	…	…	…	…	…	…	x	…	…	…	…	…	…	…	…	…
Hairy woodpecker (*Dendrocopos villosus*)	…	…	…	…	…	…	…	…	…	x	…	…	…	…	…	…	…	…	…	…	…	…
Woodpecker (Picidae)	…	…	…	…	…	…	…	…	…	…	…	…	x	…	…	…	…	…	…	…	…	…
Say's phoebe (*Sayornis saya*)	…	…	…	…	…	…	…	…	…	…	…	cf	…	…	…	…	…	…	…	…	…	…
Olive-sided flycatcher (*Contopus contopus*)	…	…	…	…	…	…	…	…	…	…	…	cf	…	…	…	…	…	…	…	…	…	…
Barn swallow (*Hirundo rustica*)	…	…	…	…	…	…	…	…	…	cf	…	…	cf	…	…	…	…	…	…	…	…	…
Cliff Swallow (*Hirundo pyrrhonota*)	…	…	…	…	…	…	…	…	…	cf	…	…	cf	…	…	…	…	…	…	…	…	…
Swallows (Hirundinidae)	…	…	…	x	…	…	…	…	…	…	…	x	…	…	…	…	…	…	…	…	…	…
Horned lark (*Eromophila alpestris*)	…	…	…	…	…	…	…	…	…	…	…	…	…	…	…	…	cf	…	…	…	…	…
Blue jay (*Cyanocitta cristata*)	x	…	…	…	…	…	…	…	…	…	…	…	…	…	…	…	…	…	…	…	…	…
Black-billed magpie (*Pica pica*)	…	…	…	…	…	…	…	…	…	x	…	…	…	…	…	…	…	…	…	…	…	…
Clark's nutcracker (*Nucifraga columbina*)	…	…	…	…	…	…	…	…	…	x	…	…	…	…	…	…	…	…	…	…	…	…
Common raven (*Corvus corax*)	…	…	…	…	…	…	…	…	…	…	…	x	x	…	…	…	…	…	…	…	…	…
Chickadee (*Parus* sp.)	…	…	…	…	…	…	…	…	…	…	…	x	…	…	…	…	…	…	…	…	…	…
Red-breasted nuthatch (*Sitta canadensis*)	x	…	…	…	…	…	…	…	…	…	…	…	…	…	…	…	…	…	…	…	…	…
Robin (*Turdus migratorius*)	…	…	…	…	…	…	…	…	…	…	…	x	…	…	…	…	…	…	…	…	…	…
Hermit thrush or Gray-cheeked thrush (*Hylocichla guttata/minima*)	…	…	…	…	…	…	…	…	…	…	…	x	…	…	…	…	…	…	…	…	…	…
Waxwing (*Bombycilla* sp.)	…	…	…	…	…	…	…	…	…	…	…	x	…	…	…	…	…	…	…	…	…	…
Common redpoll or Hoary redpoll (*Acanthis flammea/hornemanni*)	…	…	…	…	…	…	…	…	…	…	…	x	…	…	…	…	…	…	…	…	…	…
White-winged crossbill (*Loxia leucoptera*)	cf	…	…	…	…	…	…	…	…	…	…	…	…	…	…	x	…	…	…	…	…	…
Savannah sparrow (*Passerculus sandwichensis*)	…	…	…	…	…	…	…	…	…	…	…	…	…	…	…	x	…	…	…	…	…	…
Tree sparrow or Chipping sparrow (*Spizella arborea/passerina*)	…	…	…	…	…	…	…	…	…	…	…	x	…	…	…	…	…	…	…	…	…	…
Lincoln's sparrow (*Melospiza lincolnii*)	…	…	…	…	…	…	…	…	…	…	…	cf	…	…	…	…	…	…	…	…	…	…
Snow bunting (*Plectrophenax nivalis*)	…	…	…	…	…	…	…	…	…	…	…	x	…	…	…	…	…	…	…	…	…	…
Perching birds (Passeriformes)	…	…	…	…	…	…	…	…	…	…	…	…	x	…	…	…	…	…	…	…	…	…
Mammals	x	x	x	x	x	x	x	x	x	x	x	x	x	x	x	x	x	x	x	x	x	x
Masked shrew (*Sorex cinereus*)	x	…	…	x	…	…	…	…	x	x	…	…	…	…	…	…	…	…	…	…	…	…
North American water shrew (*Sorex palustris*)	x	…	…	…	…	…	…	…	…	…	…	…	…	…	…	…	…	…	…	…	…	…
Gaspé shrew (*Sorex gaspensis*)	x	…	…	…	…	…	…	…	-	…	…	…	…	…	…	…	…	…	…	…	…	…
Pygmy shrew (*Sorex hoyi*)	x	…	…	…	…	…	…	…	x	…	…	…	…	…	…	…	…	…	…	…	…	…
Dusky shrew (*Sorex monticollus*)	-	…	…	…	…	…	…	…	x	…	x	…	…	…	…	cf	…	…	…	…	…	…
Short-tailed shrew (*Blarina brevicauda*)	x	…	x	x	x	…	…	x	…	…	…	…	…	…	…	…	…	…	…	…	…	…
Shrew (*Sorex* sp.)	…	…	…	…	…	…	…	…	x	…	…	…	…	…	…	x	…	…	…	…	…	…
Shrew (Soricidae)	…	…	…	…	…	…	…	…	…	…	…	x	…	…	…	…	…	…	…	…	…	…
Hairy-tailed mole (*Parascalops breweri*)	…	…	x	…	…	…	…	…	…	…	…	…	…	…	…	…	…	…	…	…	…	…

Table 1. Continued.

Cave Faunas	Localities[a]																					
	1	2	3	4	5	6	7	8	9	10	11	12	13	14	15	16	17	18	19	20	21	22
Star-nosed mole (*Condylura cristata*)	x	…	x	…	…	…	…	…	…	…	…	…	…	…	…	…	…	…	…	…	…	…
Little brown bat (*Myotis lucifugus*)	x	…	x	x	x	x	x	…	…	…	x	…	…	…	…	…	…	…	…	…	…	…
Keen's bat (*Myotis keenii*)	…	x	-	-	x	-	-	x	…	…	…	…	…	…	…	…	…	…	…	…	…	…
Long-legged bat (*Myotis volans*)	…	…	-	-	-	-	-	-	…	x	…	…	…	…	…	…	…	…	…	…	…	…
Northern long-eared bat (*Myotis septentrionalis*)	…	…	x	x	x	-	-	-	…	-	…	…	…	…	…	…	…	…	…	…	…	…
Bat (*Myotis* sp.)	…	…	…	…	…	…	…	…	…	x	…	…	x	…	…	x	…	…	…	…	…	…
Silver-haired bat (*Lasionycterus noctivagans*)	…	…	x	…	…	…	…	…	…	x	x	…	…	…	…	…	…	…	…	…	…	…
Big brown bat (*Eptesicus fuscus*)	…	…	x	x	x	…	…	x	…	x	…	…	…	…	…	…	…	…	…	…	…	…
Eastern pipistrelle (*Pipistrellus subflavus*)	…	…	…	x	…	…	x	…	…	-	…	…	…	…	…	…	…	…	…	…	…	…
Hoary bat (*Lasiurus cinereus*)	…	…	…	…	…	…	…	…	…	x	…	…	…	…	…	…	…	…	…	…	…	…
Humans – indirect evidence (*Homo sapiens*)	…	…	…	…	…	…	…	…	…	…	…	x	x	…	…	…	…	…	x	…	…	…
American pika (*Ochotona princeps*)	…	…	…	…	…	…	…	…	x	x	x	…	…	…	…	…	…	…	…	…	…	…
Large pika (*Ochotona* sp.)	…	…	…	…	x	x	…	…	…	…	…	…	…	…	…	…	…	…	…	…	…	…
Eastern cottontail (*Sylvilagus floridanus*)	…	…	…	…	x	x	…	…	…	…	…	…	…	…	…	…	…	…	…	…	…	…
Snowshoe hare (*Lepus americanus*)	x	…	…	…	…	x	…	…	cf	cf	x	x	x	…	…	…	…	…	…	…	…	…
Arctic hare (*Lepus arcticus*)	x	…	…	x	x	…	…	…	…	…	…	x	…	…	…	…	…	…	…	…	…	…
Large hare (*Lepus* sp.)	…	…	…	…	…	…	…	…	x	…	…	…	x	…	…	…	…	…	…	…	…	…
Rabbits and hares (Leporidae)	…	…	x	…	…	…	…	…	…	…	…	…	…	…	…	…	…	…	…	…	…	…
Eastern chipmunk (*Tamias striatus*)	x	…	x	…	…	…	…	…	…	…	…	…	…	…	…	…	…	…	…	…	…	…
Least chipmunk (*Eutamias minimus*)	…	…	…	…	…	…	…	…	…	…	…	…	x	…	…	…	…	…	…	…	…	…
Chipmunk (*Eutamias* sp.)	…	…	…	…	…	…	…	…	x	x	x	…	x	…	…	…	…	…	…	…	…	…
Woodchuck (*Marmota monax*)	x	…	…	…	…	…	…	…	…	…	…	…	…	…	…	…	…	…	…	…	…	…
Hoary marmot (*Marmota caligata*)	…	…	…	…	…	…	…	…	x	x	x	…	…	…	…	…	x	…	…	…	…	…
Vancouver Island marmot (*Marmota vancouverensis*)	…	…	…	…	…	…	…	…	…	…	…	…	…	x	x	x	…	…	x	x	x	x
Marmot (Marmota sp.)	…	…	…	…	…	…	…	…	…	…	…	x	x	…	…	…	…	…	…	…	…	…
Columbian ground squirrel (*Spermophilus columbianus*)	…	…	…	…	…	…	…	…	x	x	x	…	…	…	…	…	…	…	…	…	…	…
Golden-mantled ground squirrel (*Spermophilus lateralis*)	…	…	…	…	…	…	…	…	x	x	x	…	…	…	…	…	…	…	…	…	…	…
Arctic ground squirrel (*Spermophilus parryii*)	…	…	…	…	…	…	…	…	…	…	…	x	…	…	…	…	…	…	…	…	…	…
Ground squirrel (*Spermophilus* sp.)	…	…	…	…	…	…	…	…	…	…	…	…	x	…	…	…	…	…	…	…	…	…
Niobrara prairie dog (*Cynomys niobrarensis*)	…	…	…	…	…	…	…	…	cf	…	…	…	…	…	…	…	…	…	…	…	…	…
Red squirrel (*Tamiasciurus hudsonicus*)	x	…	x	x	x	…	…	x	x	x	x	…	…	…	…	x	…	…	…	…	…	x
Tree squirrel (*Tamiasciurus* sp.)	…	…	…	…	…	…	…	…	…	…	…	…	x	…	…	…	…	…	…	…	…	…
Northern flying squirrel (*Glaucomys sabrinus*)	x	…	cf	…	…	…	…	…	…	x	…	…	-	…	…	…	…	…	…	…	…	…
Northern pocket gopher (*Thomomys talpoides*)	…	…	…	…	…	…	…	…	x	x	…	…	-	…	…	…	…	…	…	…	…	…
North American beaver (*Castor canadensis*)	x	…	…	…	…	…	x	…	…	x	…	…	x	…	…	…	…	…	…	…	…	…
Woodland deer mouse (*Peromyscus maniculatus*)	x	…	…	…	x	x	…	x	x	x	x	…	…	…	x	…	…	…	…	…	…	…

Table 1. Continued.

Cave Faunas	Localities[a]																					
	1	2	3	4	5	6	7	8	9	10	11	12	13	14	15	16	17	18	19	20	21	22
Mouse (*Peromyscus* sp.)	…	…	x	x	…	…	…	…	…	…	…	…	x	…	…	x	x	…	…	…	…	…
Bushy-tailed woodrat (*Neotoma cinerea*)	…	…	…	…	…	…	…	…	x	x	x	…	x	…	…	…	…	…	…	…	…	…
Northern red-backed vole (*Myodes* (*Clethrionomys*) *rutilus*)	…	…	…	…	…	…	…	…	…	…	x	x	…	…	…	…	…	…	…	…	…	…
Southern red-backed vole (*Myodes* (*Clethrionomys*) *gapperi*)	x	…	cf	…	…	…	…	x	x	x	…	…	x	…	…	…	…	…	…	…	…	…
Red-backed vole (*Myodes* (*Clethrionomys*) sp.)	…	…	…	x	x	…	…	…	…	…	…	…	…	…	…	…	…	…	…	…	…	…
Brown lemming (*Lemmus sibiricus*)	…	…	…	…	…	…	…	…	x	…	…	x	…	…	…	…	…	…	…	…	…	…
Southern bog lemming (*Synaptomys cooperi*)	x	…	x	…	…	…	…	…	…	…	…	…	…	…	…	…	…	…	…	…	…	…
Northern bog lemming (*Synaptomys borealis*)	x	…	…	…	…	…	…	…	x	…	…	x	…	…	…	…	…	…	…	…	…	…
Western heather vole (*Phenacomys intermedius*)	x	…	…	x	…	…	…	…	x	x	x	…	…	…	…	x	x	…	…	…	…	…
Collared lemming (*Dicrostonyx torquatus*)	…	…	…	…	…	…	…	…	x	x	…	x	x	…	…	…	…	…	…	…	…	…
Ungava collared lemming (*Dicrostonyx hudsonius*)	x	x	x	x	…	…	…	…	…	…	…	…	…	…	…	…	…	…	…	…	…	…
Muskrat (*Ondatra zibethicus*)	…	…	x	-	-	x	x	x	…	x	x	x	x	…	…	…	…	…	…	…	…	…
Sagebrush vole (*Lagurus curtatus*)	…	…	…	…	…	…	…	…	cf	…	…	…	…	…	…	…	…	…	…	…	…	…
Water vole (*Microtus richardsoni*)	…	…	…	…	…	…	…	…	x	x	…	…	…	…	…	…	…	…	…	…	…	…
Meadow vole (*Microtus pennsylvanicus*)	x	…	x	x	x	…	…	x	…	x	x	x	x	…	…	…	…	…	…	…	…	…
Rock vole (*Microtus chrotorrhinus*)	x	…	cf	…	…	…	…	…	…	…	…	…	…	…	…	…	…	…	…	…	…	…
Taiga vole (*Microtus xanthognathus*)	x	…	-	…	…	…	…	…	…	…	…	x	x	…	…	…	…	…	…	…	…	…
Woodland vole (*Microtus pinetorum*)	…	…	cf	…	…	…	…	…	…	…	…	…	…	…	…	…	…	…	…	…	…	…
Long-tailed vole (*Microtus longicaudus*)	…	…	…	…	…	…	…	…	cf	cf	…	…	…	…	…	…	x	…	…	…	…	…
Singing vole (*Microtus miurus*)	…	…	…	…	…	…	…	…	…	…	…	x	…	…	…	…	…	…	…	…	…	…
Tundra vole (*Microtus oeconomus*)	…	…	…	…	…	…	…	…	…	…	…	x	…	…	…	…	…	…	…	…	…	…
Townsend's vole (*Microtus townsendii*)	…	…	…	…	…	…	…	…	…	…	…	…	…	…	…	…	x	…	…	…	…	…
Meadow or long-tailed vole (*Microtus pennsylvanicus/longicaudus*)	…	…	…	…	…	…	…	…	…	…	…	…	x	…	…	…	…	…	…	…	…	…
Vole (*Microtus* sp.)	…	…	…	…	…	…	…	…	…	…	…	…	…	…	…	x	…	…	…	…	…	…
Meadow jumping mouse (*Zapus hudsonius*)	x	…	…	…	…	…	…	…	…	…	…	…	…	…	…	…	…	…	…	…	…	…
Woodland jumping mouse (*Napeozapus insignis*)	x	…	…	…	…	…	…	…	…	…	…	…	…	…	…	…	…	…	…	…	…	…
North American porcupine (*Erethizon dorsatum*)	x	x	x	…	…	…	…	…	…	…	x	…	x	…	…	…	…	…	…	…	…	…
Coyote (*Canis latrans*)	…	…	cf	…	…	…	…	…	x	x	…	…	…	…	…	…	…	…	…	…	…	…
Gray wolf (*Canis lupus*)	…	…	…	…	…	…	…	…	…	x	x	x	x	…	…	…	…	…	…	…	…	…
Wolf or coyote (*Canis lupus/latrans*)	…	…	…	…	…	…	…	…	…	…	x	…	…	…	…	…	…	…	…	…	…	…
Wolf or dog (*Canis lupus/familiaris*)	…	…	…	…	…	…	…	…	…	…	…	…	x	…	…	…	…	…	…	…	…	…
Canid tooth marks (Canidae)	…	…	…	…	…	…	…	…	…	…	…	…	…	…	…	…	cf	…	…	…	…	…
Arctic fox (*Alopex lagopus*)	…	…	…	x	…	…	…	…	…	…	…	x	…	…	…	…	…	…	…	…	…	…

Table 1. Continued.

Cave Faunas	Localities[a]																				
	1	2	3	4	5	6	7	8	9	10	11	12	13	14	15	16	17	18	19	20	21	22
Red fox (*Vulpes vulpes*)	…	x	…	x	…	…	…	…	x	x	…	…	x	…	…	…	…	…	…	…	…	…
Swift fox (*Vulpes velox*)	…	…	…	…	…	…	…	…	x	-	x	…	…	…	…	…	…	…	…	…	…	…
Fox (*Vulpes* sp.)	…	…	…	…	…	…	…	…	…	x	…	…	…	…	…	…	…	…	…	…	…	…
Giant short-faced bear (*Arctodus simus*)[b]	…	…	…	…	…	…	…	…	…	…	…	…	…	…	…	x	…	…	…	…	…	…
Black bear (*Ursus americanus*)	x	…	x	x	…	…	…	…	…	x	x	…	x	x	…	x	…	x	x	…	…	x
Brown bear (*Ursus arctos*)	…	x	…	…	…	…	…	…	…	x	x	x	…	…	…	x	…	…	…	…	…	…
Bear (*Ursus* sp.)	…	…	…	…	…	…	…	…	…	x	…	…	x	…	…	…	…	…	…	…	…	…
Raccoon (*Procyon lotor*)	…	…	x	…	…	…	…	…	…	…	…	…	…	…	…	…	…	…	…	…	…	…
Noble marten (*Martes americana nobilis*)[b]	…	…	…	…	…	…	…	…	…	…	…	…	…	…	…	…	cf	…	…	…	…	…
American marten (*Martes americana*)	…	…	…	x	x	…	…	…	x	x	…	x	x	…	…	…	x	…	x	…	…	x
Fisher (*Martes pennanti*)	…	…	…	…	…	…	…	…	…	x	…	-	x	…	…	…	…	…	…	…	…	…
Beringian ferret (*Mustela eversmanni*)[b]	…	…	…	…	…	…	…	…	…	…	…	x	…	…	…	…	…	…	…	…	…	…
Black-footed ferret (*Mustela nigripes*)	…	…	…	…	…	…	…	…	x	…	…	…	…	…	…	…	…	…	…	…	…	…
Least weasel (*Mustela nivalis*)	x	…	…	…	…	…	…	…	x	…	…	x	x	…	…	…	…	…	…	…	…	…
Ermine (*Mustela erminea*)	x	…	…	x	…	…	…	…	x	x	…	x	x	…	…	…	…	…	…	…	…	…
Long-tailed weasel (*Mustela frenata*)	…	…	…	…	…	…	…	…	x	x	x	…	…	…	…	…	…	…	…	…	…	…
American mink (*Mustela vison*)	…	…	…	…	…	…	…	…	…	cf	x	…	x	…	…	…	…	…	…	…	…	…
Weasel (*Mustela* sp.)	…	…	…	…	…	…	…	…	…	-	-	…	x	…	…	…	…	…	…	…	…	…
Wolverine (*Gulo gulo*)	x	…	…	…	…	…	…	…	…	x	x	…	x	…	…	…	…	…	…	…	…	…
American badger (*Taxidea taxus*)	…	…	…	…	…	…	…	…	…	x	x	…	…	…	…	…	…	…	…	…	…	…
Short-faced skunk (*Brachyprotoma obtusata*)[b]	…	…	…	…	…	…	…	…	…	…	…	x	…	…	…	…	…	…	…	…	…	…
Striped skunk (*Mephitis mephitis*)	…	…	…	…	…	x	…	…	…	x	…	…	x	…	…	…	…	…	…	…	…	…
Northern river otter (*Lontra canadensis*)	…	…	…	…	…	…	…	…	x	x	…	…	…	…	…	…	…	…	…	…	…	…
Canada lynx (*Lynx canadensis*)	…	…	…	…	…	…	…	…	…	cf	x	…	x	…	…	…	…	…	…	…	…	…
Bobcat (*Lynx rufus*)	…	…	…	…	…	…	…	…	…	cf	…	…	…	…	…	…	…	…	…	…	…	…
Cougar (*Puma concolor*)	…	…	…	…	…	…	…	…	…	…	…	x	x	…	…	…	…	…	…	…	…	…
Domestic cat (*Felis catus*)	…	…	…	…	…	…	…	…	…	…	…	…	x	…	…	…	…	…	…	…	…	…
Steppe lion (*Panthera leo spelaea*)[b]	…	…	…	…	…	…	…	…	…	…	…	x	…	…	…	…	…	…	…	…	…	…
Woolly mammoth (*Mammuthus primigenius*)[b]	…	…	…	…	…	…	…	…	…	…	…	x	…	…	…	…	…	…	…	…	…	…
Yukon horse (*Equus lambei*)[b]	…	…	…	…	…	…	…	…	…	…	…	x	…	…	…	…	…	…	…	…	…	…
Horse (*Equus* sp.)	…	…	…	…	…	…	…	…	…	x	…	…	…	…	…	…	…	…	…	…	…	…
Caribou (*Rangifer tarandus*)	x	x	…	x	…	…	…	…	…	…	…	x	…	…	…	…	…	…	…	…	…	…
Mule deer (*Odocoileus hemionus*)	…	…	…	…	…	…	…	…	cf	x	cf	…	…	…	…	…	…	…	…	…	…	…
Black-tailed deer (*Odocoileus hemionus columbianus*)	…	…	…	…	…	…	…	…	…	…	…	…	…	…	…	…	…	x	x	…	…	x
White-tailed deer (*Odocoileus virginianus*)	…	…	x	…	x	…	x	…	…	…	…	…	…	…	…	…	…	…	…	…	…	…
Deer (*Odocoileus* sp.)	…	…	…	…	…	…	…	…	…	…	…	…	x	…	…	x	…	…	…	…	…	…
Moose (*Alces alces*)	x	x	…	…	…	…	…	…	…	…	…	x	x	…	…	…	…	…	…	…	…	…
Wapiti or elk (*Cervus elaphus*)	…	…	…	…	…	…	…	x	…	…	x	x	x	…	…	…	…	…	…	…	…	…
Steppe bison (*Bison priscus*)[b]	…	…	…	…	…	…	…	…	…	…	…	x	…	…	…	…	…	…	…	…	…	…
Bison (*Bison* sp.)	…	…	…	…	…	…	…	…	…	x	x	…	x	…	…	…	…	…	…	…	…	…
American bison or cattle (*Bison bison*/*Bos taurus*)	…	…	…	…	…	…	…	…	…	x	…	…	…	…	…	…	…	…	…	…	…	…
Saiga antelope (*Saiga tatarica*)[b]	…	…	…	…	…	…	…	…	…	…	…	x	…	…	…	…	…	…	…	…	…	…

Table 1. Continued.

Cave Faunas	Localities[a]																					
	1	2	3	4	5	6	7	8	9	10	11	12	13	14	15	16	17	18	19	20	21	22
Mountain goat (*Oreamnos americanus*)	…	…	…	…	…	…	…	…	…	…	x	…	…	x	…	x	x	…	…	…	…	…
Tundra muskox (*Ovibos moschatus*)	…	…	…	…	…	…	…	…	…	…	…	x	…	…	…	…	…	…	…	…	…	…
Bighorn sheep (*Ovis canadensis*)	…	…	…	…	…	…	…	…	x	x	x	…	…	…	…	…	…	…	…	…	…	…
Dall sheep (*Ovis dalli*)	…	…	…	…	…	…	…	…	…	…	…	x	…	…	…	…	…	…	…	…	…	…

[a] Localities: 1. St. –Elzéar-de-Bonaventure Cave, Quebec, 2. Trou Otis and Spéos de la Fée caves, Quebec, 3. Mine Cave, Quebec, 4. Laflèche Cave, Quebec, 5. Elba Cave, Ontario, 6. Kelso Cave, Ontario, 7. Mt. Nemo Cave, Ontario, 8. Dickson Cave, Ontario, 9. January Cave, Alberta, 10. Eagle Cave, Alberta, 11. Rats Nest Cave, Alberta, 12. Bluefish Caves, Yukon Territory, 13. Charlie Lake Cave, British Columbia, 14. Resonance Cave, British Columbia, 15. Pellucidar I Cave, British Columbia, 16. Pellucidar II Cave, British Columbia, 17. Port Eliza Cave, British Columbia, 18. Windy Link Pot Cave, British Columbia, 19. Mariner Mountain Cave, British Columbia, 20. Golden Hinde Cave, British Columbia, 21. Clayoquot Plateau Cave, British Columbia, 22. Limestone Mountain Cave, British Columbia.
[b] Extinct or extinct in North America
Note: x = fauna present; cf = closely comparable species identified.

well above its present elevation range in this part of the Rocky Mountains (Burns, 1982; 1987).

Rats Nest Cave, a natural trap on Grotto Mountain near Exshaw, Alberta, yielded remains of fish, amphibians, reptiles, birds, two species of shrew (*Sorex arcticus* and *S. monticollus*), two species of bat (*Lasionycterus noctivagans* and *Myotis lucifugus*), the American pika *Ochotona princeps*, the snowshoe hare, the hoary marmot, two species of ground squirrel (*Spermophilus columbianus* and *Spermophilus lateralis*), the red squirrel, the deer mouse, the wood rat, three species of vole, the muskrat, the North American porcupine, the brown bear, the black bear, the gray wolf *Canis lupus*, the swift fox *Vulpes velox*, the American mink *Mustela vison*, the long-tailed weasel *Mustela frenata*, the wolverine *Gulo gulo*, the American badger *Taxidea taxus*, the Canadian lynx *Lynx canadensis*, the mule deer, the wapiti or elk, the bighorn sheep, and the mountain goat *Oreamnos americanus*. Radiocarbon dating of bone gave ages ranging from about 7,000 to 2,500 B.P. (Burns, 1989).

Yukon

Bluefish Caves (I–III; 67°08′N, 140°47′W; inset Fig. 1b; Fig. 4a), located 54 km southwest of the village of Old Crow at an elevation of 250 m, have yielded evidence of episodic human activity from about 25,000 to 10,000 B.P. I consider them to be the most significant of Canadian cave faunas because they contain evidence for the earliest humans (*Homo sapiens*) in North America, a well-marked transition between Pleistocene and Holocene sediments, flora, and fauna, and well-preserved bones representing a substantial variety of both larger and smaller mammals adapted to northern conditions. An important specimen from Cave II is a mammoth (*Mammuthus primigenius*) limb-bone flake and its parent core (Fig. 4b) AMS radiocarbon-dated to 23,500 B.P.; both flake and core were dated, the dates overlapping at one sigma, providing that average date. Since the contents of the caves constrain the range of taphonomic processes that could account for the breaking and flaking of a large mammoth bone, the flake and core were produced by humans. Further, a split caribou tibia, reminiscent of a broken fleshing tool, has been dated to 24,800 B.P. The ice-age fauna of Bluefish Caves comprises four fish species, one amphibian, at least twenty-three bird species, and thirty-five mammal species, including the mammoth, the steppe bison *Bison priscus*, the Yukon horse *Equus lambei*, the Dall sheep *Ovis dalli*, the caribou, the moose, the wapiti, the saiga antelope *Saiga tatarica*, the muskox *Ovibos moschatus*, the steppe lion *Panthera leo spelaea*, the cougar *Puma concolor*, the brown bear, the wolf, and many smaller mammals, including nine species of microtine rodents. Stone artifacts, made of exotic, high-quality cherts, were mainly found in loess that contained remains of the Late Pleistocene vertebrate fauna (Beebe, 1983; Cinq-Mars, 1979; Cinq-Mars and Morlan, 1999; Harington and Cinq-Mars, 2008; Morlan, 1989; McCuaig-Balkwill and Cinq-Mars, 1998).

British Columbia

A wealth of information about vertebrates of northeastern British Columbia spanning the last 10,800 years has come from Charlie Lake Cave (56°16′35″N, 120°56′15″W), which is about 7 km northeast of Fort St. John (Fig. 1b; Fig. 5). Following the retreat of Glacial Lake Peace from this site shortly before 10,500 years ago, the gully in front of the cave began filling with sediment, ultimately reaching a depth of more than 4 m. During this process, the site was visited occasionally by people who left stone artifacts and bones as early as 10,500 B.P. It was also visited by predators carrying their prey and by various animals that lived in the area. The basal unit (about 10,500–9,000 B.P.) produced fossils including remains of suckers *Catostomus* sp. and other unidentified fishes. Frogs also suggest nearby lakes or streams. Of the birds found, evidently the horned grebe *Podiceps auritus*, the grouse and ptarmigan of family Tetraonidae, the American coot *Fulica americana*, the short-eared owl *Asio flammeus*, and the cliff swallow *Hirundo pyrrhonota* were most common. Other bird remains collected represent the western grebe *Aechmophorus occidentalis*, medium-sized grebes of family Podice-

Table 2. Radiocarbon ages of some vertebrates from Canadian caves. Dates in parentheses are normalized.

Cave	Species	Radiocarbon Age(BP)	Lab Number[a]	Reference	Remarks
St. Elzéar Cave, Quebec	Moose (*Alces alces*)	410 ± 120	QU-714	LaSalle 1984	
	Moose (*Alces alces*)	4400 ± 130	QU-717	LaSalle 1984	
	Moose (*Alces alces*)	4390 ± 120	QU-745	LaSalle 1984	
	Moose (*Alces alces*)	5110 ± 150	QU-7016	LaSalle 1984	
Laflèche Cave, Quebec	Arctic fox (*Alopex lagopus*)	(10,800 ± 90)	TO-1197	Harington 2003b	
	Unspecified mammal bone (Mammalia)	9340 ± 80 (9310 ± 80)	Beta-83094	Harington 2003b	
Elba Cave, Ontario	Pika (*Ochotona* sp.)	8670 ± 220	TO-2566	Savage 1994; Mead and Grady 1996	
	American marten (*Martes americana*)	510 ± 60	TO-	Savage 1994	Lab number is not recorded.
January Cave, Alberta	Brown lemming (*Lemmus sibiricus*)	23,100 ± 860	GaK-5438	Burns 1980	
Eagle Cave, Alberta	Hoary marmot (*Marmota caligata*)	(29,180 ± 300)	TO-6351	Burns 1991, 1996	
	Hoary marmot (*Marmota caligata*)	(34,860 ± 470)	TO-6350	Burns 1991, 1996	
Bluefish Caves, Yukon Territory					
Cave I	Moose (*Alces alces*)	(11,570 ± 60)	CAMS-23472	Pers. comm., J. Cinq-Mars 2010	
	Caribou (*Rangifer tarandus*)	(12, 210 ± 210)	RIDDL-277	Pers. comm., J. Cinq-Mars 2010	
	Caribou (*Rangifer tarandus*)	(12,830 ± 60)	CAMS-23468	Pers. comm., J. Cinq-Mars 2010	
	Mammoth (*Mammuthus* sp.)	(12,845 ± 250)	CRNL-1220	Pers. comm., J. Cinq-Mars 2010	Butchered bone. Normalized age is average of three runs.
	Bighorn sheep (cf. *Ovis canadensis* probably *O. dalli*)	(13,580 ± 80)	CAMS-23473	Pers. comm., J. Cinq-Mars 2010	
	Woolly mammoth (*Mammuthus primigenius*)	(13,940 ± 160)	RIDDL-559	Pers. comm., J. Cinq-Mars 2010	
	Yukon horse (*Equus lambei*)	(17,440 ± 220)	RIDDL-278	Pers. comm., J. Cinq-Mars 2010	
Cave II	Bison (cf. *Bison* sp.)	(10,230 ± 140)	RIDDL-561	Pers. comm., J. Cinq-Mars 2010	
	Mammoth (*Mammuthus* sp.)	15,500 ± 130 (15,540 ± 130)	GSC-3053	Pers. comm., J. Cinq-Mars 2010	
	Mammoth (*Mammuthus* sp.)	(17,880 ± 330)	CRNL-1221	Pers. comm., J. Cinq-Mars 2010	Butchered bone.
	Mammoth (*Mammuthus* sp.)	(19,640 ± 170)	RIDDL-330	Pers. comm., J. Cinq-Mars 2010	
	Mammoth (*Mammuthus* sp.)	(20,230 ± 180)	RIDDL-223	Pers. comm., J. Cinq-Mars 2010	
	Mammoth (*Mammuthus* sp.)	(22,740 ± 90)	CAMS-23470	Pers. comm., J. Cinq-Mars 2010	
	Horse (*Equus* sp.)	22,680 ± 530 (22,760 ± 530)	CRNL-1237	Pers. comm., J. Cinq-Mars 2010	
	Mammoth (*Mammuthus* sp.)	(23,200 ± 250)	RIDDL-225	Pers. comm., J. Cinq-Mars 2010	Butchered bone core.

Table 2. Continued.

Cave	Species	Radiocarbon Age(BP)	Lab Number[a]	Reference	Remarks
	Mammoth (*Mammuthus* sp.)	(23,910 ± 200)	RIDDL-224	Pers. comm., J. Cinq-Mars 2010	Butchered bone. Bone flake that can be refitted to the above core.
	Caribou (*Rangifer tarandus*)	(24,820 ± 115)	RIDDL-226	Pers. comm., J. Cinq-Mars 2010	Butchered bone.
	Bison (*Bison* sp.)	(31,730 ± 230)	CAMS-23469	Pers. comm., J. Cinq-Mars 2010	
	Snow Goose (*Chen caerulescens*)	7670 ± 60 (7780 ± 60)	Beta-126870	Pers. comm., J. Cinq-Mars 2010	Bone has cutmarks indicating human butchering.
	Caribou or Dall sheep (*Rangifer tarandus* or *Ovis dalli*)	21,030 ± 150 (21,100 ± 150)	Beta-140679	Pers. comm., J. Cinq-Mars 2010	
Cave III	Wapiti or elk (*Cervus elaphus*)	(10,820 ± 60)	CAMS-23467	Pers. comm., J. Cinq-Mars 2010	
	Horse (*Equus* sp.)	12,290 ± 440 (12,370 ± 440)	CRNL-1236	Pers. comm., J. Cinq-Mars 2010	Butchered bone.
	Snowy Owl (*Nyctea scandiaca*)	(13,350 ± 100)	Beta-129151	Pers. comm., J. Cinq-Mars 2010	
	Saiga antelope (*Saiga tatarica*)	(13,390 ± 180)	RIDDL-279	Pers. comm., J. Cinq-Mars 2010	
	Tundra muskox (*Ovibos moschatus*)	(14,370 ± 130)	RIDDL-557	Pers. comm., J. Cinq-Mars 2010	
	Cougar (*Puma concolor*)	(18,970 ± 1490)	TO-1266	Pers. comm., J. Cinq-Mars 2010	
	Mammoth (*Mammuthus* sp.)	(22,430 ± 260)	RIDDL-558	Pers. comm., J. Cinq-Mars 2010	
	Steppe bison (*Bison priscus*)	(23,710 ± 100)	CAMS-23471	Pers. comm., J. Cinq-Mars 2010	
	Beringian ferret (*Mustela eversmanni*)	(33,550 ± 350)	TO-1196	Pers. comm., J. Cinq-Mars 2010	
Charlie Lake Cave, British Columbia	Common Raven (*Corvus corax*)	10,290 ± 100	CAMS-2317	Driver 1999	
	Common Raven (*Corvus corax*)	9490 ± 140	CAMS-2318	Driver 1999	
	Bison (*Bison* sp.)	10,770 ± 120	SFU-454	Harington 2003b	
	Bison (*Bison* sp.)	(10,560 ± 80)	CAMS-2134	Harington 2003b	
	Bison (*Bison* sp.)	10,450 ± 150	SFU-300	Harington 2003b	
	Bison (*Bison* sp.)	10,380 ± 160	SFU-378	Harington 2003b	
	Bison (*Bison* sp.)	(9980 ± 150)	RIDDL-393	Harington 2003b	
	Bison (*Bison* sp.)	9760 ± 160	SFU-355	Harington 2003b	
	Bison (*Bison* sp.)	(9670 ± 150)	CAMS-2136	Harington 2003b	
Resonance Cave, British Columbia	Mountain goat (*Oreamnos americanus*)	(12,200 ± 190)	TO-6072	Nagorsen and Keddie 2000	
Pellucidar II Cave, British Columbia	Mountain goat (*Oreamnos americanus*)	(12,070 ± 70)	TO-5006	Nagorsen and Keddie 2000	
	Deer (*Odocoileus* sp.)	8710 ± 25	UCIAMS-41053	Steffen et al. 2008	
	Black bear (*Ursus americanus*)	11,110 ± 30	UCIAMS-41052	Steffen et al. 2008	

Table 2. Continued.

Cave	Species	Radiocarbon Age(BP)	Lab Number[a]	Reference	Remarks
	Mammal bone (Mammalia)	11,465 ± 30	UCIAMS-41046	Steffen et al. 2008	
	Mammal bone (Mammalia)	11,580 ± 30	UCIAMS-41045	Steffen et al. 2008	
	Giant short-faced bear (*Arctodus simus*)	11,615 ± 30	UCIAMS-41049	Steffen et al. 2008	
	Mammal bone (Mammalia)	11,725 ± 30	UCIAMS-41047	Steffen et al. 2008	
	Giant short-faced bear (*Arctodus simus*)	11,775 ± 30	UCIAMS-41048	Steffen et al. 2008	
	Brown bear (*Ursus arctos*)	12,425 ± 35	UCIAMS-41050	Steffen et al. 2008	
	Brown bear (*Ursus arctos*)	12,440 ± 35	UCIAMS-41051	Steffen et al. 2008	
Port Eliza Cave, British Columbia	Mountain goat (*Oreamnos americanus*)	12,340 ± 50	CAMS-97342	Al-Suwaidi et al. 2006	
	Mountain goat (*Oreamnos americanus*)	16,340 ± 60	CAMS-102798	Al-Suwaidi et al. 2006	
	Savannah Sparrow (*Passerculus sandwichensis*)	16,270 ± 170	CAMS-88275	Al-Suwaidi et al. 2006	
	Vole (*Microtus* sp.)	18,010 ± 100	CAMS-74624	Al-Suwaidi et al. 2006	
	Vole (*Microtus* sp.)	16,340 ± 60	CAMS-74625	Al-Suwaidi et al. 2006	
	Vole (*Microtus* sp.)	17,100 ± 70	CAMS-102797	Al-Suwaidi et al. 2008	
	Marmot (*Marmota* sp.)	16,460 ± 170	CAMS-88274	Al-Suwaidi et al. 2008	Duplicate analysis of same bone fragment.
	Marmot (*Marmota* sp.)	16,965 ± 45	CAMS-97341	Al-Suwaidi et al. 2008	Duplicate analysis of same bone fragment.
Windy Link Pot Cave, British Columbia	Black bear (*Ursus americanus*)	9760 ± 140 (9830 ± 140)	Beta-10714	Nagorsen et al. 1995	Composite sample of two tibias, three ribs and two vertebrae.
Mariner Mountain Cave, British Columbia	Vancouver Island marmot (*Marmota vancouverensis*)	890 ± 50	TO-3562	Nagorsen et al. 1996	
	Vancouver Island marmot (*Marmota vancouverensis*)	920 ± 50	TO-3563	Nagorsen et al. 1996	
	Vancouver Island marmot (*Marmota vancouverensis*)	990 ± 50	TO-3564	Nagorsen et al. 1996	
	Vancouver Island marmot (*Marmota vancouverensis*)	850 ± 50	TO-3565	Nagorsen et al. 1996	
	Vancouver Island marmot (*Marmota vancouverensis*)	890 ± 50	TO-3566	Nagorsen et al. 1996	
	Vancouver Island marmot (*Marmota vancouverensis*)	970 ± 90	TO-3567	Nagorsen et al. 1996	

Table 2. Continued.

Cave	Species	Radiocarbon Age(BP)	Lab Number[a]	Reference	Remarks
Golden Hinde Cave, British Columbia	Vancouver Island marmot (*Marmota vancouverensis*)	830 ± 60	TO-4265	Nagorsen et al. 1996	
Clayoquot Plateau Cave, British Columbia	Vancouver Island marmot (*Marmota vancouverensis*)	2630 ± 50	TO-1224	Nagorsen et al. 1996	
	Vancouver Island marmot (*Marmota vancouverensis*)	2490 ± 50	TO-692	Nagorsen et al. 1996	
Limestone Mountain Cave, British Columbia	Vancouver Island marmot (*Marmota vancouverensis*)	1030 ± 60	TO-4266	Nagorsen et al. 1996	
	Vancouver Island marmot (*Marmota vancouverensis*)	1070 ± 60	TO-4267	Nagorsen et al. 1996	

[a] Radiocarbon-Date Laboratories: Beta – Beta Analytic Inc., Miami, Florida; CAMS – Center for Accelerator Mass Spectrometry, Lawrence Livermore Laboratories, California; CRNL – Chalk River Nuclear Laboratories, Chalk River, Ontario (no longer operating); GaK – Gakushuin University, Tokyo; GSC – Geological Survey of Canada, Ottawa, Ontario; QU – Centre de Recherche Minérales, Ministère des Richesses Naturelles, Gouvernment du Québec (no longer operating); RIDDL – Radioisotope Direct Detection Laboratory, McMaster University, Hamilton, Ontario (no longer operating); SFU – Simon Fraser University, Burnaby, British Columbia (no longer operating); TO – Isotrace Laboratory, University of Toronto, Toronto, Ontario; UCIAMS – Keck Carbon Cycle AMS Facility, Earth System Science Department, University of California, Irvine, California.

pedidae, a small rail of family Rallidae, a small wader of order Charadriiformes, the common raven *Corvus corax*, perching birds of order Passeriformes, and surface-feeding ducks of tribe Anatini, including the green-winged teal *Anas crecca*, the mallard *Anas platyrhynchos*, and the ruddy duck *Oxyura jamaicensis.* Two raven skeletons associated with Paleoindian occupations dated about 10,500 and 9500 B.P. were evidently deposited deliberately by people. Among the mammals, the snowshoe hare, the ground squirrel, small rodents including the collared lemming, and bison were most commonly represented. A small assemblage of bison *Bison* sp. from the Paleoindian components at the cave seem to have resulted from storage of frozen bison limbs in a series of meat caches that would have been difficult for scavengers to access. Other mammals were a large (possibly arctic) hare, a woodchuck or marmot *Marmota* sp., the deer mouse, the southern red-backed vole *Myodes* (*Clethrionomys*) *gapperi*, the meadow or long-tailed vole, the taiga vole *Microtus xanthognathus*, other unidentified rodents, the wolf or dog *Canis lupus/familiaris*, the least weasel *Mustela nivalis*, another small weasel, and a deer. These fossils indicate that from about 10,500 to 10,000 B.P. the landscape was open, with some water, marshes, and patches of forest, changing to forest about 10,000 years ago. By 9,000 years ago, the fauna was modern (Driver, 1988, 1998a, 1998b, 1999, 2001; Driver and Vallières, 2008; Driver et al., 1996; Harington, 1996).

Several caves on Vancouver Island (Fig. 1b), have yielded vertebrate remains. Since 1985, remains of the Vancouver Island marmot *Marmota vancouverensis* have been discovered in four high-elevation cave sites: Clayoquot Plateau, Mariner Mountain, Limestone Mountain, and Golden Hinde. Artifacts and cut marks on bones recovered in Mariner Mountain Cave indicate that the marmot remains result from human hunting. Radiocarbon dates show that these sites are prehistoric, ranging from 2,630 to 830 B.P. The remains indicate a range decline in this marmot. Although the black bear, the Columbian black-tailed deer *Odocoileus hemionus columbianus*, the American marten, and the red squirrel are represented in the fauna, the predominance of Vancouver Island marmots suggests that aboriginal people traveled to these remote areas to hunt marmots (Nagorsen et al., 1996).

Although the mountain goat is now absent from most Pacific Coast islands, including Vancouver Island, 12,000-year-old skeletal remains were found in Resonance and Pellucidar caves east of Nimpkish Lake on northern Vancouver Island. The caves are 5 km apart and are situated at an elevation of about 800 m. Limb bones of these Pleistocene mountain goats are within the size range of the modern species, suggesting a postglacial origin. Mountain goats probably became extinct on Vancouver Island during the Early Holocene (Nagorsen and Keddie, 2000).

Pellucidar II Cave is situated near Pellucidar I and Resonance caves on the eastern slope of Nimpkish Lake, at an elevation of 480 m. It is of interest because of the relatively large fauna represented there. The Late Pleistocene fauna consists of a hawk *Buteo* sp., a squirrel, a mouse

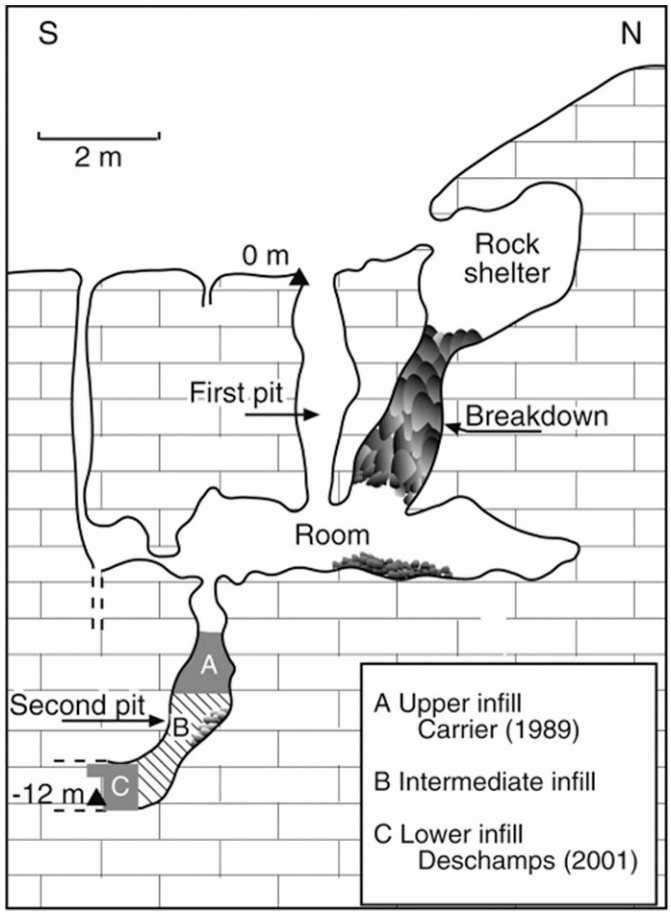

Figure 2. Mine Cave, Quebec. Cross-section diagram of the cave (Lauriol, et al., 2003).

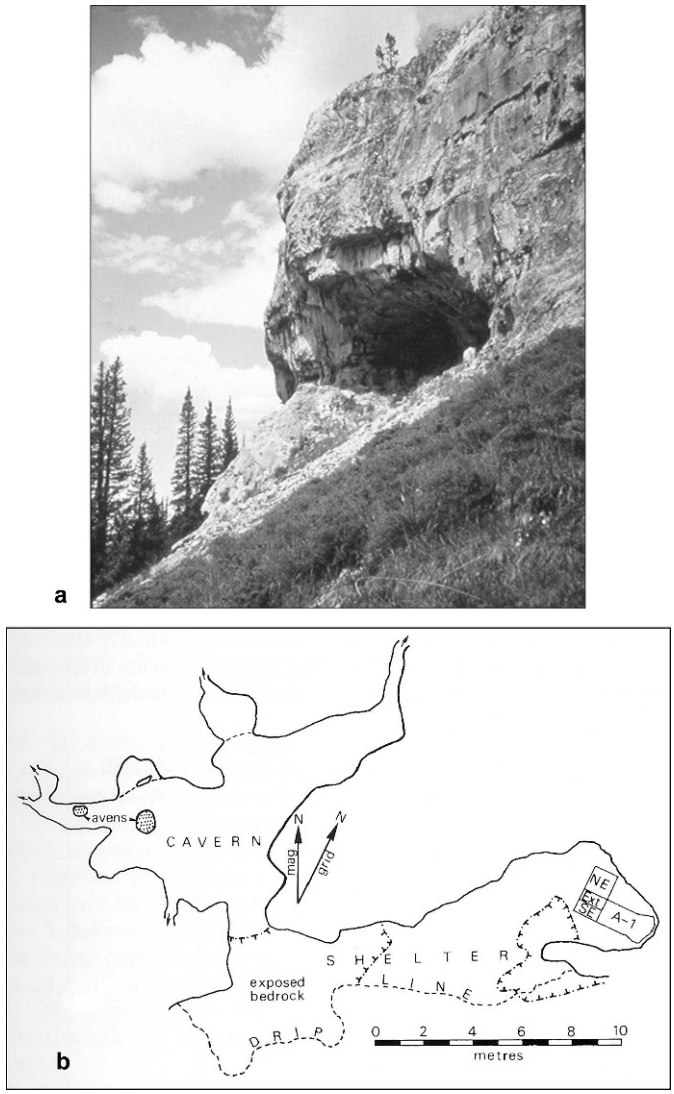

Figure 3. January Cave, Alberta. (a) Photograph of the cave entry. (b) Plan view; four test pits are marked at the far right (Burns, 1991).

Peromyscus sp., a shrew *Sorex* sp., a deer *Odocoileus* sp., the mountain goat, and several bears (extinct giant short-faced bear *Arctodus simus*, black bear, and brown bear). AMS radiocarbon dates on these bones vary from about 12,500 B.P. for a brown bear humerus to about 11,000 B.P. for a black bear humerus. Palatine and humerus fragments from the giant short-faced bear yielded radiocarbon ages of about 11,600 and 11,800 B.P., respectively. Specimens inferred to be from the Holocene on the basis of stratigraphic context include the blue grouse *Dendragrapus obscurus*, the white-winged crossbill *Loxia leucoptera*, a toad *Bufo* sp., a small snake, the red squirrel, western heather vole *Phenacomys intermedius*, another vole *Microtus* sp., a mouse *Peromyscus* sp., the marmot cf. *Marmota vancouverensis*, a small bat *Myotis* sp., the black bear, and a deer *Odocoileus* sp. The deer humerus was radiocarbon dated to about 8700 B.P. Preliminary results (Steffen et al., 2008) show that by 12,000 B.P. the coastal environment of northern Vancouver Island sustained three species of bear and other vertebrates that could have provided abundant resources for people.

Port Eliza Cave, a raised sea cave, is located on the northwestern coast of Vancouver Island at an elevation of 85 m, well above the 40 m postglacial sea level maximum (Fig. 6a, b). It formed along a fault trace and is 60 m long, varying in height from about 1 to 15 m. A diverse fish, amphibian, bird, and mammal fauna (about 3,600 specimens) was recorded from a basal unit of silty-sandy sediment greater than 50 cm deep. The fauna, yielding ages of 18,000 to 16,000 B.P., includes a salmon *Onchorhynchus* sp., the cutthroat trout *Onchorhynchus clarkii*, the three-spined stickleback *Gasterostens aculeatus*, a greenling of family Hexagrammidae, the Alaska pollock *Theragra chalcogramma*, a flatfish of order Pleuronectiformes, an Irish lord *Hemilepidotus* sp., a sculpin of family Cottidae, the Pacific tomcod *Microgadus proximus*, the western toad *Bufo boreas*, the red-throated loon *Gavia stellata*, a small alcid of family Alcidae, a cormorant *Phalacrocorax* sp., a duck, the horned lark *Eromophila alpestris*, the Savanna

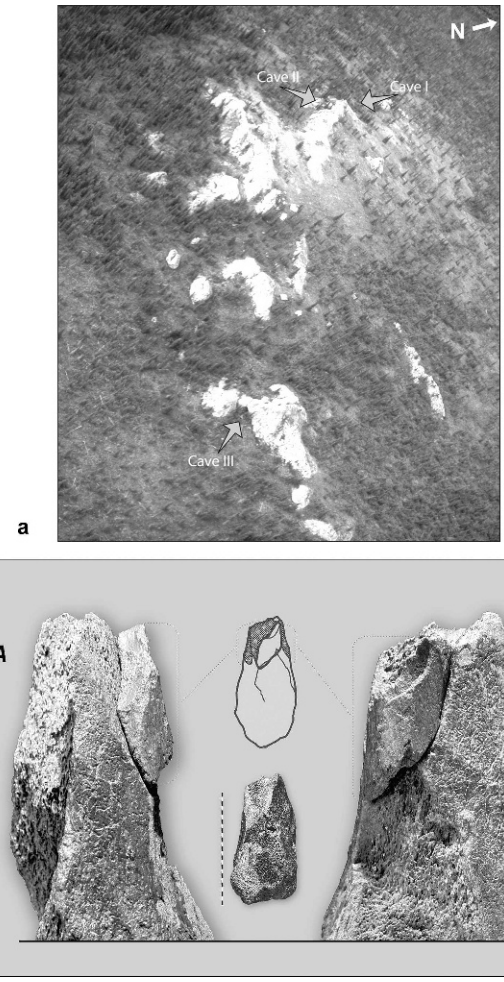

Figure 4. Bluefish Caves, Yukon. (a) Aerial view of Bluefish Caves (I–III) situated near the base of a Devonian limestone ridge. (b) A flaked mammoth bone core and its refitted flake from the lower loess unit at Bluefish Cave II, dated to around 24,000 B.P. A and B, detailed side views of the core and refitted flake; top center, schematic sketch of frontal view of core showing the position of three flake scars and the refitted flake; bottom center, frontal view of the bone core with 25 cm scale (Harington and Cinq-Mars, 2008).

sparrow *Passerculus sandwichensis*, the Townsend's vole *Microtus townsendii*, the long-tailed vole, the heather vole *Phenacomys intermedius*, the hoary marmot, the American marten, and the noble marten *Martes americana nobilis*, as well as the mountain goat and a canid (evidence from tooth marks). Fishes suggest that the shore was close enough for predators to have introduced this material to the cave. The terrestrial fauna indicates a cool, open environment with maximum summer temperatures cooler than present. A postglacial fauna consists of a mouse *Peromyscus* sp. and the mountain goat. Humans could have survived here on a mixed marine–terrestrial diet, confirming the viability of the Pacific coastal migration hypothesis for this part of the proposed route (Ward et al., 2003; Al-Suwaidi et al., 2006).

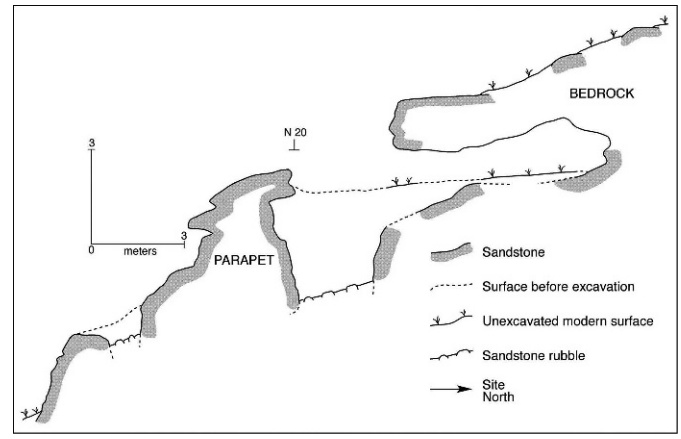

Figure 5. Charlie Lake Cave, British Columbia. Cross-section of the cave (Driver and Vallières, 2008).

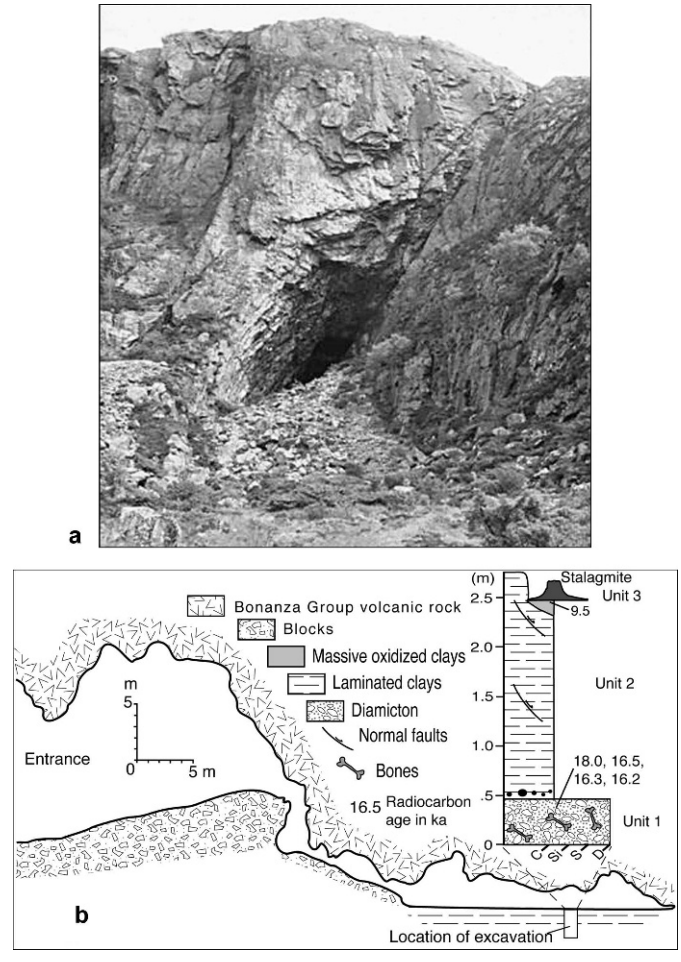

Figure 6. Port Eliza Cave, British Columbia. (a) Photograph of the cave entry. (b) Cross-section diagram of the cave (Al-Suwaidi, et al., 2006).

In 1983, cavers discovered skeletal remains of three Early Holocene (9,830 ± 140 B.P.) black bears at Windy Link Pot Cave (49°46′55″N, 125°59′10″W), situated at an elevation of about 900 m near Gold River on west-central Vancouver Island. The bears were relatively large. This cave system extends for nearly 10 km underground, with several steep drops in the cave floor, so there are many natural traps. Bones of three black-tailed deer *Odocoileus hemionus columbianus* were also discovered nearby. The bones showed no evidence of butchery or carnivore tooth marks, so the animals presumably fell to their deaths. Pollen analysis of sediment adhering to the bones indicates that the bears lived in a mixed coniferous forest with a warmer, drier climate than today (Nagorsen et al., 1995; Harington, 1996).

CONCLUSIONS

This review of twenty-two ice age vertebrate faunas, with associated data, from Canadian caves is presented to make North American and other vertebrate paleontologists more aware of the Canadian evidence. It is hoped that this summary will stimulate further studies on the cave faunas mentioned, as well as the search for more Canadian caves containing fossils that add to our knowledge of the distribution of vertebrate species, their chronological sequence and paleoenvironments, such as four caves near the mouth of the Saguenay River reported by Brassard (Beaupré and Caron 1986, p. 240–241; Harington 2003b, p. 89) and Extinction Cave in southern Manitoba's Interlake region (Oosterom, 2009).

Finds in western Canadian caves are relevant to the question of what routes early people chose to enter North America. Two modified bone specimens from Bluefish Caves, Yukon, along with a series of AMS-dated bone cores and flakes from Old Crow Basin and a bison radio-ulna from Nugget Gulch near Dawson City, Yukon, imply that an early phase of human tool-making, often involving mammoth bone, began in Eastern Beringia as early as 40,000 years ago and ended about 25,000 years ago (Cinq-Mars and Morlan, 1999; Harington and Morlan, 2002; Harington and Cinq-Mars, 2008). Further, Holen's (2006) evidence for human-modified mammoth skeletons from Kansas and Nebraska in the western United States suggests an entry-route to the heartland of North America east of the Rocky Mountains (the "ice-free corridor") before 18,000 years ago. Brown bear, with woolly mammoths (Lister and Bahn, 2007) and steppe bison (McDonald, 1981; Shapiro et al., 2004), likely reached the southern refugium in the unglaciated United States during the mid-Wisconsin ice-free period about 26,000 B.P. (Matheus et al., 2004), so that route may have been feasible for humans too. And the Port Eliza Cave fauna, Vancouver Island, indicates that people could have survived there on a mixed marine-terrestrial diet, confirming the viability of a Pacific coastal migration as early as 18,000 to 16,000 B.P. Preliminary results of the excavations at Pellucidar II Cave, Vancouver Island, show that by 12,000 B.P. the coastal vertebrate fauna could have provided abundant resources for human survival. So a later Pacific coastal migration could have occurred in latest Pleistocene–earliest Holocene time, as suggested by the oldest reliably dated, at nearly 10,000 B.P., human remains in Alaska discovered to the north in On Your Knees Cave, Prince of Wales Island (Dixon et al., 1997). Also, excavations on Haida Gwaii, Queen Charlotte Islands, since about 1995 have significantly enhanced our understanding of human history there. The archaeological record now extends to at least 10,500 B.P. (Fedje et al., 2004; Fedje and Mathewes, 2005).

Finally, it seems reasonable to suggest, as a follow-up to *Ice Age Cave Faunas of North America* (Schubert et al., 2003), that another book be published summarizing significant aspects of all North American cave faunas, perhaps following the pithy style of West's (1996) tome on the prehistory of Beringia.

ACKNOWLEDGEMENTS

I thank Camille Ek for encouraging me to collect and study vertebrate remains from the caves near La Rédemption, Quebec; Bernard Lauriol and Luc Carrier (then one of his graduate students) for allowing me to accompany them to Mine Cave, Quebec, and to identify bones (many raccoon!) from the upper 100 cm excavation; Jacques Cinq-Mars for showing me Bluefish Caves, Yukon, and for facilitating study of their well-preserved large vertebrate remains as a research associate of the Canadian Museum of Civilization; Darlene McCuaig-Balkwill for providing me with additional information on bird remains that she identified from Bluefish Caves, Yukon; Martina Steffen for allowing me to study bear remains from Pellucidar II Cave, British Columbia; Bernard Lauriol, Jacques Cinq-Mars, Jim Burns, Jon Driver and Brent Ward for assistance with Figures 2–6. Also, Jim kindly provided a faunal list for Eagle Cave from his dissertation, and Jacques sent me a list of all radiocarbon dates for Bluefish Caves. Above all, I am grateful to Gail Harington for word processing and help with the tables and illustrations. The paper has greatly benefitted from comments by Chris Jass and an anonymous reviewer.

REFERENCES

Al-Suwaidi, M., Ward, B.C., Wilson, M.C., Hebda, R.J., Nagorsen, D.W., Marshall, D., Ghaleb, B., Wigen, R.J., and Enkin, R.J., 2006, Late Wisconsinan Port Eliza Cave deposits and their implications for human coastal migration: Geoarchaeology: An International Journal, v. 21, no. 4, p. 307–332. doi: 10.1002/gea.20106.

Bateman, R.M., 1961, Mammal occurrences in escarpment caves: Ontario Field Biologist, v. 15, p. 16–18.

Beaupré, M., and Caron, D., 1986. Découvrez le Québec souterrain. Sillery, Québec Science Editeur, and Sainte-Foy, Presses de l'Université du Québec. 254 p.

Beebe, B.F., 1983, Evidence of carnivore activity in a Late Pleistocene/Early Holocene archaeological site (Bluefish Cave I), Yukon Territory, Canada, *in* Lemoine, G.M., and MacEachern, A.S., eds.,

Carnivores, Human Scavengers, and Predators: A Question of Bone Technology, Proceedings of the 15th Annual Conference of the Archaeological Association of the University of Calgary, University of Calgary, p. 1–14.

Burns, J.A., 1982, Water vole *Microtus richardsoni* (Mammalia, Rodentia) from the Late Pleistocene of Alberta: Canadian Journal of Earth Sciences, v. 19, p. 628–631.

Burns, J.A., 1987, Late Quaternary zoogeography of the northern pocket gopher, *Thomomys talpoides*, in southwestern Alberta: Canadian Field-Naturalist, v. 101, p. 419–422.

Burns, J.A., 1989, Fossil vertebrates from Rats Nest Cave, Alberta: Canadian Caver, v. 21, no. 1, p. 41–43.

Burns, J.A., 1991, Mid-Wisconsinan vertebrates and their environment from January Cave, Alberta, Canada: Quaternary Research, v. 35, p. 130–143. doi:10.1016/0033-5894(91)90100-J.

Burns, J.A., 2002, January Cave: an ancient window on the past: Alberta Archaeological Review, v. 37, p. 15–16.

Carrier, L., 1989, Le karst de Kingsmere: étude de ses remplissages, Parc de la Gatineau, Québec, [M.A. thesis], Université d'Ottawa, 120 p.

Churcher, C.S., and Fenton, M.B., 1968, Vertebrate remains from the Dickson Limestone Quarry, Halton County, Ontario, Canada: Bulletin of the National Speleological Society, v. 30, p. 11–16.

Churcher, C.S., and Karrow, P.F., 2008, The Hamilton Bar fauna: evidence for a Hypsithermal age. Canadian Journal of Earth Sciences, v. 45, p. 1487–1500.

Cinq-Mars, J., 1979, Bluefish Cave 1: a Late Pleistocene Eastern Beringian cave deposit in the northern Yukon: Canadian Journal of Archaeology, v. 3, p. 1–32.

Cinq-Mars, J., and Morlan, R.E., 1999, Bluefish Caves and Old Crow Basin: a new rapport, *in* Bonnichsen, R., and Turnmire, K.L., eds., Ice Age People of North America: Environment, Origins and Adaptations of the First Americans, Corvallis, Oregon State University Press for the Center for the Study of the First Americans, p. 200–212.

Dixon, E.J., Heaton, T.H., Fifield, T.E., Hamilton, T.D., Putnam, D.E., and Grady, F., 1997, Late Quaternary regional geoarchaeology of southeast Alaska karst: a progress report: Geoarchaeology: An International Journal, v. 12, no. 6, p. 689–712.

Driver, J.C., 1988, Late Pleistocene and Holocene vertebrates and palaeoenvironments from Charlie Lake Cave, northeast British Columbia: Canadian Journal of Earth Sciences, v. 25, p. 1545–1553.

Driver, J.C., 1998a. Human exploitation of pioneering post-glacial communities in northeastern British Columbia, Canada. 8th International Congress of the International Council for Archaeozoology (August 23–29, Victoria, British Columbia). Final Program and Abstracts, 107 p.

Driver, J.C., 1998b, Late Pleistocene collared lemming (*Dicrostonyx torquatus*) from northeastern British Columbia, Canada: Journal of Vertebrate Paleontology, v. 18, p. 816–818.

Driver, J.C., 1999, Raven skeletons from Paleoindian contexts, Charlie Lake Cave, British Columbia: American Antiquity, v. 64, p. 289–298.

Driver, J.C., 2001, Paleoecological and archaeological implications of the Charlie Lake Cave fauna, British Columbia 10,500 to 9500 B.P., *in* Gerlach, S.C., and Murray, M.S., eds., People and Wildlife in Northern North America: Essays in Honor of R. Dale Guthrie, Oxford, British Archaeological Reports International Series 944, p. 13–22.

Driver, J.C., and Vallières, C., 2008, The Paleoindian bison assemblage from Charlie Lake Cave, British Columbia: Canadian Journal of Archaeology, v. 32, p. 239–257.

Driver, J.C., Handly, M., Fladmark, K.R., Nelson, D.E., Sullivan, G.M., and Preston, R., 1996, Stratigraphy, radiocarbon dating, and culture history of Charlie Lake Cave, British Columbia: Arctic, v. 49, p. 265–277.

Fedje, D.W., and Mathewes, R.W., 2005, Conclusion: synthesis of environmental and archaeological data, *in* Fedje, D.W., and Mathewes, R.W., eds., Haida Gwaii: Human History and Environment from the Time of Loon to the Time of the Iron People, Vancouver, UBC Press, p. 372–375.

Fedje, D.W., Wigen, R.J., McLaren, D., and Mackie, Q., 2004, Archaeology and environment of karst landscapes in southern Haida Gwaii (Queen Charlotte Islands), West Coast, Canada: Paper presented at the 2004 Northwest Anthropological Conference, Eugene, Oregon. March.

Harington, C.R., 1980, A preliminary list of faunal remains from two caves (Trou Otis and Spéos de la Fée) in Gaspé, Québec, *in* Schroeder, J., ed., Le karst de plate-forme de Boischâtel et le karst barré de La Rédemption, état des connaissances, Montréal, Société Québecoise de Spéléologie, p. 95–105.

Harington, C.R., 1996, Quaternary animals: vertebrates of the ice age, *in* Ludvigsen, R., ed., Life in Stone: A Natural History of British Columbia's Fossils, Vancouver, UBC Press, p. 259–273.

Harington, C.R., 2003a, Quaternary vertebrates of Québec: a summary: Géographie physique et Quaternaire, v. 57, p. 85–94.

Harington, C.R., ed., 2003b, Annotated Bibliography of Quaternary Vertebrates of Northern North America – with Radiocarbon Dates, University of Toronto Press, 369 p.

Harington, C.R., 2006, Review of Blaine W. Schubert's, Jim I. Mead's, and Russell W. Graham's, eds., Ice Age Faunas of North America, The Palaeontology Newsletter, no. 61, p. 90–99.

Harington, C.R., and Cinq-Mars, J., 2008, Bluefish Caves – fauna and context, Beringian Research Notes, no. 19, p. 1–8.

Harington, C.R., and Morlan, R.E., 2002, Evidence for human modification of a Late Pleistocene bison (*Bison* sp.) bone from the Klondike District, Yukon Territory, Canada: Arctic, v. 55, no. 2, p. 143–147.

Holen, S.R., 2006, Taphonomy of two last glacial maximum mammoth sites in the central Great Plains of North America: a preliminary report on La Sena and Lovewell: Quaternary International, v. 142–143(2006), p. 30–43.

Karrow, P.F., 2005, Quaternary geology of the Brampton Area, Ontario Geological Survey Report 257, 59 p.

Lasalle, P., 1984, Geological setting and preliminary faunal report for St-Elzéar Cave Québec, *in* Genoways, H.H., and Dawson, M.R., eds., Contributions in Quaternary Vertebrate Paleontology: A Volume in Memorial to John E. Guilday, Carnegie Museum of Natural History Special Publication, no. 8, p. 332–346.

Lasalle, P., and Guilday, J.E., 1980, Caverne de Saint-Elzéar-de-Bonaventure, Rapport preliminaire sur les fueilles de 1977 et 1978, Quebec, Édition du Ministère de l'Énergie et des Ressources, Direction générale de la recherche géologique et minérale, DPV-750, 31 p.

Lauriol, B., Deschamps, E., Carrier, L., Grimm, W., Morlan, R., and Talon, B., 2003, Cave infill and associated biotic remains as indicators of Holocene environment in Gatineau Park (Québec, Canada): Canadian Journal of Earth Sciences, v. 40, p. 789–803.

Lister, A., and Bahn, P., 2007, Mammoths: Giants of the Ice Age, Berkeley, University of California Press, 192 p.

Matheus, P., Burns, J., Weinstock, J., and Hofreiter, M., 2004, Pleistocene brown bears in the mid-continent of North America: Science, v. 306, 1150 p. doi: 10.1126/science.1101495.

McCuaig-Balkwill, D., and Cinq-Mars, J., 1998, Migratory birds from Bluefish Caves, Eastern Beringia: 8th International Congress of the International Council for Archaeozoology (August 23–29, Victoria, B.C.) Final Program and Abstracts, 194 p.

McDonald, J.N., 1981, North American Bison: Their Classification and Evolution, Berkeley, University of California Press, 316 p.

Mead, J.I., and Grady, F., 1996, *Ochotona* (Lagomorpha) from Late Quaternary cave deposits in eastern North America: Quaternary Research, v. 45, p. 93–101.

Morlan, R.E., 1989, Paleoecological implications of Late Pleistocene and Holocene microtine rodents from Bluefish Caves, northern Yukon Territory: Canadian Journal of Earth Sciences, v. 26, p. 149–156.

Nagorsen, D.W., and Keddie, G., 2000, Late Pleistocene mountain goats (*Oreamnos americanus*) from Vancouver Island: biogeographic implications: Journal of Mammalogy, v. 81, p. 666–675. doi: 10.1644/1545-1542(2000)081<0666:LPMGOA>2.3.CO;2.

Nagorsen, D.W., Keddie, G., and Hebda, R.J., 1995, Early Holocene black bears, *Ursus americanus*, from Vancouver Island: Canadian Field-Naturalist, v. 109, p. 11–18.

Nagorsen, D.W., Keddie, G., and Luszcz, T., 1996, Vancouver Island Marmot Bones from Subalpine Caves: Archaeological and Biological Significance, Victoria, British Columbia Parks, Occasional Paper No. 4, 56 p.

Oosterom, N., 2009, Extinction Cave: unique hole in ground may yield bones of ice age creatures: The Beaver, v. 89, no. 2, 9 p.

Pigott, P., 1999, Tracking a phantom grizzly: Equinox, no. 102, p. 64–65, 68–74.

Savage, H., 1994, Prehistoric fauna in a vertical fissure cave in the Niagara Escarpment, Dufferin County, Ontario, *in* MacDonald, R.I., ed., Great Lakes Archaeology and Paleoecology: Exploring Interdisciplinary Initiatives for the Nineties: Proceedings of a Symposium presented by the Quaternary Sciences Institute, University of Waterloo, Waterloo, Ontario, September 21–22, 1991, Waterloo Ontario, Quaternary Sciences Institute publication 10.

Schubert, B.W., Mead, J.I., and Graham, R.W., eds., 2003, Ice Age Cave Faunas of North America, Bloomington, Indiana University Press, and Denver, Denver Museum of Nature and Science, 320 p.

Shapiro, B., and 27 coauthors, 2004, Rise and fall of the Beringian steppe bison: Science, v. 306, p. 1561–1565.

Steffen, M.L., Hebda, R.J., McLaren, D.S., and Fedje, D.W., 2008. P2 Cave: paleontological recovery and archaeological potential. Abstract of poster paper presented at the Northwest Anthropological Conference (April 23–26, 2008, Victoria, B.C.), Preliminary Schedule, 24 p.

Ward, B.C., Wilson, M.C., Nagorsen, D.W., Nelson, D.E., Driver, J.C., and Wigen, R.J., 2003, Port Eliza Cave: North American West Coast interstadial environment and implications for human migrations: Quaternary Science Reviews, v. 22, p. 1383–1388. doi:10.1016/S0277-3791(03)00092-1.

West, F.H., ed., 1996, American Beginnings: The Prehistory and Paleoecology of Beringia, Chicago, University of Chicago Press, 576 p.

J. F. Weishampel, J. N. Hightower, A. F. Chase, D. Z. Chase, and R. A. Patrick – Detection and morphologic analysis of potential below-canopy cave openings in the karst landscape around the Maya polity of Caracol using airborne LiDAR. *Journal of Cave and Karst Studies,* v. 73, no. 3, p. 187–196. DOI: 10.4311/2010EX0179R1

DETECTION AND MORPHOLOGIC ANALYSIS OF POTENTIAL BELOW-CANOPY CAVE OPENINGS IN THE KARST LANDSCAPE AROUND THE MAYA POLITY OF CARACOL USING AIRBORNE LIDAR

John F. Weishampel[1]*, Jessica N. Hightower[1], Arlen F. Chase[2], Diane Z. Chase[2], and Ryan A. Patrick[3]

Abstract: Locating caves can be difficult, as their entranceways are often obscured below vegetation. Recently, active remote-sensing technologies, in particular laser-based sensor systems (LiDARs), have demonstrated the ability to penetrate dense forest canopies to reveal the underlying ground topography. An airborne LiDAR system was used to generate a 1 m resolution, bare-earth digital elevation model (DEM) from an archaeologically- and speleologically-rich area of western Belize near the ancient Maya site of Caracol. Using a simple index to detect elevation gradients in the DEM, we identified depressions with at least a 10 m change within a circular area of no more than 25 m radius. Across 200 km^2 of the karst landscape, we located 61 depressions. Sixty of these had not been previously documented; the other was a cave opening known from a previous expedition. The morphologies of the depressions were characterized based on the LiDAR-derived DEM parameters, e.g., depth, opening area, and perimeter. We also investigated how the measurements change as a function of spatial resolution. Though there was a range of morphologies, most depressions were clustered around an average maximum depth of 21 m and average opening diameter of 15 m. Five depression sites in the general vicinity of the Caracol epicenter were visited; two of these were massive, with opening diameters of ~50 m, two could not be explored for lack of climbing gear, and one site was a cave opening into several chambers with speleothems and Maya artifacts. Though further investigation is warranted to determine the archaeological and geological significance of the remaining depressions, the general methodology represents an important advancement in cave detection.

Introduction

Caves have biological, geological, hydrological, and often, when near settlements of ancient cultures, anthropological significance. The detection of cave openings, classification of cave types, and mapping of cave morphologies are initial steps in documenting and conserving these sites of natural and cultural heritage. However, many caves in mesic regions remain undocumented, as the openings are often obscured by vegetation. This is especially common in Mesoamerica, where dense, structurally-complex rainforest canopies overtop numerous Maya archaeological sites (Ricketson and Kidder, 1930; Chase, 1988).

Caves are believed to have played a significant role in ancient Maya societies (e.g., Brady and Prufer, 2005; Prufer and Brady, 2005) from about 2500 BC to AD 1500. As portals to the Maya underworld, *Xibalbá*, caves served as places of religious and mythological importance in addition to functioning as shelters. They were sites of rituals, ceremonies, and burials, and they hence often contain ceramics, artwork, architectural modifications, and skeletal remains (e.g., Moyes, 2002). However, like many of the archaeological features found in the Maya polities, cave entrances are often covered by the dense tropical rainforest vegetation that reemerged after the settlements were abandoned roughly a thousand years ago.

There are several possible ways to locate caves using remote sensing. On the ground, covering a limited area, ground penetrating radar can be used to detect caves (Sellers and Chamberlain, 1998). However, the extensive below-ground root mass and the density of the above-ground vegetation preclude the use of GPR in a rainforest environment. For broad-scale prospecting, airborne- or satellite-based remote sensing is necessary. Because caves have a more stable temperature than the surface environment, there has been an effort to use thermal remote sensing on earth (Griffith, 2000) and on other planets (Cushing et al., 2007; Wynne et al., 2008) to detect cave openings. Though a temperature gradient of 7.2 °C was detected on the ground 50 to 100 m away from cave

* Corresponding Author, jweisham@mail.ucf.edu
[1] Department of Biology, University of Central Florida, Orlando, FL 32816, USA
[2] Department of Anthropology, University of Central Florida, Orlando, FL 32816, USA
[3] Interdisciplinary Studies Program, University of Central Florida, Orlando, FL 32816, USA

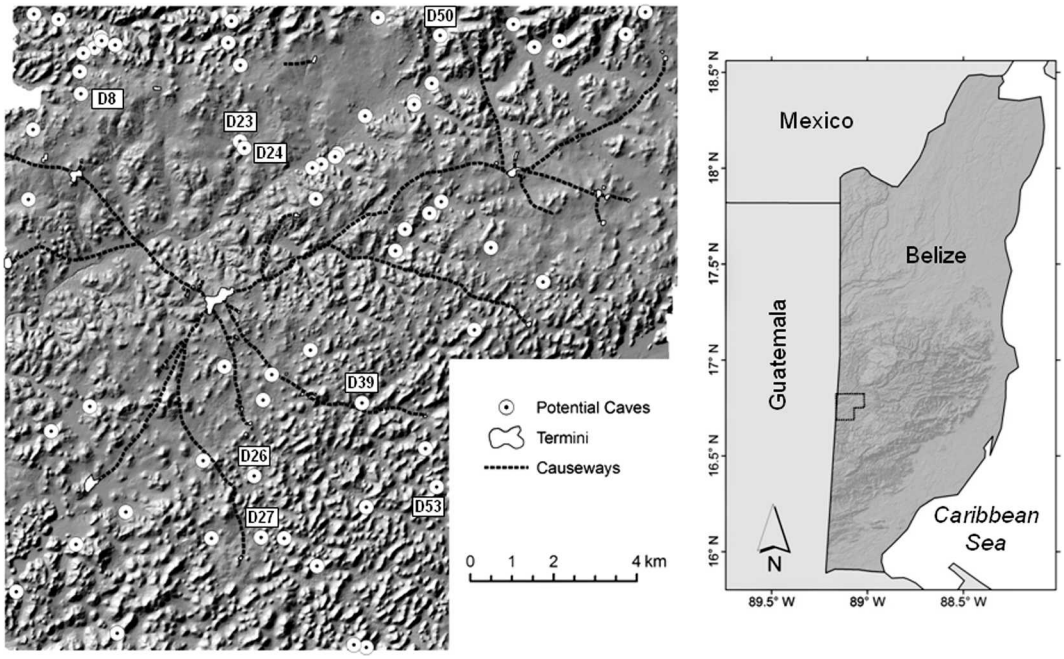

Figure 1. At right, location of 200 km^2 study area on the western border of Belize on the Vaca Plateau, shown on the hillshaded Shuttle Radar Topography Mission image of Belize. The expanded study area shows the 61 depressions more than 10 m deep on the hillshaded bare-earth image from the airborne LiDAR-derived DEM. Numbers refer to depressions specifically mentioned in this paper.

openings in Belize (Griffith, 2001), this method is challenging, given the coarse resolution of most satellite thermal sensors. Furthermore, even with finer airborne or hyperspatial satellite sensors, the sharp microclimate gradient in closed-canopy tropical rainforest regions from the ground to the upper surface of the forest canopy 20 to 30 m above may mask the temperature at the cave opening (Allee, 1926). Griffith (2001) also used an active form of remote sensing (Star 3i RADAR) to detect depressions in the surface topography of the forest canopy (Weishampel et al., 2000a) that may correspond to depressions or cave openings. This proved successful for a large ~25 m wide sinkhole, but not for depressions below the spatial resolution of the sensor. Given the ability of another active form of remote sensing (LiDAR—Light Detection and Ranging) to penetrate dense forest cover to measure ground surfaces (e.g., Weishampel et al., 2000a, 2000b; Hofton et al., 2002; Gallagher and Josephs, 2008), we assessed its ability to locate known and unknown potential cave openings and to quantify the geomorphology of their entranceways.

As part of an archaeological prospecting study (Weishampel et al., 2010), we used airborne LiDAR to map unknown Maya structures such as temples, causeways, and monuments in a 200 km^2 area around Caracol, Belize (Chase et al., 2010). In addition to anthropogenic features in the 1 m horizontal resolution digital elevation model (DEM), we identified numerous vertical depressions and surface openings. These were thought to represent cave openings, pits collapse dolines, or *chultuns* (subterranean storage chambers) that, if contemporaneous, could have been used by the ancient Maya. Here, we report our approach and findings.

CARACOL STUDY AREA

The geology of the Yucatán Peninsula consists of a porous limestone shelf that is honeycombed with sinkholes, cenotes, underground streams, lakes, and caverns. Estimated to cover about 170 km^2, Caracol is the largest Maya archaeological site in Belize. Located near the Guatemala border on the Vaca Plateau of the Cayo District (Fig. 1) west of the Maya Mountains, the Caracol landscape consists of rolling karst-defined hills and valleys ranging from about 300 to 700 m in elevation. At its cultural peak (ca. AD 700), the metropolitan population is estimated to have been greater than 100,000, which makes it one of the most populous cities in the Pre-Columbian world (Chase and Chase, 1996). Since 1950, 23 km^2 have been painstakingly surveyed on the ground (Chase, 1988; Chase and Chase, 2001). The main acropolis, comprising numerous large buildings, is at the center of several causeways that radiate outward to smaller areas called termini that also possess high concentrations of building structures.

Presently most of the remains of Caracol are hidden in the subtropical moist forests of the Chiquibul National Park (Brokaw, 1992). The average canopy height is about 25 m, with a few emergent trees extending to over 35 m.

The vertical forest structure is fairly homogeneous, with no distinct layers.

In the greater vicinity of Caracol, outside the 200 km^2 area, numerous caves have been located (Miller, 1990) and many of these are of archaeological note (McNatt, 1996; Reeder et al., 1998). The Río Frío complex 26 km to the north-northeast of the center, the Quiroz Cave 13 km to the northeast, Actun Balam 15 km to the southeast (Pendergast, 1969, 1970; Pendergast and Savage, 1971), and several other caves 30 or more km to the northeast (Moyes, 2002) all contained artifacts such as bones and pottery that indicated that they were sites of ritual use. Feld (1994) documented nine caves within the 200 km^2 Caracol area; most are within 3 km of the center. Many of these have small openings and deep shafts. Most of these are thought not to have been accessible to or not contemporary with the ancient Maya, meaning that the openings are more recent. Hence, only a few of these caves contain artifacts.

Methods and Materials

At the end of April 2009, during the end of the dry season, the National Center for Airborne Laser Mapping (NCALM; Carter et al., 2001) flew their LiDAR system, which consisted of an Optech, Inc., Gemini Airborne Laser Terrain Mapper with onboard GPS and Inertial Measurement Unit systems on board a Cessna 337 Skymaster. The timing of the flight was designed to correspond roughly to the height of leaf abscission for this forest. However, leaf-off typically does not exceed 20% at any time of the year, as most tree species maintain leaves all year long (Brokaw, 1992).

The NCALM system records four returns per pulse as it scans across a 0.5 km swath; when a pulse is transmitted, part of the pulse initially reflects off an object closest to the aircraft, usually the canopy, while the remainder of the pulse continues through gaps in the canopy, reflecting off other plant surfaces and in some cases the ground. The laser pulse rate is 167 kHz, and the scan rate is 28 Hz. At a nominal above-ground altitude of 600 to 1000 m, the system yields 10 to 15 laser shots per square meter with a height accuracy of 5 to 10 cm (one sigma) and a horizontal accuracy of 25 to 40 cm (one sigma). This system also records the relative intensity of each return. By crisscrossing (east-west and north-south) flight lines over the central Caracol area (Chase et al., 2010), 20 to 30 shots per square meter were obtained, yielding a more accurate digital elevation model.

Of the more than 20 laser shots/m^2, an average of 1.35 points/m^2 penetrated through canopy gaps to reach the ground. NCALM researchers interpolated these points to generate a 1 m resolution DEM. The DEM file for the entire 200 km^2 area was 65 MB and was analyzed using off-the-shelf software or freeware on a standard (circa 2010) desktop computer. From the bare-earth DEM rendered with a hillshade algorithm (Fig. 1), we visually identified thousands of unknown Maya settlement structures and some obvious steep surface depressions. LiDAR at Caracol has proven very effective for detecting man-made archaeological features below the canopy (Chase et al., 2010; Chase et al., 2011).

Using the Topographic Position Index (TPI) (Guisan et al., 1999) calculator within the Land Facet Corridor Designer software (Jenness et al., 2010), a plug-in application for ArcGIS (v. 9.3), we further identified numerous

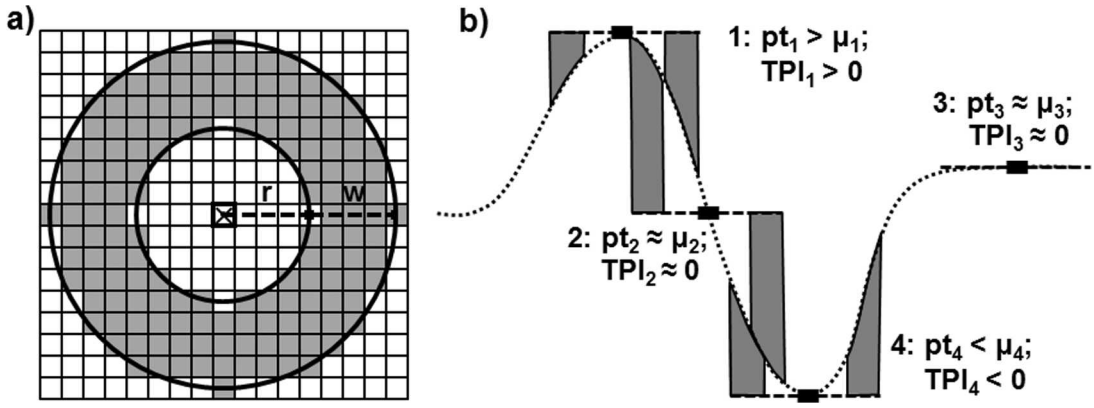

Figure 2. (a) Topographic Position Index (TPI) annulus filter that was applied to the DEM. It calculates the difference between the elevation of the focal cell (pt) designated with the 'x' and the average elevation of the gray cells (μ) in the ring surrounding it. Two parameters that can be adjusted are the inner radius (r), the distance from the center of the focal cell to the inner edge of the ring, and the annulus thickness (w), the difference between the inner and outer radii. (b) An example of a topographic cross section shows the four main terrain scenarios: 1, hump or hilltop; 2, slope; 3, level or flat; 4, depression or valley, and the associated pt, μ, and TPI values. The gray bars depict the elevations at the sides of the annuli with respect to the elevations of the focal cells (adapted from Weiss, 2001 and Jenness et al., 2010). Terrain scenarios 2 (slope) and 3 (level) are distinguished by evaluating the overall slope in the annulus.

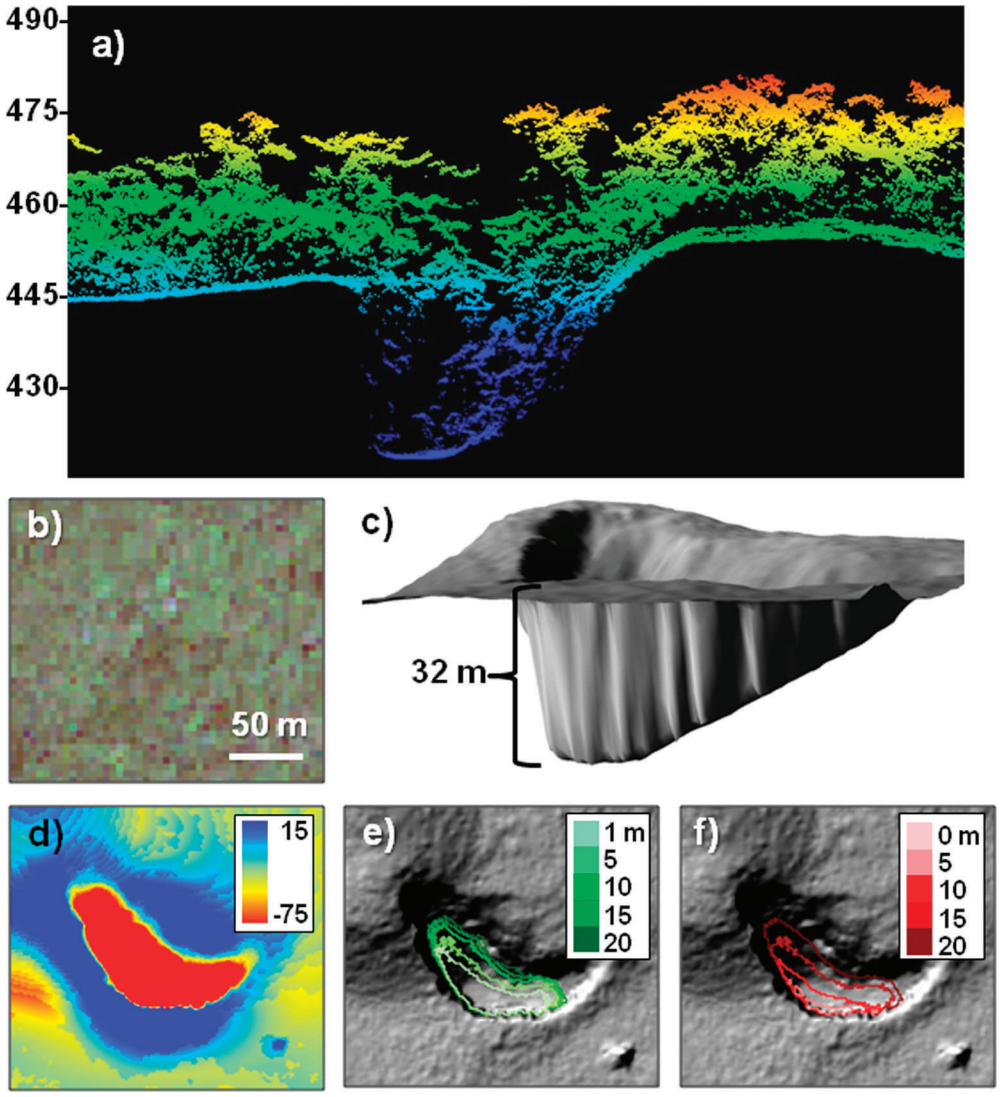

Figure 3. (a) LiDAR point-cloud data depicting forest canopy and ground surface at depression 24. The values are meters above sea level. (b) Top-down view provided by the IKONOS satellite shows complete canopy coverage over the depression. (3) 3-D rendering of the LiDAR image with vegetation removed. (d) TPI image depicting relative elevation in meters. (e) The perimeter of the area with TPI value −10 m or less as a function of annulus thickness, keeping the inner radius constant at 15 m. (f) The same as (e), but with the inner radius varying and the thickness constant at 5 m.

steep depressions that may represent cave openings. The TPI measures elevational contrast in the DEM. For each focal cell, the TPI is the difference between the elevation of the focal cell and the average elevation of all the cells in the neighborhood (Fig. 2). We used an annulus shape to define the neighborhood, i.e., cells whose center points fall between inner and outer radii. The annulus shape amplifies the difference between the focal cell and the surrounding ring.

Rasters (pixels or grid cells) with TPI values ≤ -10 m were segmented or partitioned in the DEM image as potential cave entrances (Fig. 3). This depth eliminated shallow reservoirs and chultuns previously identified in the area (Hunter-Tate 1994). Chultuns are typically bottle-shaped storage chambers about 2 m deep built by the Maya that may have served functions such as cisterns, storage, or burial sites. Given the vertical direction of the LiDAR pulse, it is unlikely that caves with side or horizontal openings would be conspicuous. Also, because of the horizontal resolution of the DEM, caves with openings smaller than 1 m^2 would most likely not be detected. Several of the previously unrecorded depressions were verified in the field during the spring of 2010.

Within a cave, terrestrial laser scanning has been shown to be an effective method to record cave morphology (González-Aguilera et al., 2009; Lerma et al., 2010). Here we apply this general technique at a coarser scale to measure the shapes of depressions that may represent cave entrances. In addition to locating steep elevational gradients, the TPI was used to characterize the geomorphology of the depressions $\geq$10 m deep located in the

DEM. From the segmented image, we used ArcGIS (v. 9.3) coupled with Hawth's Analysis Tools (Beyer, 2004) to quantify numerous parameters of the pixels associated with each depression, i.e., average depth, maximum depth, standard error of depth measures (bottom roughness), opening perimeter, opening area. As topographic features are inherently fractal surfaces (Russ, 1994), the TPI measure is a function of the annulus thickness (w) and inner radius (r) of the annulus (Fig. 3). By analyzing the morphologic parameters with differing annulus scales, we can distinguish among conical, cylindrical, and irregular or more complex openings such as multiple connected depressions or saddle backs.

Lastly, an ordination using principal-components analysis was performed on the LiDAR-derived morphologic parameters for vertical depressions 10 m or more deep. This was done to understand the range of karst depressions that could be detected by LiDAR in the landscape around Caracol as a function of the inner radius and width of the annulus.

Results and Discussion

Depression Identification and Field Verification

Sixty-one depressions 10 or more meters deep were identified in the 200 km^2 DEM by visually scanning the image from top to bottom and left to right for patches that were deeper (darker) than their surroundings and by using the Topographic Position Index filter. These were fairly well distributed across the Caracol landscape, but were more common in the hilly terrain on the outskirts of the region with the highest concentration of monumental architecture, which is also the hub of the half-dozen causeways that radiate outward. Only one depression, Cohune Ridge Cave, which is west of depression 50 in Figure 1, had been previously known (Feld, 1994). Other known cave openings (Feld, 1994) were either too shallow or were horizontal, and not detected by the LiDAR scan. Five of the previously unrecorded depressions relatively close to the epicenter were located in the field. All had vegetation above the depression that obscured it from traditional passive remote-sensing techniques. Two of these had massive openings, depressions 23 (1919 m^2) and 24 (1550 m^2). During this ground verification, we did not take depth and width measurements on the ground for comparison with the LiDAR-derived measurements. The former was inaccessible without vertical equipment; the latter was explored in a cursory fashion and did not appear to contain Maya artifacts. Of the remaining three one was simply a steep rock face adjacent to a hill, one had an opening of 6 m^2 and a steep shaft >15 m deep that was inaccessible without vertical equipment, and the last one

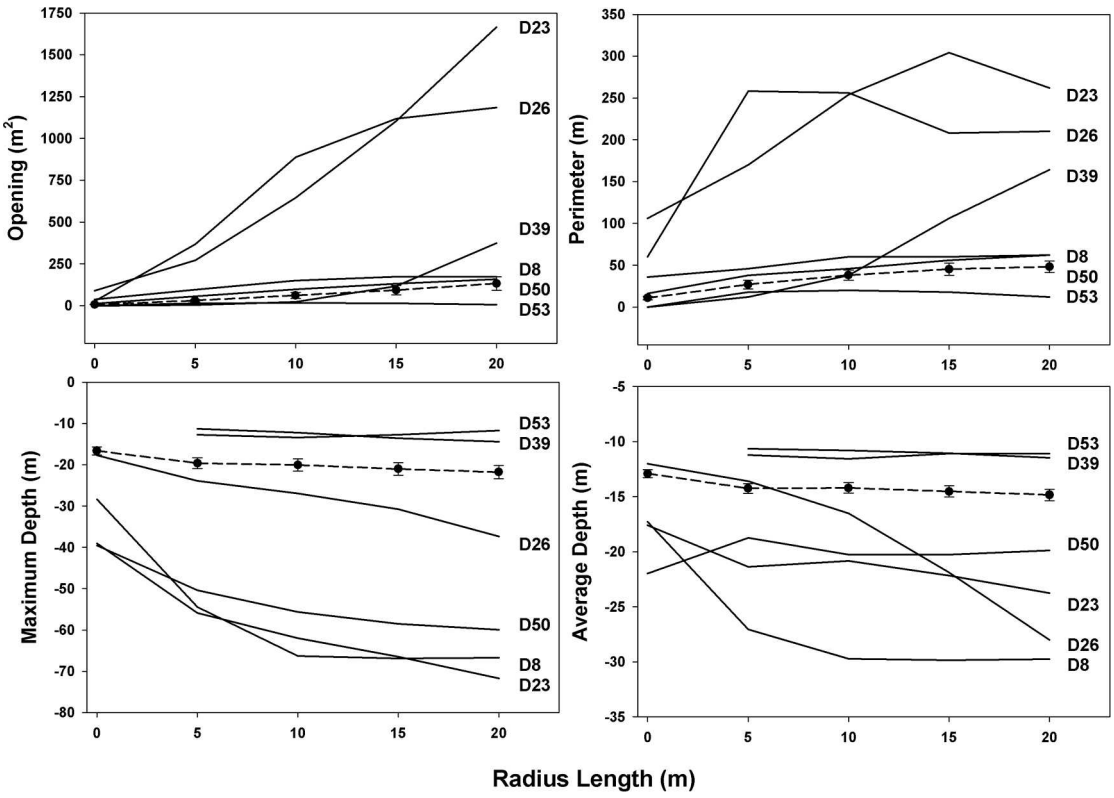

Figure 4. Change in morphologic parameters of selected potential cave opening in Figure 1 derived with TPI from the DEM as a function of inner radius (r), keeping the annulus thickness constant (w = 5 m). The points on the dashed line are the averages of the 61 depressions at least 10 m deep, with one standard error indicated.

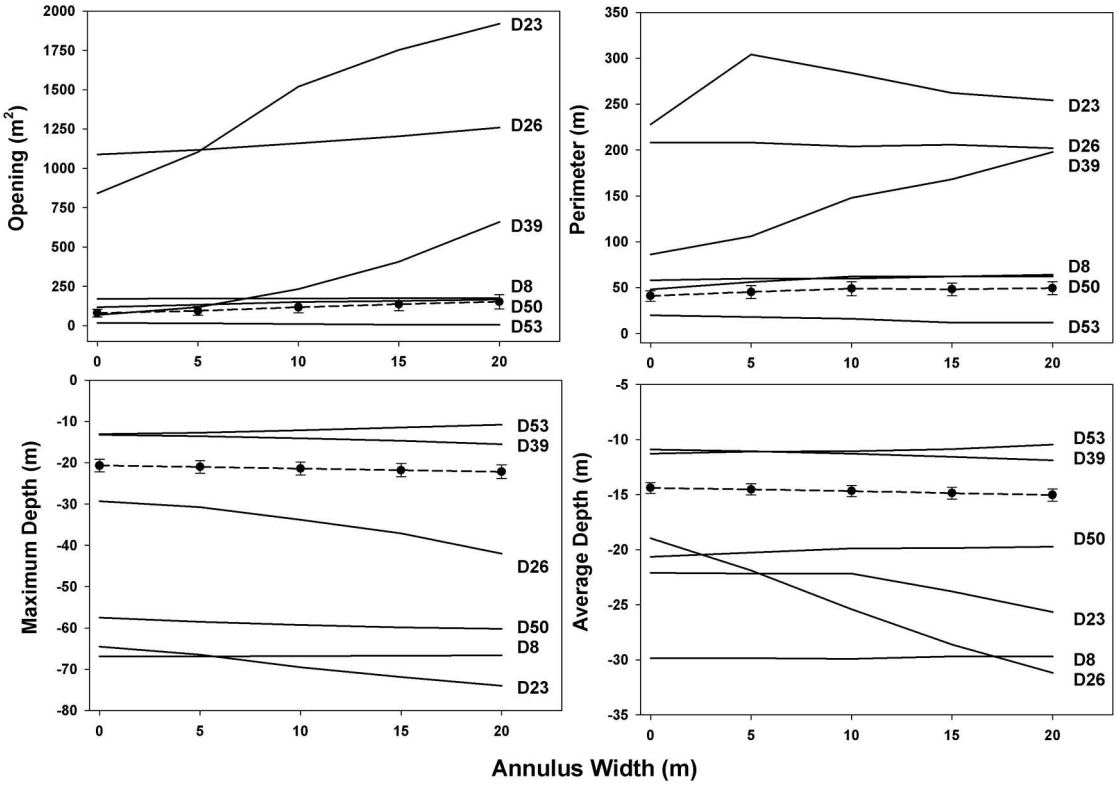

Figure 5. Change in morphologic parameters of potential cave openings derived with TPI from the DEM as a function of annulus thickness (w) keeping the inner radius constant (r = 15). The points on the dashed line are the averages of the 61 depressions at least m deep, with one standard error indicated.

was an accessible cave with an opening of 8 m^2. For this cave, the LiDAR detected a maximum depth of 10.9 m. It was explored and found to consist of several rooms with speleothems such as soda straw stalactites, stalagmites, flowstone, and splash cup structures, as well as archaeological features such as human bones and pottery.

MORPHOLOGIC CHARACTERIZATION

Based on an annulus thickness of 20 m and an inner radius of 15 m (Fig. 4), the average depression opening was 149.3 m^2 (SD=359.8 m^2), and the average maximum depth was 21.5 m (SD=13.8). Based on an annulus thickness of 5 m and an inner radius of 20 m (Fig. 5), the average

Table 1. Eigenvectors associated with the principal component analysis of the LiDAR-derived parameters that characterize the 61 depression morphologies. The numbers in parentheses are the percentages of variance explained by the principal components axes. Slopes are functions of the annulus inner radius (r; w = 5) and thickness (w; r = 15) as shown in Figures 4 and 5.

Parameters	PC1 (52.5%)	PC2 (22.9%)	PC3 (9.1%)
Maximum Depth	−0.23	−0.36	0.32
Average Depth	−0.23	−0.42	0.04
Standard Error of Depth	−0.07	0.41	−0.22
Opening Area	0.35	−0.11	0.04
Perimeter	0.35	−0.16	−0.06
Slope Max Depth (r)	−0.24	−0.35	0.28
Slope Avg Depth (r)	−0.21	−0.32	−0.30
Slope Area (r)	0.35	−0.08	0.12
Slope Perimeter (r)	0.30	−0.29	−0.11
Slope Max Depth (w)	−0.32	−0.00	−0.26
Slope Avg Depth (w)	−0.26	−0.03	−0.58
Slope Area (w)	0.30	−0.24	−0.20
Slope Perimeter (w)	0.12	−0.34	−0.39

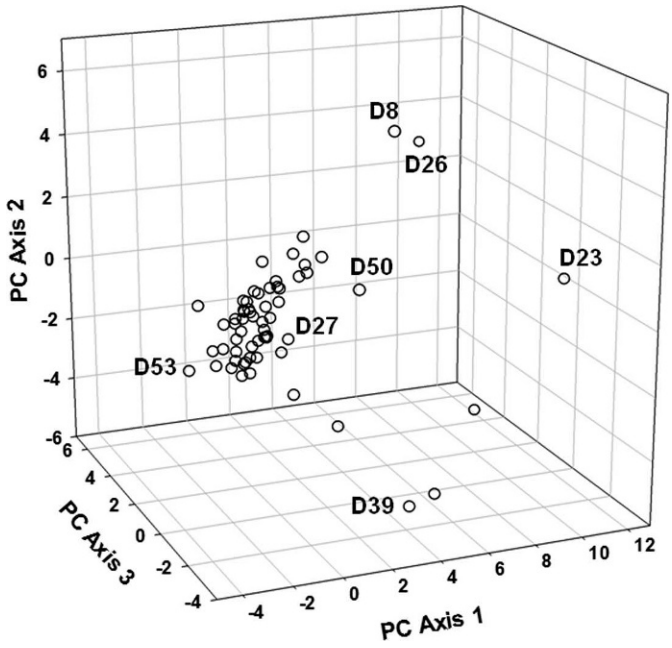

Figure 6. Ordination of depressions based on morphological characters derived using TPI for different scales of annulus width and radius length. The numbered markers correspond to depressions on Figure 1 that represent the extremities for the three principal component axes except number 27, which corresponds to the depression whose morphology most resembled the mean.

depression opening was 130.4 m^2 (SD=313.5); the average maximum depth was 21.1 m (SD=13.5). The general trends with increasing annulus thickness (holding the inner radius constant at 15 m) and inner radius (holding the thickness constant at 5 m) showed slight increases in opening area and perimeter length and slight increases in maximum and average depths (Figs. 4 and 5). However, these effects varied substantially for individual depressions.

The first three principal components (PC) axes accounted for 84.5% of the variance (Table 1). The first PC axis was positively weighted on parameters that characterized the morphology of the depressions' opening, its area and perimeter. The second PC axis was negatively weighted on parameters that characterized the depressions' average and maximum depth and standard error of depth. The third PC axis was negatively weighted on parameters that are related to scaling effects, i.e., slopes of parameter measures as a function of r and w. The ordination showed little distinct grouping of depression morphologies (Fig. 6). All but about ten of these depression morphologies were concentrated slightly on the negative side of PC Axis 1 and near the zero intercept of PC Axis 2 and PC Axis 3. This implies that the depressions tend to be smaller than the average, which is probably skewed by the few much larger depressions. D27, the depression closest to the average of the 61 depressions, based on their positions in the ordination space, had an average depth of 13.2 m (13.5 m), a maximum depth of 25.3 m (24.8 m), and an opening of 86 m^2 (67 m^2) with r = 20 m and w = 15 m (r = 5 m and w = 20 m). The hillshaded rendering of this nearly average depression is shown in Figure 7. The irregular bottom is the cause of the discrepancy between the average and maximum depths. Its conical shape resulted in its opening area and maximum depth being related to the scale of both the annulus width and radius length.

The depressions with extreme morphologies, as represented by the PC axes, are rendered in Figure 8. The first PC axis shows two depressions that are distinguished by opening area; D53 has an opening of 5 m^2 and D23 has an opening of 1919 m^2 when analyzed with an annulus thickness of 20 m and inner radius of 15 m. The second PC axis juxtaposes a narrow, deep D8 and a broad, shallow D39. The standard error of the depth measure is among the highest and lowest for D8 and D39, respectively. The third PC axis contrasts a slightly slanted, flat-sided D26 and a complex, sharply recessed D50. Average depth increased for D26 and decreased for D50 with increasing annulus thickness. The decrease for D50 was unusual and the greatest among the 61 depressions.

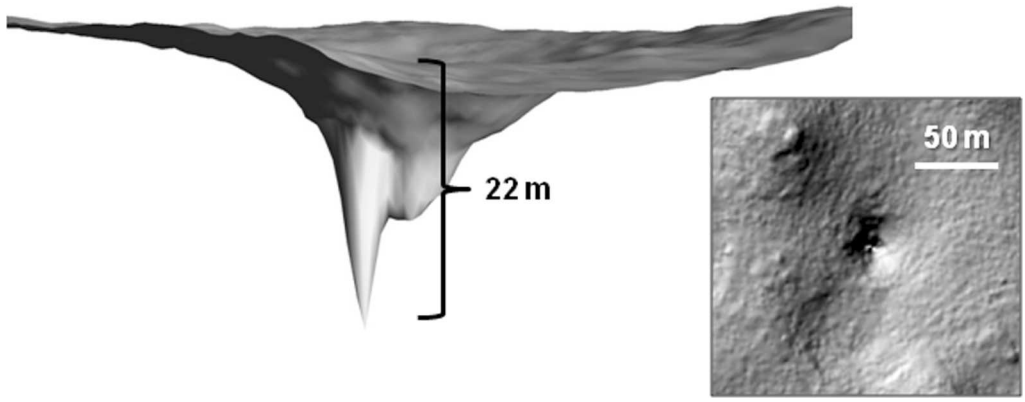

Figure 7. Bare-earth 3-D rendering and top-down view of depression 27, the one with the most typical morphology, closest to the centroid of the 61 depressions in the volume defined by the three principal component axes of ordination space (Fig. 6).

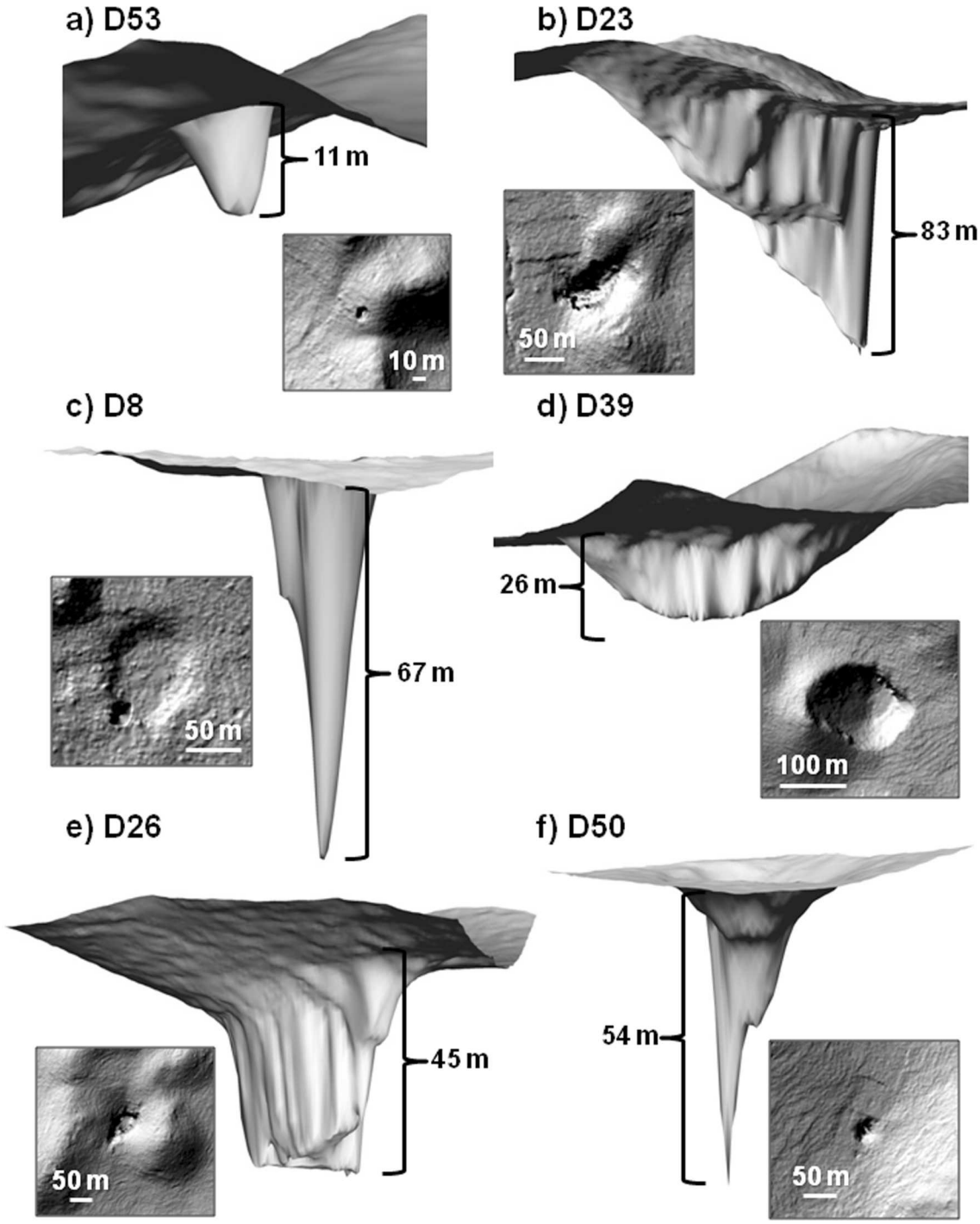

Figure 8. Morphologies of some depressions at the extremes in the three ordination axes (Fig. 6). Hillshaded 3-D renderings and top-down views of depression 53 juxtaposed with depression 23 for PC Axis 1, depression 8 juxtaposed with depression 39 for PC Axis 2, and depression 26 juxtaposed with depression 50 for PC Axis3.

This type of morphological analysis shows the range of shapes and sizes of the depressions and provides some level of guidance for future exploration; it may help indicate how the depression was formed and provide information as to the historic accessibility of the depression for the ancient Maya, as well as for current archaeologists.

Conclusions

Remote sensing of geomorphological features in a karst landscape is not particularly novel (e.g., Siart et al., 2009); however, detecting fine-scale (1 m horizontal resolution) karstic features across a densely forested landscape as

described here is unprecedented. Through this airborne LiDAR study, we detected 60 previously undocumented vertical depressions, shafts, and cave entrances that pockmark the karstic landscape beneath the dense rainforest canopy of western Belize. This study demonstrates the capability of LiDAR to detect surface features that may represent entrances to subterranean geological complexes. As prospecting for openings is often laborious, time-consuming work, this application of LiDAR should improve the efficiency of cave location. However, as many caves used by the Maya have horizontal or very small openings, ground searches on foot are necessary for a comprehensive inventory.

Though there are several ways to partition DEM landscapes into a variety of terrain types (e.g., Yokoyama et al., 2002; Denizman, 2003; Iwahashi and Pike, 2007; Stepinski and Bagaria, 2009; Patel and Sarkar, 2010; Prima and Yoshida, 2010), the Topographic Position Index seemed effective at locating and quantifying the geomorphology of these recessed features. Somewhat unexpectedly, the LiDAR sensor system flying at an altitude of nearly 1 km was able to record a variety of geomorphologies from these vertical depressions. This rich dataset shows some of these depressions to be very deep (>50 m) with massive openings (>350 m across); others are deep (>25 m) with relatively narrow (<5 m across) openings. Most of these depressions represent caves that were contemporary with the ancient Maya and likely contain artifacts, but a few may be more recent. As only a tenth of these depressions have been located and explored on the ground, it is important that these potentially culturally significant sites remain undisturbed until their archaeological context can be realized.

Acknowledgments

This research was supported by NASA Grant #NNX08AM11G through the Space Archaeology program and the University of Central Florida–University of Florida–Space Research Initiative (UCF-UF-SRI). We appreciated conversations with Jaime Awe, Holley Moyes, and Cameron Griffith, members of the Western Belize Regional Cave Project (WBRCP), about caving and cave detection using remote sensing techniques in Belize. The expertise of James Angelo with Fusion and the National Center for Airborne Laser Mapping (NCALM), Ramesh Shrestha, Clint Slatton, Bill Carter, and Michael Sartori, helped to make this study possible.

References

Allee, W.C., 1926, Measurement of environmental factors in the tropical rain-forest of Panama, Ecology, v. 7, p. 273–302.

Beyer, H.L., 2004, Hawth's Analysis Tools for ArcGIS, available at: www.spatialecology.com/htools, [accessed September 24, 2010].

Brady, J.E., and Prufer, K.M., 2005, In the Maw of the Earth Monster: Mesoamerican Ritual Cave Use: Austin, University of Texas Press, 438 p.

Brokaw, N.V.L., 1992, Vegetation and tree flora in the central area of the Caracol archaeological reserve, Belize: Manomet, Massachusetts, Manomet Observatory for Conservation Science, 28 p.

Carter, W., Shrestha, R., Tuell, G., Bloomquist, D., and Sartori, M., 2001, Airborne laser swath mapping shines new light on Earth's topography: Eos, v. 82, 549, 550, 555 p.

Chase A.F., 1988, Jungle surveying: mapping the archaeological site of Caracol, Belize: Point of Beginning, v. 13, p. 10–24.

Chase, A.F., and Chase, D.Z., 1996, A mighty Maya nation: how Caracol built an empire by cultivating its 'middle class': Archaeology, v. 49, p. 66–72.

Chase, A.F., and Chase, D.Z., 2001, Ancient Maya causeways and site organization at Caracol, Belize: Ancient Mesoamerica, v. 12, p. 273–281.

Chase, A.F., Chase, D.Z., and Weishampel, J.F., 2010, Lasers in the jungle: airborne sensors reveal a vast Maya landscape: Archaeology, v. 63, no. 4, p. 27–29.

Chase, A.F., Chase, D.Z., Weishampel, J.F., Drake, J.B., Shrestha, R.L., Slatton, K.C., Awe, J.J., and Carter, W.E., 2011, Airborne LiDAR, archaeology, and the ancient Maya landscape at Caracol, Belize: Journal of Archaeological Science, v. 38, p. 387–398. doi: 10.1016/j.jas.2010.09.018.

Cushing, G.E., Titus, T.N., Wynne, J.J., and Christensen, P.R., 2007, THEMIS observes possible cave skylights on Mars: Geophysical Research Letters, v. 34, L17201 p. doi: 10.1029/2007GL030709.

Denizman, C., 2003, Morphometric and spatial distribution parameters of karstic depressions, lower Suwanee River basin, Florida: Journal of Cave and Karst Studies, v. 65, p. 29–35.

Feld, W.A., 1994, The caves of Caracol: initial impressions, *in* Chase, D.Z., and Chase, A.F., eds., Studies in the archaeology of Caracol, Belize. San Francisco, Pre-Columbian Art Research Institute Monograph 7, p. 76–82.

Gallagher, J.M., and Josephs, R.L., 2008, Using LiDAR to detect cultural resources in a forested environment: an example from Isle Royale National Park, Michigan, USA: Archaeological Prospection, v. 15, p. 187–206. doi: 10.1002/arp.333.

González-Aguilera, D., Muñoz-Nieto, A., Gómez-Lahoz, J., Herrero-Pascual, J., and Gutierrez-Alonso, G., 2009, 3D digital surveying and modeling of cave geometry: application to Paleolithic rock art: Sensors, v. 9, p. 1108–1127. doi: 10.3390/s90201108.

Griffith, C., 2000, Remote sensing in cave research, available at: www.archaeology.org/online/features/belize/remote.html, [accessed September 24, 2010].

Griffith, C., 2001, Locating Cave Sites: Results of our remote-sensing research, available at: www.archaeology.org/interactive/belize/newremote.html, [accessed March 2, 2011].

Guisan, A., Weiss, S.B., and Weiss, A.D., 1999, GLM versus CCA spatial modeling of plant species distribution: Plant Ecology, v. 143, p. 107–122. doi: 10.1023/A:1009841519580.

Hofton, M.A., Rocchio, L.E., Blair, J.B., and Dubayah, R., 2002, Validation of vegetation canopy lidar sub-canopy topography measurements for a dense tropical forest: Journal of Geodynamics, v. 34, p. 491–502. doi: 10.1016/S0264-3707(02)00046-7.

Hunter-Tate, C.C., 1994, The chultuns of Caracol, *in* Chase, D.Z., and Chase, A.F., eds., Studies in the archaeology of Caracol, Belize. San Francisco, Pre-Columbian Art Research Institute Monograph 7, p. 64–75.

Iwahashi, J., and Pike, R.J., 2007, Automated classifications of topography from DEMs by an unsupervised nested-means algorithm and a three-part geometric signature: Geomorphology, v. 86, p. 409–440. doi: 10.1016/j.geomorph.2006.09.012.

Jenness, J., Brost, B., and Beier, P., 2010, Land Facet Corridor Designer, available at: www.jennessent.com/downloads/LandFacetCorredor.zip, [accessed September 24, 2010].

Lerma, J.L., Navarro, S., Cabrelles, M., and Villaverde, V., 2010, Terrestrial laser scanning and close range photogrammetry for 3D archaeological documentation: the Upper Palaeolithic cave of Parpalló as a case study: Journal of Archaeological Science, v. 37, p. 499–507. doi: 10.1016/j.jas.2009.10.011.

McNatt, L., 1996, Cave archaeology of Belize: Journal of Cave and Karst Studies, v. 58, p. 81–99.

Miller, T., 1990, Caves and caving in Belize, Caves and Caving, no. 49, p. 2–4.

Moyes, H., 2002, The use of GIS in the spatial analysis of an archaeological cave site: Journal of Cave and Karst Studies, v. 64, p. 9–16.

Patel, P.P., and Sarkar, A., 2010, Terrain characterization using SRTM data: Journal of Indian Society of Remote Sensing, v. 38, p. 11–24. doi: 10.1007/s12524-010-0008-8.

Pendergast, D.M., 1969, The Prehistory of Actun Balam, British Honduras: Toronto, Royal Ontario Museum Occasional Paper 16, Art and Archaeology, 68 p.

Pendergast, D.M., 1970, A. H. Anderson's Excavations at Rio Frio Cave E, British Honduras (Belize): Toronto, University of Toronto, Royal Ontario Museum Occasional Paper 20, Art and Archaeology, 59 p.

Pendergast, D.M., and Savage, H.G., 1971, Excavations at Eduardo Quiroz Cave British Honduras (Belize): Toronto, University of Toronto, Royal Ontario Museum Occasional Paper 21, Art and Archaeology, 123 p.

Prima, O.D.A., and Yoshida, T., 2010, Characterization of volcanic geomorphology and geology by slope and topographic openness: Geomorphology, v. 118, p. 22–32. doi: 10.1016/j.geomorph.2009.12.005.

Prufer, K.M., and Brady, J.E., 2005, Stone Houses and Earth Lords: Maya Religion in the Cave Context: Boulder, University Press of Colorado, 392 p.

Reeder, P., Brady, J.E., and Webster, J., 1998, Geoarchaeological investigations on the northern Vaca Plateau, Belize: Mexicon, v. 20, p. 37–41.

Ricketson, O. Jr., and Kidder, A.V., 1930, An archaeological reconnaissance by air in Central America: Geographical Review, v. 20, p. 177–206.

Russ, J.C., 1994, Fractal Surfaces, New York, Plenum Press, 309 p.

Sellers, B., and Chamberlain, A., 1998, Cave detection using ground penetrating radar: The Archaeologist, no. 31, p. 20–21.

Siart, C., Bubenser, O., and Eitel, B., 2009, Combining digital elevation data (SRTM/ASTER), high resolution satellite imagery (Quickbird) and GIS for geomorphological mapping: A multi-component case study on Mediterranean karst in Central Crete: Geomorphology, v. 112, p. 106–121. doi: 10.1016/j.geomorph.2009.05.010.

Stepinski, T.F., and Bagaria, C., 2009, Segmentation-based unsupervised terrain classification for generation of physiographic maps: IEEE Geoscience and Remote Sensing Letters, v. 6, p. 733–737. doi: 10.1109/LGRS.2009.2024333.

Weishampel, J.F., Blair, J.B., Dubayah, R., Clark, D.B., and Knox, R.G., 2000a, Canopy topography of an old-growth tropical rainforest landscape: Selbyana, 21, p. 79–87.

Weishampel, J.F., Blair, J.B., Knox, R.G., Dubayah, R., and Clark, D.B., 2000b, Volumetric lidar return patterns from an old-growth tropical rainforest canopy: International Journal of Remote Sensing, v. 21, p. 409–415. doi: 10.1080/014311600210939.

Weishampel, J.F., Chase, A.F., Chase, D.Z., Drake, J.B., Shrestha, R.L., Slatton, K.C., Awe, J.J., Hightower, J., and Angelo, J., 2010, Remote sensing of ancient Maya land use features at Caracol, Belize related to tropical rainforest structure, *in* Forte, M., Campana, S., and Liuzza, C., eds., Space, Time, Place: Third International Conference on Remote Sensing Archaeology: Oxford, Archaeopress, BAR International Series 2118, p. 45–52.

Weiss, A., 2001, Topographic position and landform analysis, available at: www.jennessent.com/downloads/TPI-poster-TNC_18x22.pdf, [accessed September 24, 2010].

Wynne, J.J., Titus, T.N., and Diaz, G.C., 2008, On developing thermal cave detection techniques for earth, the moon and mars: Earth and Planetary Science Letters, v. 272, p. 240–250. doi: 10.1016/j.epsl.2008.04.037.

Yokoyama, R., Shirawawa, M., and Pike, R.J., 2002, Visualizing topography by openness: a new application of image processing to digital elevation models: Photogrammetric Engineering & Remote Sensing, v. 68, p. 257–265.

Ø. Hammer, S.E. Lauritzen, and B. Jamtveit – Stability of dissolution flutes under turbulent flow. *Journal of Cave and Karst Studies,* v. 73, no. 3, p. 181–186. DOI: 10.4311/2011JCKS0200

STABILITY OF DISSOLUTION FLUTES UNDER TURBULENT FLOW

ØYVIND HAMMER[1*], STEIN E. LAURITZEN[2], AND BJØRN JAMTVEIT[1]

Abstract: Dissolution of a solid surface under turbulent fluid flow can lead to the formation of periodic ripple-like structures with a wavelength dependent upon flow velocity. A model coupling hydrodynamics with mass transport and dissolution kinetics shows that the shape stability of these structures can be explained from fundamental principles. The effects of a subgrid diffusion boundary layer must be included in the dissolution model to produce realistic results. The importance of including not only the mean flow velocity, but also the turbulent component of flow, in the dissolution model is emphasized. The numerical experiments also compare dissolution profiles for gypsum and calcite.

INTRODUCTION

Limestone dissolution under turbulent, high-velocity flow commonly leads to a certain surface roughness morphology known as scallops. Such scallops can have complex, three-dimensional shapes, but can also take the form of ripples or flutes oriented normal to the flow direction (Curl, 1966, 1974; Goodchild and Ford, 1971; Blumberg and Curl, 1974; Thomas, 1979; Gale, 1984; Villien, et al. 2005).

One of the most interesting properties of dissolution flutes is that their profiles are stable in time, while migrating both vertically as the surface is globally dissolved and in the downstream direction in a soliton-like manner (Blumberg and Curl, 1974). Such behavior is maintained as long as the flute with profile $y(x,t)$ obeys the one-dimensional transport equation with horizontal velocity v_x and an added term v_y for the mean dissolution rate (corresponding to vertical displacement velocity):

$$\frac{\partial y}{\partial t} = -v_x \frac{\partial y}{\partial x} - v_y. \quad (1)$$

This equation refers to dissolution rates in the vertical direction, and x is the horizontal (i.e., not tangential to the profile). The free parameters v_x and v_y allow for a family of possible dissolution profiles all compatible with a given flute shape. These parameters also imply a certain angle of translation of the flute with respect to the horizontal, as $\tan\theta = v_y / v_x$.

The dissolution rate in a direction normal to the surface can be calculated geometrically as (cf. Curl 1966, eq. 15)

$$\frac{\partial y'}{\partial t} = \frac{\frac{\partial y}{\partial t}}{\sqrt{1+\left(\frac{\partial y}{\partial x}\right)^2}} = \frac{-v_x \frac{\partial y}{\partial x} - v_y}{\sqrt{1+\left(\frac{\partial y}{\partial x}\right)^2}}. \quad (2)$$

Curl (1966) and Blumberg and Curl (1974) provided careful theoretical analysis and experimental results on dissolution scallops and flutes in gypsum. They found that the Reynolds number calculated from flute wavelength and main-channel maximum velocity remained fairly constant at Re = 23300 over a large range of flow velocities, implying an inverse relationship between flow velocity and flute wavelength. Bird et al. (2009) presented a full 3D fluid-dynamics simulation of flow over static dissolution scallops, confirming several of the observations of flow patterns described by Blumberg and Curl (1974). A recent review of dissolution scallops was given by Meakin and Jamtveit (2010).

The purpose of this paper is to couple a simple 2D fluid dynamics model to a dissolution model, and to compare the simulation dissolution profiles with the dissolution profiles required for the stability of experimental flute shapes.

METHODS

The numerical experiments all use a fixed two-dimensional flute geometry reported from laboratory experiments with gypsum at Re = 23300, flute wavelength 5.1 cm (Blumberg and Curl 1974). The empirical sine series of flute geometry normalized to flute wavelength is

$$\hat{Y} = 0.112\sin\pi\hat{X} + 0.028\sin2\pi\hat{X} - 0.004\sin3\pi\hat{X}. \quad (3)$$

To reduce boundary effects, hydrodynamics were simulated using three consecutive flutes, and subsequent study concentrated on the central flute. The total simulated area was 15.24 by 5.08 cm. A grid size of 612 by 204 gave a resolution of h = 0.25 mm. The Navier-Stokes code NaSt2D-2.0 (Griebel et al. 1997; Bauerfeind, 2006) was used with a k-ε turbulence model. In addition to the mean velocity vector field **u**, this code also produces the eddy (turbulent) viscosity v_t that can be regarded as a measure of

* Corresponding Author
[1] Physics of Geological Processes, University of Oslo, PO Box 1048 Blindern, 0316 Oslo, Norway
[2] Department of Earth Science, University of Bergen, Allegaten 41, 5007 Bergen, Norway

degree of local turbulence (Boussinesq approximation). The results of the computational fluid dynamics were cross-validated using the k-ε turbulence model provided in an independent finite volume, unstructured mesh code, OpenFoam version 1.6 (www.openfoam.com). The velocity and eddy viscosity fields given by the two programs were practically identical.

The equations for scalar transport of dissolved species were approximated using explicit finite difference methods. The advection term was implemented with a second-order Lax-Wendroff difference scheme (Lax and Wendroff, 1960). Turbulent mixing was approximated using the Reynolds analogy, where mixing is modeled as diffusion with a turbulent (eddy) diffusivity that can be orders of magnitude larger than molecular diffusivity. The turbulent diffusivity is defined as

$$\Gamma = \frac{v_t}{\sigma_t}, \tag{4}$$

where v_t is turbulent viscosity and σ_t is the turbulent Prandtl number. We used $\sigma_t = 1.0$. The complete transport equation for the concentration c with mean velocity field $\mathbf{u}$ becomes

$$\frac{\partial c}{\partial t} = -\mathbf{u}\cdot\nabla c + \nabla\cdot(\Gamma\nabla c). \tag{5}$$

Precipitation and dissolution rates under flow can be largely dependent upon the thickness of a diffusive boundary layer (e.g., Buhmann and Dreybrodt 1985; Liu and Dreybrodt 1997; Opdyke et al., 1987). The diffusive boundary layer can be only a few micrometers thick at high flow rates and is not captured with the grid size used here. For example, Curl (1966) reports a transfer coefficient $k = 3.4 \times 10^{-3}$ cm s^{-1} under conditions typical for flute formation. With a molecular diffusion coefficient of $D = 1.2 \times 10^{-5}$ cm^2 s^{-1}, this corresponds to a diffusive boundary layer thickness $\varepsilon = 35$ μm. The thickness of the diffusive boundary layer can be defined as the point where molecular and turbulent diffusivities are equal. With y the perpendicular distance from the solid-liquid interface into the liquid, molecular diffusion dominates in the region $y < \varepsilon$. With D the molecular diffusivity, we then have

$$\Gamma(\varepsilon) = \frac{v_t(\varepsilon)}{\sigma_t} = D. \tag{6}$$

Away from the boundary the eddy viscosity v_t (y') is nearly linear, vanishing near the boundary (Kleinstein, 1967). This is in accordance with the eddy viscosity profile seen from the NaSt2D-2.0 solution down to the first liquid cell over the boundary ($y' = 250$ μm). Near the boundary, the eddy viscosity profile becomes more complex and generally follows a power law with 3 as exponent (Kleinstein, 1967). However, this nonlinearity is expected to be found in a layer much thinner than the grid size. We therefore roughly estimate the subgrid values of the eddy viscosity v_t (y') by linear interpolation between the surface (v_t (0) = 0) and the prescribed value in the first cell. The thickness ε of the diffusive boundary layer can then be computed from Equation (6).

An alternative estimation of the diffusive boundary layer thickness is based on the viscous boundary layer thickness, which is much larger. The viscous boundary layer thickness δ can be defined as the height where turbulent diffusivity is equal to kinematic viscosity v and can be estimated by linear interpolation of turbulent diffusivity from the first grid cell to the interface, as above. The diffusive boundary layer thickness is then estimated using an empirical relation

$$\varepsilon = \frac{\delta}{\sigma^{\alpha}}, \tag{7}$$

where $\sigma = \upsilon D$ is the Schmidt number. The exponent α is assumed to be between 1/3 and 1/4 (Wüest and Lorke 2003). With $\sigma \approx 10^3$ and $Sc \approx 1/3$, we have $\varepsilon \approx 0.1\delta$.

The molar dissolution rate of gypsum follows the rate law of Opdyke et al. (1987):

$$R = \frac{D}{\varepsilon}\left(\left[\mathrm{Ca}^{2+}_{\mathrm{eq}}\right] - \left[\mathrm{Ca}^{2+}\right]\right), \tag{8}$$

where $\left[Ca^{2+}_{eq}\right]$ is the equilibrium concentration of 15.4 mM at 20 °C. A more complex, second-order equation was given by Raines and Dewers (1997) and Villien et al. (2005). This reaction adds calcium to the solution, modifying the boundary condition of Equation (5) at the solid-water interface. The transport equations are applied to calcium concentration only. Because the fluid dynamics are many magnitudes faster than the rate of movement of the interface due to dissolution, we run the fluid dynamics in a static geometry, where the boundary conditions are not moving.

Dissolution of calcite uses the method described by Hammer et al. (2008) with the rate equation of Plummer et al. (1978). This requires the modeling of reaction and transport of three species in solution, [CO_2], [Ca^{2+}] and the sum of the carbonate and bicarbonate concentrations $[\mathrm{c}] = \left[\mathrm{HCO}_3^-\right] + \left[\mathrm{CO}_3^{2-}\right]$. The Plummer et al. (1978) rate computed from the concentrations in the fluid cell above the interface is multiplied with an approximate empirical function of the diffusive boundary layer thickness ε, derived from Table 2 in Liu and Dreybrodt (1997):

$$b = 0.02 + \frac{0.001}{\varepsilon + 0.001}. \tag{9}$$

The transport equations use cyclic boundary conditions at the inflow and outflow boundaries. In order to keep the system away from equilibrium, maintaining dissolution over time, a sink for the dissolved species was provided by setting the concentrations to zero at the upper boundary of the domain. For the calcite model, [CO_2] was set to 0.1 mM at the upper boundary.

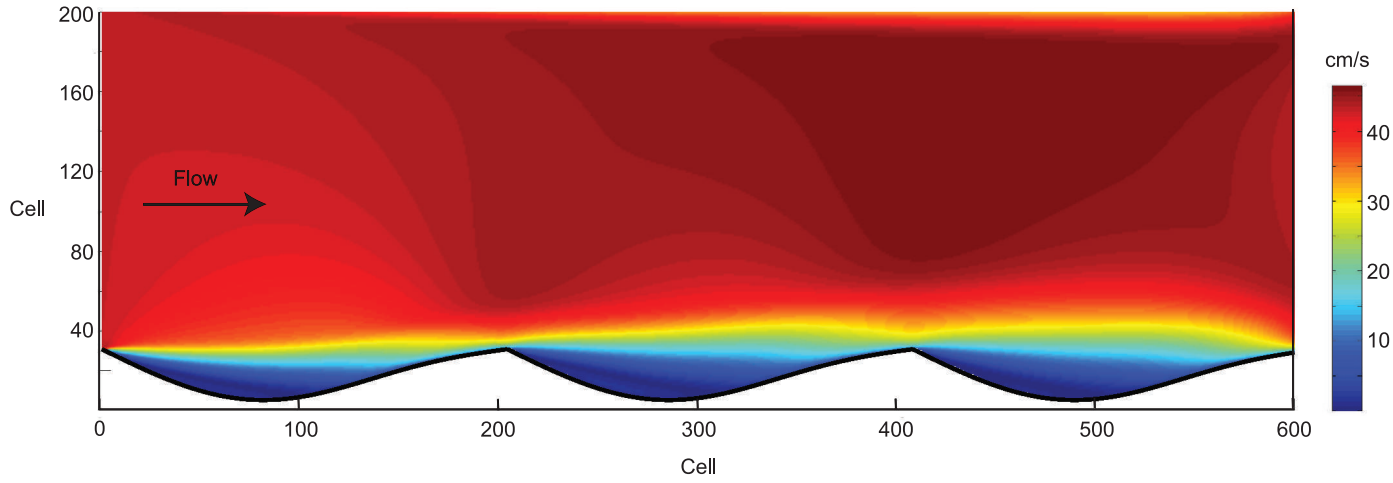

Figure 1. The geometry of the simulation, with the absolute value of mean-field flow velocity (cm/s). Flow from left to right.

Results

The model geometry and mean flow velocity are shown in Figure 1. The flow streamlines in Figure 2 demonstrate flow separation at the crest and the formation of a back eddy. The flow reattachment point is found near the lower end of the stoss side, while the region of maximal eddy viscosity is localized further up the slope. The mean velocity profile away from the fluted wall is precisely logarithmic up to a distance of about 1 cm, after which it starts to diverge from logarithmic towards the middle of the channel due to the inflow and outflow boundary conditions.

Figure 3 shows the Ca concentration field from the dissolution of gypsum, and the simulated dissolution profile together with a theoretical profile (rate normal to the surface) calculated from Equations (2) and (3). Apart from a ragged appearance due to the discretization grid, the simulation result is similar to the theoretical profile, with a sharp decrease in dissolution rate after the crest followed by a gradual increase to a maximum about halfway up the stoss side. However, the recovery of dissolution rate downstream from the crest is somewhat delayed in the simulation compared with the theoretical profile.

To assess the sensitivity to grid resolution, the complete simulation (fluid dynamics, transport and dissolution) was repeated on a twice coarser grid (306 by 102, $h = 0.5$ mm), and also with a 1 mm grid. The dissolution profiles were indistinguishable in shape between these runs, but overall dissolution rate scaled with roughly the square root of h. We ascribe this scale difference to the decrease as cell size increases in average concentration of dissolved species in the first cell over the interface. However, since the shape of the profile is unaffected, this grid dependence does not influence conclusions about the stability of the flutes.

The calcite dissolution profile (Fig. 4) seems further removed from the ideal profile than for the gypsum case, with a more gentle decrease in dissolution rate after the crest and without a clear maximum on the stoss side. Another difference between the two simulations is the smaller amplitude of the dissolution profile compared with the average value for calcite than for gypsum. This implies a larger k/v_x value for calcite, and therefore, a larger angle of flute translation with respect to the horizontal. Using the

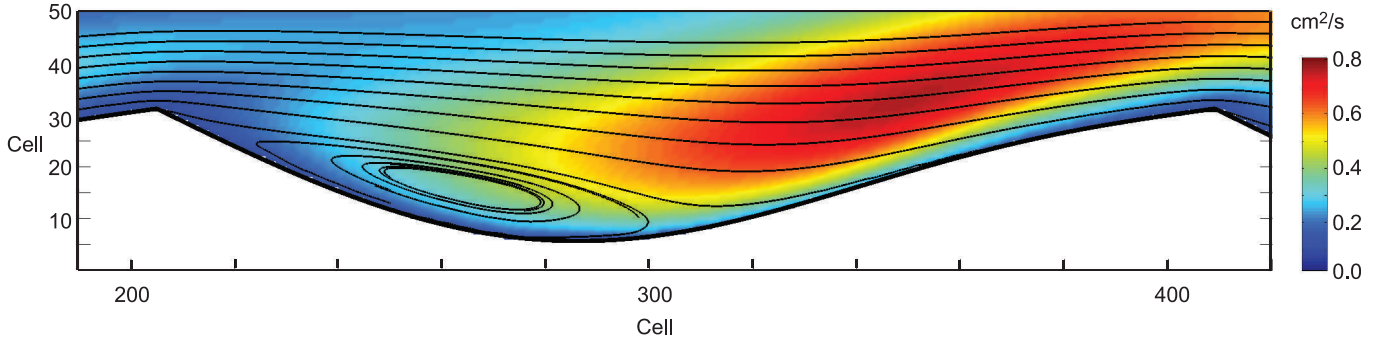

Figure 2. The central part of the modeled domain, with mean-field flow streamlines (black). The eddy viscosity field (colors) indicates degree of local turbulence.

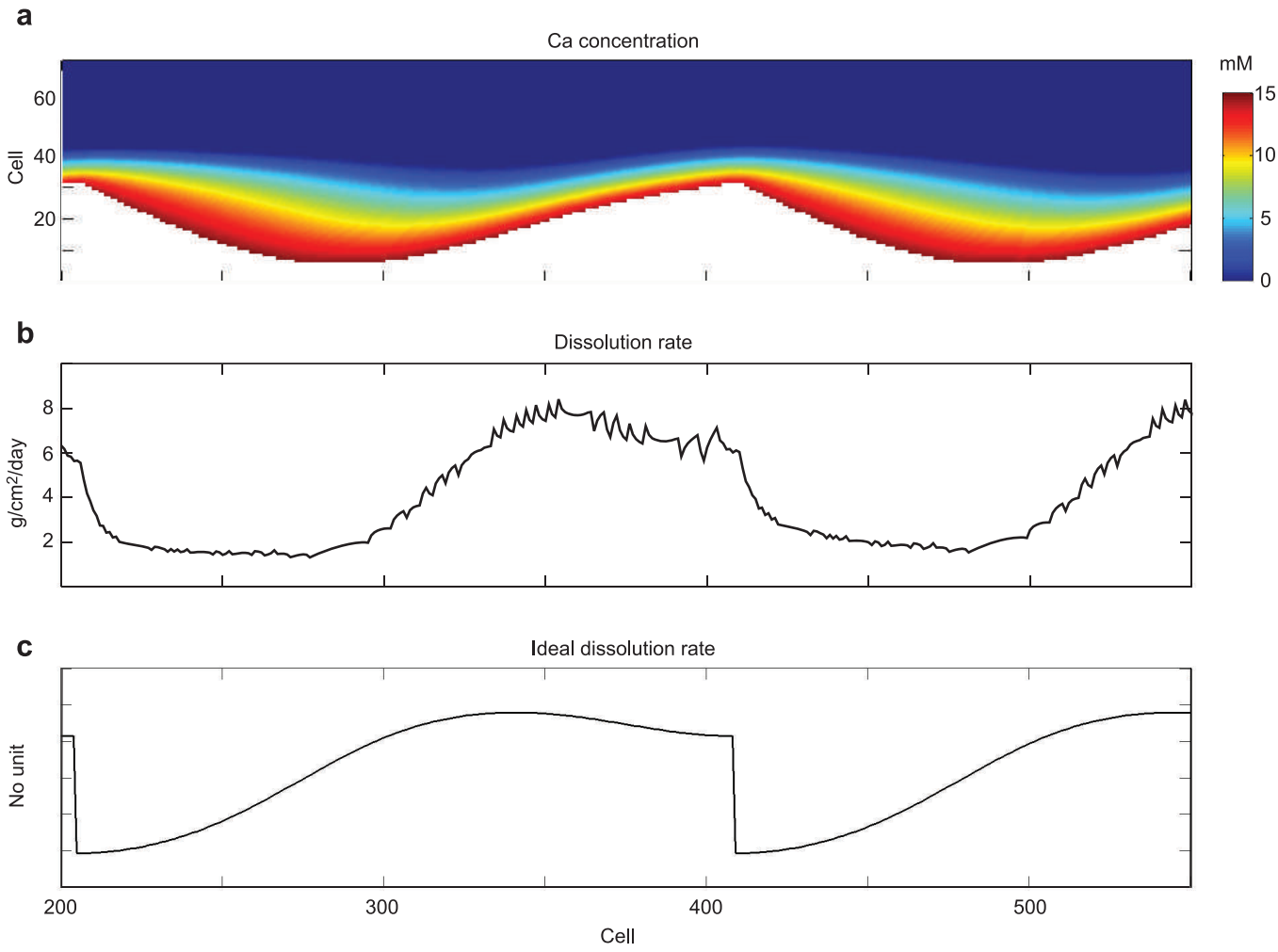

Figure 3. Results from simulation coupling hydrodynamics with gypsum dissolution. a: Calcium concentration in solution (mM). b: Simulated dissolution rate profile, aligned with fig. 3a. c: Theoretical dissolution profile for stable flutes, calculated from Equations 2 and 3.

ratio between mean dissolution rates in the horizontal and vertical directions, the angle at which the flute moves into the dissolving face can be computed as about 54 degrees for the gypsum simulation, compared with the 61 ± 2 degrees reported by Blumberg and Curl (1974) and 80 degrees for the calcite simulation. These differences can only be due to the different equations used for dissolution kinetics, possibly indicating that the rate equation of Plummer et al. (1978) or Equation (9) above is not fully applicable under the conditions simulated here.

The correspondence between ideal and modeled dissolution curve can be illustrated by plotting the $\partial y/\partial t$ from the simulation against $\partial y/\partial x$. According to Equation (1), this relationship should be linear, with slope $-v_x$. By setting $-v_y$ equal to the average dissolution rate from the simulation, the ideal slope can be calculated as $-v_x = v_y/\tan\theta$. As shown in Figure 5 for the gypsum case, the displacement of the dissolution profile downstream of the crest compared to the theoretical case gives too low slope of a on the lee side of the trough, overcompensating for an excessive slope on the stoss side. Near the bottom of the trough and near the top of the crest, the data follow a more linear trend.

DISCUSSION

The simple model described above seems sufficient to capture the essential aspects of the stability of dissolution flutes. The inclusion of turbulent mixing and the thinning of the laminar boundary layer under turbulence are necessary for reproducing a dissolution maximum close to the predicted position. The displacement of the dissolution maximum from the reattachment point and closer to the position of maximum eddy viscosity may indicate that dissolution in this region is controlled more by turbulence effects than by the angle of flow with respect to the surface, as suggested by Bird et al. (2009). On the other hand, the underestimation of dissolution rate near the reattachment point may indicate that the balance between the influence

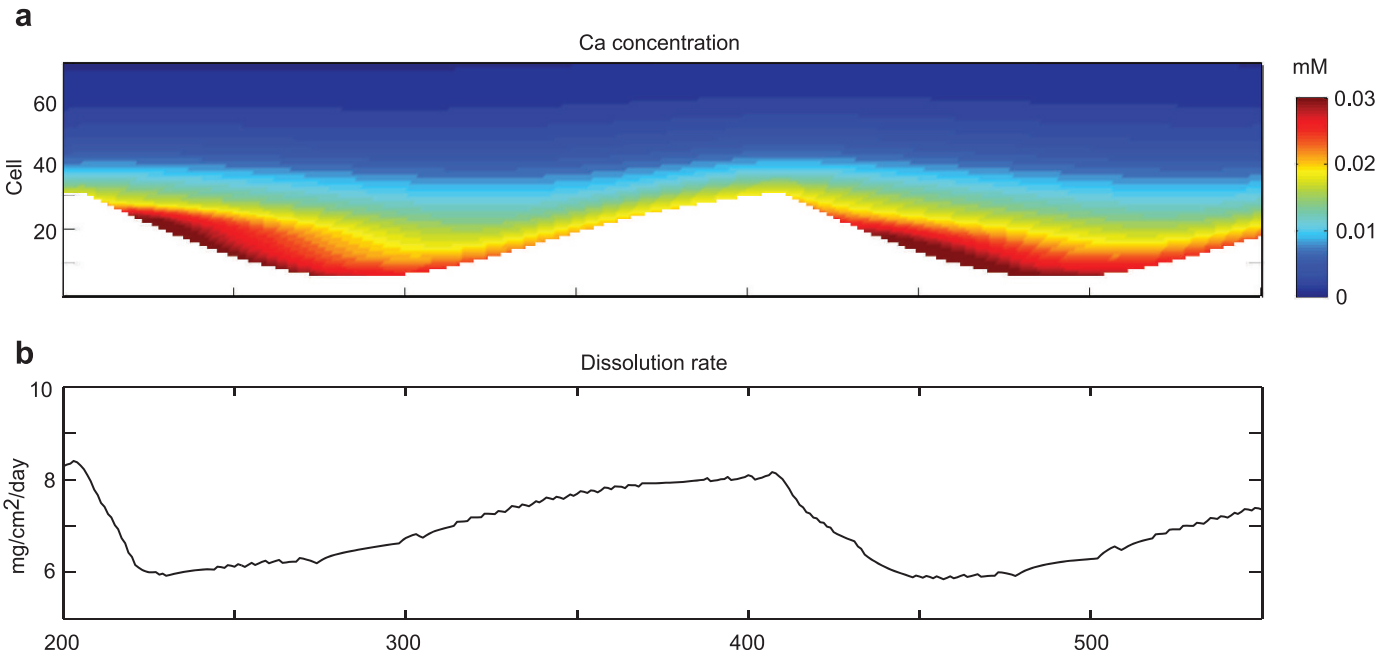

Figure 4. Results from simulation coupling hydrodynamics with calcite dissolution. a: Calcium concentration in solution. b: Simulated dissolution rate profile.

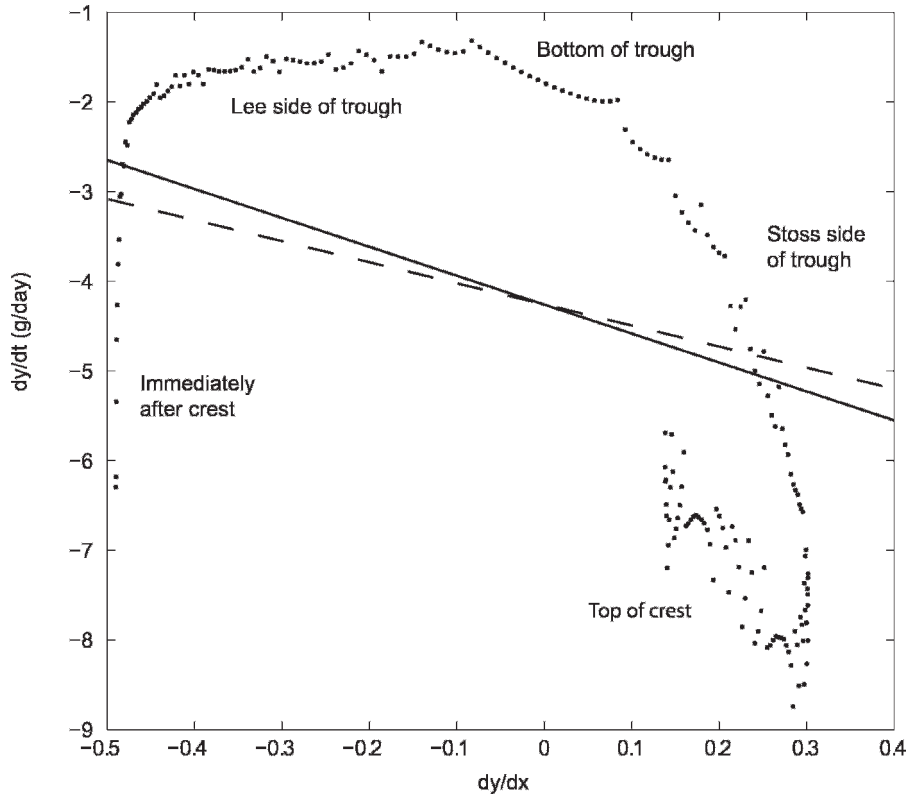

Figure 5. A plot of the result from the gypsum dissolution model, cf Equation (1) in text. Local slope of the flute profile ($\partial y/\partial x$) versus velocity of surface dissolution in the vertical direction ($\partial y/\partial t$). Dashed line: Theoretical relationship for stable flutes based on the experimental dissolution angle of 61° (Blumberg and Curl, 1974). Solid line: Theoretical relationship based on the angle of 54° resulting from the simulation.

of mean flow advection and turbulence needs further tuning to reproduce the theoretical result. More advanced turbulence modeling (including the simulation of unsteady turbulence by, for example, large eddy simulation) and also improved empirical or theoretical models for dissolution kinetics may prove useful in this respect. The exact profile of eddy viscosity very close to the solid-fluid interface (here assumed linear), which influences the estimation of diffusive boundary layer thickness, may also be a factor.

The poorer results of the calcite model compared to the gypsum model are interesting. The only difference between the two simulations is in the dissolution kinetics. It is possible that the different solution and dissolution kinetics of the calcite system would lead to a different stable flute shape than for the gypsum system, and that the gypsum flute geometry used in the simulation does not represent the steady state for calcite. However, the calcite flute shapes illustrated by Curl (1966; Fig. 3) do not appear very different from the gypsum flutes. It is therefore possible that the calcite dissolution model used here does not fully reflect the kinetics in the natural system.

ACKNOWLEDGEMENTS

Thanks to Luiza Angheluta and two anonymous reviewers for useful comments on the manuscript.

This study was supported by a Center of Excellence grant to PGP from the Norwegian Research Council.

REFERENCES

Bauerfeind, K., 2006, Fluid Dynamic Computations with NaSt2D-2.0, Open-source Navier-Stokes solver, http://home.arcor.de/drklaus.bauerfeind/nast/eNaSt2D.html [accessed February 28, 2011].

Bird, A.J., Springer, G.S., Bosch, R.F., and Curl, R.L., 2009, Effects of surface morphologies on flow behavior in karst conduits, *in* Proceedings, 15th International Congress of Speleology: Kerrville, Texas, National Speleological Society, p. 1417–1421.

Blumberg, P.N., and Curl, R.L., 1974, Experimental and theoretical studies of dissolution roughness: Journal of Fluid Mechanics, v. 65, p. 735–751. doi:10.1017/S0022112074001625.

Buhmann, D., and Dreybrodt, W., 1985, The kinetics of calcite dissolution and precipitation in geologically relevant situations of karst areas. 1. Open system: Chemical Geology, v. 48, p. 189–211. doi:10.1016/0009-2541(85)90046-4.

Curl, R.L., 1966, Scallops and flutes: Transactions of Cave Research Group of Great Britain, v. 7, p. 121–160.

Curl, R.L., 1974, Deducing flow velocity in cave conduits from scallops: National Speological Society Bulletin, v. 36, p. 1–5.

Gale, S., 1984, The hydraulics of conduit flow in carbonate aquifers: Journal of Hydrology, v. 70, p. 309–327. doi:10.1016/0022-1694(84)90129-X.

Goodchild, M.F., and Ford, D.C., 1971, Analysis of scallop patterns by simulation under controlled conditions: Journal of Geology, v. 79, p. 52–62.

Griebel, M., Dornseider, T., and Neunhoeffer, T., 1997, Numerical Simulation in Fluid Dynamics: A Practical Application (SIAM monographs on mathematical modeling and computation 3), Philadelphia, Society for Industrial and Applied Mathematics, 217 p.

Hammer, Ø., Dysthe, D.K., Lelu, B., Lund, H., Meakin, P., and Jamtveit, B., 2008, Calcite precipitation instability under laminar, open-channel flow: Geochimica et Cosmochimica Acta, v. 72, p. 5009–5021. doi:10.1016/j.gca.2008.07.028.

Kleinstein, G., 1967, Generalized law of the wall and eddy viscosity model for wall boundary layers: American Institute of Aeronautics and Astronautics Journal, v. 5, p. 1402–1407.

Lax, P.D., and Wendroff, B., 1960, Systems of conservation laws: Communications on Pure and Applied Mathematics, v. 13, p. 217–237. doi: 10.1002/cpa.3160130205.

Liu, Z., and Dreybrodt, W., 1997, Dissolution kinetics of calcium carbonate minerals in H_2O–CO_2 solutions in turbulent flow: The role of the diffusion boundary layer and the slow reaction $H_2O + CO_2 \leftrightarrows HCO_3^-$: Geochimica and Cosmochimica Acta, v. 61, p. 2879–2889. doi 10.1016/S0016-7037(97)00143-9.

Meakin, P., and Jamtveit, B., 2010, Geological pattern formation by growth and dissolution in aqueous systems: Proceedings of the Royal Society of London A, v. 466, p. 659–694. doi: 10.1098/rspa.2009.0189.

Opdyke, B.N., Gust, G., and Ledwell, J.R., 1987, Mass transfer from smooth alabaster surfaces in turbulent flows: Geophysical Research Letters, v. 14, p. 1131–1134. doi:10.1029/GL014i011p01131.

Plummer, L.N., Wigley, T.M.L., and Parkhurst, D.L., 1978, The kinetics of calcite dissolution in CO_2-water systems at 5 degrees to 60 degrees C and 0.0 to 1.0 atm CO_2: American Journal of Science, v. 278, p. 179–216. doi: 10.2475/ajs.278.2.179.

Raines, M.A., and Dewers, T.A., 1997, Mixed transport/reaction control of gypsum dissolution kinetics in aqueous solutions and initiation of gypsum karst: Chemical Geology, v. 140, p. 29–48. doi:10.1016/S0009-2541(97)00018-1.

Thomas, R.M., 1979, Size of scallops and ripples formed by flowing water: Nature, v. 277, p. 281–283. doi:10.1038/277281a0.

Villien, B., Zheng, Y., and Lister, D., 2005, Surface dissolution and the development of scallops: Chemical Engineering Communications, v. 192, p. 125–136. doi: 10.1080/00986440590473272.

Wüest, A., and Lorke, A., 2003, Small-scale hydrodynamics in lakes: Annual Review of Fluid Dynamics, v. 35, p. 373–412. doi: 10.1146/annurev.fluid.35.101101.161220.

J. F. Weishampel, J. N. Hightower, A. F. Chase, D. Z. Chase, and R. A. Patrick – Detection and morphologic analysis of potential below-canopy cave openings in the karst landscape around the Maya polity of Caracol using airborne LiDAR. *Journal of Cave and Karst Studies,* v. 73, no. 3, p. 187–196. DOI: 10.4311/2010EX0179R1

DETECTION AND MORPHOLOGIC ANALYSIS OF POTENTIAL BELOW-CANOPY CAVE OPENINGS IN THE KARST LANDSCAPE AROUND THE MAYA POLITY OF CARACOL USING AIRBORNE LIDAR

John F. Weishampel[1]*, Jessica N. Hightower[1], Arlen F. Chase[2], Diane Z. Chase[2], and Ryan A. Patrick[3]

Abstract: Locating caves can be difficult, as their entranceways are often obscured below vegetation. Recently, active remote-sensing technologies, in particular laser-based sensor systems (LiDARs), have demonstrated the ability to penetrate dense forest canopies to reveal the underlying ground topography. An airborne LiDAR system was used to generate a 1 m resolution, bare-earth digital elevation model (DEM) from an archaeologically- and speleologically-rich area of western Belize near the ancient Maya site of Caracol. Using a simple index to detect elevation gradients in the DEM, we identified depressions with at least a 10 m change within a circular area of no more than 25 m radius. Across 200 km^2 of the karst landscape, we located 61 depressions. Sixty of these had not been previously documented; the other was a cave opening known from a previous expedition. The morphologies of the depressions were characterized based on the LiDAR-derived DEM parameters, e.g., depth, opening area, and perimeter. We also investigated how the measurements change as a function of spatial resolution. Though there was a range of morphologies, most depressions were clustered around an average maximum depth of 21 m and average opening diameter of 15 m. Five depression sites in the general vicinity of the Caracol epicenter were visited; two of these were massive, with opening diameters of ~50 m, two could not be explored for lack of climbing gear, and one site was a cave opening into several chambers with speleothems and Maya artifacts. Though further investigation is warranted to determine the archaeological and geological significance of the remaining depressions, the general methodology represents an important advancement in cave detection.

Introduction

Caves have biological, geological, hydrological, and often, when near settlements of ancient cultures, anthropological significance. The detection of cave openings, classification of cave types, and mapping of cave morphologies are initial steps in documenting and conserving these sites of natural and cultural heritage. However, many caves in mesic regions remain undocumented, as the openings are often obscured by vegetation. This is especially common in Mesoamerica, where dense, structurally-complex rainforest canopies overtop numerous Maya archaeological sites (Ricketson and Kidder, 1930; Chase, 1988).

Caves are believed to have played a significant role in ancient Maya societies (e.g., Brady and Prufer, 2005; Prufer and Brady, 2005) from about 2500 BC to AD 1500. As portals to the Maya underworld, *Xibalbá*, caves served as places of religious and mythological importance in addition to functioning as shelters. They were sites of rituals, ceremonies, and burials, and they hence often contain ceramics, artwork, architectural modifications, and skeletal remains (e.g., Moyes, 2002). However, like many of the archaeological features found in the Maya polities, cave entrances are often covered by the dense tropical rainforest vegetation that reemerged after the settlements were abandoned roughly a thousand years ago.

There are several possible ways to locate caves using remote sensing. On the ground, covering a limited area, ground penetrating radar can be used to detect caves (Sellers and Chamberlain, 1998). However, the extensive below-ground root mass and the density of the above-ground vegetation preclude the use of GPR in a rainforest environment. For broad-scale prospecting, airborne- or satellite-based remote sensing is necessary. Because caves have a more stable temperature than the surface environment, there has been an effort to use thermal remote sensing on earth (Griffith, 2000) and on other planets (Cushing et al., 2007; Wynne et al., 2008) to detect cave openings. Though a temperature gradient of 7.2 °C was detected on the ground 50 to 100 m away from cave

* Corresponding Author, jweisham@mail.ucf.edu
[1] Department of Biology, University of Central Florida, Orlando, FL 32816, USA
[2] Department of Anthropology, University of Central Florida, Orlando, FL 32816, USA
[3] Interdisciplinary Studies Program, University of Central Florida, Orlando, FL 32816, USA

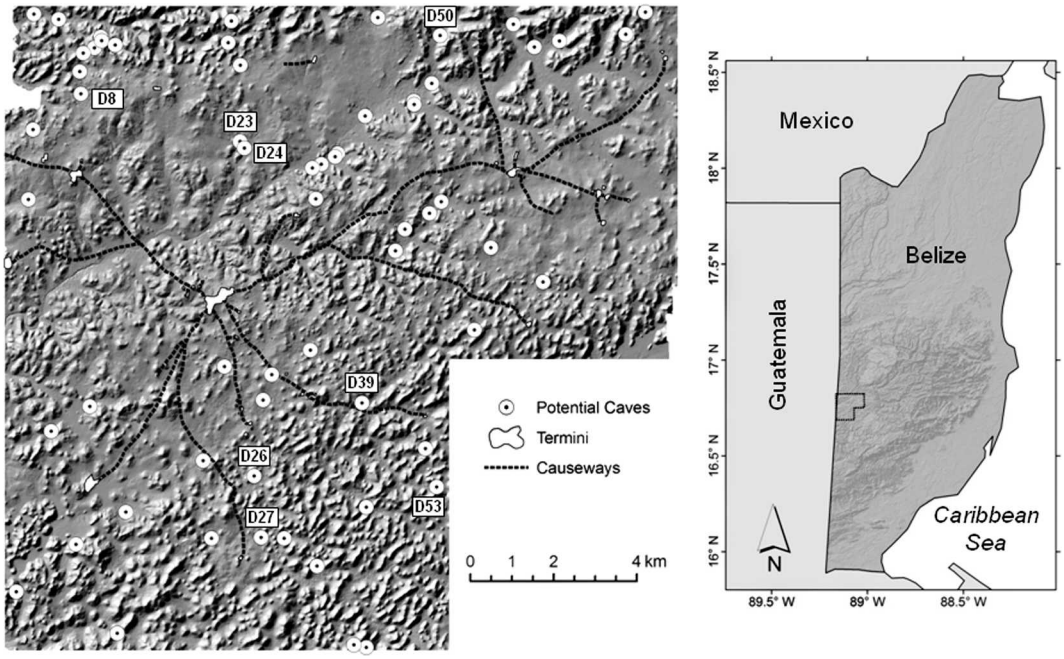

Figure 1. At right, location of 200 km^2 study area on the western border of Belize on the Vaca Plateau, shown on the hillshaded Shuttle Radar Topography Mission image of Belize. The expanded study area shows the 61 depressions more than 10 m deep on the hillshaded bare-earth image from the airborne LiDAR-derived DEM. Numbers refer to depressions specifically mentioned in this paper.

openings in Belize (Griffith, 2001), this method is challenging, given the coarse resolution of most satellite thermal sensors. Furthermore, even with finer airborne or hyperspatial satellite sensors, the sharp microclimate gradient in closed-canopy tropical rainforest regions from the ground to the upper surface of the forest canopy 20 to 30 m above may mask the temperature at the cave opening (Allee, 1926). Griffith (2001) also used an active form of remote sensing (Star 3i RADAR) to detect depressions in the surface topography of the forest canopy (Weishampel et al., 2000a) that may correspond to depressions or cave openings. This proved successful for a large ~25 m wide sinkhole, but not for depressions below the spatial resolution of the sensor. Given the ability of another active form of remote sensing (LiDAR—Light Detection and Ranging) to penetrate dense forest cover to measure ground surfaces (e.g., Weishampel et al., 2000a, 2000b; Hofton et al., 2002; Gallagher and Josephs, 2008), we assessed its ability to locate known and unknown potential cave openings and to quantify the geomorphology of their entranceways.

As part of an archaeological prospecting study (Weishampel et al., 2010), we used airborne LiDAR to map unknown Maya structures such as temples, causeways, and monuments in a 200 km^2 area around Caracol, Belize (Chase et al., 2010). In addition to anthropogenic features in the 1 m horizontal resolution digital elevation model (DEM), we identified numerous vertical depressions and surface openings. These were thought to represent cave openings, pits collapse dolines, or *chultuns* (subterranean storage chambers) that, if contemporaneous, could have been used by the ancient Maya. Here, we report our approach and findings.

CARACOL STUDY AREA

The geology of the Yucatán Peninsula consists of a porous limestone shelf that is honeycombed with sinkholes, cenotes, underground streams, lakes, and caverns. Estimated to cover about 170 km^2, Caracol is the largest Maya archaeological site in Belize. Located near the Guatemala border on the Vaca Plateau of the Cayo District (Fig. 1) west of the Maya Mountains, the Caracol landscape consists of rolling karst-defined hills and valleys ranging from about 300 to 700 m in elevation. At its cultural peak (ca. AD 700), the metropolitan population is estimated to have been greater than 100,000, which makes it one of the most populous cities in the Pre-Columbian world (Chase and Chase, 1996). Since 1950, 23 km^2 have been painstakingly surveyed on the ground (Chase, 1988; Chase and Chase, 2001). The main acropolis, comprising numerous large buildings, is at the center of several causeways that radiate outward to smaller areas called termini that also possess high concentrations of building structures.

Presently most of the remains of Caracol are hidden in the subtropical moist forests of the Chiquibul National Park (Brokaw, 1992). The average canopy height is about 25 m, with a few emergent trees extending to over 35 m.

The vertical forest structure is fairly homogeneous, with no distinct layers.

In the greater vicinity of Caracol, outside the 200 km^2 area, numerous caves have been located (Miller, 1990) and many of these are of archaeological note (McNatt, 1996; Reeder et al., 1998). The Río Frío complex 26 km to the north-northeast of the center, the Quiroz Cave 13 km to the northeast, Actun Balam 15 km to the southeast (Pendergast, 1969, 1970; Pendergast and Savage, 1971), and several other caves 30 or more km to the northeast (Moyes, 2002) all contained artifacts such as bones and pottery that indicated that they were sites of ritual use. Feld (1994) documented nine caves within the 200 km^2 Caracol area; most are within 3 km of the center. Many of these have small openings and deep shafts. Most of these are thought not to have been accessible to or not contemporary with the ancient Maya, meaning that the openings are more recent. Hence, only a few of these caves contain artifacts.

Methods and Materials

At the end of April 2009, during the end of the dry season, the National Center for Airborne Laser Mapping (NCALM; Carter et al., 2001) flew their LiDAR system, which consisted of an Optech, Inc., Gemini Airborne Laser Terrain Mapper with onboard GPS and Inertial Measurement Unit systems on board a Cessna 337 Skymaster. The timing of the flight was designed to correspond roughly to the height of leaf abscission for this forest. However, leaf-off typically does not exceed 20% at any time of the year, as most tree species maintain leaves all year long (Brokaw, 1992).

The NCALM system records four returns per pulse as it scans across a 0.5 km swath; when a pulse is transmitted, part of the pulse initially reflects off an object closest to the aircraft, usually the canopy, while the remainder of the pulse continues through gaps in the canopy, reflecting off other plant surfaces and in some cases the ground. The laser pulse rate is 167 kHz, and the scan rate is 28 Hz. At a nominal above-ground altitude of 600 to 1000 m, the system yields 10 to 15 laser shots per square meter with a height accuracy of 5 to 10 cm (one sigma) and a horizontal accuracy of 25 to 40 cm (one sigma). This system also records the relative intensity of each return. By crisscrossing (east-west and north-south) flight lines over the central Caracol area (Chase et al., 2010), 20 to 30 shots per square meter were obtained, yielding a more accurate digital elevation model.

Of the more than 20 laser shots/m^2, an average of 1.35 points/m^2 penetrated through canopy gaps to reach the ground. NCALM researchers interpolated these points to generate a 1 m resolution DEM. The DEM file for the entire 200 km^2 area was 65 MB and was analyzed using off-the-shelf software or freeware on a standard (circa 2010) desktop computer. From the bare-earth DEM rendered with a hillshade algorithm (Fig. 1), we visually identified thousands of unknown Maya settlement structures and some obvious steep surface depressions. LiDAR at Caracol has proven very effective for detecting man-made archaeological features below the canopy (Chase et al., 2010; Chase et al., 2011).

Using the Topographic Position Index (TPI) (Guisan et al., 1999) calculator within the Land Facet Corridor Designer software (Jenness et al., 2010), a plug-in application for ArcGIS (v. 9.3), we further identified numerous

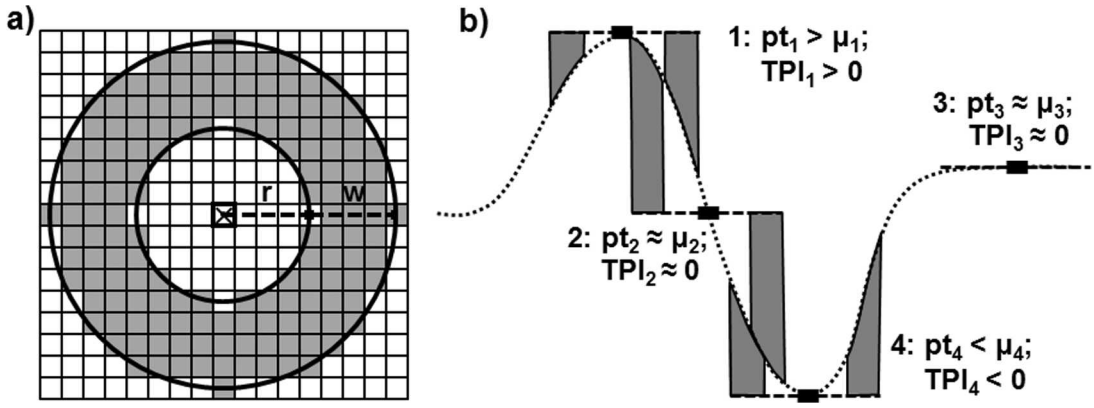

Figure 2. (a) Topographic Position Index (TPI) annulus filter that was applied to the DEM. It calculates the difference between the elevation of the focal cell (pt) designated with the 'x' and the average elevation of the gray cells (μ) in the ring surrounding it. Two parameters that can be adjusted are the inner radius (r), the distance from the center of the focal cell to the inner edge of the ring, and the annulus thickness (w), the difference between the inner and outer radii. (b) An example of a topographic cross section shows the four main terrain scenarios: 1, hump or hilltop; 2, slope; 3, level or flat; 4, depression or valley, and the associated pt, μ, and TPI values. The gray bars depict the elevations at the sides of the annuli with respect to the elevations of the focal cells (adapted from Weiss, 2001 and Jenness et al., 2010). Terrain scenarios 2 (slope) and 3 (level) are distinguished by evaluating the overall slope in the annulus.

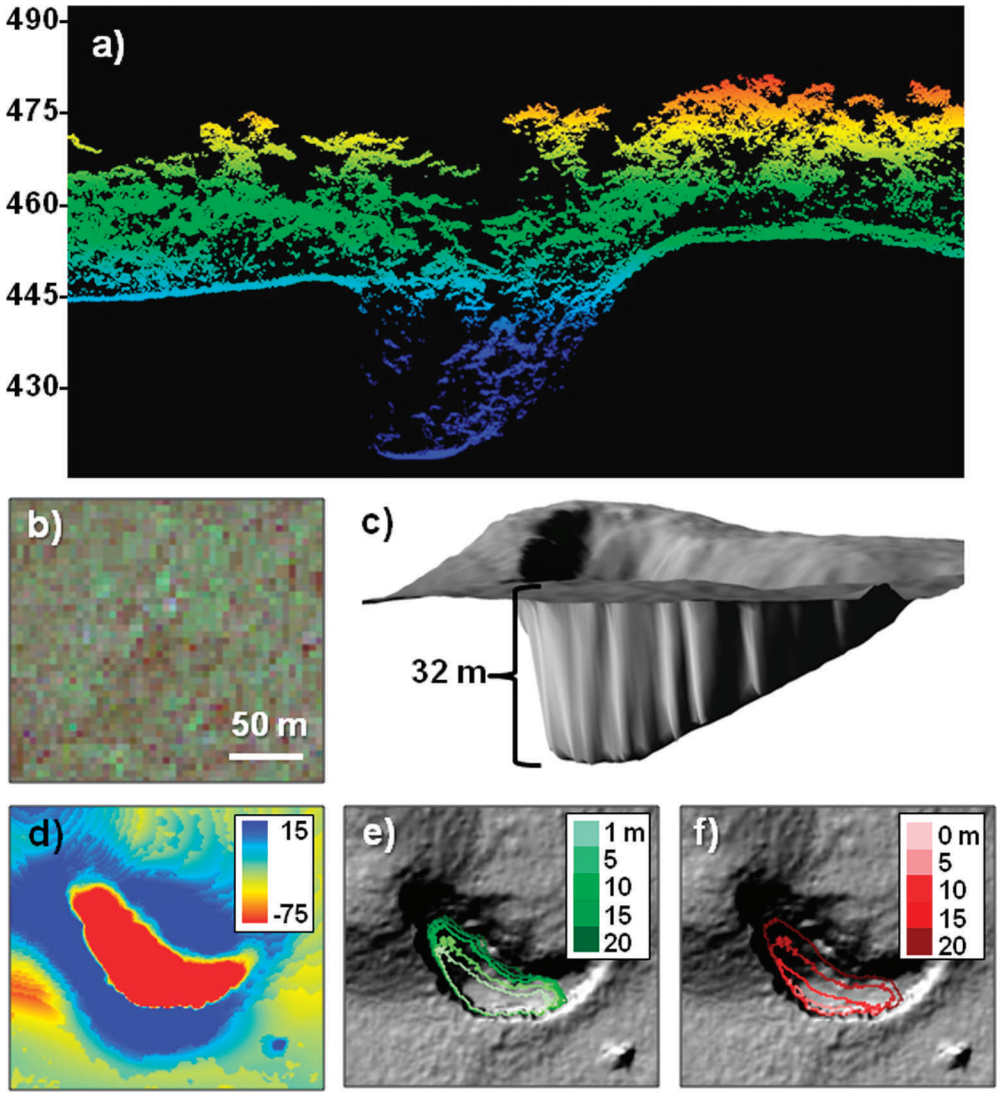

Figure 3. (a) LiDAR point-cloud data depicting forest canopy and ground surface at depression 24. The values are meters above sea level. (b) Top-down view provided by the IKONOS satellite shows complete canopy coverage over the depression. (3) 3-D rendering of the LiDAR image with vegetation removed. (d) TPI image depicting relative elevation in meters. (e) The perimeter of the area with TPI value −10 m or less as a function of annulus thickness, keeping the inner radius constant at 15 m. (f) The same as (e), but with the inner radius varying and the thickness constant at 5 m.

steep depressions that may represent cave openings. The TPI measures elevational contrast in the DEM. For each focal cell, the TPI is the difference between the elevation of the focal cell and the average elevation of all the cells in the neighborhood (Fig. 2). We used an annulus shape to define the neighborhood, i.e., cells whose center points fall between inner and outer radii. The annulus shape amplifies the difference between the focal cell and the surrounding ring.

Rasters (pixels or grid cells) with TPI values ≤ -10 m were segmented or partitioned in the DEM image as potential cave entrances (Fig. 3). This depth eliminated shallow reservoirs and chultuns previously identified in the area (Hunter-Tate 1994). Chultuns are typically bottle-shaped storage chambers about 2 m deep built by the Maya that may have served functions such as cisterns, storage, or burial sites. Given the vertical direction of the LiDAR pulse, it is unlikely that caves with side or horizontal openings would be conspicuous. Also, because of the horizontal resolution of the DEM, caves with openings smaller than 1 m^2 would most likely not be detected. Several of the previously unrecorded depressions were verified in the field during the spring of 2010.

Within a cave, terrestrial laser scanning has been shown to be an effective method to record cave morphology (González-Aguilera et al., 2009; Lerma et al., 2010). Here we apply this general technique at a coarser scale to measure the shapes of depressions that may represent cave entrances. In addition to locating steep elevational gradients, the TPI was used to characterize the geomorphology of the depressions $\geq$10 m deep located in the

DEM. From the segmented image, we used ArcGIS (v. 9.3) coupled with Hawth's Analysis Tools (Beyer, 2004) to quantify numerous parameters of the pixels associated with each depression, i.e., average depth, maximum depth, standard error of depth measures (bottom roughness), opening perimeter, opening area. As topographic features are inherently fractal surfaces (Russ, 1994), the TPI measure is a function of the annulus thickness (w) and inner radius (r) of the annulus (Fig. 3). By analyzing the morphologic parameters with differing annulus scales, we can distinguish among conical, cylindrical, and irregular or more complex openings such as multiple connected depressions or saddle backs.

Lastly, an ordination using principal-components analysis was performed on the LiDAR-derived morphologic parameters for vertical depressions 10 m or more deep. This was done to understand the range of karst depressions that could be detected by LiDAR in the landscape around Caracol as a function of the inner radius and width of the annulus.

Results and Discussion

Depression Identification and Field Verification

Sixty-one depressions 10 or more meters deep were identified in the 200 km^2 DEM by visually scanning the image from top to bottom and left to right for patches that were deeper (darker) than their surroundings and by using the Topographic Position Index filter. These were fairly well distributed across the Caracol landscape, but were more common in the hilly terrain on the outskirts of the region with the highest concentration of monumental architecture, which is also the hub of the half-dozen causeways that radiate outward. Only one depression, Cohune Ridge Cave, which is west of depression 50 in Figure 1, had been previously known (Feld, 1994). Other known cave openings (Feld, 1994) were either too shallow or were horizontal, and not detected by the LiDAR scan. Five of the previously unrecorded depressions relatively close to the epicenter were located in the field. All had vegetation above the depression that obscured it from traditional passive remote-sensing techniques. Two of these had massive openings, depressions 23 (1919 m^2) and 24 (1550 m^2). During this ground verification, we did not take depth and width measurements on the ground for comparison with the LiDAR-derived measurements. The former was inaccessible without vertical equipment; the latter was explored in a cursory fashion and did not appear to contain Maya artifacts. Of the remaining three one was simply a steep rock face adjacent to a hill, one had an opening of 6 m^2 and a steep shaft >15 m deep that was inaccessible without vertical equipment, and the last one

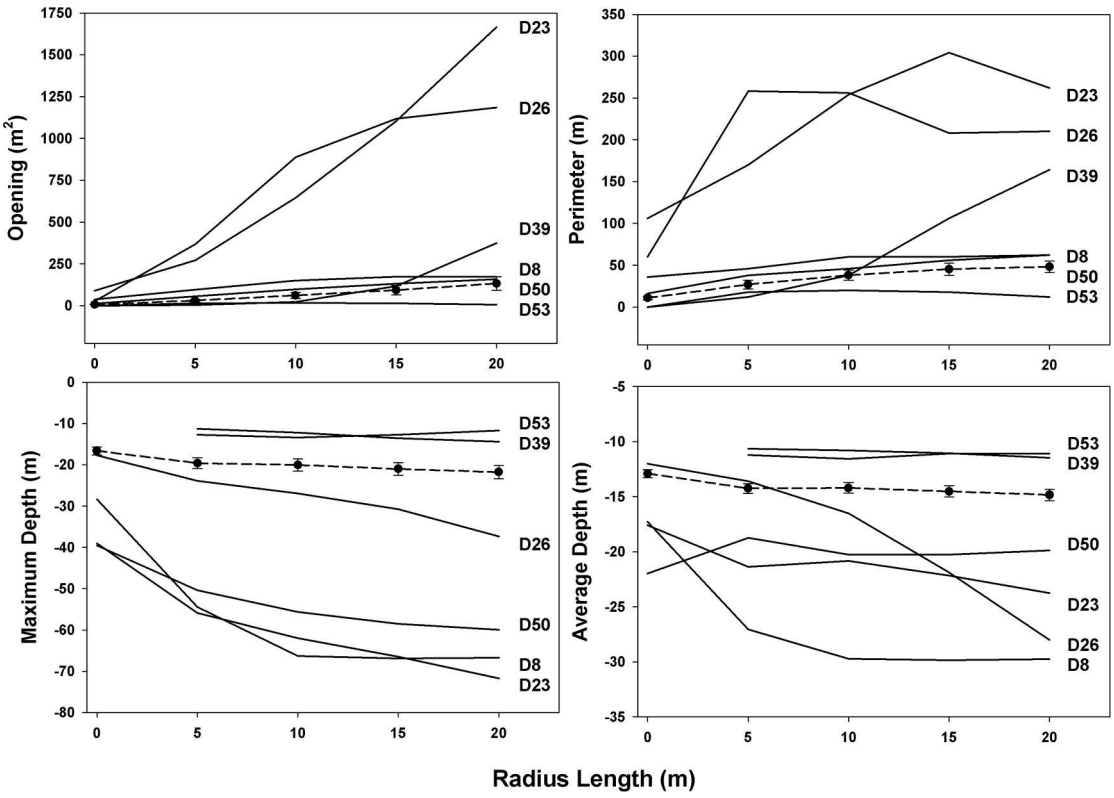

Figure 4. Change in morphologic parameters of selected potential cave opening in Figure 1 derived with TPI from the DEM as a function of inner radius (r), keeping the annulus thickness constant (w = 5 m). The points on the dashed line are the averages of the 61 depressions at least 10 m deep, with one standard error indicated.

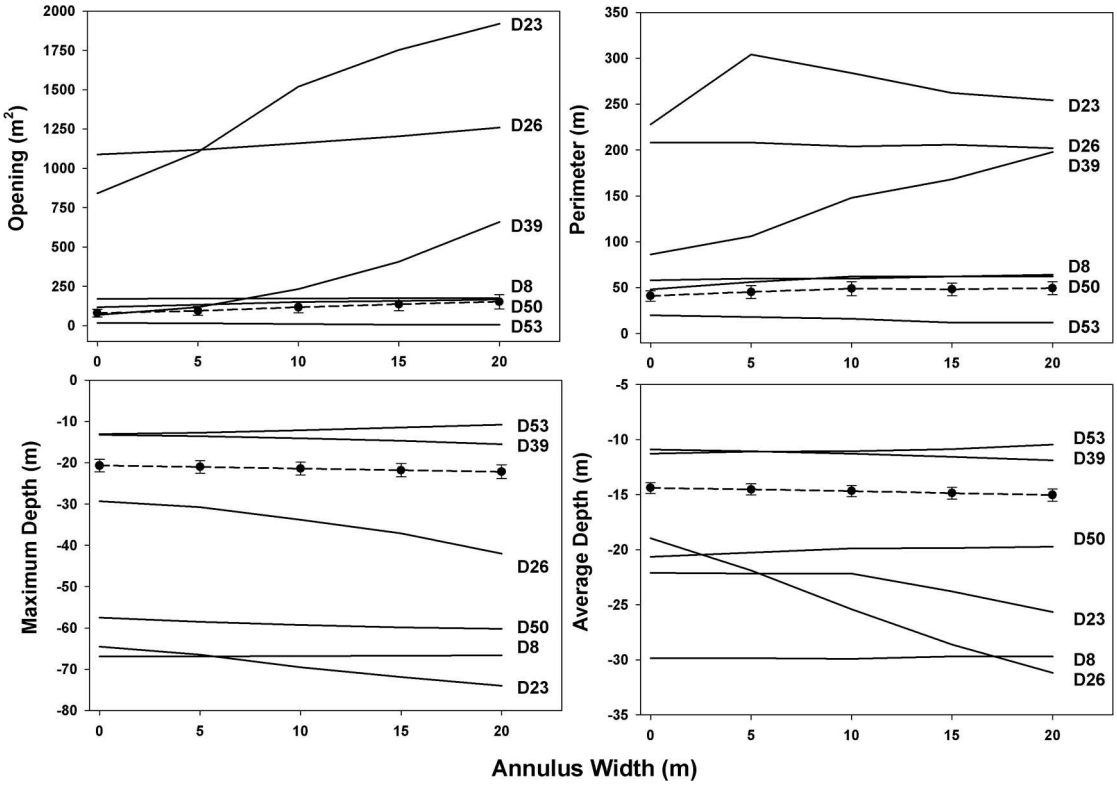

Figure 5. Change in morphologic parameters of potential cave openings derived with TPI from the DEM as a function of annulus thickness (w) keeping the inner radius constant (r = 15). The points on the dashed line are the averages of the 61 depressions at least m deep, with one standard error indicated.

was an accessible cave with an opening of 8 m^2. For this cave, the LiDAR detected a maximum depth of 10.9 m. It was explored and found to consist of several rooms with speleothems such as soda straw stalactites, stalagmites, flowstone, and splash cup structures, as well as archaeological features such as human bones and pottery.

MORPHOLOGIC CHARACTERIZATION

Based on an annulus thickness of 20 m and an inner radius of 15 m (Fig. 4), the average depression opening was 149.3 m^2 (SD=359.8 m^2), and the average maximum depth was 21.5 m (SD=13.8). Based on an annulus thickness of 5 m and an inner radius of 20 m (Fig. 5), the average

Table 1. Eigenvectors associated with the principal component analysis of the LiDAR-derived parameters that characterize the 61 depression morphologies. The numbers in parentheses are the percentages of variance explained by the principal components axes. Slopes are functions of the annulus inner radius (r; w = 5) and thickness (w; r = 15) as shown in Figures 4 and 5.

Parameters	PC1 (52.5%)	PC2 (22.9%)	PC3 (9.1%)
Maximum Depth	−0.23	−0.36	0.32
Average Depth	−0.23	−0.42	0.04
Standard Error of Depth	−0.07	0.41	−0.22
Opening Area	0.35	−0.11	0.04
Perimeter	0.35	−0.16	−0.06
Slope Max Depth (r)	−0.24	−0.35	0.28
Slope Avg Depth (r)	−0.21	−0.32	−0.30
Slope Area (r)	0.35	−0.08	0.12
Slope Perimeter (r)	0.30	−0.29	−0.11
Slope Max Depth (w)	−0.32	−0.00	−0.26
Slope Avg Depth (w)	−0.26	−0.03	−0.58
Slope Area (w)	0.30	−0.24	−0.20
Slope Perimeter (w)	0.12	−0.34	−0.39

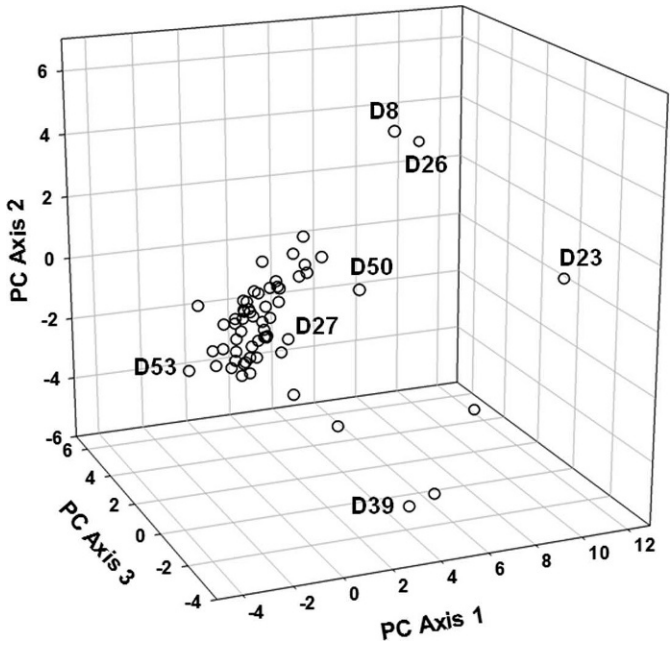

Figure 6. Ordination of depressions based on morphological characters derived using TPI for different scales of annulus width and radius length. The numbered markers correspond to depressions on Figure 1 that represent the extremities for the three principal component axes except number 27, which corresponds to the depression whose morphology most resembled the mean.

depression opening was 130.4 m^2 (SD=313.5); the average maximum depth was 21.1 m (SD=13.5). The general trends with increasing annulus thickness (holding the inner radius constant at 15 m) and inner radius (holding the thickness constant at 5 m) showed slight increases in opening area and perimeter length and slight increases in maximum and average depths (Figs. 4 and 5). However, these effects varied substantially for individual depressions.

The first three principal components (PC) axes accounted for 84.5% of the variance (Table 1). The first PC axis was positively weighted on parameters that characterized the morphology of the depressions' opening, its area and perimeter. The second PC axis was negatively weighted on parameters that characterized the depressions' average and maximum depth and standard error of depth. The third PC axis was negatively weighted on parameters that are related to scaling effects, i.e., slopes of parameter measures as a function of r and w. The ordination showed little distinct grouping of depression morphologies (Fig. 6). All but about ten of these depression morphologies were concentrated slightly on the negative side of PC Axis 1 and near the zero intercept of PC Axis 2 and PC Axis 3. This implies that the depressions tend to be smaller than the average, which is probably skewed by the few much larger depressions. D27, the depression closest to the average of the 61 depressions, based on their positions in the ordination space, had an average depth of 13.2 m (13.5 m), a maximum depth of 25.3 m (24.8 m), and an opening of 86 m^2 (67 m^2) with r = 20 m and w = 15 m (r = 5 m and w = 20 m). The hillshaded rendering of this nearly average depression is shown in Figure 7. The irregular bottom is the cause of the discrepancy between the average and maximum depths. Its conical shape resulted in its opening area and maximum depth being related to the scale of both the annulus width and radius length.

The depressions with extreme morphologies, as represented by the PC axes, are rendered in Figure 8. The first PC axis shows two depressions that are distinguished by opening area; D53 has an opening of 5 m^2 and D23 has an opening of 1919 m^2 when analyzed with an annulus thickness of 20 m and inner radius of 15 m. The second PC axis juxtaposes a narrow, deep D8 and a broad, shallow D39. The standard error of the depth measure is among the highest and lowest for D8 and D39, respectively. The third PC axis contrasts a slightly slanted, flat-sided D26 and a complex, sharply recessed D50. Average depth increased for D26 and decreased for D50 with increasing annulus thickness. The decrease for D50 was unusual and the greatest among the 61 depressions.

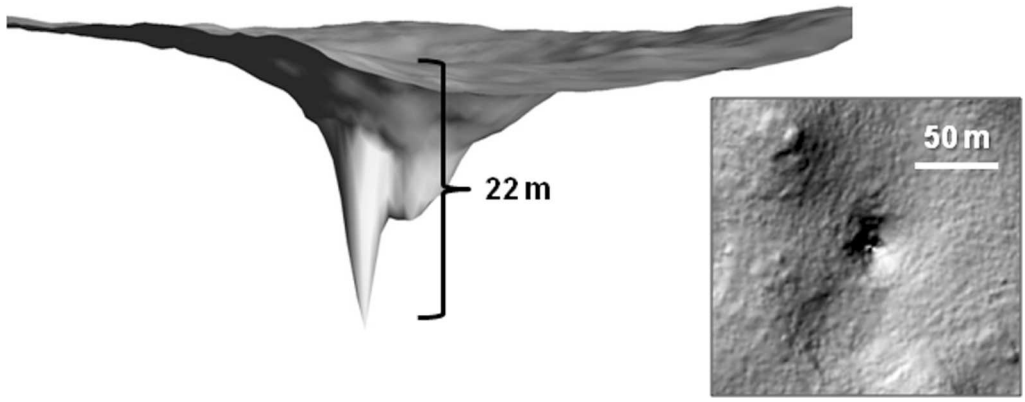

Figure 7. Bare-earth 3-D rendering and top-down view of depression 27, the one with the most typical morphology, closest to the centroid of the 61 depressions in the volume defined by the three principal component axes of ordination space (Fig. 6).

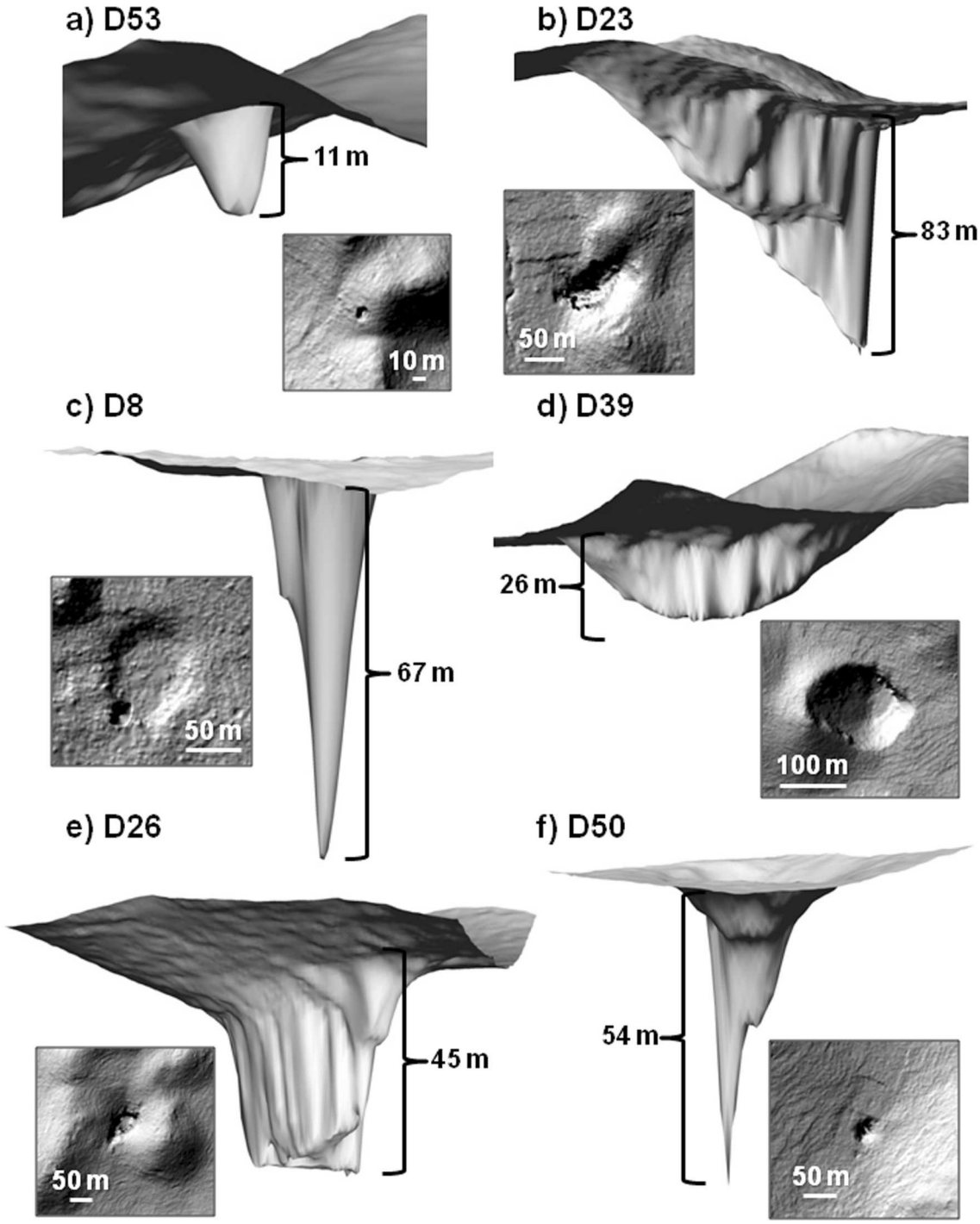

Figure 8. Morphologies of some depressions at the extremes in the three ordination axes (Fig. 6). Hillshaded 3-D renderings and top-down views of depression 53 juxtaposed with depression 23 for PC Axis 1, depression 8 juxtaposed with depression 39 for PC Axis 2, and depression 26 juxtaposed with depression 50 for PC Axis3.

This type of morphological analysis shows the range of shapes and sizes of the depressions and provides some level of guidance for future exploration; it may help indicate how the depression was formed and provide information as to the historic accessibility of the depression for the ancient Maya, as well as for current archaeologists.

Conclusions

Remote sensing of geomorphological features in a karst landscape is not particularly novel (e.g., Siart et al., 2009); however, detecting fine-scale (1 m horizontal resolution) karstic features across a densely forested landscape as

described here is unprecedented. Through this airborne LiDAR study, we detected 60 previously undocumented vertical depressions, shafts, and cave entrances that pockmark the karstic landscape beneath the dense rainforest canopy of western Belize. This study demonstrates the capability of LiDAR to detect surface features that may represent entrances to subterranean geological complexes. As prospecting for openings is often laborious, time-consuming work, this application of LiDAR should improve the efficiency of cave location. However, as many caves used by the Maya have horizontal or very small openings, ground searches on foot are necessary for a comprehensive inventory.

Though there are several ways to partition DEM landscapes into a variety of terrain types (e.g., Yokoyama et al., 2002; Denizman, 2003; Iwahashi and Pike, 2007; Stepinski and Bagaria, 2009; Patel and Sarkar, 2010; Prima and Yoshida, 2010), the Topographic Position Index seemed effective at locating and quantifying the geomorphology of these recessed features. Somewhat unexpectedly, the LiDAR sensor system flying at an altitude of nearly 1 km was able to record a variety of geomorphologies from these vertical depressions. This rich dataset shows some of these depressions to be very deep (>50 m) with massive openings (>350 m across); others are deep (>25 m) with relatively narrow (<5 m across) openings. Most of these depressions represent caves that were contemporary with the ancient Maya and likely contain artifacts, but a few may be more recent. As only a tenth of these depressions have been located and explored on the ground, it is important that these potentially culturally significant sites remain undisturbed until their archaeological context can be realized.

Acknowledgments

This research was supported by NASA Grant #NNX08AM11G through the Space Archaeology program and the University of Central Florida–University of Florida–Space Research Initiative (UCF-UF-SRI). We appreciated conversations with Jaime Awe, Holley Moyes, and Cameron Griffith, members of the Western Belize Regional Cave Project (WBRCP), about caving and cave detection using remote sensing techniques in Belize. The expertise of James Angelo with Fusion and the National Center for Airborne Laser Mapping (NCALM), Ramesh Shrestha, Clint Slatton, Bill Carter, and Michael Sartori, helped to make this study possible.

References

Allee, W.C., 1926, Measurement of environmental factors in the tropical rain-forest of Panama, Ecology, v. 7, p. 273–302.

Beyer, H.L., 2004, Hawth's Analysis Tools for ArcGIS, available at: www.spatialecology.com/htools, [accessed September 24, 2010].

Brady, J.E., and Prufer, K.M., 2005, In the Maw of the Earth Monster: Mesoamerican Ritual Cave Use: Austin, University of Texas Press, 438 p.

Brokaw, N.V.L., 1992, Vegetation and tree flora in the central area of the Caracol archaeological reserve, Belize: Manomet, Massachusetts, Manomet Observatory for Conservation Science, 28 p.

Carter, W., Shrestha, R., Tuell, G., Bloomquist, D., and Sartori, M., 2001, Airborne laser swath mapping shines new light on Earth's topography: Eos, v. 82, 549, 550, 555 p.

Chase A.F., 1988, Jungle surveying: mapping the archaeological site of Caracol, Belize: Point of Beginning, v. 13, p. 10–24.

Chase, A.F., and Chase, D.Z., 1996, A mighty Maya nation: how Caracol built an empire by cultivating its 'middle class': Archaeology, v. 49, p. 66–72.

Chase, A.F., and Chase, D.Z., 2001, Ancient Maya causeways and site organization at Caracol, Belize: Ancient Mesoamerica, v. 12, p. 273–281.

Chase, A.F., Chase, D.Z., and Weishampel, J.F., 2010, Lasers in the jungle: airborne sensors reveal a vast Maya landscape: Archaeology, v. 63, no. 4, p. 27–29.

Chase, A.F., Chase, D.Z., Weishampel, J.F., Drake, J.B., Shrestha, R.L., Slatton, K.C., Awe, J.J., and Carter, W.E., 2011, Airborne LiDAR, archaeology, and the ancient Maya landscape at Caracol, Belize: Journal of Archaeological Science, v. 38, p. 387–398. doi: 10.1016/j.jas.2010.09.018.

Cushing, G.E., Titus, T.N., Wynne, J.J., and Christensen, P.R., 2007, THEMIS observes possible cave skylights on Mars: Geophysical Research Letters, v. 34, L17201 p. doi: 10.1029/2007GL030709.

Denizman, C., 2003, Morphometric and spatial distribution parameters of karstic depressions, lower Suwanee River basin, Florida: Journal of Cave and Karst Studies, v. 65, p. 29–35.

Feld, W.A., 1994, The caves of Caracol: initial impressions, *in* Chase, D.Z., and Chase, A.F., eds., Studies in the archaeology of Caracol, Belize. San Francisco, Pre-Columbian Art Research Institute Monograph 7, p. 76–82.

Gallagher, J.M., and Josephs, R.L., 2008, Using LiDAR to detect cultural resources in a forested environment: an example from Isle Royale National Park, Michigan, USA: Archaeological Prospection, v. 15, p. 187–206. doi: 10.1002/arp.333.

González-Aguilera, D., Muñoz-Nieto, A., Gómez-Lahoz, J., Herrero-Pascual, J., and Gutierrez-Alonso, G., 2009, 3D digital surveying and modeling of cave geometry: application to Paleolithic rock art: Sensors, v. 9, p. 1108–1127. doi: 10.3390/s90201108.

Griffith, C., 2000, Remote sensing in cave research, available at: www.archaeology.org/online/features/belize/remote.html, [accessed September 24, 2010].

Griffith, C., 2001, Locating Cave Sites: Results of our remote-sensing research, available at: www.archaeology.org/interactive/belize/newremote.html, [accessed March 2, 2011].

Guisan, A., Weiss, S.B., and Weiss, A.D., 1999, GLM versus CCA spatial modeling of plant species distribution: Plant Ecology, v. 143, p. 107–122. doi: 10.1023/A:1009841519580.

Hofton, M.A., Rocchio, L.E., Blair, J.B., and Dubayah, R., 2002, Validation of vegetation canopy lidar sub-canopy topography measurements for a dense tropical forest: Journal of Geodynamics, v. 34, p. 491–502. doi: 10.1016/S0264-3707(02)00046-7.

Hunter-Tate, C.C., 1994, The chultuns of Caracol, *in* Chase, D.Z., and Chase, A.F., eds., Studies in the archaeology of Caracol, Belize. San Francisco, Pre-Columbian Art Research Institute Monograph 7, p. 64–75.

Iwahashi, J., and Pike, R.J., 2007, Automated classifications of topography from DEMs by an unsupervised nested-means algorithm and a three-part geometric signature: Geomorphology, v. 86, p. 409–440. doi: 10.1016/j.geomorph.2006.09.012.

Jenness, J., Brost, B., and Beier, P., 2010, Land Facet Corridor Designer, available at: www.jennessent.com/downloads/LandFacetCorredor.zip, [accessed September 24, 2010].

Lerma, J.L., Navarro, S., Cabrelles, M., and Villaverde, V., 2010, Terrestrial laser scanning and close range photogrammetry for 3D archaeological documentation: the Upper Palaeolithic cave of Parpalló as a case study: Journal of Archaeological Science, v. 37, p. 499–507. doi: 10.1016/j.jas.2009.10.011.

McNatt, L., 1996, Cave archaeology of Belize: Journal of Cave and Karst Studies, v. 58, p. 81–99.

Miller, T., 1990, Caves and caving in Belize, Caves and Caving, no. 49, p. 2–4.

Moyes, H., 2002, The use of GIS in the spatial analysis of an archaeological cave site: Journal of Cave and Karst Studies, v. 64, p. 9–16.

Patel, P.P., and Sarkar, A., 2010, Terrain characterization using SRTM data: Journal of Indian Society of Remote Sensing, v. 38, p. 11–24. doi: 10.1007/s12524-010-0008-8.

Pendergast, D.M., 1969, The Prehistory of Actun Balam, British Honduras: Toronto, Royal Ontario Museum Occasional Paper 16, Art and Archaeology, 68 p.

Pendergast, D.M., 1970, A. H. Anderson's Excavations at Rio Frio Cave E, British Honduras (Belize): Toronto, University of Toronto, Royal Ontario Museum Occasional Paper 20, Art and Archaeology, 59 p.

Pendergast, D.M., and Savage, H.G., 1971, Excavations at Eduardo Quiroz Cave British Honduras (Belize): Toronto, University of Toronto, Royal Ontario Museum Occasional Paper 21, Art and Archaeology, 123 p.

Prima, O.D.A., and Yoshida, T., 2010, Characterization of volcanic geomorphology and geology by slope and topographic openness: Geomorphology, v. 118, p. 22–32. doi: 10.1016/j.geomorph.2009.12.005.

Prufer, K.M., and Brady, J.E., 2005, Stone Houses and Earth Lords: Maya Religion in the Cave Context: Boulder, University Press of Colorado, 392 p.

Reeder, P., Brady, J.E., and Webster, J., 1998, Geoarchaeological investigations on the northern Vaca Plateau, Belize: Mexicon, v. 20, p. 37–41.

Ricketson, O. Jr., and Kidder, A.V., 1930, An archaeological reconnaissance by air in Central America: Geographical Review, v. 20, p. 177–206.

Russ, J.C., 1994, Fractal Surfaces, New York, Plenum Press, 309 p.

Sellers, B., and Chamberlain, A., 1998, Cave detection using ground penetrating radar: The Archaeologist, no. 31, p. 20–21.

Siart, C., Bubenser, O., and Eitel, B., 2009, Combining digital elevation data (SRTM/ASTER), high resolution satellite imagery (Quickbird) and GIS for geomorphological mapping: A multi-component case study on Mediterranean karst in Central Crete: Geomorphology, v. 112, p. 106–121. doi: 10.1016/j.geomorph.2009.05.010.

Stepinski, T.F., and Bagaria, C., 2009, Segmentation-based unsupervised terrain classification for generation of physiographic maps: IEEE Geoscience and Remote Sensing Letters, v. 6, p. 733–737. doi: 10.1109/LGRS.2009.2024333.

Weishampel, J.F., Blair, J.B., Dubayah, R., Clark, D.B., and Knox, R.G., 2000a, Canopy topography of an old-growth tropical rainforest landscape: Selbyana, 21, p. 79–87.

Weishampel, J.F., Blair, J.B., Knox, R.G., Dubayah, R., and Clark, D.B., 2000b, Volumetric lidar return patterns from an old-growth tropical rainforest canopy: International Journal of Remote Sensing, v. 21, p. 409–415. doi: 10.1080/014311600210939.

Weishampel, J.F., Chase, A.F., Chase, D.Z., Drake, J.B., Shrestha, R.L., Slatton, K.C., Awe, J.J., Hightower, J., and Angelo, J., 2010, Remote sensing of ancient Maya land use features at Caracol, Belize related to tropical rainforest structure, *in* Forte, M., Campana, S., and Liuzza, C., eds., Space, Time, Place: Third International Conference on Remote Sensing Archaeology: Oxford, Archaeopress, BAR International Series 2118, p. 45–52.

Weiss, A., 2001, Topographic position and landform analysis, available at: www.jennessent.com/downloads/TPI-poster-TNC_18x22.pdf, [accessed September 24, 2010].

Wynne, J.J., Titus, T.N., and Diaz, G.C., 2008, On developing thermal cave detection techniques for earth, the moon and mars: Earth and Planetary Science Letters, v. 272, p. 240–250. doi: 10.1016/j.epsl.2008.04.037.

Yokoyama, R., Shirawawa, M., and Pike, R.J., 2002, Visualizing topography by openness: a new application of image processing to digital elevation models: Photogrammetric Engineering & Remote Sensing, v. 68, p. 257–265.

M. E. Slay and S. J. Taylor – *Brackenridgia ashleyi* (Isopoda: Trichoniscidae): Range extension with notes on ecology. *Journal of Cave and Karst Studies,* v. 73, no. 3, p. 197–200. DOI: 10.4311/2011LSC0221

BRACKENRIDGIA ASHLEYI (ISOPODA: TRICHONISCIDAE): RANGE EXTENSION WITH NOTES ON ECOLOGY

Michael E. Slay[1]* and Steven J. Taylor[2]

Abstract: We collected *Brackenridgia ashleyi* from ten caves in Arkansas and Missouri. From the type locality at Tumbling Creek Cave, Taney County, Missouri, we extended the range of the species 138 km north-northeast into Pulaski County, Missouri, 67 km south-southwest into Newton County, Arkansas, and 96 km southeast into Izard County, Arkansas. The new records reported here, in combination with detection of this species at previously inventoried sites, suggest that this species is widely distributed in the Ozarks. However, the relatively intensive sampling efforts required indicate the *B. ashleyi* is rare and easily overlooked.

Introduction

The genus *Brackenridgia* (Isopoda: Trichoniscidae) includes ten species, nearly all described from subterranean habitats, mostly in the western United States and Mexico (Lewis, 2004). With the exception of *B. heroldi* in California, all of the species are troglobionts (Sket, 2008) and occur in widely separated karst areas. *Brackenridgia cavernarum* has the widest distribution, known from two areas in Texas and one location in New Mexico (Lewis, 2004). Three species are known from individual caves: *B. sphinxensis* (Arizona; Shultz, 1984), *B. palmitensis* (Mexico; Reddell, 1981, p. 95), and *B. ashleyi* described on the basis of specimens from Tumbling Creek Cave, Taney County, Missouri, by Lewis (2004).

In Missouri, trichoniscid isopods were reported from Tumbling Creek Cave, Missouri (Craig, 1975; Gardner, 1986), and these specimens ultimately were included in the description of *B. ashleyi* by Lewis (2004). In addition to *B. ashleyi,* other trichoniscids have been recorded from caves in the Ozark ecoregion of Arkansas, Missouri, and Oklahoma. Gardner (1986) reported, from several caves in Carter, Crawford, Howell, and Taney counties in the Missouri Ozarks, *Miktoniscus* and *Amerigoniscus* (as *Caucasonethes*; North American *Caucasonethes* were placed in *Amerigoniscus* by Vandel (1950, 1977)). In Arkansas, *Miktoniscus* has been reported from Clay Cave, Izard County (McDaniel and Smith, 1976), and from Foushee Cave, Independence County (Youngsteadt and Youngsteadt, 1978). Recent records of trichoniscids in Arkansas (Graening et al., 2007) include *Brackenridgia* from a cave in Marion County, *Haplothalmus danicus* from a cave in Benton County, and *Miktoniscus* (determined by G. Schultz) from single caves in Newton and Searcy counties. We report new records from caves in Missouri and Arkansas, broadening the range of *B. ashleyi* to include much of the central Ozarks and changing its global conservation status, an assessment of extinction risk as defined by NatureServe (2011), through addition of new localities.

Materials and Methods

During 2003–2009, we collected *B. ashleyi* from caves in Missouri and Arkansas. Usually, we discovered individuals by visually inspecting woody debris, animal feces, or other organic material. In several caves, we recorded soil temperature (2 cm below the surface), air temperature (10 cm above the surface), and relative humidity to further define the habitats that yielded trichoniscid isopods. We preserved specimens in 70 to 80% ethanol and sent them to J. J. Lewis for identification. Specimens from Arkansas were deposited in the University of Arkansas Arthropod Museum, Fayetteville. Specimens from Missouri were deposited in the Crustacean Collection at the Illinois Natural History Survey, Champaign.

Results

New localities and records for *Brackenridgia ashleyi*—Arkansas: Izard County, Clay Cave, 10 July 2008, M. Slay and M. Kottmyer, 1 individual (Dark 2). Marion County, Forest Trail Ridge Cave, 8 June 2004, M. Slay and C. Bitting, 1 individual (087 Hand); 12 June 2008, M. Slay, D. Fong, and M. Kottmyer, 11 individuals; Forest Trail Pit, 11 June 2008, M. Slay, D. Fong, and M. Kottmyer, 2 individuals; Overlook(ed) Cave, 11 June 2008, M. Slay, D. Fong, and M. Kottmyer, 2 individuals. Newton County, Toney Barnes Cave, 16 September 2004, M. Slay and C. Bitting, 1 individual. Stone County, Blanchard Springs Caverns, 11 March 2009, M. Slay and M. Kottmyer, 3 individuals (Dripstone Tour behind first set of bleachers); Rowland Cave, 14 August 2008, M. Slay, C. Slay, and M. Kottmyer, 6 individuals (start of Breakdown passage), 1 ovigerous female (between station

* Corresponding Author
[1] The Nature Conservancy, 601 North University Avenue, Little Rock, AR 72205, USA mslay@tnc.org
[2] Illinois Natural History Survey, University of Illinois at Urbana-Champaign, 1816 South Oak Street, Champaign, IL 61820, USA sjtaylor@illinois.edu

D and station E); Upper Shelter Cave, 11 July 2008, M. Slay and M. Kottmyer, 12 individuals. Missouri: Pulaski County, Andy's Cave #2, 11 April 2004, S. Taylor, M. Slay, and JoAnn Jacoby, 6 individuals (335 Hand); Martin Cave, 23 March 2003, S. Taylor and V. Block, 1 individual (MAR-002 Hand), 29 March 2003, S. Taylor and V. Block, 1 individual (362 Hand), 1 individual (316 Hand).

New localities and records for *Brackenridgia* sp.—Arkansas: Marion County, Morning Star Mine #6, 26 May 2004, M. Slay and C. Bitting, 1 individual (034 Hand); Toney Bend Mine #3, 23 July 2004, M. Slay and C. Bitting, 4 individuals (122 Hand), 3 individuals (120 Hand). Missouri: Pulaski County, Wilson Cave, 5 January 2004, S. Taylor and M. Slay, 1 individual (093 Hand), 8 January 2004, S. Taylor and M. Slay, 2 individuals (159 Hand).

In Rowland Cave, we collected *B. ashleyi* on moist soil mixed with old bones of bats, organic debris, and rocks. In Clay Cave, we collected specimens on clay floors from old, blackened, damp wood full of casings and feces. Similarly, in Blanchard Springs Caverns, we collected individuals from damp pieces of decayed wood; however, the pieces of wood were on top of rocks in a large pile of breakdown blocks. In Pulaski County, Missouri, we always collected the species on clay floors, sometimes with scattered bat guano present. All of our collections and observations of this isopod occurred in sections of caves characterized by complete darkness. In four caves (Clay Cave, Forest Trail Ridge Cave, Martin Cave, and Rowland Cave), we recorded temperature and relative humidity at locations where *B. ashleyi* was present. Average temperature of the soil (n = 14) was 13.6 °C (SE ± 0.3 °C) with a range of 12.1–16.6 °C. Average temperature of the air (n = 13) was 14.3 °C (SE ± 0.3 °C) with a range of 13.1–17.1 °C. Average relative humidity (n = 13) was 94.6% (SE ± 1%) with a range of 85.5–98.2%.

Collectively, we observed the species during all seasons and in eight (January, March, April, May, June, July, August, and September) of the twelve calendar months. In Martin Cave, we consistently observed the species during four visits over a period of nineteen months (documenting it in March 2003 and January, May, and September 2004). In Blanchard Springs Caverns, we observed it twice over a five-month period (March and July 2009). At a smaller time scale, daily visits to several caves in Arkansas over a period of five days in June 2008 yielded some consecutive observations of *B. ashleyi*. In Forest Trail Pit, we observed individuals the first four days, but not the final day. In Overlook(ed) Cave, we observed individuals the first three days, but not the last two days.

Overall, when any individuals were found, the number was low, with fewer than five individuals observed 87% of the time. Of 30 observations, 17 detected a single individual, 9 detected two to four individuals, and 4 yielded more than five individuals. We observed the greatest numbers of individuals in Rowland Cave, Forest Trial Ridge Cave, and Upper Shelter Cave, where ten, eleven, and twelve individuals of *B. ashleyi* were observed, respectively.

Bioinventories in Pulaski County, Missouri, included fifty-seven caves, thirty-three of which were visited on more than one occasion for bioinventory using timed-area searches, pitfall trapping, or quadrat sampling. Qualitative sampling was conducted at the remaining caves, but this isopod was only detected in three of the caves in Pulaski County.

Discussion

Brackenridgia ashleyi is now confirmed from ten additional sites in Arkansas and Missouri, and these new locations extend the range of the species 138 km north-northeast into Pulaski County, Missouri, 67 km south-southwest into Newton County, Arkansas, and 96 km southeast into Izard County, Arkansas, from the type locality at Tumbling Creek Cave, Taney County, Missouri (Fig. 1). Specimens of *Brackenridgia* were collected from three other caves, but these individuals could not be identified to species. It is possible that these three caves also are locations for *B. ashleyi*, but additional specimens are needed for confirmation. Earlier records attributed to other genera may, in part, be misidentifications of *B. ashleyi* (such as records of *Miktoniscus* in Arkansas and Missouri; Lewis, 2004). Several caves where we recorded this species had been sampled previously for macroinvertebrates, notably Blanchard Springs Caverns and Rowland Cave, which were inventoried by Graening et al. (2003). The new records reported here, in combination with detection of this species at previously inventoried sites, suggest that this species is widely distributed in the Ozarks. However, the relatively intensive sampling efforts required indicate the *B. ashleyi* is rare and easily overlooked.

Acknowledgements

We thank J. J. Lewis (Lewis and Associates LLC) for identifying material and persons listed in records of collection for assistance during fieldwork. S. R. Ahler (University of Kentucky), J. Proffitt, K. Lohraff, and R. Edging (Natural Resources Branch, Fort Leonard Wood, Missouri) provided critical advice and information for fieldwork in Missouri. Funding and logistical support was provided by the Arkansas Game and Fish Commission, The Nature Conservancy (Arkansas Field Office), the Illinois State Museum Society, the United States Army Corps of Engineers, the United States Forest Service (Ozark National Forest), and the United States National Park Service (Buffalo National River).

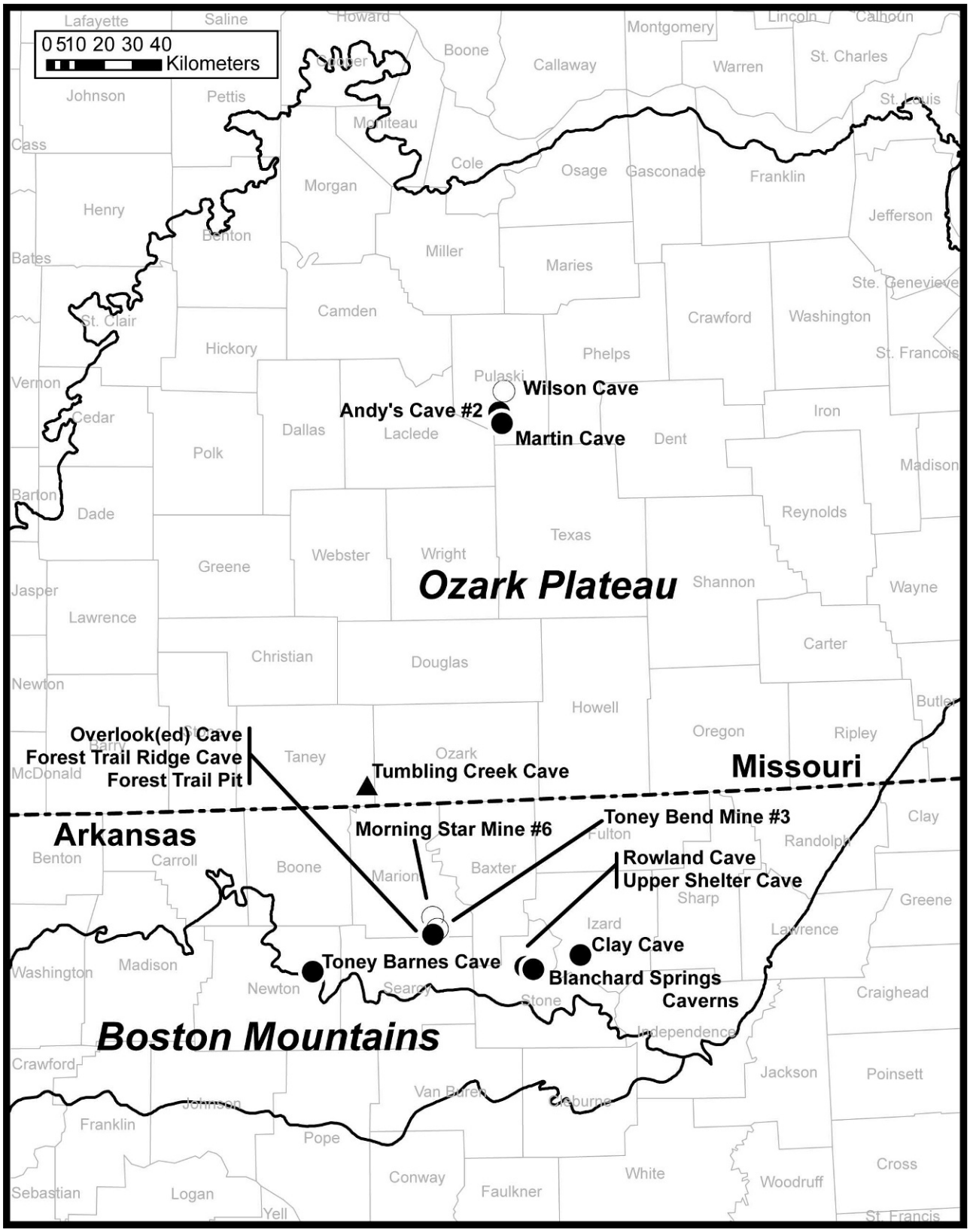

Figure 1. Known distribution of *Brackenridgia ashleyi* (closed circles, triangle) showing type locality (triangle) and *Brackenridgia* sp. (open circles, material probably attributable to this species).

References

Craig, J.L., 1975, A checklist of the invertebrate species recorded from Missouri subterranean habitats: Missouri Speleology, v. 15, no. 2, p. 1–10.

Gardner, J.E., 1986, Invertebrate Fauna from Missouri Caves and Springs: Missouri Department of Conservation Natural History Series No. 3, 72 p.

Graening, G.O., Slay, M.E., Fenolio, D.B., and Robinson, H.W., 2007, Annotated checklist of the Isopoda (Subphlyum Crustacea: Class Malacostraca) of Arkansas and Oklahoma, with emphasis on subterranean habitats: Proceedings of the Oklahoma Academy of Science, v. 87, p. 1–14.

Graening, G.O., Slay, M.E., and Tinkle, K., 2003, Subterranean biodiversity of Arkansas, part 1: bioinventory and bioassessment of caves in the Sylamore Ranger District, Ozark National Forest, Arkansas: Journal of the Arkansas Academy of Sciences, v. 57, p. 44–58.

Lewis, J.J., 2004, *Brackenridgia ashleyi*, a new species of terrestrial isopod from Tumbling Creek Cave, Missouri (Isopoda: Oniscidea: Trichoniscidae): Proceedings of the Biological Society of Washington, v. 117, p. 176–185.

McDaniel, V., and Smith, K., 1976, Cave fauna of Arkansas: selected invertebrate taxa: Proceedings of the Arkansas Academy of Science, v. 30, p. 57–60.

NatureServe, 2011, NatureServe Explorer: An online encyclopedia of life [web application], Version 7.1, NatureServe, Arlington, Virginia, http://www.natureserve.org/explorer, [accessed 18 May 2011].

Reddell, J.R., 1981, A Review of the Cavernicole Fauna of Mexico, Guatemala, and Belize, Austin, Texas Memorial Museum bulletin 27, 327 p.

Schultz, G.A., 1984, *Brackenridgia sphinxensis* n. sp. from a cave with notes on other species from Arizona and California (Isopoda, Oniscoidea): The Southwestern Naturalist, v. 29, p. 309–319.

Sket, B., 2008, Can we agree on an ecological classification of subterranean animals?: Journal of Natural History, v. 42, p. 1549–1563. doi: 10.1080/00222930801995762.

Vandel, A., 1950, Biospeologica LXXI. Campagne spéologique de C. Bolivar et R. Jeannel dans l'Amerique du Nord (1928). Isopodes terrestres recueillis par C. Bolivar et R. Jeannel (1928) et le Dr. Henrot (1946): Archives de Zoologie expérimentale et générale, v. 87, p. 183–210.

Vandel, A., 1977, Les espèces appartenant au genre *Amerigoniscus* Vandel, 1950 (Crustacés, Isopodes, Oniscoïdes): Bulletin de la Société d'Histoire naturelle de Toulouse, v. 113, p. 303–310.

Youngsteadt, N., and Youngsteadt, J., 1978, Biosurvey of invertebrates in Foushee Cave, IN-371, with notes on vertebrate observations: AACtivitieS, v. 84, p. 12–15.

R. Curl – Comment on "Coastal Caves in Bahamian Eolian Calcarenites: Differentiating Between Sea Caves and Flank Margin Caves Using Quantitative Morphology". *Journal of Cave and Karst Studies,* v. 73, no. 3, p. 201. DOI: 10.4311/jcks2010es0190

COMMENT ON "COASTAL CAVES IN BAHAMIAN EOLIAN CALCARENITES: DIFFERENTIATING BETWEEN SEA CAVES AND FLANK MARGIN CAVES USING QUANTITATIVE MORPHOLOGY"

RANE CURL
2805 Gladstone Ave., Ann Arbor, MI 48104, ranecurl@umich.edu

Waterstrat et al. (JCKS (2010), **72** (2) 61–74) compared means of geometric measurements of sea and flank margin caves with the Student t-test and concluded that these different types of caves could be "statistically differentiated." However, their use of the t-test is dependent on the data being normally distributed. The data that were analyzed, cave area to perimeter ratio, entrance-width to maximum-width ratio and short-axis to long-axis ratio, are all skewed to the right, generally have large standard deviations relative to their means, and are all non-negative. The data for at least some of the cases they analyzed may be normalized by a logarithmic transformation, yielding a close fit to log-normal distributions. This is shown in Figure 1 as log-normal probability plots of data for Flank Margin caves (FM) and San Salvador sea caves (SC) from Waterstrat (2007 – cited by the authors), where the natural logarithm of the area to perimeter ratio, $log_e(A/P)$, is plotted versus the standard unit-normal variable z corresponding to the unbiased estimator for the cumulative of the data, $F(k) = k/(n+1)$, where k is an order statistic of the data and n is the number of caves in a sample. Log-normal distributions of the data would yield straight lines. The linearity of the data is quite good, as shown by the correlation coefficients.

For these data, the respective means for $log_e(A/P)$ for FM and SC caves are 0.581 and 0.392, and their corresponding standard deviations are 0.682 and 0.411. A two-sided t-test of the difference of the these means is not significant at the 5% level of significance (los), contrary to the authors' conclusion based on applying the t-test to the unnormalized data. An additional interesting comparison can be made for the standard deviations of $log_e(A/P)$ for FM and SC caves. The slopes of the regression lines in Figure 1, which approximate the respective standard deviations, are clearly different. The variance ratio of the two data sets is 2.75, which is significant at a 1% los in a Snedecor F-test.

Waterstrat (2007) sorted data for flank margin caves and sea caves based on the general presence of speleothems in the former and their lack in the later, along with various dissolutional features, although the sorting of caves between the two types was also, in part, subjective. However the authors' statements that these statistical comparisons differentiate between sea caves and flank margin caves requires examination, if by differentiate they mean to use the comparisons for sorting the two types of caves into sea or flank margin caves. If a cave has, say, a value of $A/P = 1$ (m) ($log_e(A/P) = 0$), it is not possible to decided whether it is a sea cave or flank margin cave from the distribution data in Figure 1. This will be true in all cases where the statistical distributions of data sets overlap. For the data in Figure 1, a differentiation of type may be possible for large $log_e(A/P)$, where only flank margin caves have values over about 1.5, but even then, one needs to be concerned about the reasons for sea caves not being observed above that value, which may be because of inadequate discovery. This problem is even more obvious in the comparison of the variances of $log_e(A/P)$ of the two groups of caves. Even though the variances of the data for the two cave types are significantly different, this is no help in deciding whether a particular cave is one or the other type: both the mean and variance of the data for a cave type are not properties of individual caves, but rather of cave populations.

Still, both the mean and variance of data for a particular cave type, differentiated by other observations, are characteristics of the each cave type, and would be bases for testing geomorphic process models for their development. For example, how do the dissolutional and erosional processes make the variance of the $log_e(A/P)$ data for flank margin caves about 2.75 times greater than that for the San Salvador sea caves, or, fundamentally, why are these data apparently log-normally distributed?

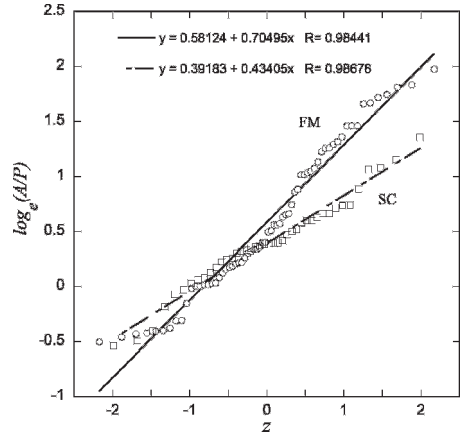

Figure 1. Log-normal probability plots of area/perimeter (*A/P*) data for flank margin caves (FM) and San Salvador sea caves (SC), from Waterstrat (2007). *Z* is the standard unit-normal variable corresponding to the estimated cumulative probability for each data point.

B. Mixon – Comment on "Coastal Caves in Bahamian Eolian Calcarenites: Differentiating Between Sea Caves and Flank Margin Caves Using Quantitative Morphology". *Journal of Cave and Karst Studies,* v. 73, no. 3, p. 202. DOI: 10.4311/jcks2011es0195

COMMENT ON "COASTAL CAVES IN BAHAMIAN EOLIAN CALCARENITES: DIFFERENTIATING BETWEEN SEA CAVES AND FLANK MARGIN CAVES USING QUANTITATIVE MORPHOLOGY"

BILL MIXON
14045 North Green Hills Loop, Austin, Texas 78737, bmixon@alumni.uchicago.edu

Waterstrat et al. (JCKS (2010), **72** (2) 61–74) calculated means of various geometric properties of collections of sea caves and flank-margin caves with the professed aim of showing that they can be statistically distinguished. If this is meant to be useful for determining whether a given coastal cave is one sort or the other, the results are useless, because the standard deviations of the distributions are larger than the differences in the means—a fancy way of saying that the distributions overlap substantially.

If the intention of the paper is to show that the two types of caves differ in the various properties to a statistically significant extent, it is hardly noteworthy. Statistical tests such as Student's t are useful in cases where the natural assumption is that there is no difference between two classes, a typical example being whether a new drug is more effective than an old one. In the case of caves, I can state with full confidence that any sufficiently large collections of caves formed by different mechanisms, or indeed by the same mechanism in different geological environments, will differ significantly in shape, however that is defined. Indeed, the authors point out various qualitative features that can be used to differentiate flank-margin caves from sea caves. When anyone familiar with coastal caves can usually tell from a glance at its map which category a cave belongs to, it is not surprising that extremely high levels of statistical significance can be reached, limited only by the number of data points available.

One of the parameters investigated by the authors is not even dimensionless. Given two collections of caves that match one-to-one in shape exactly, but with one collection being systematically 1% longer than the other, their mean ratios of perimeter to area will differ to any level of significance you like, given large enough samples.

W.J. Waterstrat, J.E. Mylroie, A.M. Owen, and J.R. Mylroie – Reply to Comments on: Coastal Caves in Bahamian Eolian Calcarenites: Differentiating Between Sea Caves and Flank Margin Caves Using Quantitative Morphology. *Journal of Cave and Karst Studies,* v. 73, no. 3, p. 203. DOI: 10.4311/2011ES0216

REPLY TO COMMENTS ON: COASTAL CAVES IN BAHAMIAN EOLIAN CALCARENITES: DIFFERENTIATING BETWEEN SEA CAVES AND FLANK MARGIN CAVES USING QUANTITATIVE MORPHOLOGY

Willipa J. Waterstrat, John E. Mylroie, Athena M. Owen, and Joan R. Mylroie
Department of Geosciences, Mississippi State University, Mississippi State, MS 39762

We thank Rane Curl and Bill Mixon for their insight into the statistics of sea cave and flank margin cave morphometry.

We agree that the data are not normally distributed, which puts the results of Waterstrat et al. (2010) into question as use of the Student T-test would be then inappropriate. We agree with Curl's attempt to normalize the data with a log transformation, and the data certainly are closer to normal than they were before the natural log transformation. However, we do not agree that the data are now normal. The log transformed data fail the Anderson-Darling test for normality ($p=0.026$), and the Shapiro-Wilk test for normality ($p=0.018$). This still invalidates the use of the Student T-test as it assumes normality. However, when we conduct the Wilcoxon-Rank Sum Test (the non-parametric equivalent of the Student T-test) with the natural log transformed A/P ratios, we find that the Flank Margin Caves and San Salvador Sea Caves are not significantly different ($p=0.457$), as Curl noted using the Student T-test. Further work needs to be done to confirm or reject the use of the various other ratios discussed in Waterstrat et al. (2010).

To clarify Curl's statement about the use of speleothems to differentiate cave types, the controls for this work were sea caves developed in Holocene eolianites, which by definition, could not contain flank margin caves of Pleistocene age, and flank margin caves near higher paleo-shorelines entered by ceiling collapse or vadose shafts, with no lateral opening to a past sea-level highstand. These end-member caves allowed qualitative comparison of diagnostic features unique to each cave type. The various measurements subsequently used were an attempt to quantify these observations.

In regard to Bill Mixon's statements, comparison of caves from differing geologic environments would certainly be expected to give different results; how they differ was the important question. In carbonate islands, one cannot tell at a glance of a cave map if a cave is a sea cave or a flank margin cave; that is precisely why the quantitative attempt was undertaken. These San Salvador caves are developed in geologically identical Quaternary eolianites, and the caves formed in geologically recent time, and can be overprinted. As a result, criteria for differentiation are subtle. The issue of dimensionless ratios is irrelevant; hydraulic radius is an area to perimeter ratio of well known effectiveness in stream hydrology.

The authors thank Mr. Erik Larson for his application and evaluation of the statistics discussed above.

GUIDE TO AUTHORS

The *Journal of Cave and Karst Studies* is a multidisciplinary journal devoted to cave and karst research. The *Journal* is seeking original, unpublished manuscripts concerning the scientific study of caves or other karst features. Authors do not need to be members of the National Speleological Society, but preference is given to manuscripts of importance to North American speleology.

LANGUAGES: The *Journal of Cave and Karst Studies* uses American-style English as its standard language and spelling style, with the exception of allowing a second abstract in another language when room allows. In the case of proper names, the *Journal* tries to accommodate other spellings and punctuation styles. In cases where the Editor-in-Chief finds it appropriate to use non-English words outside of proper names (generally where no equivalent English word exists), the *Journal* italicizes them. However, the common abbreviations i.e., e.g., et al., and etc. should appear in roman text. Authors are encouraged to write for our combined professional and amateur readerships.

CONTENT: Each paper will contain a title with the authors' names and addresses, an abstract, and the text of the paper, including a summary or conclusions section. Acknowledgments and references follow the text.

ABSTRACTS: An abstract stating the essential points and results must accompany all articles. An abstract is a summary, not a promise of what topics are covered in the paper.

STYLE: The *Journal* consults The Chicago Manual of Style on most general style issues.

REFERENCES: In the text, references to previously published work should be followed by the relevant author's name and date (and page number, when appropriate) in parentheses. All cited references are alphabetical at the end of the manuscript with senior author's last name first, followed by date of publication, title, publisher, volume, and page numbers. Geological Society of America format should be used (see http://www.geosociety.org/pubs/geoguid5.htm). Please do not abbreviate periodical titles. Web references are acceptable when deemed appropriate. The references should follow the style of: Author (or publisher), year, Webpage title: Publisher (if a specific author is available), full URL (e.g., http://www.usgs.gov/citguide.html) and date when the web site was accessed in brackets; for example [accessed July 16, 2002]. If there are specific authors given, use their name and list the responsible organization as publisher. Because of the ephemeral nature of websites, please provide the specific date. Citations within the text should read: (Author, Year).

SUBMISSION: Effective July 2007, all manuscripts are to be submitted via AllenTrack, a web-based system for online submission. The web address is http://jcks.allentrack2.net. Instructions are provided at that address. At your first visit, you will be prompted to establish a login and password, after which you will enter information about your manuscript (e.g., authors and addresses, manuscript title, abstract, etc.). You will then enter your manuscript, tables, and figure files separately or all together as part of the manuscript. Manuscript files can be uploaded as DOC, WPD, RTF, TXT, or LaTeX. A DOC template with additional manuscript specifications may be downloaded. (Note: LaTeX files should not use any unusual style files; a LaTeX template and BiBTeX file for the *Journal* may be downloaded or obtained from the Editor-in-Chief.) Table files can be uploaded as DOC, WPD, RTF, TXT, or LaTeX files, and figure files can be uploaded as TIFF, EPS, AI, or CDR files. Alternatively, authors may submit manuscripts as PDF or HTML files, but if the manuscript is accepted for publication, the manuscript will need to be submitted as one of the accepted file types listed above. Manuscripts must be typed, double spaced, and single-sided. Manuscripts should be no longer than 6,000 words plus tables and figures, but exceptions are permitted on a case-by-case basis. Authors of accepted papers exceeding this limit may have to pay a current page charge for the extra pages unless decided otherwise by the Editor-in-Chief. Extensive supporting data will be placed on the *Journal*'s website with a paper copy placed in the NSS archives and library. The data that are used within a paper must be made available. Authors may be required to provide supporting data in a fundamental format, such as ASCII for text data or comma-delimited ASCII for tabular data.

DISCUSSIONS: Critical discussions of papers previously published in the *Journal* are welcome. Authors will be given an opportunity to reply. Discussions and replies must be limited to a maximum of 1000 words and discussions will be subject to review before publication. Discussions must be within 6 months after the original article appears.

MEASUREMENTS: All measurements will be in Systeme Internationale (metric) except when quoting historical references. Other units will be allowed where necessary if placed in parentheses and following the SI units.

FIGURES: Figures and lettering must be neat and legible. Figure captions should be on a separate sheet of paper and not within the figure. Figures should be numbered in sequence and referred to in the text by inserting (Fig. x). Most figures will be reduced, hence the lettering should be large. Photographs must be sharp and high contrast. Color will generally only be printed at author's expense.

TABLES: See http://www.caves.org/pub/journal/PDF/Tables.pdf to get guidelines for table layout.

COPYRIGHT AND AUTHOR'S RESPONSIBILITIES: It is the author's responsibility to clear any copyright or acknowledgement matters concerning text, tables, or figures used. Authors should also ensure adequate attention to sensitive or legal issues such as land owner and land manager concerns or policies.

PROCESS: All submitted manuscripts are sent out to at least two experts in the field. Reviewed manuscripts are then returned to the author for consideration of the referees' remarks and revision, where appropriate. Revised manuscripts are returned to the appropriate Associate Editor who then recommends acceptance or rejection. The Editor-in-Chief makes final decisions regarding publication. Upon acceptance, the senior author will be sent one set of PDF proofs for review. Examine the current issue for more information about the format used.

ELECTRONIC FILES: The *Journal* is printed at high resolution. Illustrations must be a minimum of 300 dpi for acceptance.

Journal of Cave and Karst Studies

Volume 73 Number 3 December 2011

Article 125
Geographical and Geological Data from Caves and Mines Infected with White-Nose Syndrome (WNS) before September 2009 in the Eastern United States
Christopher S. Swezey and Christopher P. Garrity

Article 158
Karst Springs as Habitats for Rare and Protected Plant Species: A New Inland Locality of a Halophyte Plant *Batrachium baudotii* (Ranunckaceae) in a Karst Spring in Central Europe
Krzysztof Spałek and Jaroslaw Proćków

Article 162
Quaternary Cave Faunas of Canada: A Review of the Vertebrate Remains
C.R. Harington

Article 181
Stability of Dissolution Flutes under Turbulent Flow
Øyvind Hammer, Stein E. Lauritzen, and Bjørn Jamtveit

Article 187
Detection and Morphologic Analysis of Potential Below-Canopy Cave Openings in the Karst Landscape around the Maya Polity of Caracol using Airborne Lidar
John F. Weishampel, Jessica N. Hightower, Arlen F. Chase, Diane Z. Chase, and Ryan A. Patrick

Article 197
Brackenridgia Ashleyi (Isopoda: Trichoniscidae): Range Extension with Notes on Ecology
Michael E. Slay and Steven J. Taylor

Article 201
Comment on "Coastal Caves in Bahamian Eolian Calcarenites: Differentiating between Sea Caves and Flank Margin Caves using Quantitative Morphology"
Rane Curl

Article 202
Comment on "Coastal Caves in Bahamian Eolian Calcarenites: Differentiating between Sea Caves and Flank Margin Caves using Quantitative Morphology"
Bill Mixon

Article 203
Reply to Comments on : Coastal Caves in Bahamian Eolian Calcarenites: Differentiating between Sea Caves and Flank Margin Caves using Quantitative Morphology
Willipa J. Waterstrat, John E. Mylroie, Athena M. Owen, and Joan R. Mylroie